Title

SURFACE SCIENCE AND HIGH PRESSURE REACTION STUDIES OF THIOPHENE HYDRODESULFURIZATION OVER Mo SINGLE CRYSTAL CATALYSTS

Author

Gellman, A.J.

Publication Date

1985-07-01

Lawrence Berkeley Laboratory
UNIVERSITY OF CALIFORNIA

Materials & Molecular Research Division

SURFACE SCIENCE AND HIGH PRESSURE REACTION STUDIES OF THIOPHENE HYDRODESULFURIZATION OVER Mo SINGLE CRYSTAL CATALYSTS

A.J. Gellman
(Ph.D. Thesis)

July 1985

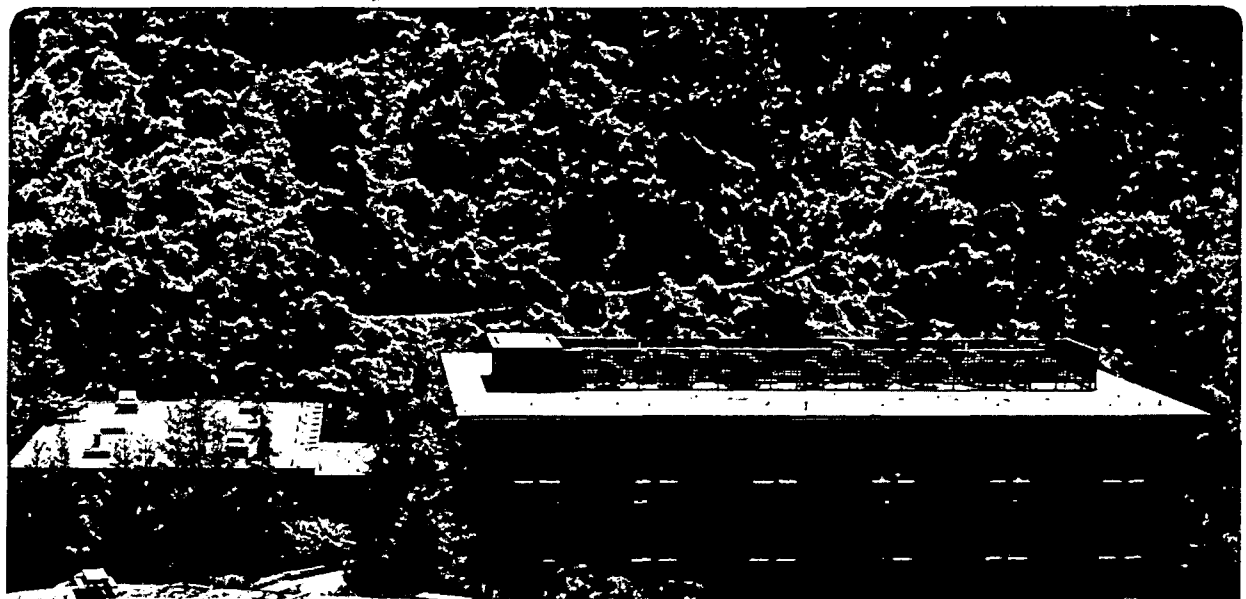

Prepared for the U.S. Department of Energy under Contract DE-AC03-76SF00098

DISCLAIMER

SURFACE SCIENCE AND HIGH PRESSURE REACTION STUDIES OF THIOPHENE HYDRODESULFURIZATION OVER MO SINGLE CRYSTAL CATALYSTS

by

Andrew John Gellman

Materials and Molecular Research Division
Lawrence Berkeley Laboratory and Department of Chemistry
University of California, Berkeley, California 94720

Surface Science and High Pressure Reaction Studies of Thiophene Hydrodesulfurization over Mo Single Crystal Catalysts

Andrew John Gellman

Abstract

Surface science experiments combined with high pressure reaction studies have been used to investigate the hydrodesulfurization (HDS) of thiophene over Mo single crystal catalysts. Characterization of the sulfided Mo(100) surface and the surface chemistry of thiophene on Mo have been performed under UHV conditions while HDS reaction were performed at pressures of 1 atm.

At low coverages (θ_S<0.5) sulfur atoms are adsorbed on the Mo(100) surface in the fourfold hollow site. As the sulfur coverage is increased past θ_S=0.67 a second binding site becomes occupied. The simultaneous occupation of two binding sites is induced by repulsive interactions between adsorbed atoms. The heat of adsorption at low coverages is 110 kcal/mole and drops to 75-90 kcal/mole at high coverages.

At high coverages thiophene adsorbs on the Mo(100) surface in both a reversibly bound state that desorbs upon heating and an irreversibly bound state that decomposes. The irreversibly bound molecule decomposes via a low temperature mechanism (175K - 350K) and a second, high temperature process in the range 600K - 680K. The adsorbed molecule is π-bonded to the surface with its sulfur atom bound in a chemical environment similar to that in gas phase thiophene. The α-CH bonds are weakened to a greater extent by their interaction with the surface than

the β-CH bonds. During the low temperature decomposition process α-CH bond scission occurs prior to β-CH bond scission. This adsorbed species is stable on the surface to temperatures >600K (the temperature at which high pressure HDS reactions are performed).

The high pressure HDS reaction mechanism proceeds via initial desulfurization to yield butadiene. The subsequent hydrogenation reactions producing butenes and butane proceed via a hydrocarbon intermediate that saturates its available binding sites on the surface. Sulfiding of the surface selectively blocks these binding sites and thus selectively blocks butene and butane production.

The initial desulfurization step of the thiophene HDS reaction occurs via a mechanism that does not deposit sulfur onto the metal surface i.e. not via the Lipsch-Schuit mechanism. A mechanism involving direct hydrogenation of CS bonds to produce H_2S is consistent with these results. An intramolecular dehydrodesulfurization mechanism, as proposed by Kolboe, cannot be ruled out.

G. A. Somorjai

Acknowledgments

The work presented in this thesis has benefitted greatly from a number of collaborations and the interest of many individuals. My greatest debt of gratitude is to Prof. Gabor Somorjai for his unfaltering support, tutelage and friendship over the past four years. In addition to introducing me to the field of surface science he has provided me with a unique perspective on science in general, the ways in which interesting scientific problems can be identified and approached, and the role of science in society. Furthermore, and of equal importance, he has created a research group providing an excellent learning environment. The wide ranging backgrounds of its members and of the fields under study has produced a group of individuals with broad scientific interests and a group in which it is possible to actively interest people in all types of problems.

I would like to thank the people with whom I have worked either directly or indirectly on various portions of this research. These include Eddie Tysoe, Fransisco Zaera, Mark Bussel, Mario Farias, Miquel Salmeron and Dave Kelly. Some of the experiments have been performed at the Exxon Research and Engineering Co. in Clinton, NJ and I must thank many of the people there for their interest in this work. In particular, my thanks go to John Gland and Ed Kollin for the use of some of their equipment and for their hospitality during my stay in Clinton. In addition to the work presented in this thesis I have enjoyed working with Mark Logan, Randy Yeates, John Turner, and Chun-si Zhang on a number of projects not mentioned in this thesis. Finally, my thanks go to Berkeley undergraduates Dave Neiman and Dave Arthur who

worked with me on a number of projects.

For their excellent advice and help during the times of stress when equipment was not working, or at least wouldn't work for me, I am thankful to Keith Frank and Dan Colomb who are, I think, among the best technicians one could hope to work with. I would like to thank Jim Severns, Hank Brendle and Glenn Baum for their help in fixing many electronic and vacuum related problems. Furthermore, my thanks go to all the MMRD support staff for their help in solving all types of problems.

My thanks go to Mathew Mate, Dave Godbey, Kao Chi-Tzu, Dan Strongin and Mark Bussel for their critical reading of various chapters of this thesis, and to Prof. Somorjai, Prof. Searcy and Prof. Pimentel for reviewing it in its entirety.

Finally, I would like to thank to thank my family and friends for the many good times that I have enjoyed over the past four years. To my parents in particular my thanks for always showing their interest in my work and for never believing anything just because I said it. Within the group I would like to thank everyone for taking the time to consider my questions and in turn for asking hard questions, for the many late-night pitchers of beer, and for the many interesting discussions absolutely unrelated to surface science.

This work was supported by the Director, Office of Energy Research, Office of Basic Energy Sciences, Materials Science Division of the U.S. Department of Energy under Contract No. DE-AC03-76SF00098.

Table of Contents

Table of Figures

4. The Chemistry of Thiophene on the Mo(100) Surface

Table of Tables

Chapter 1. Introduction

Catalytic processes are vital components of the chemical, energy and petroleum industries. They form the basis for the syntheses of many economically important compounds and materials including polymers, fertilizers from ammonia synthesis, and synthesis of light hydrocarbons from coal. Catalysts are used throughout the petroleum refining industry for cleaning of crude stocks, cracking of heavy crudes and reforming and upgrading processes. The heterogeneous catalysts used for many of these are extremely complex and very poorly understood, often consisting of mixtures of metals in various oxidation states or chemical environments dispersed on high surface area support materials. The lack of understanding of these catalysts is due in part to their complexity and in part to a lack of analytical tools for their study.

There now exist, however, a large number of techniques for the study of the surfaces of small ($\sim 1 cm^2$) samples and of adsorbates on these surfaces (1,2). It is possible to obtain information about surface composition, structure, electronic structure, the local chemical environments of surface atoms, and various other physical and chemical characteristics of material surfaces and adsorbates. These techniques have been applied to the study of a number of catalytically interesting systems (1,3). The approach has been to study well defined surfaces, usually of catalytically important metals, under ultra-high vacuum (UHV) conditions in which they can be kept clean for fairly long periods of time (hrs.). The study of these surfaces and of adsorbates on these surfaces has been coupled with the use of an isolation cell in which high pressure reactions can be performed over

these well characterized catalysts (4). The work presented in this thesis represents the first attempt to study such a system in which the catalyst is not a metal but, in this case, a sulfide.

Hydrotreating or hydroprocessing catalysis is used to remove contaminants from crude stocks. This process has become increasingly important as sources of clean petroleum are being consumed and the industry is forced to rely on crudes with higher concentrations of undesirable compounds. The contaminant compositions of a number of crudes are listed in Table 1.1 and, as can be seen, many are high in sulfur, nitrogen and oxygen content (5). Not listed is the metals content which can be in 100 ppm range. The four processes included under the heading of hydrotreating catalysis are hydrodesulfurization (HDS), hydrodenitrogenation (HDN), hydrodeoxygenation (HDO), and hydrodemetallation (HDM). The need to remove sulfur from crude petroleum arises from the fact that many of the Pt hydroforming catalysts used to upgrade petroleum octane number are extremely sensitive to poisoning by small amounts of sulfur. Furthermore, the burning of sulfur containing compounds produces SO_2 which is a highly undesirable pollutant. Similarly, many of the nitrogen containing compounds are poisons for the acidic hydrogenation catalysts used in petroleum refining and must be removed early on in the process. Metal contaminants must be removed because they are often irreversibly deposited on the catalyst, plugging pores and thus inhibiting the transport of reactants and products in and out of catalyst pellets (6,7).

The most common forms of sulfur present in crude petroleum are thiols, sulfides, disulfides and thiophenes. These are progressively more difficult to desulfurize in that same order, with the thiophenes

Table 1.1 Compositions of Several Crude Stocks (wt.%) (5)

	C	H	N	S	O
Arab Light Atmospheric Resid	84.8	11.8	0.2	3.6	0.1
Utah Coal Oil	83.3	8.8	1.0	0.3	6.6
Athabasca Bitumen	83.3	10.4	0.4	4.6	1.3
Shale Oil	86.3	11.4	2.0	0.9	-
Utah A Coal	74.8	5.5	1.4	0.5	6.1

being much less active than the others. As a result thiophene and its derivatives are the most commonly used models for the study of hydrodesulfurization with thiophene, benzothiophene and dibenzothiophene (Fig. 1.1) being the most common among these (8). In most cases these are, again, progressively more difficult to desulfurize in the order in which they are listed. The conditions typically used for the process are temperatures of 300° - 450°C and pressures as high as 200 atm. of hydrogen. Reactors are of the trickle-bed type in which the feed is introduced at the top and flows downward through a bed of catalyst particles.

HDS catalysts are usually mixed metal catalysts using either Mo or W as the base metal and Co or Ni as a promoter. Metal loadings can be as high as 20% with a ratio of base metal to promoter of about 3:1. They are produced by impregnation of the support material, usually γ-Al_2O_3, with solutions of molybdates and Co nitrates followed by calcining in oxygen. Sulfiding is accomplished either by treatment in an H_2/H_2S mixture or by allowing the catalyst to become sulfided in the petroleum feed. Catalyst lifetimes are from 1 yr. for those used with heavy petroleum fractions to 10 yrs. for those used with light fractions (6), the primary causes of deactivation being the buildup of coke deposits and the plugging of catalyst particle pores by metals (9).

Although the Mo and W catalysts are by far the most common there are a number of metals that are more active. A study of the activity of a series of transition metal sulfides showed that the first row sulfides were relatively poor catalysts for the HDS of dibenzothiophene. In the second and third rows activity peaked for the

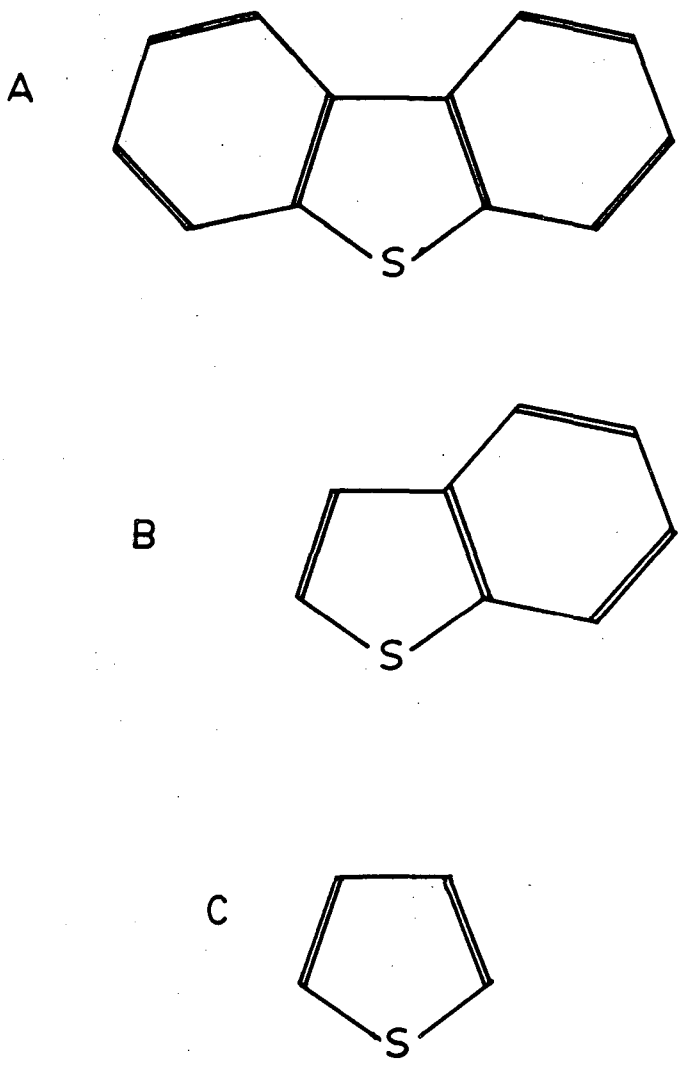

Fig. 1.1 Three compounds used as models in studies of HDS catalysis. A) Dibenzothiophene, B) Benzothiophene, C) Thiophene

sulfides of Ru and Os (10,22). A correlation was drawn between activity and the heat of formation of the sulfide showing that the optimum occurred at $\Delta H_f \approx 40$ kcal/mole. This was extended to the mixed metal catalysts to show that those that had the highest activity had average heats of formation of the two metal sulfides that were about 40 kcal/mole. From this it was inferred that an optimum metal-sulfur bond strength is needed to induce C-S bond breaking and yet allow facile removal of sulfur from the surface (23).

The active form of the HDS catalyst has been the subject of a great deal of controversy. The original models proposed that the oxidized form of the catalyst (prior to sulfiding) consists of a MoO_3 monolayer on the Al_2O_3 substrate (11-13). Sulfiding resulted in the substitution of sulfur for oxygen in the topmost layer of the catalyst (14,15). More recent work using X-ray photoelectron (16,17) and X-ray absorption spectroscopy (18) suggests that, although there is always some Mo present in its oxidized form, the active component of the catalyst is MoS_2. MoS_2 is certainly known to be an active HDS catalyst and exhibits the same Co promotion effects as the supported catalyst. The structure of MoS_2 is shown in Fig. 1.2. It is a laminar compound formed of layers of Mo atoms sandwiched between two layers of sulfur. These are then stacked over each other with very weak bonding between layers. The basal planes of these MoS_2 sheets are completely sulfided and expose no metal atoms. It has been suggested that these are inactive in catalysis and that it is the edges or defects in this material, at which Mo atoms are exposed, that are the catalytically active sites. Studies of the adsorption of organic molecules on the basal plane of MoS_2 have shown that it is indeed, relatively inert

MoS_2 -

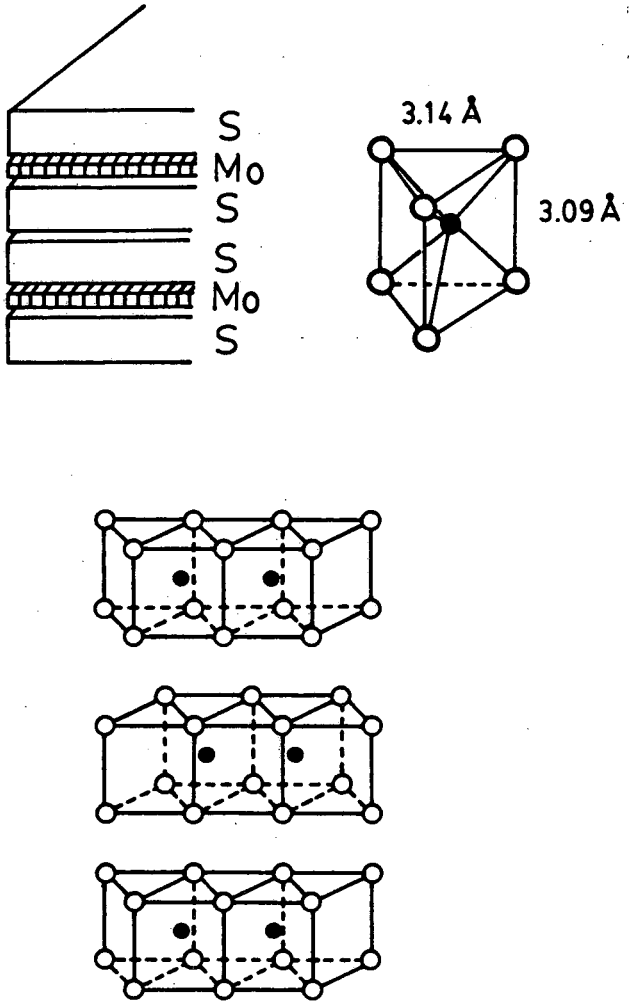

Fig. 1.2 MoS_2- the active component of HDS catalysts.

and that it will only physisorb molecules at very low temperatures (19).

The reaction that has been studied in this work is the HDS of thiophene, depicted in Fig. 1.3. The thermodynamic parameters of the reaction are listed in Table 1.2 and it is clear that the most favoured product is butane. While this product is favoured thermodynamically its production consumes the greatest amount of hydrogen, and thus is economically undesirable. The appearance of butadiene in the product mixture has lead to the proposal that the reaction proceeds via initial production of butadiene followed by its hydrogenation to butene and butane (20). The kinetics of the reaction have been studied several times over supported catlysts and have been reviewed recently (8). These have been interpreted in terms of Langmuir-Hinshelwood mechanisms to show that thiophene and H_2S compete for binding sites. The reaction rates have a first order dependence on the hydrogen pressure and there is some question as to whether hydrogen is dissociated on the catalyst. Certainly hydrogen adsorption on metallic Mo is dissociative (21) and the work presented here suggests that this is true under catalytic conditions. Finally, it is fairly widely held that the desulfurization and hydrogenation reactions occur at different sites on the catalyst. This is based on the observation that desulfurization is subject to inhibition by the presence of H_2S while hydrogenation is not (6,7).

The aim of the work described in this thesis is to study the HDS of thiophene over well characterized catalytic surfaces. The approach has been from two directions and the work is divided into four distinct sections. Although single crystal samples of MoS_2 are available, they

THE HYDRODESULFURIZATION OF THIOPHENE

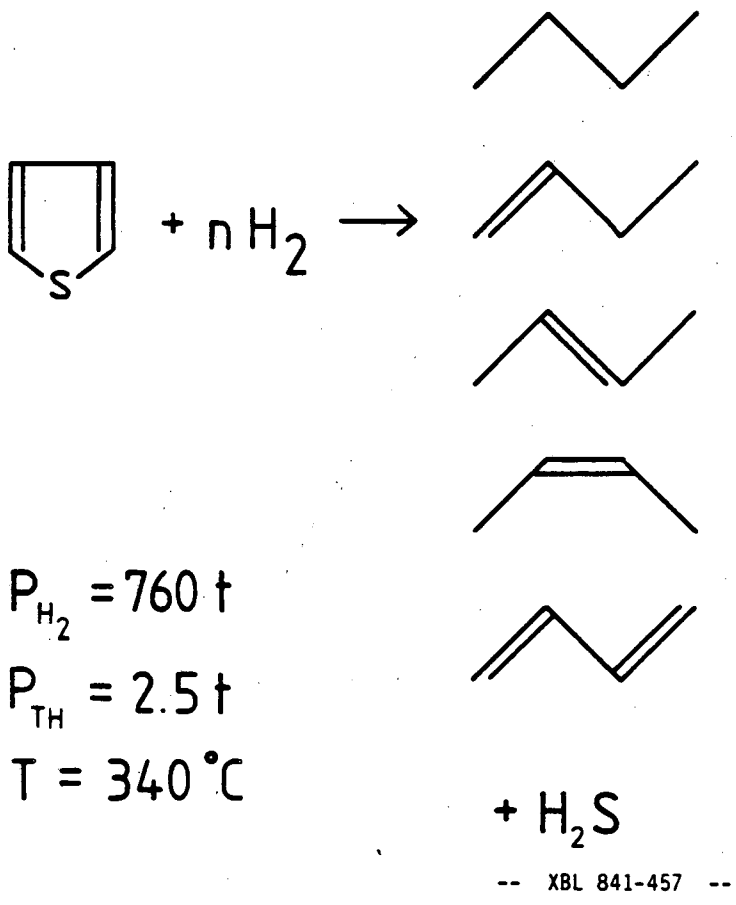

-- XBL 841-457 --

Fig. 1.3 The thiophene HDS reaction.

Table 1.2 Thermodynamic Parameters for Thiophene HDS

Reaction	ΔH°_{298} (kcal/mole)	ΔS (cal/mole/K)	ΔG°_{298} (kcal/mole)
Th + $2H_2$ → Butadiene + H_2S	-5.9	-13.3	-1.9
Th + $3H_2$ → 1-Butene + H_2S	-32.2	-37.6	-21.
Th + $3H_2$ → t2-Butene + H_2S	-35.0	-40.2	-22.9
Th + $3H_2$ → c2-Butene + H_2S	-34.0	-39.2	-22.2
Th + $4H_2$ → Butane + H_2S	-62.4	-68.2	-41.9

are extremely thin samples on which the sulfided basal plane is the predominantly exposed surface. This being the inactive plane it is not of direct interest. The weak interaction between the layers of MoS_2 causes the crystals to be very fragile and it is not possible to cut the single crystals at an angle to the basal plane to produce a well ordered surface composed of edges and defects. As a result this work has used metal single crystal samples as catalysts. The first section of this thesis describes the characterization of sulfur overlayers on the Mo(100) surface and the second is a study of the adsorption of thiophene on these surfaces. The kinetics of the high pressure reaction and the effects of surface modification on the reaction rates are described in the third section. Finally, the last chapter is devoted to a study using labelled sulfur on the surface to examine the nature of the initial step in the HDS reaction mechanism.

1.1 References

1. G.A. Somorjai, Chemistry in Two Dimensions: Surfaces, Cornell Univ. Press, Ithaca, NY, 1981
2. G. Ertl, J. Kuppers, Low Energy Electrons in Surface Chemistry, Verlag-Chimie, Germany, 1974
3. F. Zaera, A.J. Gellman, G.A. Somorjai, submitted to Acc. Chem. Res.
4. D.W. Blakely, E. Kozak, B.A. Sexton, G.A. Somorjai, J. Vac. Sci. & Tech., 13 (1976) 1091
5. L. Rollman, J. Catal., 46 (1977) 243
6. B.C. Gates, J.R. Katzer, G.C.A. Schuit, Chemistry of Cat. Processes, McGraw-Hill, NY, 1979
7. C.N. Satterfield, Heterogeneous Catalysis in Practice, McGraw-Hill, NY, 1980
8. M.L. Vrinat, Appl. Cat., 6 (1983) 137
9. T. Ohtsuka, Catal. Rev.- Sci. & Eng., 16(2) (1977) 291
10. T.A. Pecoraro, R.R. Chianelli, J. Catal., 67 (1981) 430
11. F.E. Massoth, G. MuraliBhar, Fourth Int. Conf. on the Chemistry and Uses of Molybdenum, Climax Moly. Co., Golden Co., 1982
12. E. Furminsky, Catal. Rev.- Sci. & Eng., 22(3) (1980) 371
13. P. Grange, Catal. Rev.- Sci. & Eng., 21(1) (1980) 135
14. J.M.J. Lipsch, G.C.A. Schuit, J. Catal., 15 (1969) 179
15. F.E. Massoth, J. Catal., 50 (1977) 190
16. R.A. Walton, J. Catal., 44 (1976) 325
17. G.C. Stevens, T. Edmonds, J. Catal., 44 (1976) 488
18. B.C. Clausen et. al., J. Phys. Chem., 85 (1981) 3868
19. M. Salmeron, G.A. Somorjai, A. Wold, R.R. Chianelli, K.S. Liang,

Chem. Phys. Lett., 90(2) (1982) 105

20. P.J. Owens, C.H. Amberg, Adv. Chem. Ser., 33 (1961) 181

21. H.R. Han, L.D. Schmidt, J. Phys. Chem., 75(2) (1971) 227

22. S. Harris, R.R. Chianelli, J. Catal., 86 (1984) 400

23. R.R. Chianelli, T.A. Pecoraro, T. R. Halbert, W.-H. Pan, E.I. Stiefel, J. Catal., 86 (1984) 226

Chapter 2. Experimental Techniques and Apparatus.

This work has benefitted from the application of a fairly wide variety of techiques both for surface analysis and the study of catalytic reactions. Most of the techniques applied, with the possible exception of the ^{35}S radiotracer experiments, are fairly "standard" in the sense that they have been used by many researchers in the study of surface related phenomenon. This work has used each as an analytical tool and is focussed on the problem of hydrodesulfurization rather than the study of a particular surface analysis technique or spectroscopy. Each of these tools has been described in great depth in a number of reviews and in many cases the detailed description of each spectroscopy goes far beyond the scope of this discussion. Hence, this section will be limited to describing each technique only to the depth necessary to understand its basic application to the problems studied in this work.

2.1 Apparatus

The experiments described here were performed in three stainless steel ultra-high vacuum (UHV) chambers. Each such chamber has various characteristics making it suitable for particular types of work.

2.1.1 Thermal Desorption Chamber

The chamber used for performing Thermal Desorption Spectroscopy (TDS) is shown schematically in Fig. 2.1. The belljar is a commercially available model (Varian) pumped by both an oil diffusion pump and an ion pump to base pressures of $1\text{-}2\times10^{-10}$ torr. The chamber is equipped

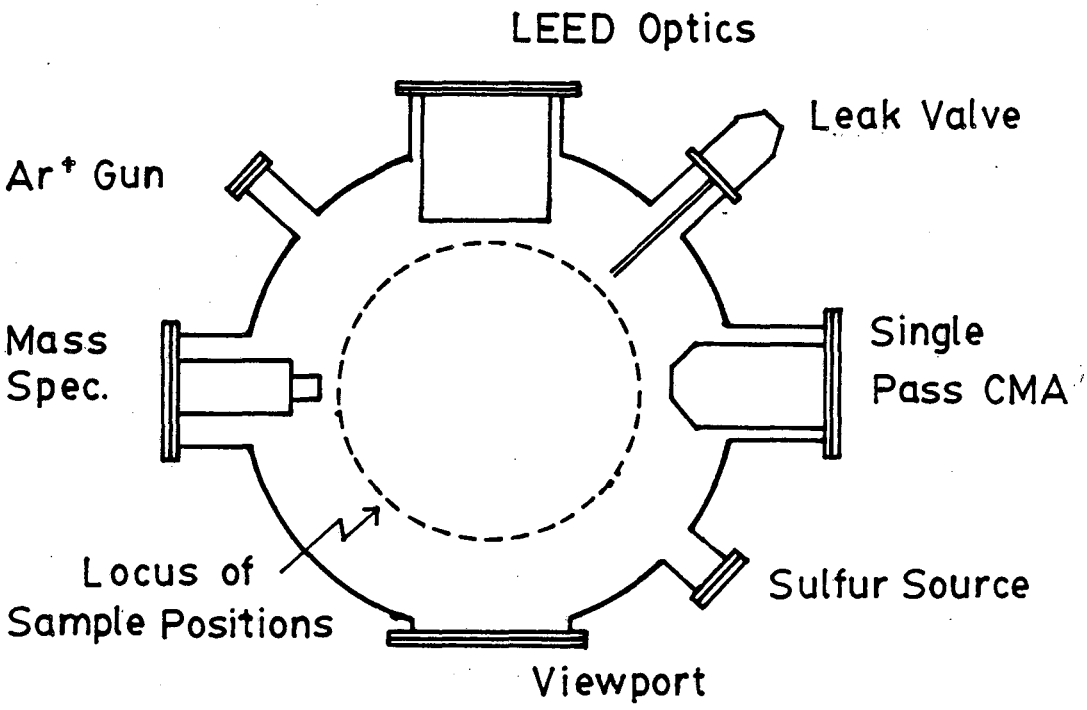

Fig. 2.1 Schematic diagram of the chamber used for thermal desorption experiments.

with the following:

- A crystal manipulator allowing x,y,z motion and rotation of the sample. The crystal can be heated resistively to 2000K and cooled to 150K through copper braids attached to two liquid nitrogen reservoirs.
- A single pass cylindrical mirror analyzer (PHI 10-155) with an internal electron gun for performing Auger Electron Spectroscopy.
- A four-grid optics (PHI 15-120) for performing Low Energy Electron Diffraction (LEED).
- An Ar^+ ion sputtering gun (PHI 04-161) for cleaning of the surface.
- A quadrupole mass spectrometer (UTI 100C) for analysis of background gases and performing desorption spectroscopy. This was interfaced to a Commodore PET computer to allow simultaneous monitoring of up to eight masses during desorption experiments.
- An electrolytic sulfur source for controlled sulfur deposition. (see Sec. 2.3)
- Two leak valves for controlled leaking of gases into the UHV chamber.

2.1.2 Photoemission Chamber

The UHV chamber used for all the photoemission experiments is depicted in Fig. 2.2. It is pumped solely by a liquid nitrogen trapped oil diffusion pump and attains base pressures of $1\text{-}2\times10^{-10}$ torr. The chamber equipped with the following:

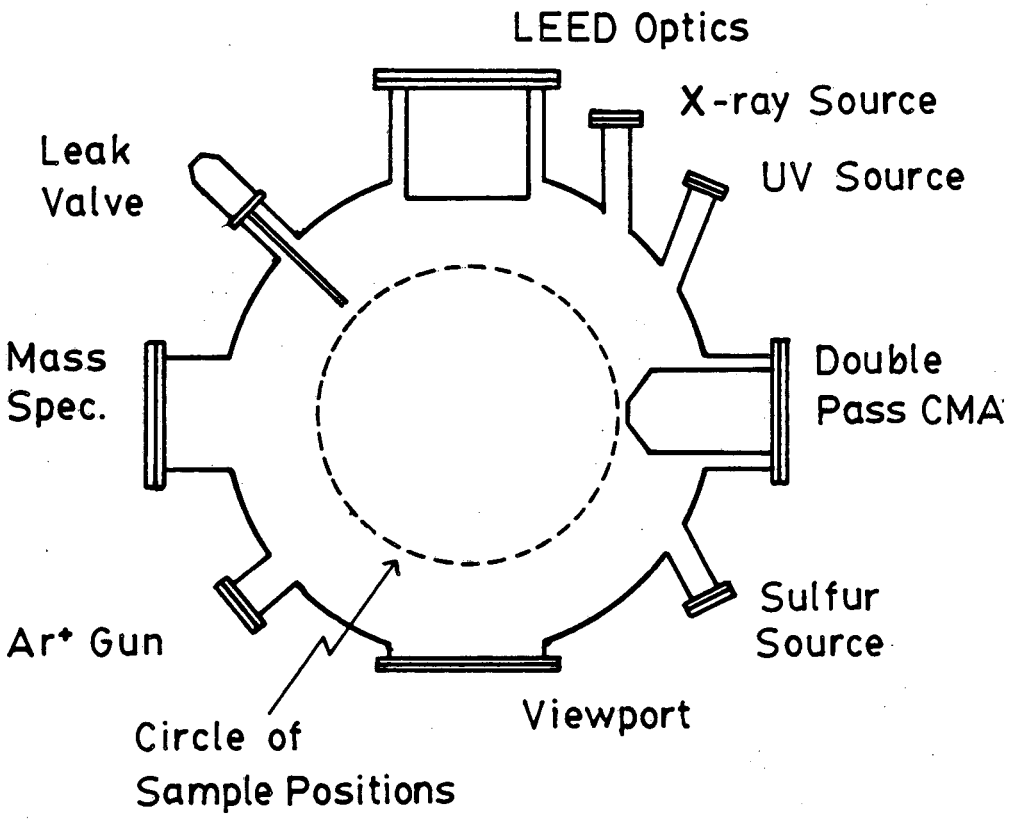

Fig. 2.2 Schematic diagram of the chamber used for UV and X-ray photoemission spectroscopy.

- An off-axis crystal manipulator providing x,y,z and rotational motion and in addition rotational motion of the crystal about a vertical axis through the plane of its surface. The crystal can be resistively heated to 1900K and cooled to 125K.
- A double pass cylindrical mirror analyzer (PHI 15-25G) for electron energy analysis during AES, XPS and UPS measurments.
- An X-ray source (PHI 04-151) fitted with a Mg anode providing 1235.6 eV K_α radiation for XPS measurments.
- An UV lamp (GCA/McPherson 630) providing He I radiation for UPS measurments.
- A mass spectrometer (see Sec. 2.1.1).
- A LEED optics assembly (see Sec. 2.1.1).
- A sputter ion gun (see Sec. 2.1.1).
- A leak valve (see Sec. 2.1.1).
- An electrlytic sulfur source (see Sec 2.3).
- A Commodore PET computer for data aquisition during AES, XPS, and UPS experiments.

2.1.3 High Pressure / UHV Chamber

The high pressure reactions and the ^{35}S experiments were performed in a specially designed chamber equipped with a high pressure isolation cell (Fig. 2.3) (1). This chamber is pumped by an ion pump and a titanium sublimation pump reaching ultimate vacuum of $6\text{-}8\times10^{-10}$ torr. The chamber is equipped with the following:

- An on-axis crystal manipulator modified for compatibility with the high pressure cell (Fig. 2.4). This manipulator allows

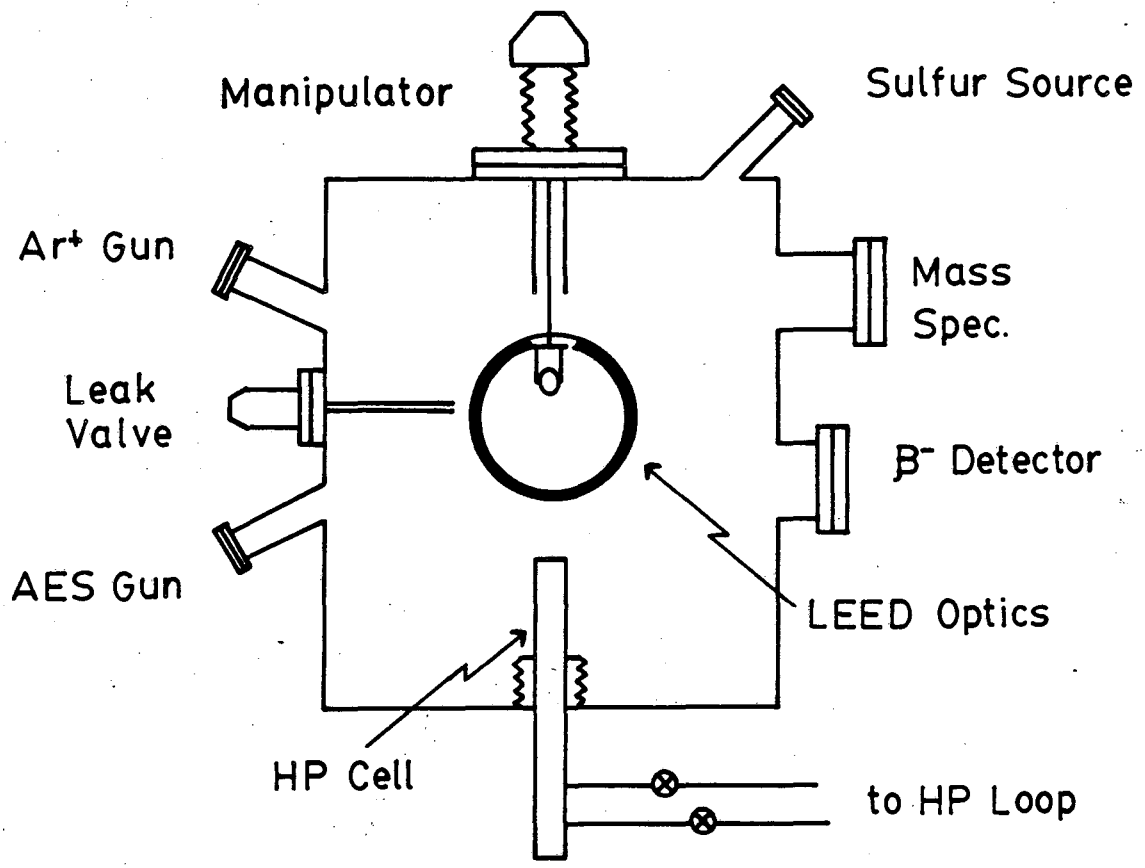

Fig. 2.3 Schematic diagram of the chamber used for high pressure reaction studies and ^{35}S radiotracer experiments.

x,y,z and rotational motion and heating of the sample to 1900K. No cooling was necessary.

- A high pressure isolation cell (Fig. 2.4) that, when enclosed over the sample, can be pressurized to 1 atm. with no degradation of vacuum in the UHV chamber.
- A reaction loop attached to the high pressure cell (Fig. 2.5, see Sec. 2.10).
- A gas chromatograph (Perkin-Elmer 3920B) for analysis of the contents of the reaction loop.
- A solid state β^- detector installed for the radiotracer experiments (see Sec 2.9).
- A LEED optics assembly (see Sec 2.1.1).This was also used as a retarding field analyzer for AES.
- An ion sputter gun (see Sec 2.1.1).
- Three leak valves (see Sec. 2.1.1).
- An electrolytic sulfur source (see Sec. 2.3).

The ultimate base pressure of such chambers, equipped with high pressure isolation cells, is limited by the presence of the cell whose walls are continuously contaminated with hydrocarbons and water from high pressure reactions. It seems that a future design in which the cell is completely retracted from the UHV chamber, when not in use, would greatly improve the vacuum. Such a modification would be extremely worthwhile.

HIGH PRESSURE CELL

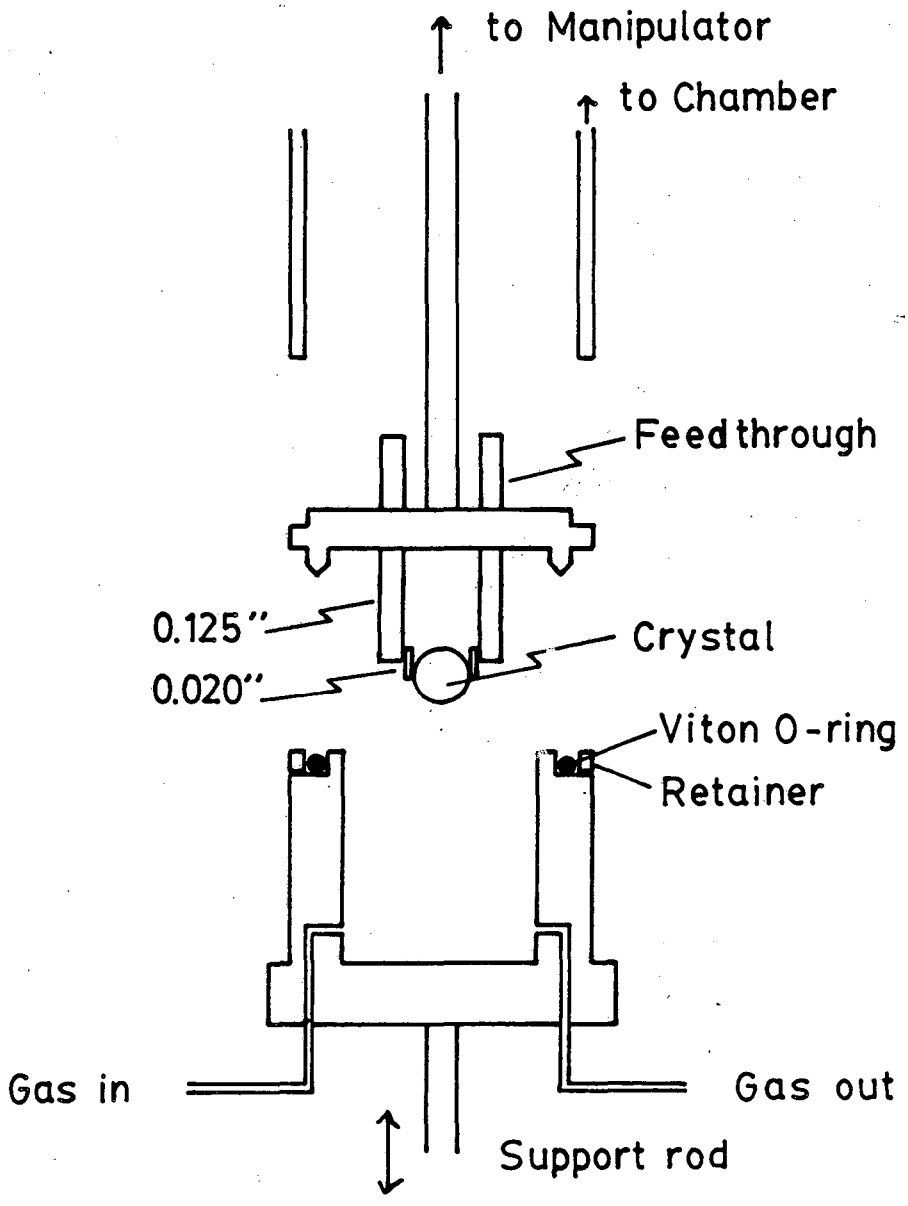

Fig. 2.4 The high pressure cell and adapted manipulator with crystal mounted in the typical manner.

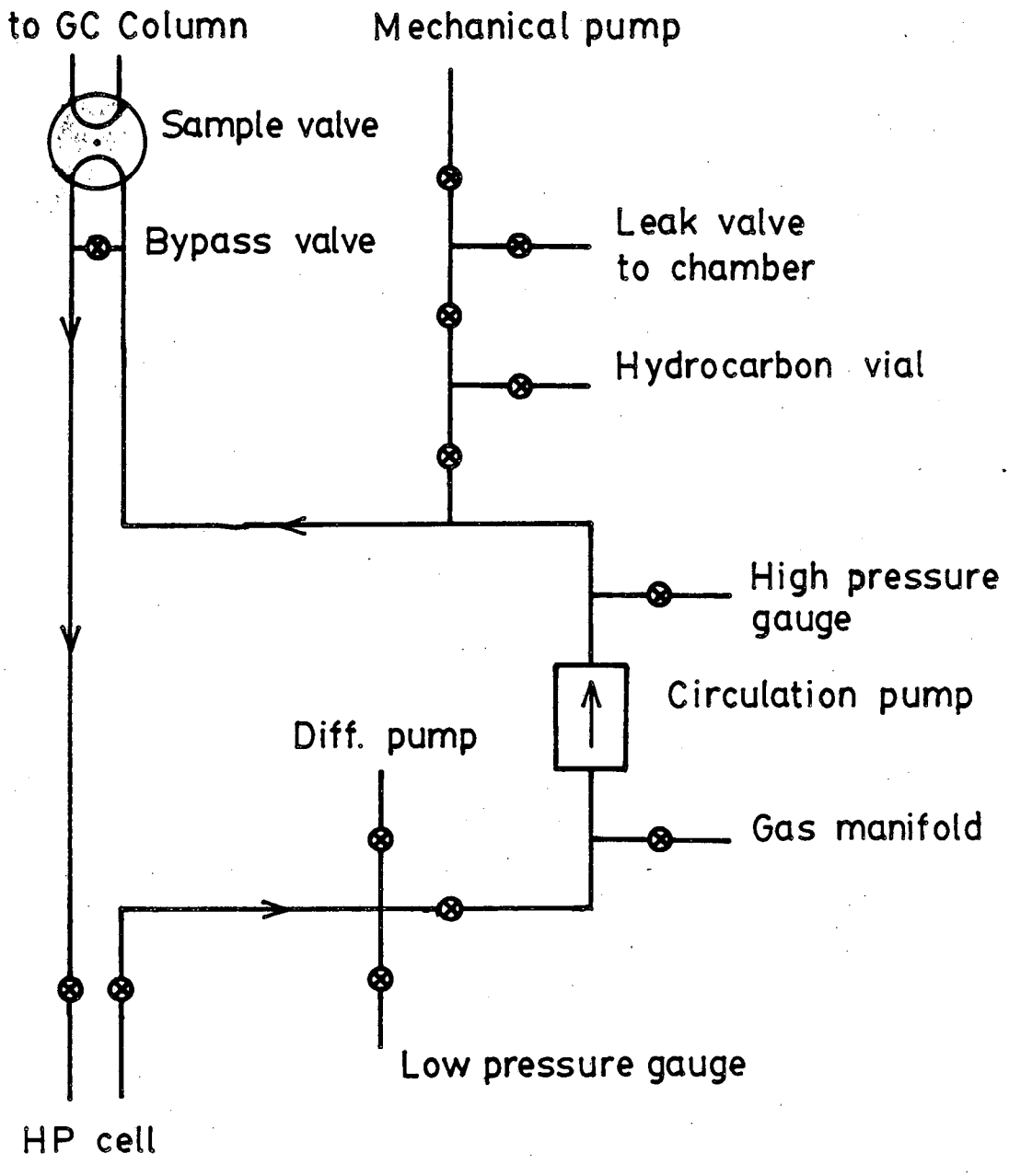

Fig. 2.5 Schematic of the high pressure closed loop batch reactor attached to the high pressure cell.

2.2 Materials / Materials Preparation

2.2.1 Mo Single Crystals

The molybdenum single crystal rods were obtained from the Materials Research Corp. They were oriented using Laue back-diffraction and cut by spark erosion in thin slices of 1. - 0.5 mm thickness. A mirror finish was achieved using standard metallurgical polishing techniques. Crystals were mounted by spotwelding them between two Ta posts as illustrated in Fig 2.4. This configuration allowed rapid resistive heating and subsequent cooling. This configuration allows optimal heating of the crystal without simultaneous heating of the support rods to excessive temperatures. This is necessary during catalytic reactions to ensure minimal contribution of the supports to catalytic activity (2). With this configuration it is possible to heat the crystal to 1900K while the temperature of the support rods does not exceed 800K.

The choice of materials for mounting the crystals is critical. For work purely under UHV conditions the materials must have the following characteristics:

1) They must be easily spotwelded to the Mo sample which limits the choice drastically.
2) They must be able to withstand heating to high temperatures (>1900K).

For this work Ta is the ideal choice. Studies involving high pressure hydrogen treatments place the following restriction:

3) Materials must not embrittle in hydrogen at high temperatures (<700K).

Although much of the high pressure reaction work was performed using Ta supports the best combination was finally found to be the use of Mo for the main support rods and Re for the .020" spacers.

The major surface contaminant of the Mo samples was carbon. This was cleaned from the surface by repeated treatments in oxygen ($1x10^{-8}$ - $1x10^{-7}$ torr) at temperatures of 1100K - 1500K. Carbon was completely removed from the bulk of the crystal by alternately treating with oxygen and heating to 1900K to segregate further carbon. The initial proceedure required from hours to days after which the crystals remained relatively free of carbon. Oxygen was removed from the surface either by heating the crystal to 2100K or by dosing with small amounts of ethylene (< 10^{-6} torr•sec) at temperatures of about 1100K. Sulfur was removed by heating to 1900K at which it desorbs into vacuum.

2.2.2 Reagents

A number of hydrocarbon reagents were used to model the hydrotreating reactions. These are listed in Table 2.1 with suppliers and specifications. Each is a liquid at room temperature with a high enough vapour pressure to allow use as reactants without necessitating heating of the entire reaction loop. The reagents were cleaned of all high vapour pressure contaminants by repeated freeze-thaw treatments during which the sample was frozen in liquid nitrogen, evacuated and then allowed to thaw.

Table 2.1 Reagents

Compound	Supplier	Purity	Vap. Press.(Rm.T.)
1. Thiophene	Aldrich	99+%	80 torr
2. Tetrahydro-thiophene	Aldrich	99%	20 torr
3. 1,3, Butadiene	Matheson	99%	gas
4. H_2	Matheson		gas
5. H_2S	Matheson		gas

2.2.3 $C^{35}S_2$

The radiotracer sulfur was obtained by custom synthesis of CS_2, at great expense ($100/mg) and after undue frustration, from New England Nuclear (Lot No. 1800-281). The sample was shipped in two breakseal tubes at a total radio-concentration of 100 mC/mmole. Radiochemical purity was stated to be in excess of 99%. The material was purified by the freeze-thaw technique described above.

2.3 Electrochemical Sulfur Source

Sulfur deposition under UHV conditions was achieved by a rather novel method using a solid state electrochemical cell. Most surface science investigations of adsorbed sulfur layers have deposited sulfur on metal surfaces by exposure to H_2S followed by heating of the sample to dissociate the molecule and desorb hydrogen as H_2. This procedure results in the exposure of the entire chamber to H_2S which, because of its relatively low pumping speed, is highly undesirable. The electrochemical cell used here was first developed by Wagner (7) and is depicted in Fig. 2.6.

The cell is made by compressing a Pt gauze (anode), a pellet of Ag_2S, a pellet of AgI (ionic conductor), and a silver disc (cathode) in a glass tube. The Ag_2S can be prepared by dipping Ag into molten sulfur and the AgI is precipitated from a $AgNO_3$ / KI solution and pressed into a pellet. The assembly can be heated by passing current through a foil wrapped about the glass tube assembly.

Operation of the cell is achieved by applying a potential across the cell using the circuit in Fig. 2.7. At a potential of 0.2V the

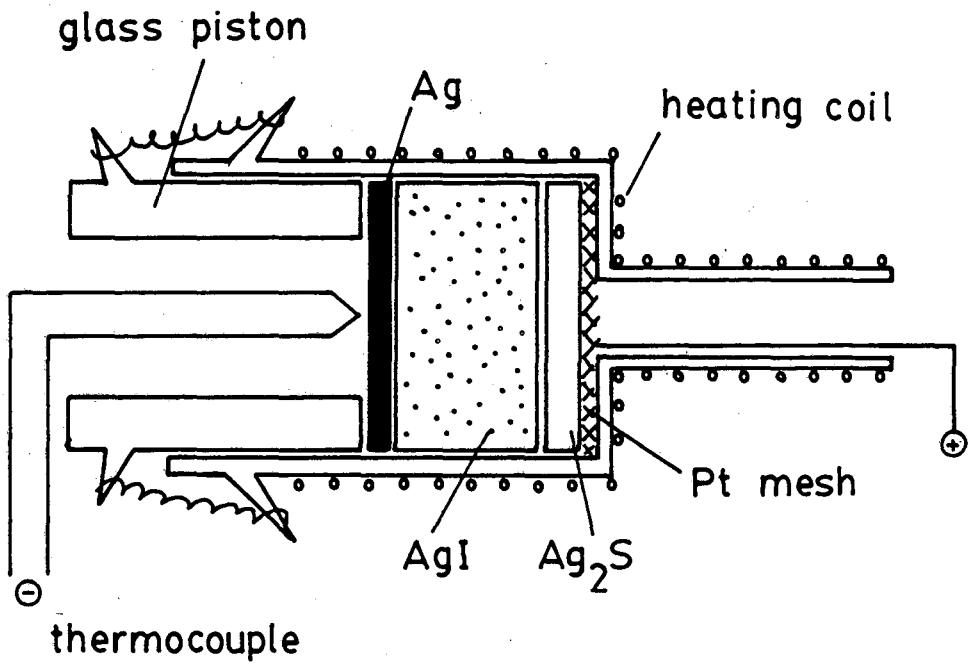

Fig. 2.6 Electrolytic source used for sulfur deposition.

SULFUR SOURCE CIRCUIT

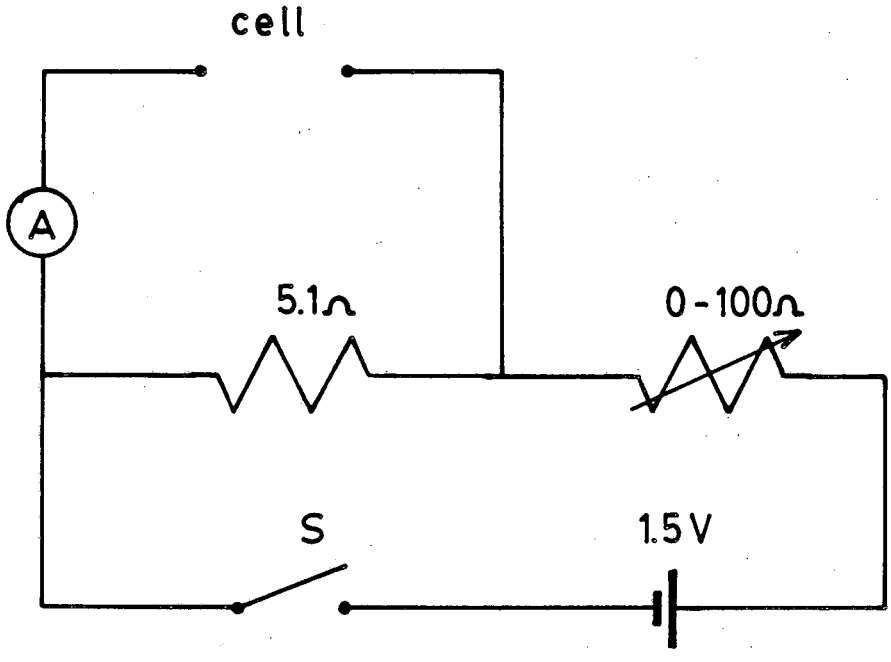

Fig. 2.7 Circuit used to bias the sulfur source.

electrolytic decomposition of the Ag_2S begins, producing sulfur at the anode.

$Ag_2S + 2e^- \rightarrow 2Ag + S^{2-}$	-0.705V (21)
$S^{2-} \rightarrow 2e^- + S$	+0.508V
$Ag_2S \rightarrow 2Ag + S$	-0.197V

The sulfur desorbs from the anode primarily as S_2, as determined by mass spectroscopy. Under optimal conditions it was possible to obtain fluxes of S_2 high enough to deposit sulfur on the surface at rates of about one monolayer/ min. with no apparent increase in the background pressure of the chamber. In order to pass sufficient current through the cell it was normally necessary to heat the assembly to temperatures between 125°C and 175°C, thereby increasing the ionic conductivity of the AgI. If over-heated it is impossible to maintain a 0.2V potential across the cell using the simple circuit shown in Fig. 2.7 and the decomposition of the Ag_2S does not occur.

2.4 Auger Electron Spectroscopy (AES)

Auger spectroscopy is used in this work primarily as a tool for the determination of the elemental composition of the near surface region of the sample. The technique is inherently surface sensitive due to the fact that Auger electrons, in most cases and certainly in ours, have energies that fall into the range in which they have very short mean free paths through metals (3) (Fig. 2.8). Because of this property most of the work done to date in the field of surface analysis has used either ion or electron spectroscopies of one form or another

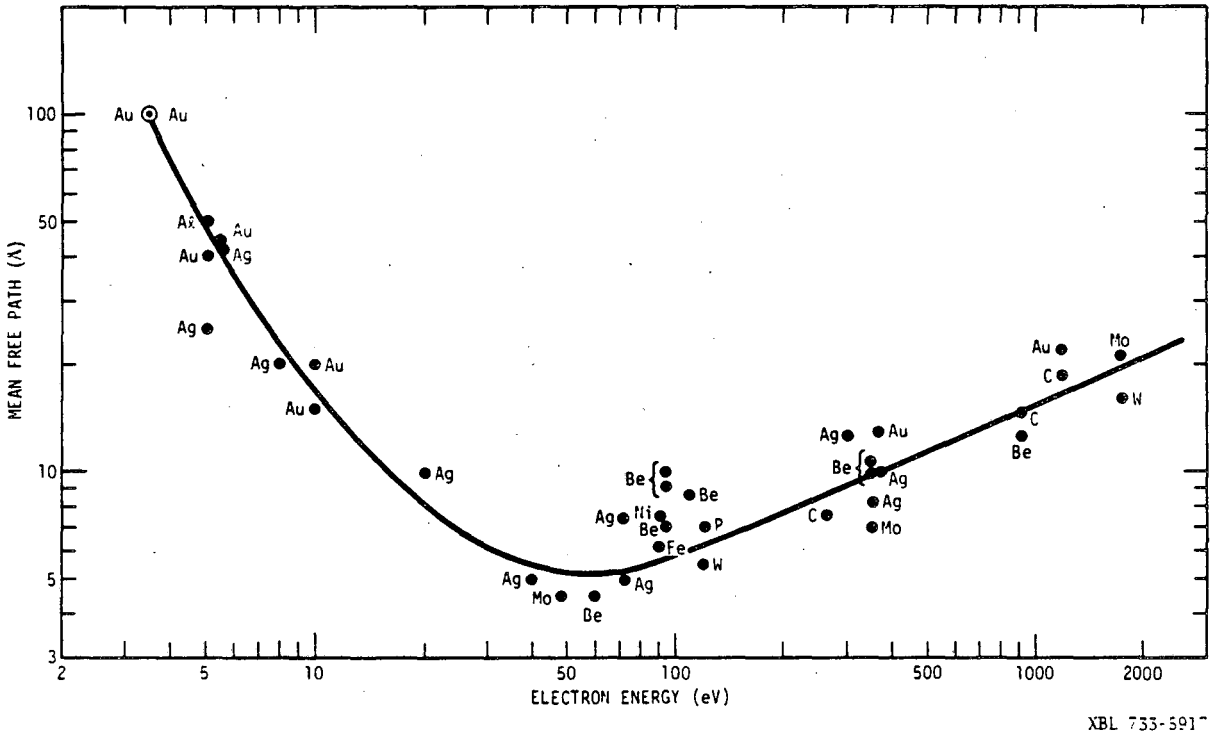

Fig. 2.8 Universal curve of electron mean free paths through various metals vs. electron energy.

to achieve adequate surface sensitivity.

The theory of the Auger process has been described in detail in a number of articles and books (4,5). It is depicted schematically in Fig. 2.9. The experiment is performed by having a beam of high energy electrons incident on the surface ionizing atoms to create core holes. The excited state ion can then decay either by X-ray emission or by an auto-ionization process in which an electron from a higher lying level decays into the core hole simultaneously ionizing a second electron into the continuum. The kinetic energy of the detected electron is determined by the various energy levels involved in the process and is characteristic of the atom from which it originated. This energy can be given roughly as

$$E_{kin} = (E_K - E_{LI}) - (E_{LIII} - e \cdot \phi_{sp}).$$

The first term in parentheses is the amount of energy liberated by the decay of the electron at orbital energy level E_{LI} into the core hole (E_K). The second term is that amount of energy necessary to take the electron from the orbital at energy level E_{LIII} to the vacuum level of the spectrometer (ϕ_{sp} is the work function of the spectrometer and the energy levels are all referred to the Fermi level).

A typical energy distribution curve of electrons scattered from a surface by the incident beam is shown in Fig. 2.10. The broad feature at low kinetic energies is the secondary electron yield arising from the emission of electrons by multiple scattering processes. This portion of the distribution contains little information and superimposes a large background on the Auger electron distribution. As a

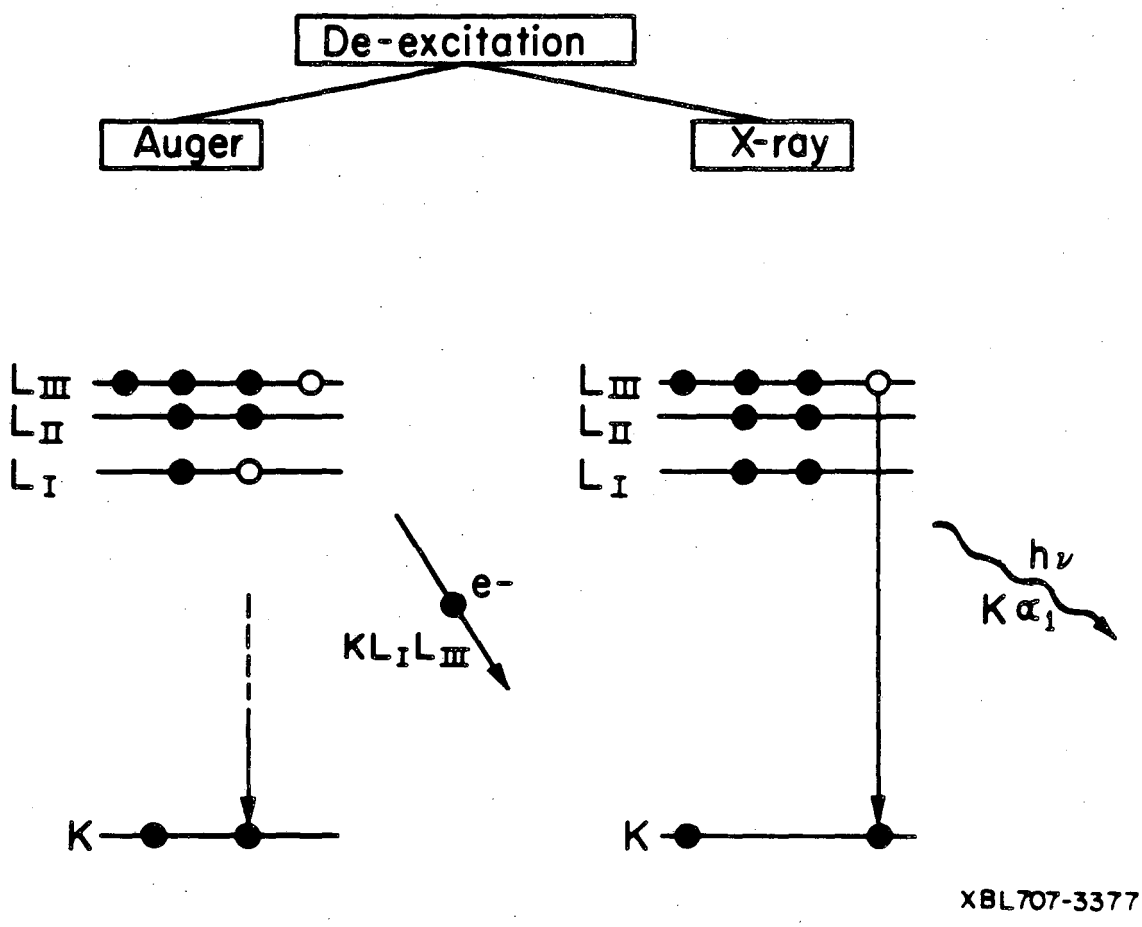

Fig. 2.9 Schematic of the Auger and X-ray florescence processes.

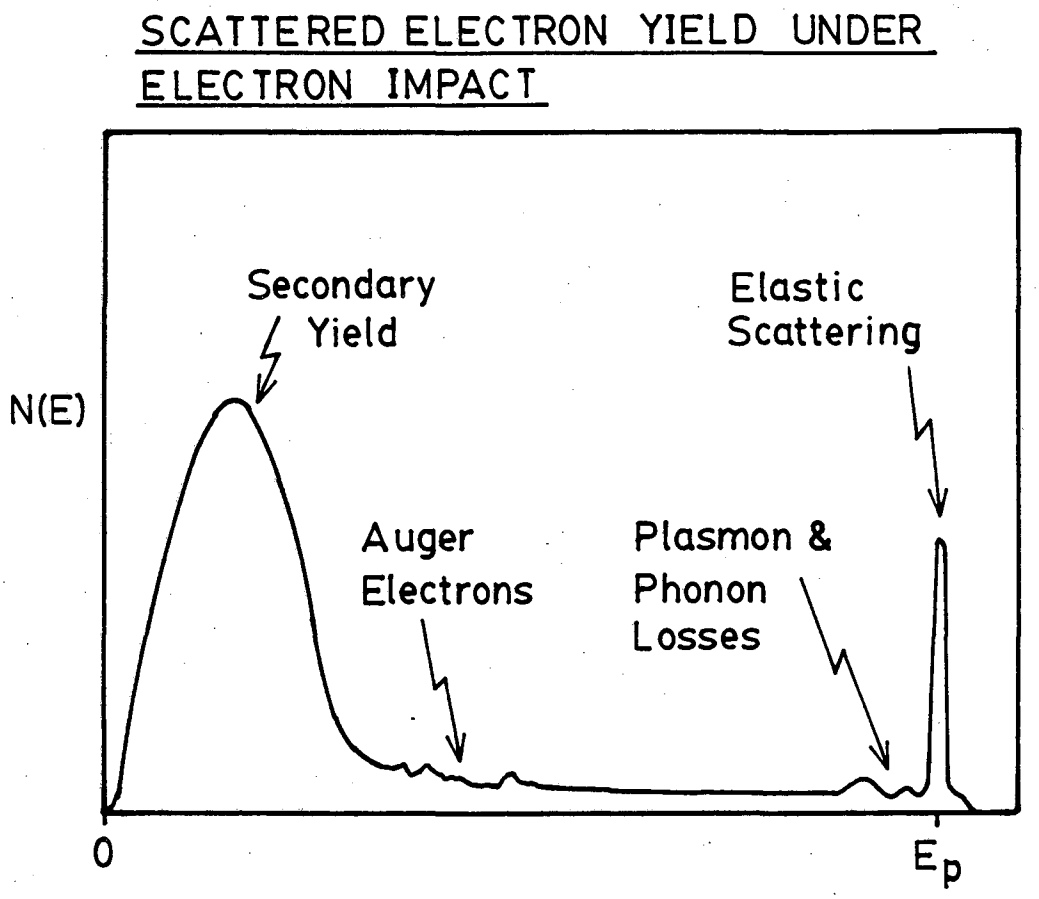

Fig. 2.10 Energy distribution of electrons scattered from a metal surface during high energy electron impact.

result it has become conventional to enhance the Auger signal by displaying the electron distribution in derivative mode. Auger spectra from the clean Mo(100) surface and the Mo surface with adsorbed S,C, and O are illustrated in Fig. 2.11. If the Auger peak shape is independent of coverage

$$N(E,\theta) = \theta \times f(E)$$

then the derivative at some energy E_0 will be proportional to the coverage. If the maxima and minima of f'(E) occur at E_{max} and E_{min} respectively then the peak to peak height in the N'(E) spectrum will be proportional to the coverage(6).

$$N'(E_{max}) - N'(E_{min}) = \theta \times [f'(E_{max}) - f'(E_{min})]$$

$$= \theta \times \text{constant}$$

Although it is experimentally difficult to reproduce absolute peak heights it is fairly easy to reproduce the ratio of adsorbate to substrate Auger peaks at a given coverage. This ratio can then be calibrated against coverage to allow quick determination of surface compositions.

In the case of submonolayer amounts of sulfur on the Mo(100) surface the sulfur AES peak height is directly proportional to the coverage

$$I_S(\theta) = \theta \cdot I_S(1).$$

The substrate signal is assumed to vary linearly between the clean surface signal and a screened signal from that portion of the surface

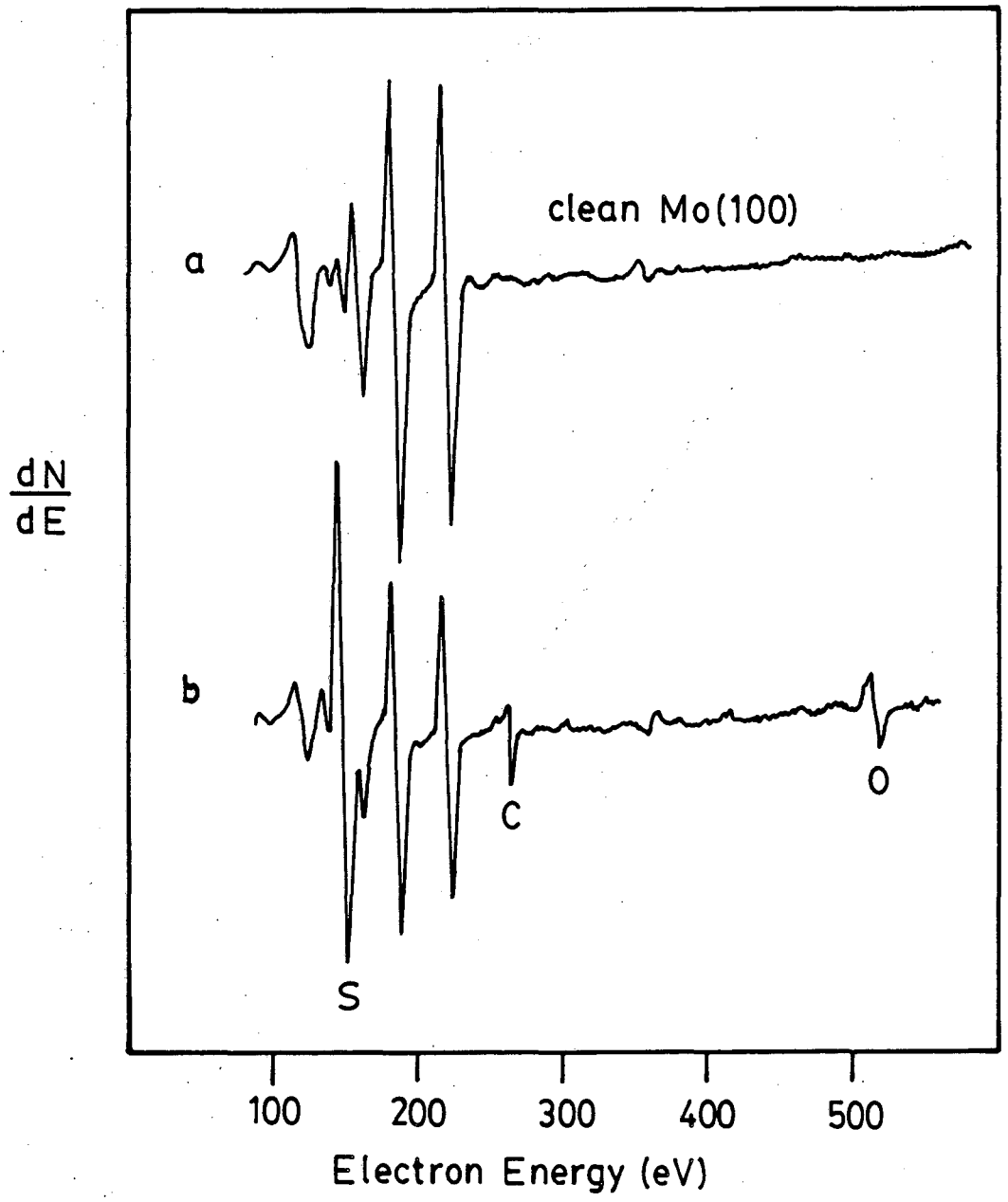

Fig. 2.11 Auger spectra in dN/dE mode of the clean Mo(100) surface and the Mo(100) surface contaminated with sulfur (150 eV), carbon (272 eV) and oxygen (515 eV).

that is covered with sulfur.

$$I_{Mo}(\theta) = \theta \cdot I_{Mo}(1) + (1-\theta) \cdot I_{Mo}(0).$$

Therefore:

$$r = \frac{I_S}{I_{Mo}} = \frac{\theta \cdot I_S(1)}{I_{Mo}(0) + \theta \cdot [I_{Mo}(1) - I_{Mo}(0)]}$$

Finally:

$$\theta = \frac{r}{\alpha + (1-\beta)} \qquad \alpha = I_S(1)/I_{Mo}(0)$$

$$\beta = I_{Mo}(1)/I_{Mo}(0)$$

In practice this simple calibration method has to be modified slightly due to the presence of a small Mo peak that overlaps the sulfur peak at 150 eV. The final calibration expression becomes:

$$\theta = \frac{r - \gamma}{(\alpha + \alpha\gamma - \gamma) + (1 - \beta) \cdot r}$$

$$\gamma = I_{Mo_{150}}(0) \; / \; I_{Mo_{221}}(0)$$

A typical curve is shown in Fig. 2.12.

2.5 Low Energy Electron Diffraction (LEED)

LEED is one of the most important structural tools of the surface science community. The schematic representation of the experiment is shown in Fig. 2.13 depicting a low energy electron beam (50-250eV), incident on the surface, back diffracting from the surface lattice and being imaged on a phosphorus screen. This work has used LEED primarily

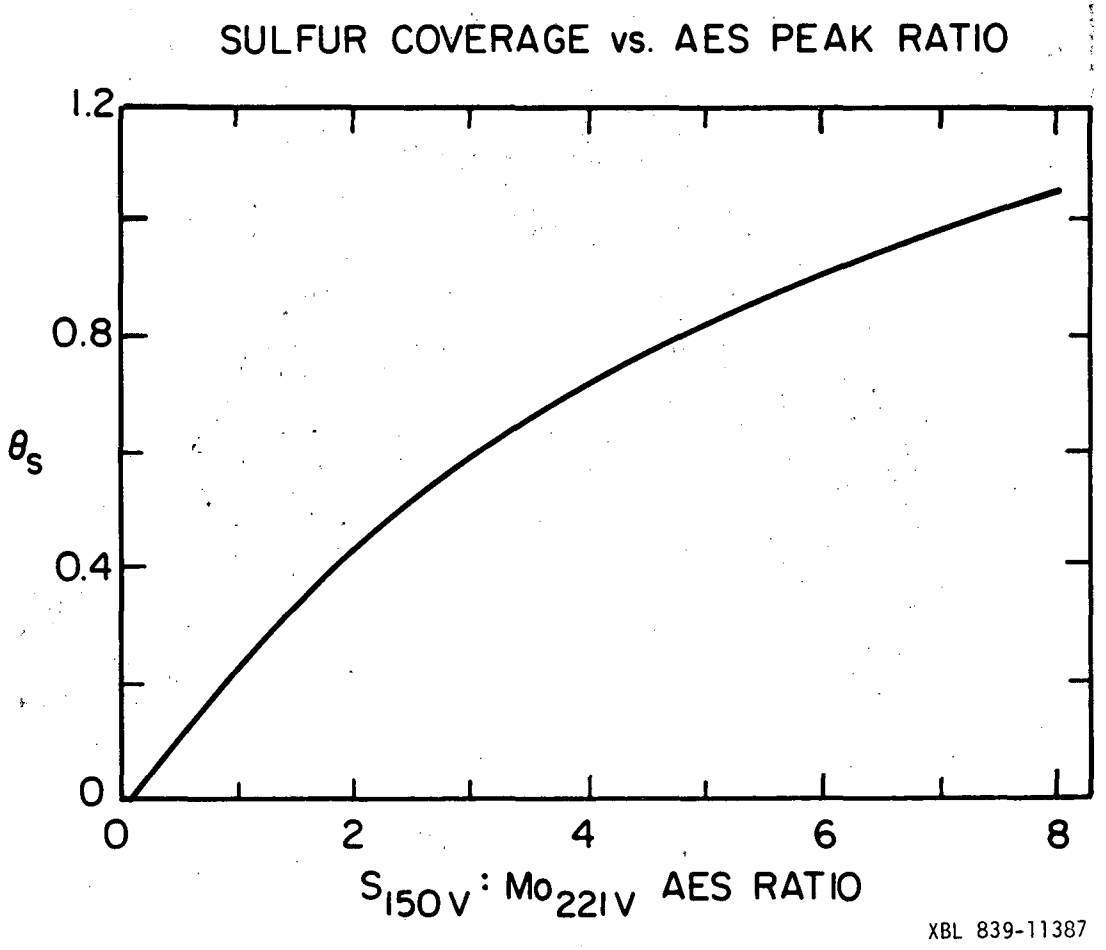

Fig. 2.12 Calibration curve of sulfur coverage (θ_S) vs. S_{150}:Mo_{221} AES peak height ratio.

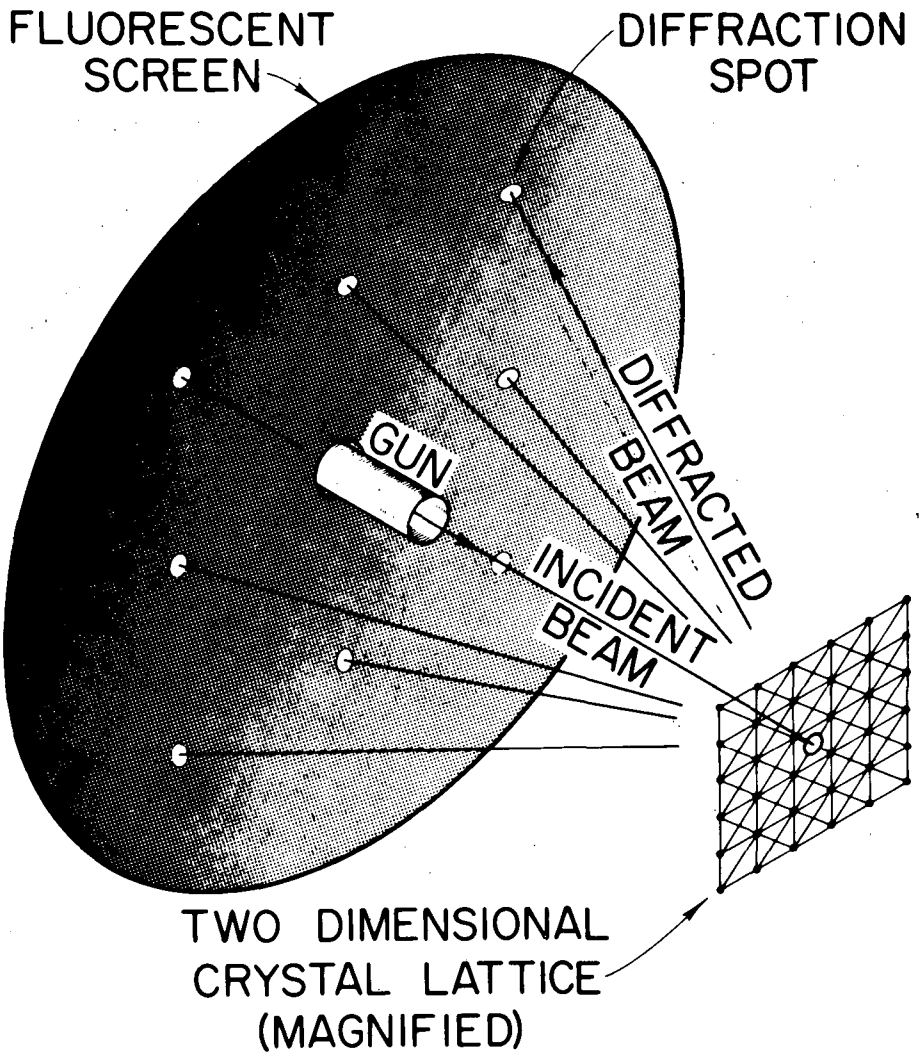

$$\underset{\sim}{k}' = \underset{\sim}{k} + \underset{\sim}{G}$$

to examine the periodicity of the ordered structures produced by sulfur overlayers on the Mo(100) surface. A relatively simple analysis of the diffraction patterns allows the determination of the unit cell parameters of the ordered overlayers. Examination of the diffracted intensity as a function of the electron energy can, in principle, yield detailed structural information but requires extensive analysis. The theory of such dynamical LEED analysis has been described elsewhere (4,8) and has not yet been applied to the systems studied in this work.

The kinematic theory of LEED used in this work assumes single scattering events. Starting with the formalism presented by Ertl (4) we think of scattering from a two dimensional lattice as depicted in Fig. 2.14. The scattering amplitude at a point that is far from the surface ($r>>|\underset{\sim}{R}|$) is given by

$$\Psi = \Psi_0 \left(\frac{1}{r} e^{i\underset{\sim}{k}\cdot\underset{\sim}{r}}\right) \int\int_S F(\underset{\sim}{R},\underset{\sim}{k},\underset{\sim}{k}_0)\, e^{i(\underset{\sim}{k}-\underset{\sim}{k}_0)\cdot\underset{\sim}{R}}\, dA$$

The first term is the spherically scattered wave, $\underset{\sim}{R}$ is a vector from an arbitrary lattice point serving as the origin to any point on the surface. $F(\underset{\sim}{R},\underset{\sim}{k},\underset{\sim}{k}_0)$ is the scattering factor at point $\underset{\sim}{R}$, and $e^{i(\underset{\sim}{k}-\underset{\sim}{k}_0)}$ is the phase lag between a wave scattered at the origin and one scattered at point $\underset{\sim}{R}$. The integral is taken over the whole surface. The periodicity of the lattice manifests itself in the periodicity of the scattering factor

$$\begin{aligned} F(R,\underset{\sim}{k},\underset{\sim}{k}_0) &= F[(n+x)\underset{\sim}{a} + (m+y)\underset{\sim}{b},\ \underset{\sim}{k},\ \underset{\sim}{k}_0] \\ &= F[x\underset{\sim}{a} + y\underset{\sim}{b},\ \underset{\sim}{k},\ \underset{\sim}{k}_0] \end{aligned}$$

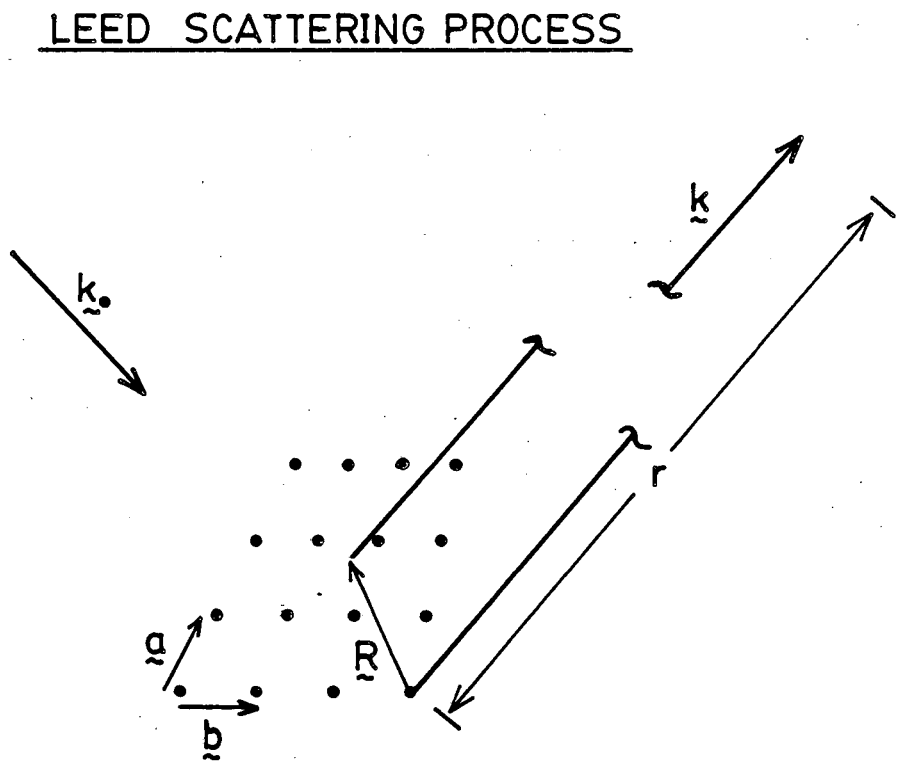

Fig. 2.14 Schematic depiction of electron scattering from a 2D-lattice.

and so, the amplitude can be rewritten as

$$\Psi = \Psi_o\left(\frac{1}{r} e^{i\underset{\sim}{k}\cdot\underset{\sim}{r}}\right) \sum_n \sum_m e^{i\Delta\underset{\sim}{k}(n\underset{\sim}{a}+m\underset{\sim}{b})} \int\int_C F(x\underset{\sim}{a}+y\underset{\sim}{b})\, e^{i\Delta\underset{\sim}{k}(x\underset{\sim}{a}+y\underset{\sim}{b})}\, dA$$

where the integral is over the unit cell and $\underset{\sim}{a}$ and $\underset{\sim}{b}$ are the unit cell vectors. The intensity of the diffracted wave into a given direction is given by

$$I = |\Psi|^2 \propto |\underline{F}|^2 \cdot |\underline{G}|^2$$

where $\underline{F}$ is the structure factor and $\underline{G}$ is the lattice factor. The lattice factor is given by

$$G = \sum_n e^{i\Delta\underset{\sim}{k}\cdot n\underset{\sim}{a}} \cdot \sum_m e^{i\Delta\underset{\sim}{k}\cdot m\underset{\sim}{b}}$$

This factor only has non-zero values when

$$\underset{\sim}{a}\cdot\Delta\underset{\sim}{k} = 2\pi h$$

and

$$\underset{\sim}{b}\cdot\Delta\underset{\sim}{k} = 2\pi k$$

These are the Laue conditions for surface diffraction which determine the directions or values of $\Delta\underset{\sim}{k}$ into which diffraction will occur. These are

$$\Delta\underset{\sim}{k} = 2\pi(h\underset{\sim}{a}^{-1} + k\underset{\sim}{b}^{-1})$$

where the reciprocal lattice vectors are given by

$$\underset{\sim}{a}\cdot\underset{\sim}{a}^{-1} = 1 \qquad \underset{\sim}{a}\cdot\underset{\sim}{b}^{-1} = 0$$
$$\underset{\sim}{b}\cdot\underset{\sim}{a}^{-1} = 0 \qquad \underset{\sim}{b}\cdot\underset{\sim}{b}^{-1} = 1$$

The Ewald construction (4) demonstrates that the LEED pattern is in fact a direct representation of the lattice in reciprocal space.

The LEED work performed in this research has primarily been concerned with the overlayer lattice produced by the adsorption of an adsorbate on an ordered substrate. If the relationship between the overlayer lattice and the substrate can be given by the following matrix equation

$$\begin{vmatrix} a' \\ b' \end{vmatrix} = \underset{\approx}{M} \begin{vmatrix} a \\ b \end{vmatrix}$$

where $\underset{\sim}{a}'$ and $\underset{\sim}{b}'$ are the over layer lattice vectors and $\underset{\sim}{a}$ and $\underset{\sim}{b}$ are the substrate lattice vectors, then the relation ship between the reciprocal lattices is given by

$$\begin{vmatrix} a'^{-1} \\ b'^{-1} \end{vmatrix} = \underset{\approx}{M}^{t^{-1}} \begin{vmatrix} a^{-1} \\ b^{-1} \end{vmatrix}$$

In general the matrix $\underset{\approx}{M}^{t^{-1}}$ is determined directly from the LEED patterns and can be inverted and transposed to obtain the real space lattice matrix $\underset{\approx}{M}$. The overlayer structures are often identified by the matrix $\underset{\approx}{M}$.

The structure factor $\underline{F}$ contains the detailed scattering information at each point in the unit cell used to calculate the diffaction spot intensities. There is a special case in which the surface unit cell has glide plane symmetry that results in the structure factor being zero for some values of (h,k) and thus systematic abscences in

the LEED pattern. For a given $\underset{\sim}{k}$, $\underset{\sim}{k}_0$ and unit cell the scattering factor is given by

$$F(x\underset{\sim}{a} + y\underset{\sim}{b},\underset{\sim}{k},\underset{\sim}{k}_0) = f(x,y)$$

A glide plane along the a axis of the unit cell implies that

$$f(x,y) = f(x+1/2,1-y)$$

The structure factor, assuming normal lattice vectors, becomes

$$\underline{F} = \int_0^1 \int_0^1 f(x,y) \exp[i\Delta\underset{\sim}{k}\cdot(x\underset{\sim}{a}+y\underset{\sim}{b})]\, dx\, dy\, ab$$

and for values of $\Delta\underset{\sim}{k}$ allowed by the Laue conditions is

$$\underline{F} = \int_0^1 \int_0^1 f(x,y) \exp(i2\pi hx) \exp(i2\pi ky)\, dx\, dy\, ab\ .$$

If we split the integral over dx and substitute $x = x'+1/2$ and $y = 1-y'$, keeping in mind the symmetry of $f(x,y)$ we get

$$\underline{F} \propto \int_0^1 \int_0^{1/2} f(x,y) \exp(i2\pi hx) \exp(i2\pi ky)\, dx\, dy + \exp(ih\pi) \int_0^1 \int_0^{1/2} f(x,y) \exp(i2\pi hx) \exp(-i2\pi ky)\, dx\, dy\ .$$

For k=0 it is clear that F will be identically zero for values of h = 1,3,5..... and thus thus that the corresponding diffraction beams will be absent. The presence or lack of such systematic absences can be an important clue to the arrangement of atoms within the lattice unit cell.

2.6 Thermal Desorption Spectroscopy (TDS)

Thermal Desorption Spectroscopy has been used in this work primarily to determine metal-adsorbate bond strengths and to study decompos-

ition kinetics. The experiment is performed by first exposing the sample to a gas phase adsorbate ($P \leq 10^{-8}$). The sample is then heated at a constant rate and the desorption of species from the surface is monitored with a mass spectrometer. Desorbing species can be the result of a simple desorption process, the reaction of two or more adsorbed molecules or the fragments of a decomposition process. The simple desorption spectrum of deuterium from a Mo(100) surface is shown in Fig. 2.15.

The rate of desorption at a given temperature is given by

$$R = A\ \theta^n\ \nu_n\ \exp(-E_d/RT)$$

where A is the area of the sample, θ is the adsorbate coverage, n is the order of the desorption process in coverage, ν_n is the pre-exponential factor and E_d is the barrier to desorption. During the desorption cycle the expression for the rate of change of the number of gas phase molecules in the chamber is given by (9)

$$KV \frac{dP}{dt} = R(t) - KSP$$

P - pressure

K - molecules/volume/pressure

S - pumping speed (volume/time)

V - chamber volume

which can be reduced to

$$aR(t) = \frac{dP}{dt} + \frac{P}{\tau}$$

$a = 1/KV$

τ = characteristic pumping time

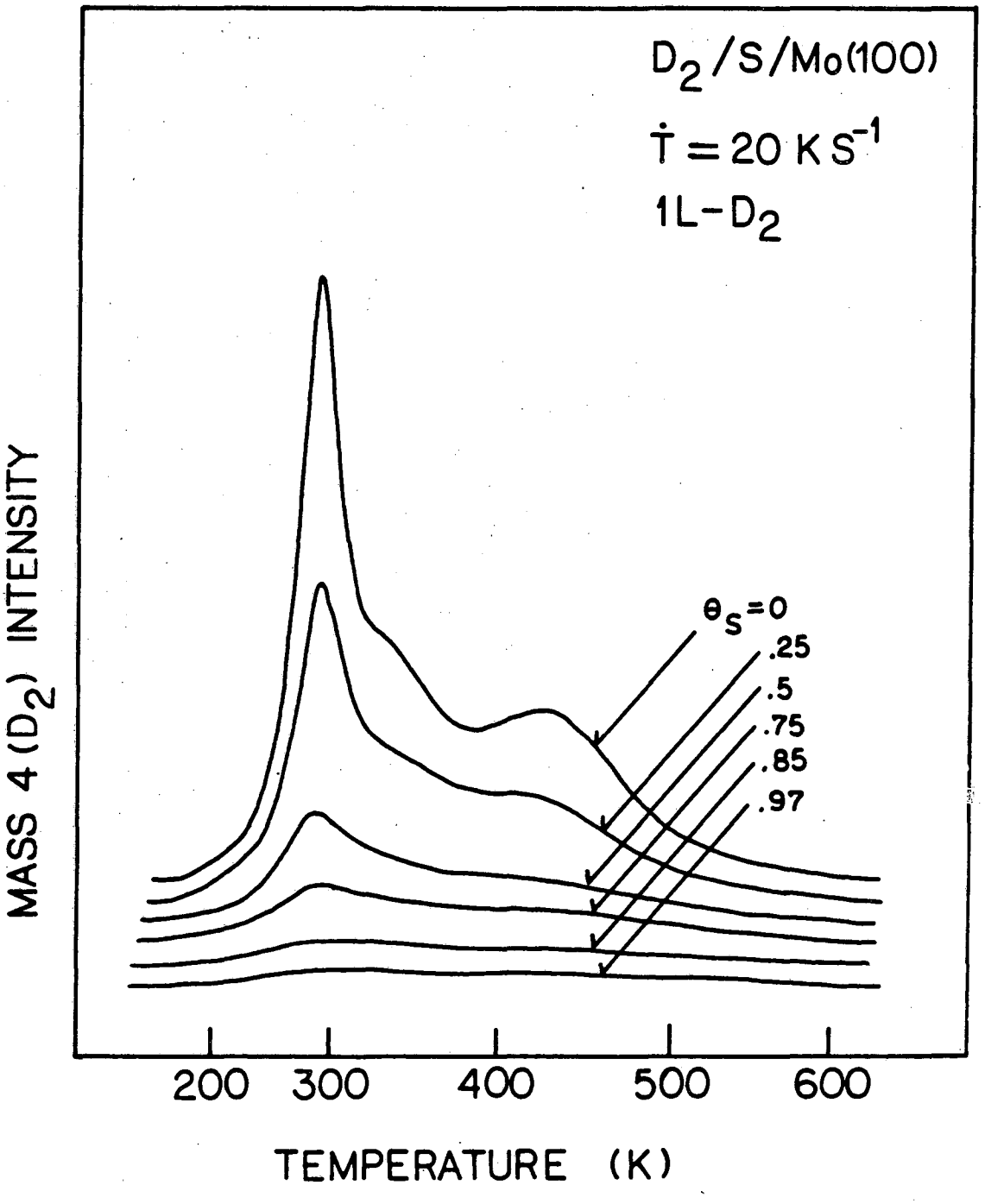

XBL 837-10688

Fig. 2.15 Thermal Desorption Spectra (TDS) of D_2 from the Mo(100) surface after varying exposures to D_2.

For high pumping speeds ($\tau \to 0$)

$$R(t) \propto P.$$

At a constant heating rate $T = T_0 + \beta \cdot t$ the expression relating the desorption rate parameters to the temperature of maximum desorption rate is given by (9)

$$\frac{E_d}{RT_m^2} = \frac{\nu_1}{\beta} \exp(-E_d/RT_m) \qquad n = 1$$

$$\frac{E_d}{RT_m^2} = \frac{\nu_2}{\beta} \theta_0 \exp(-E_d/RT_m) \qquad n = 2$$

for first and second order desorption respectively. It is possible to obtain both E_d and ν_n from spectra taken over a wide range of heating rates. Alternately, it is often assumed for first order processes that the pre-exponential factor is $\nu_1 = 10^{13}$ sec^{-1}.

Other analyses of the desorption equations use both the peak width and the temperature of maximum desorption to estimate ν_n and E_d (10,11, 12). The disadvantages of such schemes are that peak widths can be very sensitive to experimental conditions, in particular, slow pumping speeds and uneven heating of the crystal. In addition, peak widths are very sensitive to coverage dependent desorption energies (13). Such phenomenon are the result of adsorbate-adsorbate interactions and can be significant. Modelling studies of the desorption experiment have in fact concluded that the simple assumption stated above can give results that are better than approaches relying upon peak widths (13).

2.7 Ultra-violet Photoelectron Spectroscopy (UPS)

Ultra-violet photoelectron spectroscopy serves as a probe of the valence electron energy levels of adsorbates and of the valence bands of clean metals. UV photons (He I, 21.2 eV) impinging on the sample excite electrons from valence levels into the vacuum continuum. The energy of the electron upon arrival at the analyzer is given by the expression

$$E_{kin} = h\nu - E_b - e\phi_{sp}$$

where E_b is the binding energy of the initial state orbital and ϕ_{sp} is the work function of the spectrometer. The energy distribution of these electrons reflects the density of states of the orbitals from which they originate.

The theory of the photoemission process has been discussed in a number of works (4,14). In practice the number of electrons excited to some energy $E_j > E_F$ from an occupied level at $E_i < E_F$ is proportional to the product of the densities of states at both energies and the transition probability between the two. These factors combine to make the complete understanding of the photoemission spectra of clean metal surfaces extremely difficult, requiring detailed theoretical analysis. This being the case it might seem that the addition of adsorbates to the surface should only complicate the situation. In fact, examination of adsorbate energy levels for relatively large molecules reveals that orbitals not participating in bonding are unperturbed from their gas phase values with the exception of a constant shift in value due to the screening by the metal(15,22). Those orbitals participating in

bonding are shifted with respect to the non-bonding orbitals and can be identified as such. Thus it is possible to make some qualitative arguments about the bonding of adsorbates. Although the inherent lack of resolution of surface electron spectroscopy results in broad features and hinders the identification of orbitals.

2.8 X-ray Photoelectron Spectroscopy (XPS)

X-ray Photoelectron Spectroscopy serves as a probe of the energies of the core levels of surface atoms. The experiment is identical to the UPS experiment with the exception that the exciting photon is an x-ray, in this case the K_α line of a Mg source (1253.6 eV). The much higher energies of x-rays as compared to UV photons allows a much greater range of binding energies to be sampled.

A given element has core level energies that are characteristic of that element and as such can be used to determine surface composition in much the same way as Auger electrons. In addition, the x-ray photoelectron yield from a given atom is proportional to its concentration at the surface and can be used to determine coverages. The limitations of XPS as a surface analysis tool in this respect are its low total yields and the fact that the high electron energies limit its surface sensitivity.

The power of XPS lies in the fact that the core level binding energies are sensitive to the valence electron distribution or chemical state of the atom. Detailed discussions of such binding energy shifts can be found in several texts (5,16). A simple picture of the core-valence interaction is one in which the core electron lies within a sphere of charge (q_v) having a radius r_v. The core electron potential

then becomes

$$U = \frac{q_v e}{r_v}$$

where e is the electron charge. In a situation in which the valence orbitals are perturbed by bonding interactions the expected shift in the core level binding energy between the molecular atom and the free atom is

$$\Delta E_b = \frac{q_v^m e}{r_v^m} - \frac{q_v^a e}{r_v^a} \quad .$$

In the case of oxidation, or the bonding of an atom to a more electronegative species one expects q_v^m to decrease and r_v^m to increase. The resulting value of ΔE_b is negative, i.e. a shift of the core level energy to lower values.

2.9 ^{35}S Radiotracer Experiments

The use of radioactive labelled sulfur has proven to be extremely useful in this work. The general technique has been applied before using ^{14}C labelled ethylene on Pt surfaces (17) and is applicable to any problem in which it is necessary to discriminate between a species that is adsorbed on a surface under well controlled UHV conditions from one that is deposited during a high pressure reaction. In this particular work the technique has been used to study the hydrogenation of surface sulfur under hydrodesulfurization reaction conditions.

Overlayers labelled with ^{35}S were produced on the Mo(100) surface by the room temperature deposition of labelled CS_2 via a gas leak

valve fitted with a doser. Heating of the crystal to ~1100K was sufficient to dissociate the CS_2 and, at high coverages (>0.5 monolayers), cause the carbon to dissolve into the bulk of the crystal. This process leaves a sulfur overlayer that is identical to one that could otherwise be produced by simple sulfur deposition. Two such exposures totalling, $30\text{-}45 \times 10^{-8}$ torr·sec, were usually sufficient to produce a sulfur coverage of 0.75 monolayers ordered into a c(4x2) lattice. Additional exposure and heating sequences do not deposit additional sulfur on the surface. Apparently the sulfur overlayer at θ_S=0.75 blocks CS_2 decomposition.

Carbon will, in general, segregate from the bulk of a Mo crystal to the clean metal surface and is the major contaminant in unused samples. Using Auger spectroscopy it has been noticed in this work that in the presence of surface sulfur the reverse is true and that surface carbon will in fact dissolve into the bulk of the crystal at high temperatures. A similar phenomenon has been noted in the case of Ni and discussed in terms of a change in the heat of segregation of carbon with sulfur coverage. In the case of Mo this fortuitous state of affairs allows the preparation of well characterized ^{35}S labelled overlayers that are free of carbon.

Detection of β^- radiation is accomplished using the surface barrier detector (Ortec TA-23-25-300) depicted in Fig. 2.16. Signal is collected and amplified using the scheme illustrated schematically in Fig. 2.17. The detector is a piece of N-type silicon with a depletion layer serving as the detection region. Front and back faces are coated with gold and a bias is applied across the detector. Free charge car-

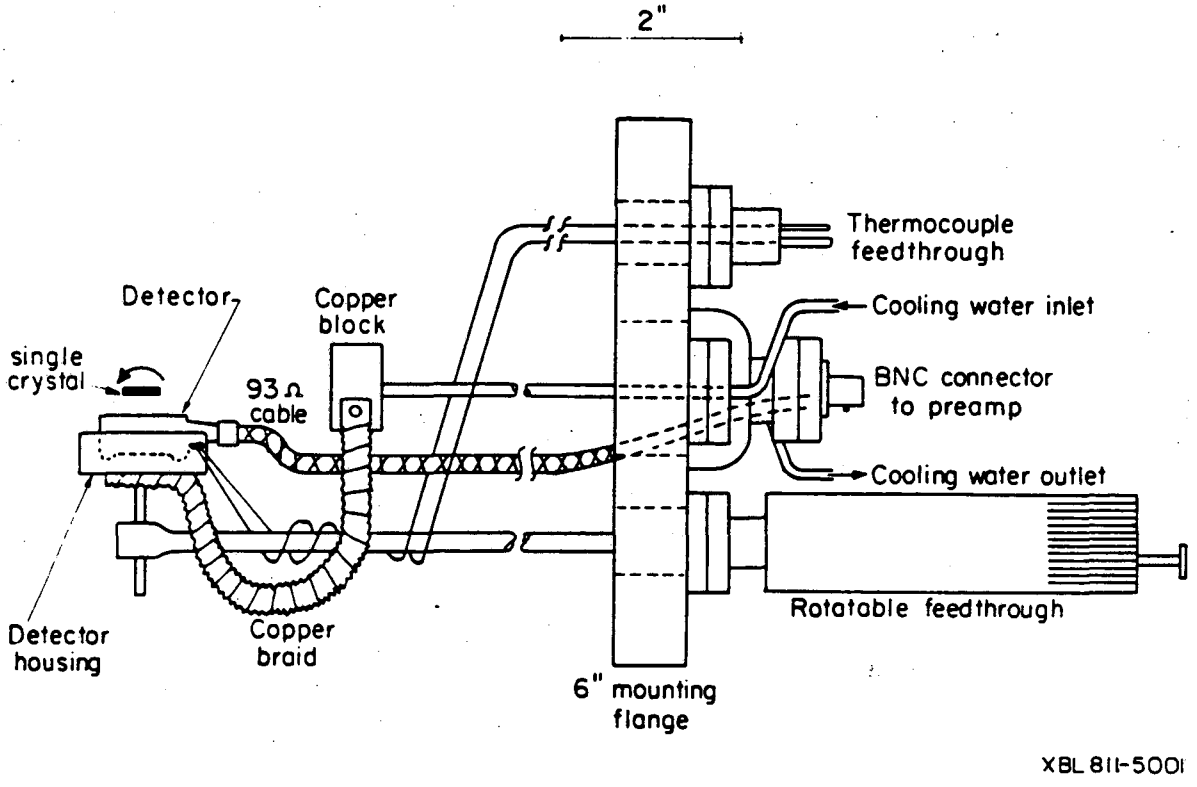

Fig. 2.16 β^- particle detector and mount.

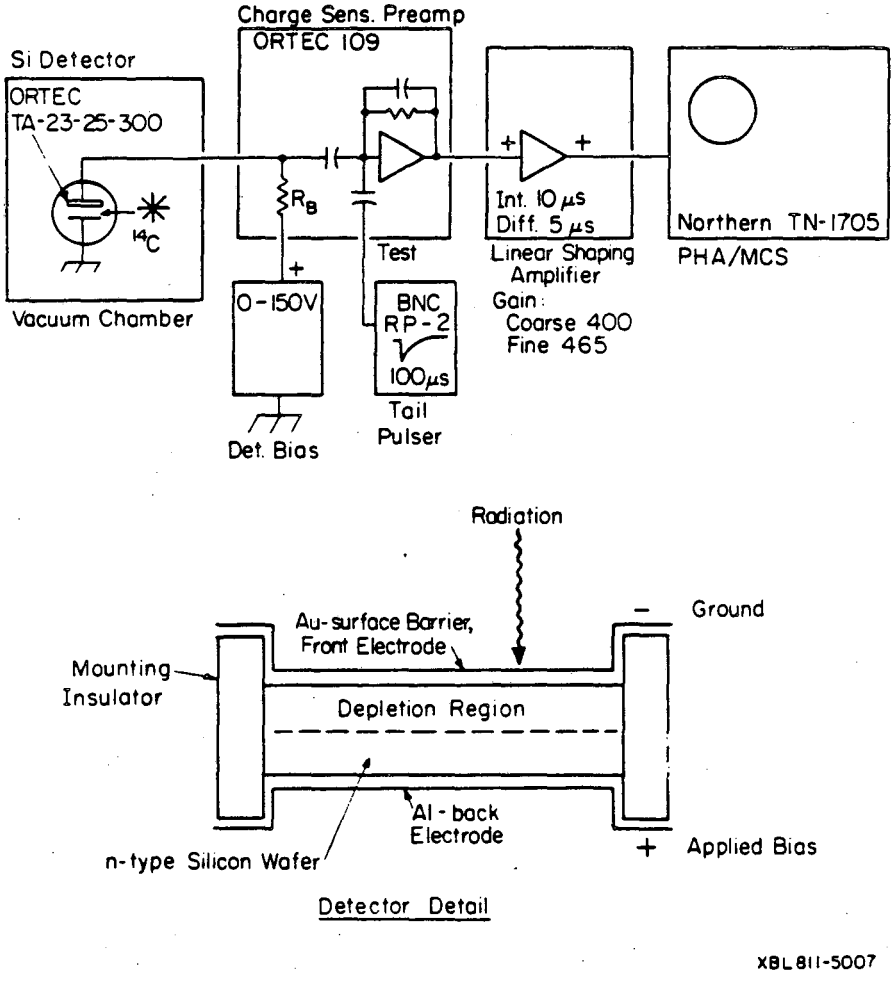

Fig. 2.17 β^- particle detector and data collection electronics.

riers created in the depletion region are seperated in by the electric field and a current pulse is detected at the gold contacts that is proportional to the energy of the impinging β^- particles (19). The detection system is very sensitive to external noise and a number of precautions had to be taken to minimize these problems. All ionizers and filaments within the vacuum chamber had to be turned off during operation and the viewport was covered to exclude any light. In order to avoid contamination of the detector with ^{35}S during dosing it was turned away from the crystal. When in use the detector was positioned as closely to the crystal as possible and was cooled to -35°C to reduce dark current.

2.10 High Pressure Reaction Experiments

High pressure catalytic reactions were performed over single crystal surfaces using the high pressure isolation cell. After preparation and characterization of the sample under UHV conditions the cell was enclosed over the crystal bringing it into contact with the reaction loop (Fig. 2.5). The organic component of the reaction mixture was leaked into the loop first to pressures of 0.1-10 torr followed by hydrogen (100 - 800 torr). Both gases were circulated about the loop by a micropump (Micropump 120-000-100) for approximately 30 minutes to ensure complete mixing. Circulation times were found to be on the order of 2-3 minutes and mixing was completed in 10-15 minutes as determined by monitoring with a gas chromatograph.

Once mixing was complete the reaction was initiated by heating the sample resistively. Crystal temperature was maintained at a set value

to within ±1K by a temperature controller. The reaction mixture was sampled periodically (15-20 min.) and analyzed using a gas chromatograph. The products were seperated on a 19% picric acid on Carbowax column and detected using a flame ionization detector. The following temperature program was used:

T_o = 50°C 4 min.

Ramp 32°C/min.

T_f = 110°C 4 min.

and gave product separations similar to that shown in Fig. 2.18. Integration of peak areas was performed by an electronic integrator (Spectra Physics Minigrator). Calibration of product retention times was performed using known standards and the flame ionization detector was calibrated with a standard CH_4/N_2 mixture.

After completion of the reaction the crystal was cooled to room temperature and the loop evacuated to ~100-500 μ using a mechanical pump. The high pressure cell was then isolated from the remainder of the loop and evacuated for ~2hrs. to a pressure of <1 μ using a liquid nitrogen trapped oil diffusion pump. At this point it was possible to open the cell and, after an initial burst in the chamber pressure to ~5×10^{-8} torr, achieve a vacuum of 2×10^{-9} torr within ~30 seccc. It should be noted that when dealing with such organics as thiophene that have low vapour pressures and extremely low pumping speeds a 2 hr. evacuation of the cell is necessary. High pressure exposures to gases such as H_2 and CO require much shorter pump down times of 5-15 min.

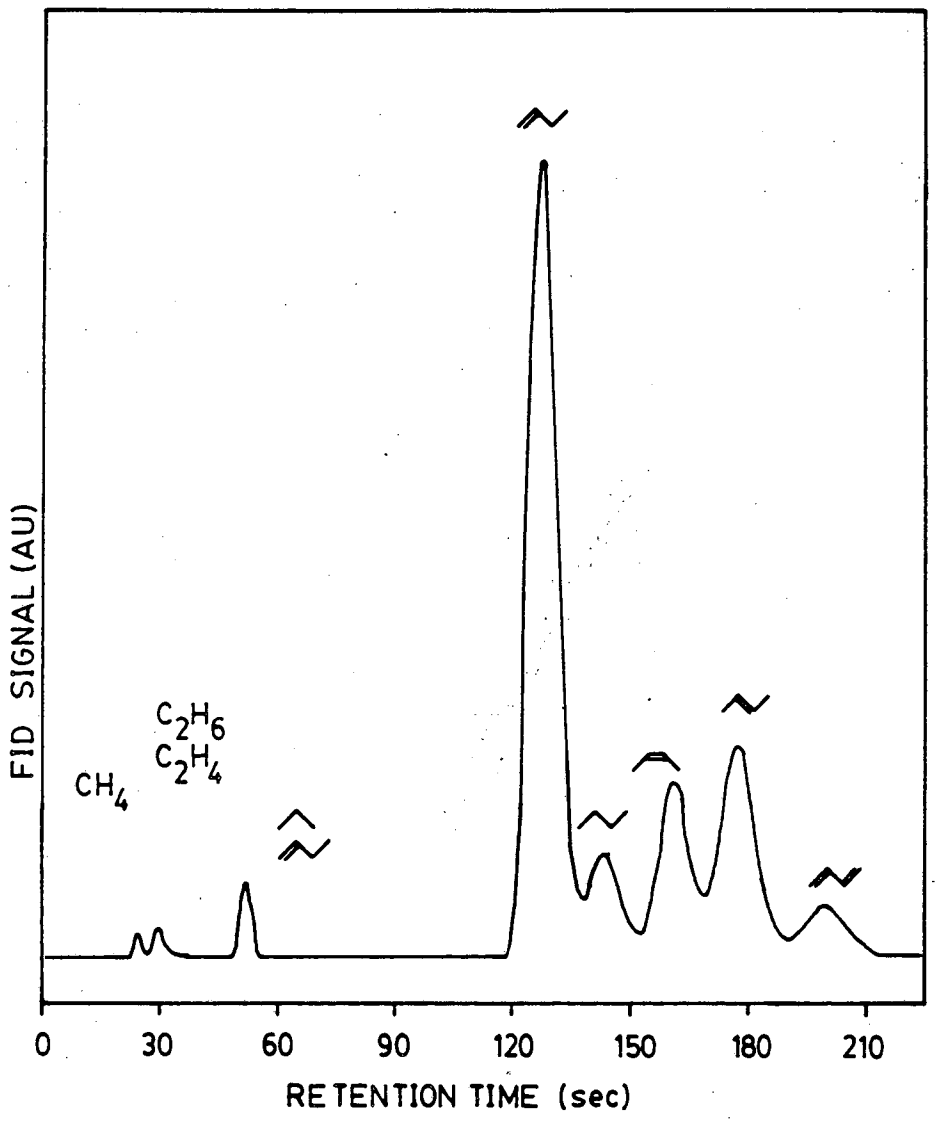

Fig. 2.18 Typical gas chromatogram of thiophene HDS products.

2.11 High Resolution Electron Energy Loss Spectroscopy

Low energy electrons incident on a metal surface exhibit small energy losses due to inelastic interactions with the vibrational modes of adsorbates. The spectrometer used for HREELS, depicted in Fig. 2.19, consists of two 127° electrostatic sectors. A monochromator sector produces low energy electrons (2-6 eV) while the analyzer sector collects electrons scattered from the crystal surface.

The theory of HREELS is discussed in detail elsewhere (20). Briefly, low energy electrons can interact inelastically with the vibrational modes of adsorbates via two mechanisms. The first is a long range interaction with the dynamic dipole moment of the mode and the second is a short range interaction termed impact scattering. In either case most such electrons appear to the loss side of the elastically scattered electrons and yield a spectrum such as that shown in Fig. 2.20.

The analysis of such a vibrational spectrum begins with a comparison of adsorbate modes with the modes of the gas phase species. Identification of modes involving hydrogen atoms can be made using selectively dueterated molecules. Unfortunately, the poor resolution (50 cm^{-1}) limits isotopic labelling techniques to the identification of these modes only. Finally, the presence of a dipole image in the metal introduces a surface selection rule. Modes with dipole derivatives purely parallel to the surface will be inactive in dipole scattering. The absence of expected modes can thus be used to determine adsorbate orientation on the surface.

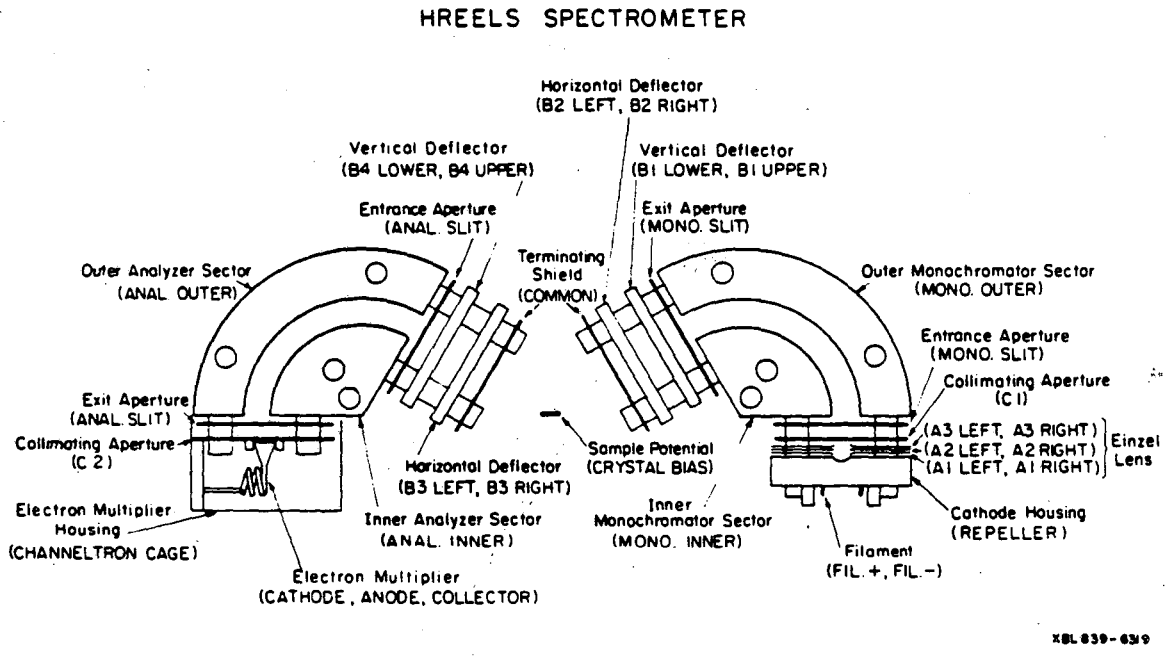

Fig. 2.19 Schematic diagram of HREELS spectrometer.

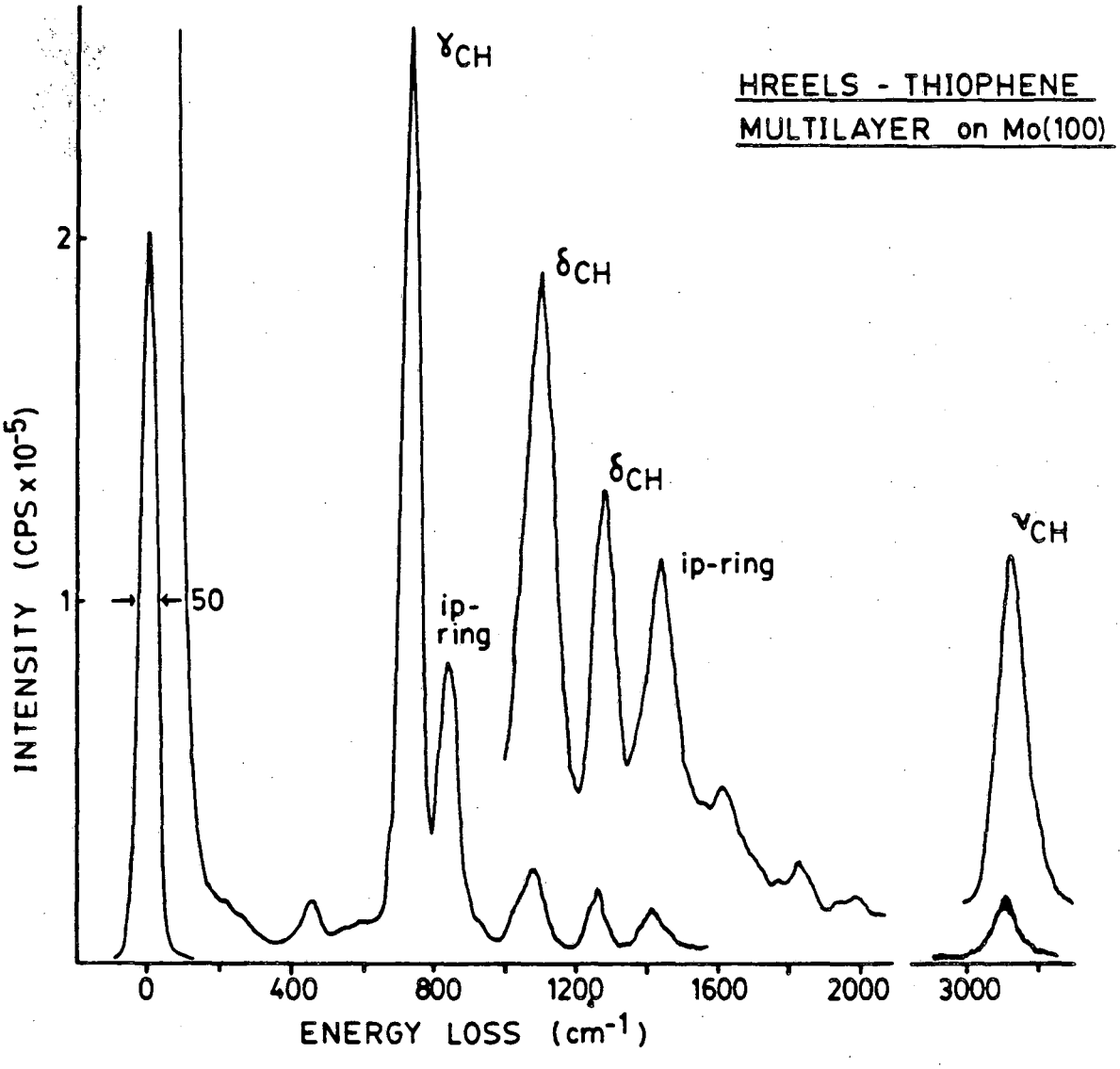

Fig. 2.20 HREEL spectrum of multilayer thiophene on the Mo(100) surface at T ≈ 100K.

2.12 References

1. D.W. Blakely, E. Kozak, B.A. Sexton, G.A. Somorjai, J. Vac. Sci. Technol., 13 (1976) 1091
2. W.D. Gillespie, Ph.D. Thesis, U.C. Berkeley, Berkeley, CA 1980
3. G.A. Somorjai, "Chemistry in Two Dimensions: Surfaces", Cornell Univ. Press, 1981, Ithaca, NY
4. G. Ertl, J. Kuppers, "Low Energy Electrons and Surface Chemistry", Verlag-Chemie, 1974, Germany
5. D. Briggs, M.P. Seah, "Practical Surface Analysis by Auger and X-ray Photoelectron Spectroscopy", Wiley, 1983, New York
6. N. Taylor, Rev. Sci. Instr., 40 (1969) 792
7. C. Wagner, J. Chem. Phys., 21 (1953) 1819
8. M.A. Van Hove, S.Y. Tong, "Surface Crystallography by LEED", Springer-Verlag, 1979, Berlin
9. P.A. Redhead, Vacuum, 12 (1962) 203
10. C.M. Chan, R. Aris, W.H. Weinberg, Appl. of Surf. Sci., 1 (1978) 360
11. C.M. Chan, W.H. Weinberg, Appl. of Surf. Sci., 1 (1978) 377
12. D. Edwards, Surf. Sci., 54 (1976) 1
13. J.M. Soler, N. Garcia, Surf. Sci., 124 (1983) 563
14. D.W. Turner, C. Baker, A.D. Baker, C.R. Brundle, Molecular Photoelectron Spectroscopy, Interscience, NY 1970
15. B.J. Bandy, D.R. Lloyd, N.V. Richardson, Surf. Sci., 89 (1979) 344
16. T.A. Carlson, Photoelectron and Auger Spectroscopy, Plenum Press, 1975, New York
17. F. Zaera, Ph.D. Thesis, Univ. of California, Berkeley, CA 1984
18. R. Ramanathan, M. Quinlan, H. Wise, Chem. Phys. Lett., 106 (1984) 87
19. Silicon Charged Particle Radiation Dectectors Instrumentation Manual,

EG&G Ortec Corp.

20. H. Ibach, D.L. Mills, Electron Energy Loss Spectroscopy and Surface Vibrations, Academic Press, 1982, New York

21. Handbook of Chemistry and Physics, 59th ed., CRC Press, Florida 1979

Chapter 3. Characterization of the Sulfided Mo(100) Surface

3.1 Introduction

The investigation of the catalytic activity of the Mo-S system was initiated by a study of the adsorption of sulfur on the single crystal metal surface. The aim of this study has been the determination of the sulfur adsorption site, the structure of the overlayers formed at various coverages and the examination of the nature of the sulfur-metal bond and the interactions between adsorbed sulfur atoms. Although some characterization of the Mo(110) (1) and Mo(111) (2,3) surfaces has been performed, the Mo(100) plane has been the focus of this work. This is due, in part, to its high symmetry and in part to the fact that there have been several prior studies of sulfur adsorption on this surface. Given that the active component of the industrial HDS catalysts is MoS_2, whose basal plane has hexagonal symmetry it might have been desirable to choose a single crystal plane having the same symmetry. Molybdenum, however, having a body centered cubic (bcc) structure has no hexagonally close packed surface. The (111) plane has the correct symmetry but also a very rough morphology and as a result presents a very complicated adsorption system (3). Following a similar line of argument, that it is the edge sites in the MoS_2 that are thought to be the active sites, it would seem that a stepped surface would be interesting. Although some study has been made of such a surface it is not significantly different in catalytic activity from the Mo(100) surface.

The work to date studying the adsorption of sulfur on the Mo(100) surface has primarily made use of LEED and AES (4-8). At this point in

time there is a fairly wide consensus concerning the LEED patterns produced by these overlayers and the coverages at which they occur. The most recent work includes a very thorough discussion of the LEED patterns and is in complete agreement with this investigation (8). The accompanying discussion of the structure of the corresponding sulfur overlayers, however, leaves in question the exact positions of the sulfur atoms within the lattice unit cells at high coverages. It is clear that at coverages ≤ 0.5 monolayers the sulfur atoms sit in the fourfold hollow site while at coverages of one monolayer some additional site is occupied. The distribution of atoms between binding sites in the intermediate coverage regime is still in question but will be addressed in this chapter.

By comparison with the LEED studies, much less work has been done to study the nature of the Mo-S bond and has been limited to the use of electron energy loss spectroscopy (ELS) (9) and some work function measurements (8,10). The work presented here has added to these the use of UV and X-ray photoelectron spectroscopies which have contributed not only to the understanding of the bonding but also to the question of adsorption site. Finally, the adsorption of S_2 and desorption of atomic sulfur have been studied and can be understood in terms of the proposed overlayer structures.

3.2 Calibration of the Sulfur Coverage

The calibration of the AES signal from sulfur overlayers on the Mo(100) surface has been discussed in Sec. 2.4. The approach used has been to define a function relating θ_S to $r = {}^{I}S_{150} / {}^{I}Mo_{221}$ in terms

of three parameters.

$$\theta_S = \frac{r - \gamma}{(\alpha+\alpha\gamma-\gamma) + (1-\beta)r}$$

$$\alpha = I_S(1) \;/\; I_{Mo}(0)$$

$$\beta = I_{Mo}(1) \;/\; I_{Mo}(0)$$

$$\gamma = I_{Mo_{150}}(0) \;/\; I_{Mo}(0)$$

$I_{Mo_{150}}(0)$ is the amplitude of the Mo Auger peak at 150 eV from the clean surface while I_S and I_{Mo} refer to the sulfur and Mo peaks at 150 eV and 221 eV respectively. In general, these paramenters depend upon the configuration of the spectrometer and can be obtained either from measurements of the relative AES peak heights (AES ratio) at three known coverages or absolute measurements of the spectral peak heights at two known coverages. Given that one of these points can be the clean surface, one must at least be able to obtain an AES spectrum of a surface at a well determined coverage. In general, this is one of the hardest problems in surface science. In this case, however, there are three seperate approaches to calibrating the coverage and there is complete concensus on this point in the literature.

Table 3.1 lists the four LEED patterns (discussed in Sec. 3.3) produced by the sulfur overlayer on the Mo(100) surface, the corresponding ranges of AES ratios at which they occur and the corresponding surface lattice unit cell sizes. The sizes of the unit cells are given in multiples of the substrate unit cell size and must contain integral numbers of sulfur atoms. Quick comparison of the AES ratios and unit cell sizes suggests that the c(2x2), $\begin{vmatrix} 2 & \bar{1} \\ 1 & 1 \end{vmatrix}$, c(4x2), and p(2x1) unit cells should contain integral multiples of 1,2,3, and 2 sulfur atoms respectively. These yield coverages of 1/2, 2/3, 3/4 and 1, or integral

Table. 3.1 S:Mo AES ratios, Coverage ranges and Temperature of Formation of LEED patterns for Sulfur on Mo(100)

Structure	Unit Cell Size[a]	AES[b] Ratio $I_S:I_{Mo}$	Sulfur Coverage Range	Temperature Range (K)[c]
p(2x1)	2	2.15 - 2.3	0.99 - 1.05	400 - 850
c(4x2)	4	1.6 - 2.0	0.75 - 0.9	1100 - 1320
$\begin{vmatrix} 2 & \bar{1} \\ 1 & 1 \end{vmatrix}$	3	1.3 - 1.45	0.65 - 0.7	1360 - 1410
c(2x2)	2	0.25 - 1.1	0.15 - 0.55	1450 - 1800

a. Overlayer lattice cell size relative to substrate lattice.

b. Measured using single-pass CMA.

c. Temperature range in which the structure is formed from starting with an adsorbed sulfur multilayer.

multiples of these. Given that the atomic diameter of sulfur is 2.1Å (11) and the unit cell parameters of the p(2x1) lattice are 3.1Å x 6.2Å it seems unlikely that four or more sulfur atoms could occupy this unit cell and thus that this lattice occurs at one monolayer coverage. These arguments have, so far, ignored the possibility of gross reconstruction of the Mo(100) surface during sulfur adsorption and the possibility of overlayers of greater than one atomic thickness.

The work of Clarke (5) studying these sulfur overlayers has included an analysis of the diffraction spot intensities vs. electron energy for the c(2x2) structure. The analysis shows close agreement between these intensity profiles and those predicted for a model in which the unit cell contains one sulfur atom adsorbed in the fourfold hollow position. Such an analysis should be fairly sensitive to the possible reconstruction mentioned above and thus serves as a good calibration of the c(2x2) lattice as the half monolayer coverage structure.

Finally, absolute sulfur coverage measurements have been made using ^{35}S on the Mo(110) surface (1). This calibration has recently been carried over to the Mo(100) surface (8) and agrees with the calibration obtained from the initial examination of the LEED patterns. Using this calibration for each of the LEED patterns it has been possible to obtain AES spectra of the surface at well defined sulfur cover-coverages and thus to determine the parameters α, β and γ. The resulting calibration curve has been shown in Fig. 2.12.

3.3 Sulfur Overlayer Structures

3.3.1 The Clean Mo(100) Surface

Fig. 3.1 shows the LEED pattern of the clean Mo(100) surface. Molybdenum has a bcc structure and hence the termination of the bulk structure along the (100) plane has a square surface lattice and produces a square diffraction pattern. The real space structure of the surface is also shown in Fig. 3.1 and, as can be seen, has a relatively exposed second layer. Although this lattice is the correct surface structure for T>300K the clean surface has been shown to undergo a complex reconstruction at lower temperatures to a lattice that has what is close to c(2x2) periodicity with respect to the unreconstructed surface lattice (12,13). Analysis of the diffraction intensity vs. electron energy profiles has shown that the lattice parameters of the unreconstructed surface are 3.14Å x 3.14Å, identical to those of the bulk termination plane (14,15). In the direction normal to the surface, however, there is a contraction of the first and second layer spacings by ~10% and ~1% respectively.

3.3.2 The c(2x2) Structure

In the coverage range $0.15 \leq \theta_S \leq 0.55$ the surface LEED pattern corresponds to a c(2x2) lattice. The diffraction pattern is displayed in Fig. 3.2 with the real space lattice and the real space structure. Analysis of the I-V profiles has shown that the sulfur atom is in fact adsorbed in the fourfold hollow site at a distance of 1.04Å above the surface plane with a Mo-S bond length of 2.45Å (5). The appearance

Fig. 3.1 LEED pattern and corresponding structure of the clean Mo(100) surface.

Mo(100) - LEED Pattern

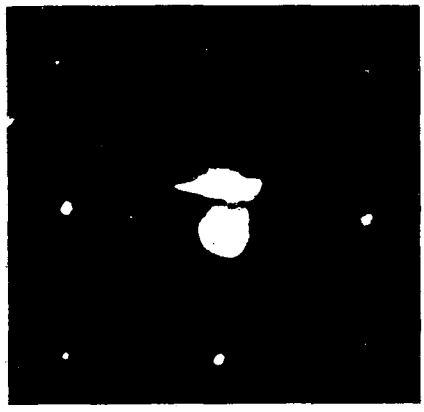

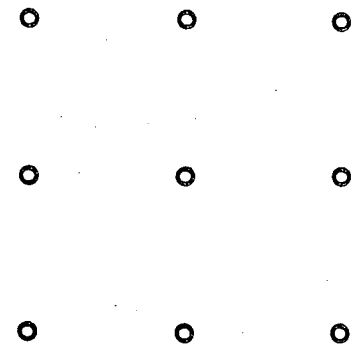

- Real Space Structure

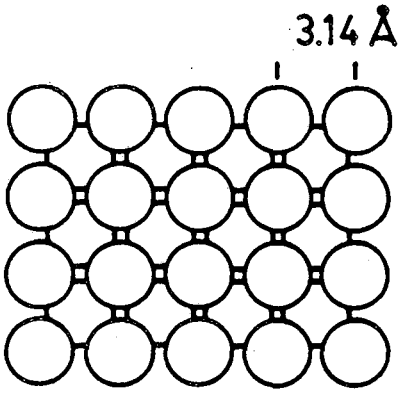

Top view

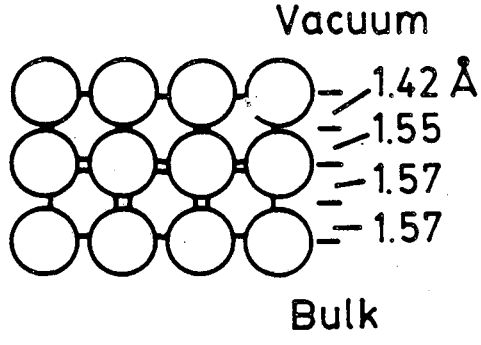

Side view

Fig. 3.2 LEED pattern of the c(2x2) sulfur structure on the Mo(100) surface. The pattern is drawn to the right of the picture with the open circles (o) representing substrate diffraction spots and the solid circles (•) the extra spots due to overlayer diffraction. The real space structure is depicted at bottom (A) with the overlayer lattice (B).

c(2x2) - LEED Pattern

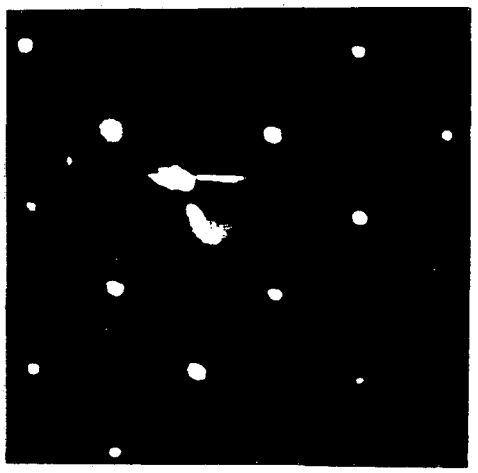

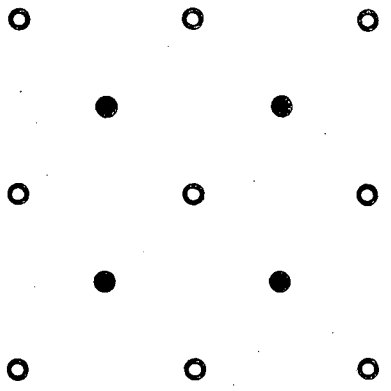

- Real Space Lattice

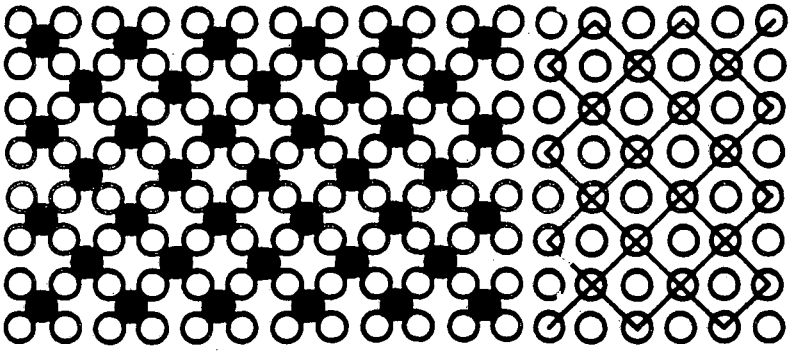

A B

of the c(2x2) pattern at sulfur coverages much less than the stoichiometric half monolayer implies that at low coverages the sulfur atoms coalesce into islands. Apparently the interaction potential between sulfur atoms on the surface at low coverages is attractive, at least to nearest neighbour distances.

3.3.3 The $\begin{vmatrix} 2 & \bar{1} \\ 1 & 1 \end{vmatrix}$ Structure

In the coverage region $0.65 \leq \theta_S \leq 0.70$ the LEED pattern correspond to an overlayer lattice described by the matrix $\underset{\approx}{M} = \begin{vmatrix} 2 & \bar{1} \\ 1 & 1 \end{vmatrix}$. This pattern is shown in Fig. 3.3 with the real space lattice and two possible overlayer structures. It is not possible to describe this lattice in the simplified notation proposed by Wood (16) due to the fact that the angle subtended by the unit cell vectors differs from that of the substrate lattice vectors. As shown the LEED pattern is complicated by the fact that the overlayer lattice can have two equivalent orientations with respect to the substrate.

There have been no analyses of the I/V profiles for the $\begin{vmatrix} 2 & \bar{1} \\ 1 & 1 \end{vmatrix}$ overlayer and so the exact structure is not known. The lattice contains three Mo atoms per unit cell and corresponds to a stiochiometric coverage of 2/3. Thus the unit cell can contain two sulfur atoms in any positions. The structures proposed have been restricted to models in which the atoms sit in sites of high symmetry i.e. the fourfold hollow or a bridging position.

At coverages intermediate between θ_S=0.5 and θ_S=0.67 the LEED patterns display streaks of diffraction intensity between the (1/2,1/2) spots of the c(2x2) pattern and the (1/3,2/3) and (2/3,1/3) spots of

Fig. 3.3 LEED pattern of the (2,-1,1,1) sulfur overlayer lattice. Two possible structures are presented (A,B). The open circles (o) represent Mo atoms and the solid circles (•) sulfur atoms. The overlayer lattice is depicted in C.

$\begin{bmatrix} 2 & \bar{1} \\ 1 & 1 \end{bmatrix}$ - LEED Pattern

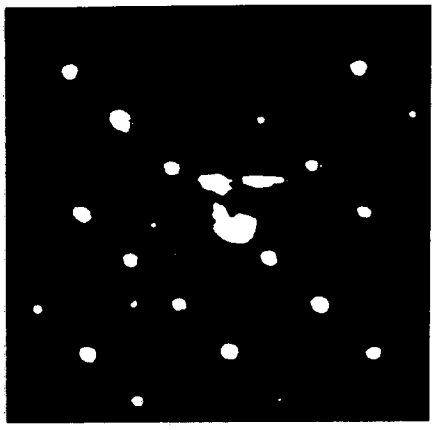

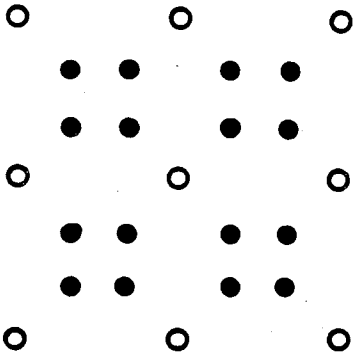

- Real Space Lattice

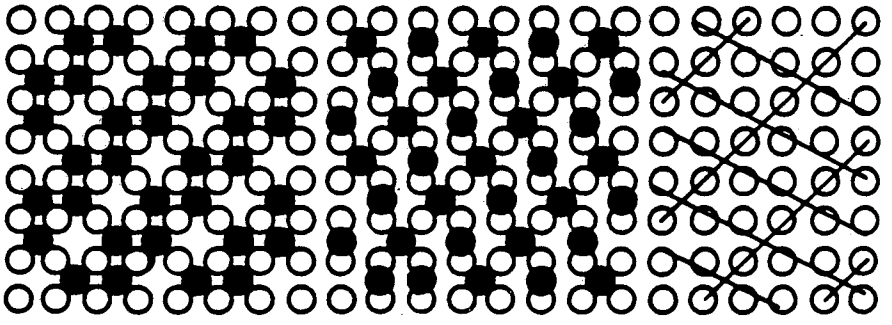

the $\begin{vmatrix} 2 & \bar{1} \\ 1 & 1 \end{vmatrix}$ pattern. These features are shown in Fig. 3.4 and have been discussed by Maurice et. al. (8) in terms of a continuous increase in the density of anti-phase domains in the c(2x2) lattice as the coverage exceeds θ_S = 1/2. Such anti-phase domains are depicted in Fig. 3.4 and it should be noted that such a growth mechanism should lead smoothly to overlayer structure A in Fig. 3.3 composed purely of atoms in the fourfold hollow sites.

3.3.4 The c(2x4) Structure

In the coverage range $0.70 \leq \theta_S \leq 0.85$ the LEED pattern corresponds to a c(4x2) overlayer lattice. This pattern is shown in Fig. 3.5 and again has contributions from two equivalent domains of the overlayer. The overlayer lattice contains four Mo atoms and, since it corresponds to a stoichiometric coverage of θ_S=0.75, three sulfur atoms. Three possible overlayer structures are shown in which atoms have been restricted to sit in either hollow or bridging positions.

The transition between the 2/3 monolayer to the 3/4 monolayer coverages is accompanied by LEED patterns formed of the c(4x2) pattern superimposed on the $\begin{vmatrix} 2 & \bar{1} \\ 1 & 1 \end{vmatrix}$ pattern. This suggests a nucleated growth of the c(4x2) structure and a surface composed of islands of each structure rather than the smooth transition that occurs between the 1/2 and 2/3 monolayer coverages.

3.3.5 The p(2x1) Structure

The LEED pattern of the surface covered by one monolayer of sulfur is from a p(2x1) lattice present in two domains (Fig. 3.6). Note that

Fig. 3.4 The streaked LEED pattern observed during the transition from the c(2x2) structure to the (2,-1,1,1) structure. The real space structure shows c(2x2) domains separated by anti-phase boundaries.

c(2×2) -$\begin{bmatrix} 2 & \bar{1} \\ 1 & 1 \end{bmatrix}$ Transition - LEED Pattern

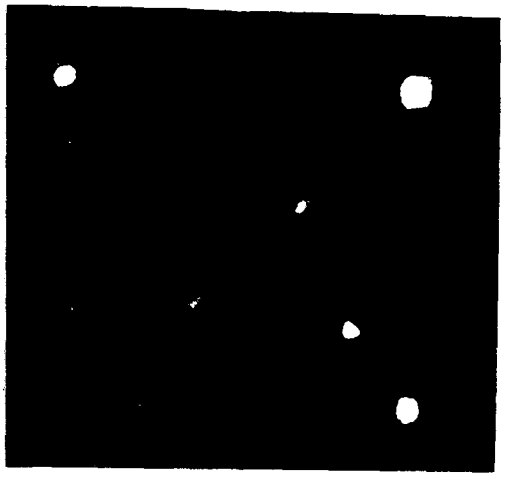

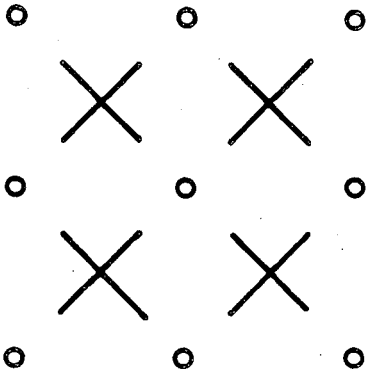

- Antiphase domain structure

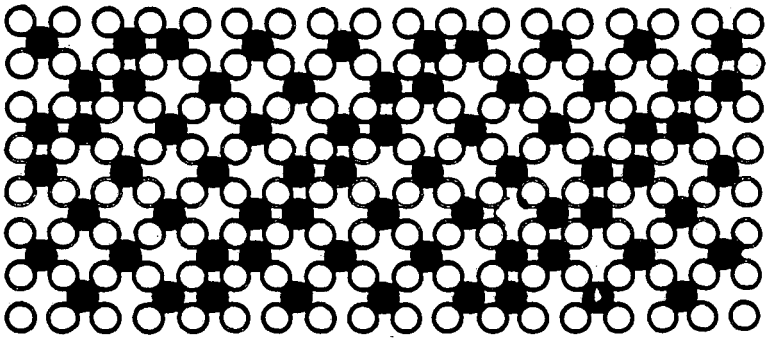

Fig. 3.5 LEED pattern of the c(4x2) sulfur overlayer lattice. Three possible structures are presented (A,B,C). The overlayer lattice is depicted in D.

c(4x2) - LEED Pattern

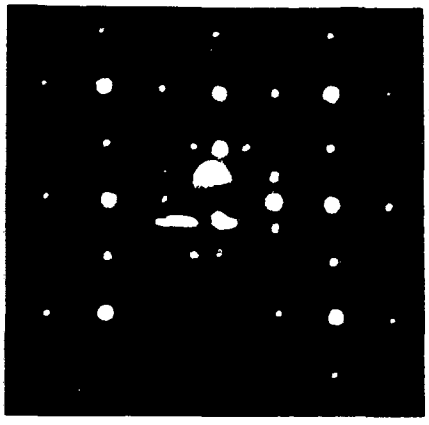

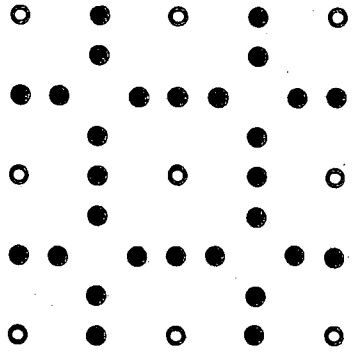

- Real Space Lattice

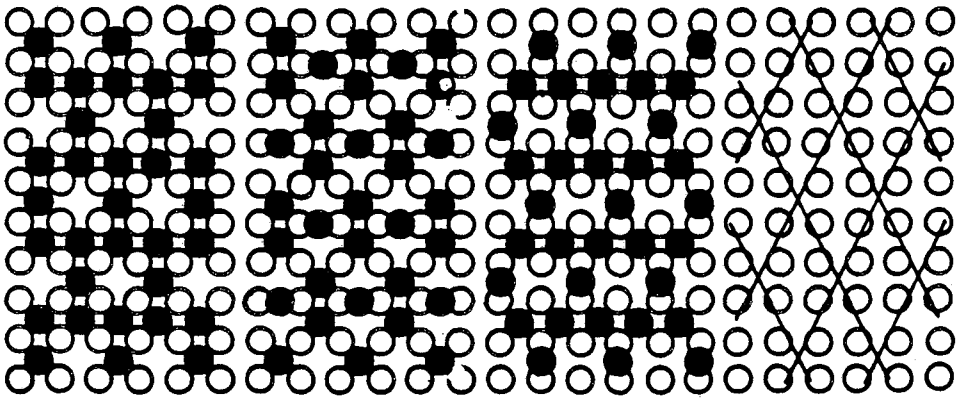

this overlayer has two sulfur atoms and two molybdenum atoms per unit cell in a lattice that is primitive. In order for the lattice to be primitive the atoms must occupy two inequivalent binding sites, as suggested by structure A, in which one atom is found in a fourfold hollow and the other in a bridging position. It is clear that such a configuration serves to increase the average sulfur-sulfur distance over that of a structure in which all atoms are in hollow sites. This configuration is, in fact, psuedo-hexagonal.

The structure depicted in Fig. 3.6 B has been proposed as a possible p(2x1) lattice in which the sulfur atoms occupy identical but inequivalent sites, although not ones of high symmetry (5). Examination of this structure, however, reveals the presence of a glide plane parallel to the $\underset{\sim}{a}$ lattice vector. Such a symmetry element should result in systematic absences of the (0,n+1/2) spots (see Sec. 2.5) and the LEED pattern depicted in Fig. 3.7. These spots are, however, present in the observed pattern and thus we can eliminate the corresponding structure.

The p(2x1) structure at the monolayer coverage implies the coadsorption of sulfur in two distinct binding sites. While at the half monolayer it is clear that there is only one binding site, the fourfold hollow, the structures at intermediate coverages can be composed of sulfur atoms in either one or two sites. This problem will be addressed at a later point in the chapter.

Fig. 3.6 LEED pattern of the p(2x1) sulfur overlayer lattice. Two possible structures are presented (A,B). The overlayer lattice is depicted in C.

p(2x1) - LEED Pattern

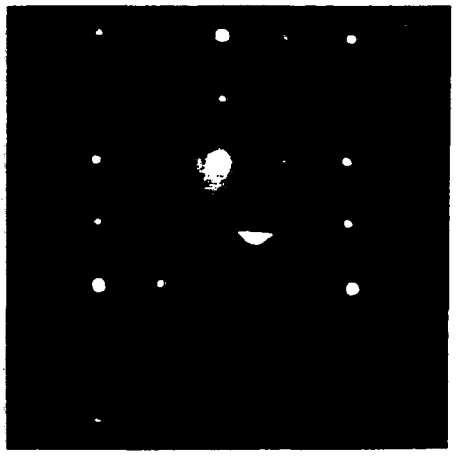

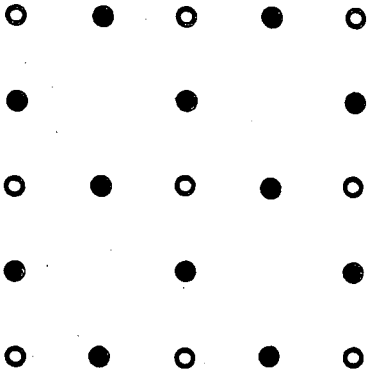

- Real Space Lattice

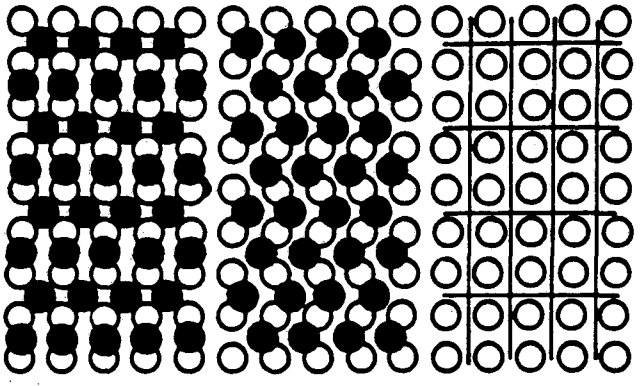

LEED Pattern - p(2x1) Lattice with Glide Plane

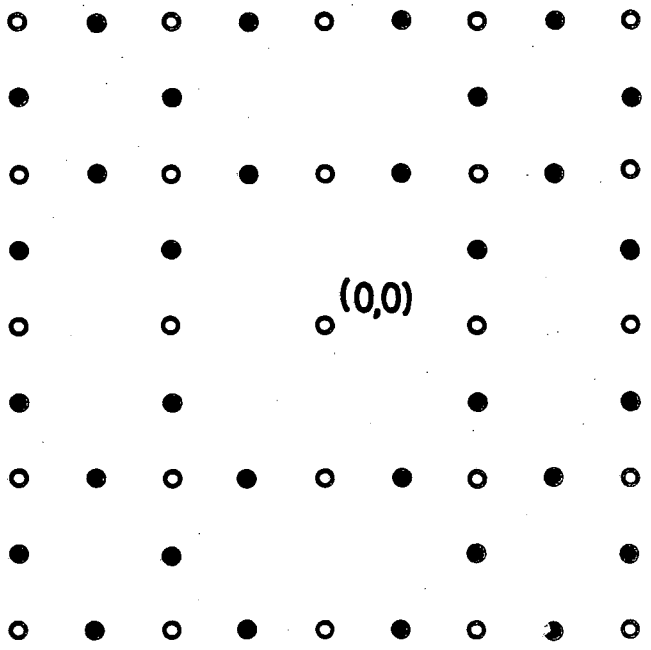

Fig. 3.7 The LEED pattern expected from a p(2x1) overlayer having glide plane symmetry, as in Fig. 3.6B.

3.3.6 Other LEED Patterns

In addition to the LEED patterns that have been discussed above, patterns corresponding to c(4x4) and ($\sqrt{5}$x$\sqrt{5}$)R26° lattices have been reported (5,7), but not observed consistently. The c(4x4) pattern only occurs at very low coverages of $\theta_S \approx 0.12$. The ($\sqrt{5}$x$\sqrt{5}$)R26° pattern occurs at coverages of $\theta_S \approx 0.6$ and is often observed in the presence of oxygen which is known itself to form the same overlayer lattice (17). It is possible that the adsorbed oxygen in some manner nucleates this structure and that on the occasions when there is only sulfur apparent on the surface, oxygen is still present, but at levels below its detection limit (≈10%). In any case it is seems that these two structures are only weakly stable and they certainly do not appear in a reproducible fashion.

3.4 Adsorption and Desorption of Sulfur

The adsorption of sulfur on the Mo(100) surface has been studied using sulfur in the form of S_2 from the electrochemical source. Fig. 3.8a shows the S_{150} and Mo_{221} AES signals as a function of time during exposure to S_2 at room temperature. It is clear that the sulfur uptake occurs at a constant rate until near-saturation coverage is reached at about one monolayer. At this point the sticking coefficient drops and the sulfur uptake decreases markedly. This type of behaviour suggests adsorption of S_2 into a weakly bound, precursor state, and subsequent adsorption to the metal surface, resulting in an apparently constant sticking coefficient over a wide range of coverages (34). Fig.s 3.8b &c compare the S uptake curve with typical curves expected for cases

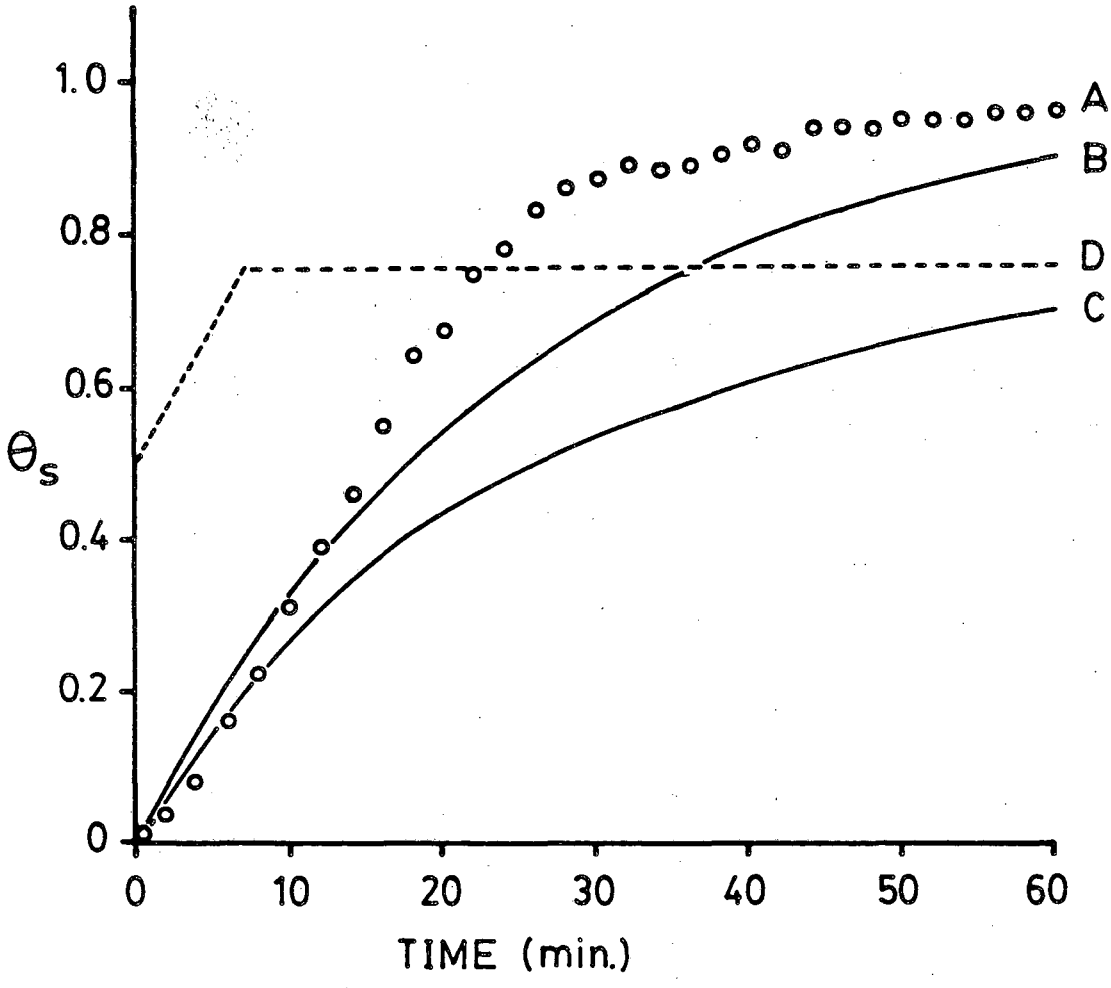

Fig. 3.8 Sulfur coverage vs. time of the Mo(100) surface under exposure to a constant flux of S_2 (A). Calculated uptake curves for first order Langmuir growth (B) and second order Langmuir growth (C) using a flux of 0.05 monolayers/min. Uptake curve observed on starting with a surface having a half monolayer c(2x2) sulfur coverage.

of Langmuir type growth, in which the only atoms that will adsorb to the surface are those that are incident directly upon exposed metal atoms (34). Continued exposure of our sample results in the slow uptake of sulfur to produce multilayer growth. The fact that such multilayers can be grown indicates that there is a significant adsorption energy for sulfur upon sulfur and that a precursor state can exist. Adsorption at temperatures of ~150K allowed facile growth of thick sulfur overlayers.

LEED experiments performed on surfaces produced by S_2 adsorption on clean surfaces at room temperature or below reveal no ordering of the adsorbate layer. Annealing to temperatures of ~450K is necessary to desorb any multilayer sulfur and induce ordering (Fig. 3.9). Adsorption on partially sulfided surfaces, however, yields different results. Starting with a surface sulfur coverage of θ_S=0.5, in a c(2x2) structure, and exposing the crystal to S_2 at room temperature results in the adsorption of sulfur and the spontaneous formation of the $\begin{vmatrix} 2 & \bar{1} \\ 1 & 1 \end{vmatrix}$ structure followed by the c(4x2) overlayer structure. At this point, however, no further adsorption of sulfur is possible, as shown in Fig. 3.8d. In order to reach a one monolayer coverage ordered into a p(2x1) lattice it is necessary to adsorb sulfur on an initially clean surface and subsequently anneal the crystal to induce order. It is apparent that the adsorption of sulfur on an ordered matrix of sulfur differs from adsorption on a clean surface.

Fig. 3.9 shows the decrease in the S:Mo AES ratio as a surface initially covered with multilayers of adsorbed sulfur is annealled to increasing temperatures. In addition, the corresponding LEED patterns are listed. The sharp drop at low temperatures results from the desorp-

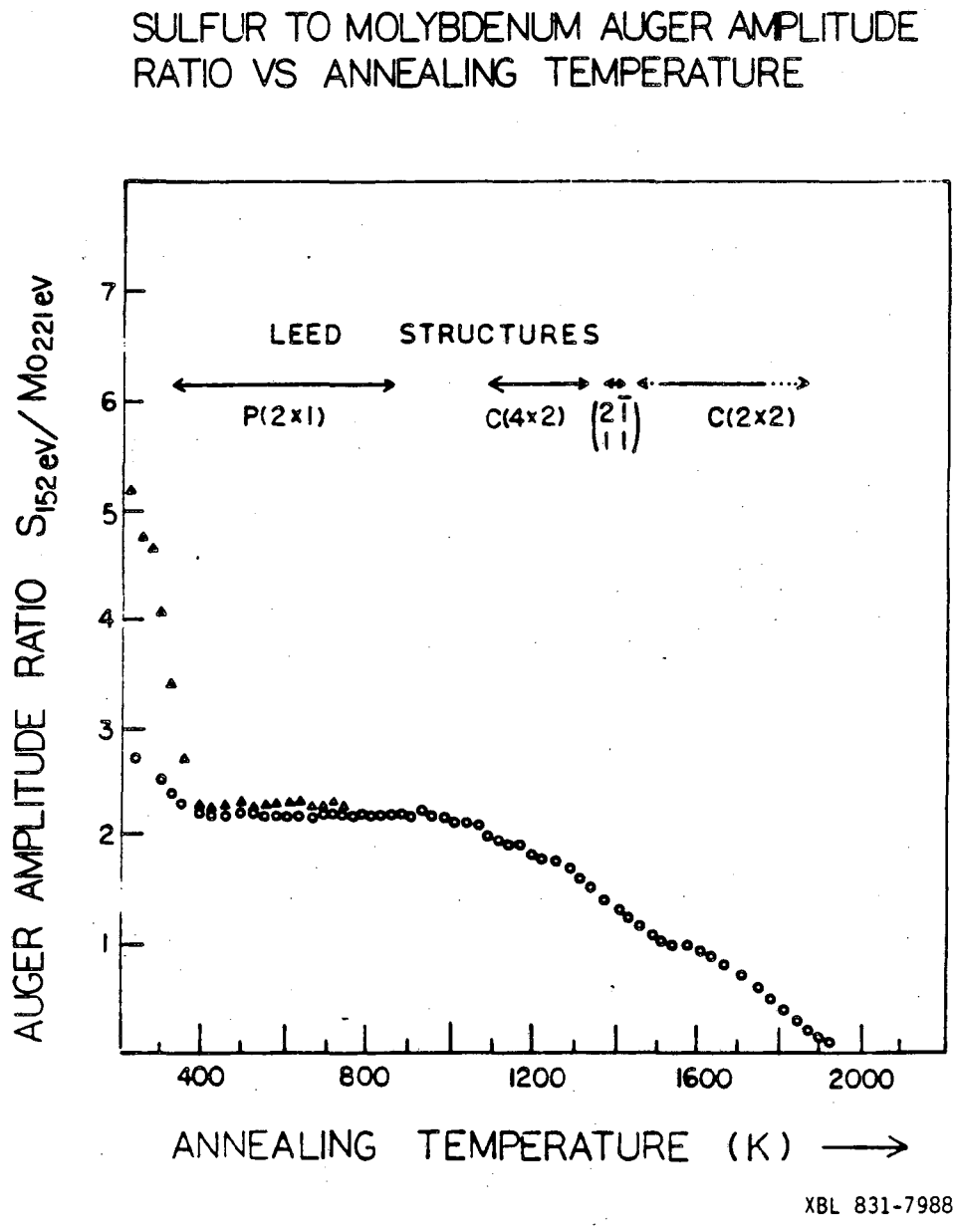

Fig. 3.9 S:Mo AES ratio vs. temperature during annealing of a surface initially covered with multilayer sulfur. AES measurements were all made at room temperature after annealing at elevated temperatures for ~20 sec.

tion of multilayer sulfur followed by the formation of the monolayer p(2x1) structure. This lattice is stable up to temperatures of ~1100K at which further desorption begins and the submonolayer structures appear.

The thermal desorption spectra (TDS) of sulfur from the Mo(100) surface are shown in Fig. 3.10 for several different initial sulfur coverages. The four features observed are similar to those observed during sulfur desorption from the W(100) surface (18). At low coverages there is one desorption peak of atomic sulfur at 1800K that does not shift with coverage and appears to be the result of a first order process. Assuming a pre-exponential factor of 10^{13} sec^{-1}, which is probably valid for an atomic desorption process (19), we calculate a Mo-S bond strength of ~110 kcal/mole. At higher coverages $\theta_S \geq 0.67$ a second feature appears as a shoulder to the low temperature side of the low coverage peak. This feature is somewhat poorly resolved and appears to have a maximum in the temperature range 1300K - 1500K and a desorption energy in the range 75 - 90 kcal/mole. These two features arise from atomic desorption at monolayer and submonolayer coverages in which the sulfur is bound directly to the metal surface.

The other features appear only for initial coverages in excess of one monolayer. The sharp desorption feature at ~1150K is accompanied by S_2 desorption and has a shape reminiscent of a zero-order desorption process. Zero-order desorption is characteristic of bulk compound vapourization. This feature is not highly reproducible, as can be seen from the experiment depicted in Fig. 3.9 in which the sulfur coverage drops to one monolayer after heating to only 400K. It is possible that this feature arises from the decompostion of MoS_2 which might be

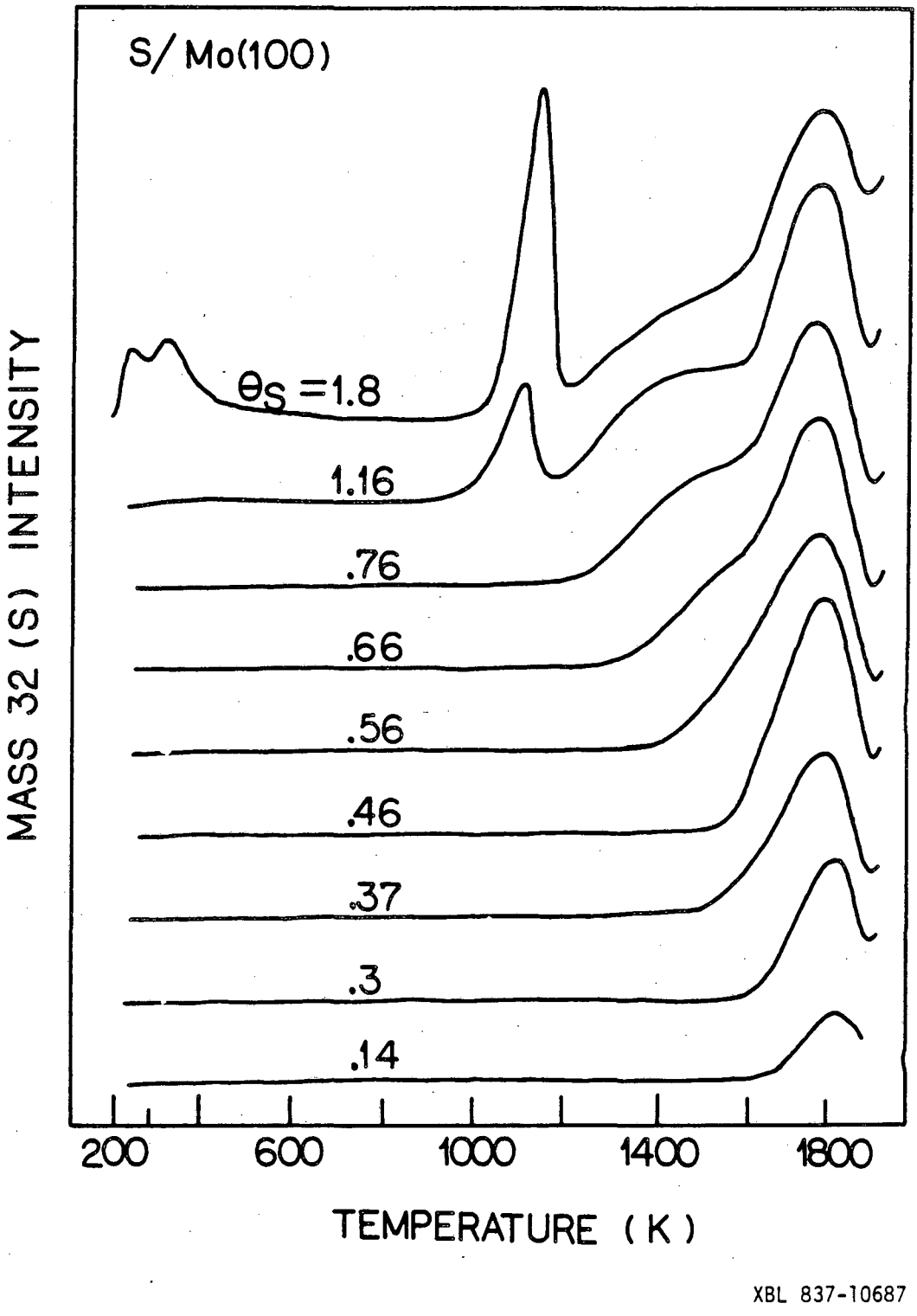

Fig. 3.10 TDS of sulfur from the Mo(100) surface at several initial sulfur coverages. Heating rate is 20 K/sec.

expected to occur at this temperature. The equilibrium vapour pressure of S_2 over MoS_2 at this temperature can be calculated at 10^{-6} torr.

At the lowest temperatures (300K - 400K) S_2 desorbs from the multilayer condensed sulfur phase. The fact that sulfur will desorb from the overlayers in this temperature range supports the previous suggestion that sulfur adsorption at room temperatures can occur through an intermediate, precursor state i.e. sulfur adsorbed on sulfur.

3.5 Bonding of Sulfur to the Surface

X-ray and UV photoelectron spectroscopies have been used to study the bonding of sulfur on the Mo(100) surface in each of the four overlayer structures. Fig 3.11 shows the UV photoemission spectrum of the clean metal surface. This is identical to angle integrated spectra reported elsewhere (20). There are a number of studies of this and of angle resolved spectra which have been interpreted using calculations of the density of electronic states at the surface (21-23). There does not seem to be complete concensus on its interpretation, however, some calculations suggest that the two peaks at -0.3 eV and -2.6 eV below the Fermi level arise from surface localized states (21). The adsorption of sulfur results in a sharp drop in intensity of the -0.3 eV peak suggesting that this might in fact be the case.

In this work sulfur deposition has been accomplished using a source of S_2. Fig. 3.12 shows the UP spectrum of multilayer sulfur deposited on the Mo(100) surface at ~150K. Photoemission from the metal d-bands is almost completely attenuated and the remaining features correspond very closely to the four highest lying features of the gas phase S_2

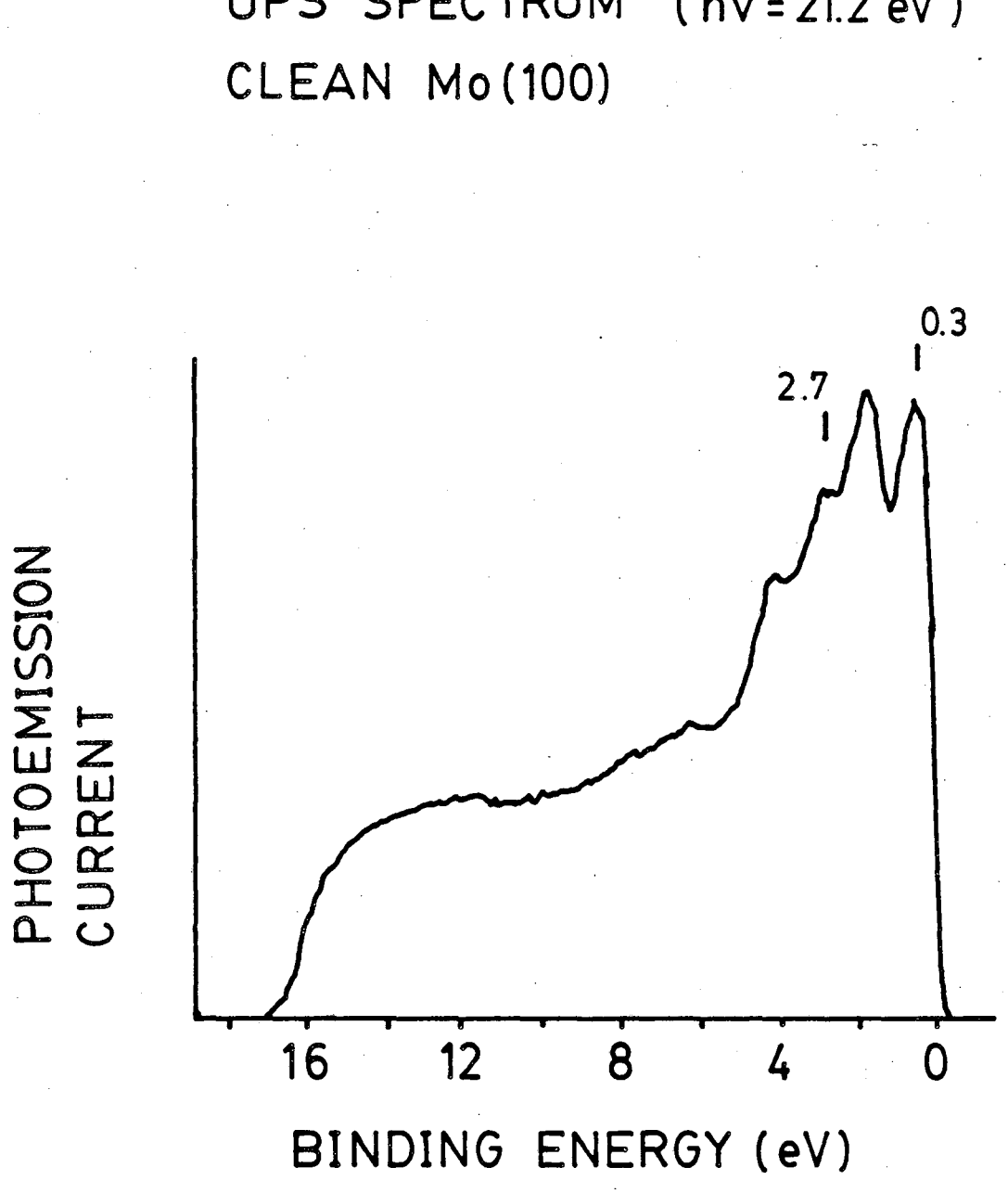

Fig. 3.11 He I UP spectrum of the clean Mo(100) surface.

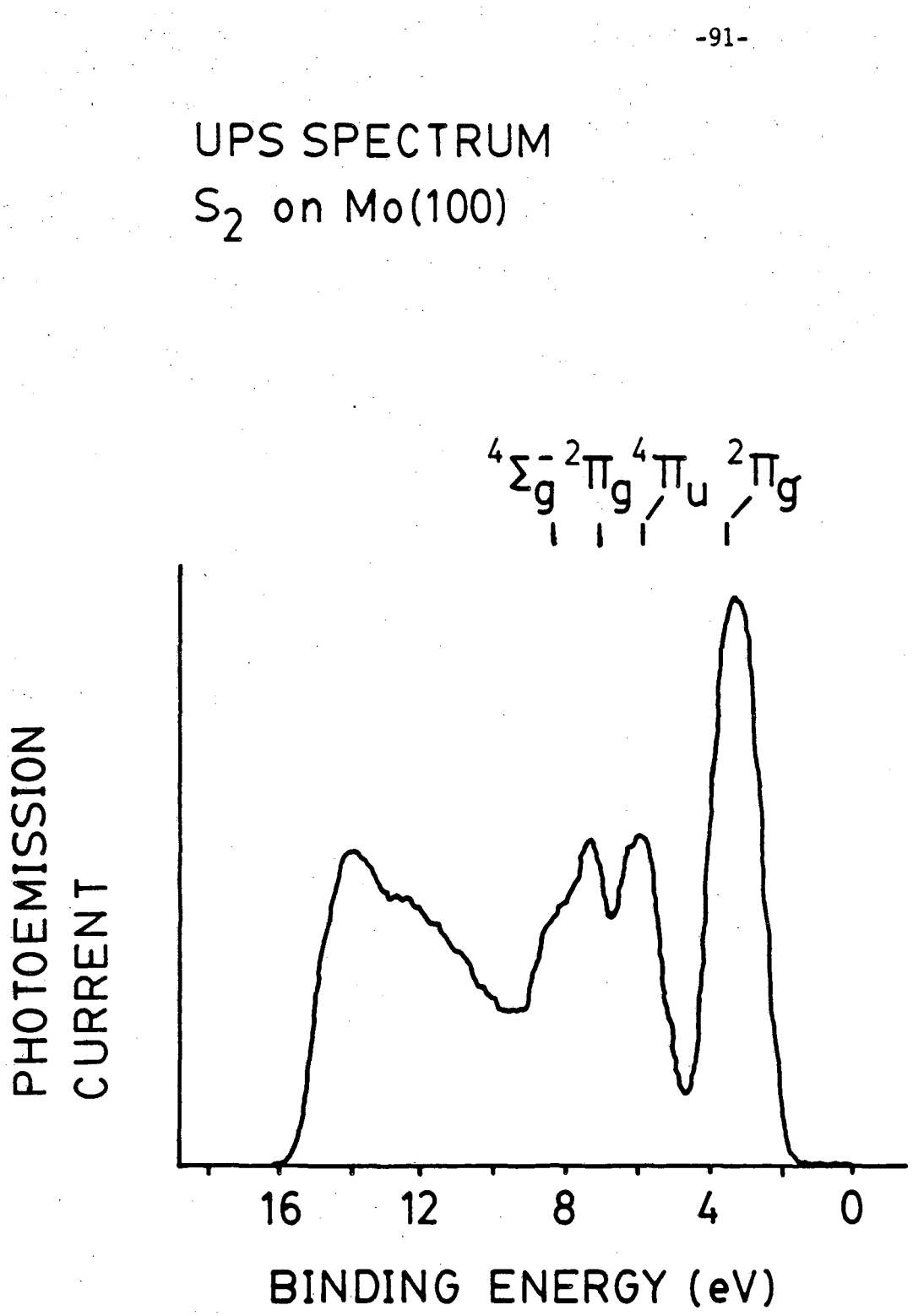

Fig. 3.12 He I UP spectrum of multilayer S_2 on the Mo(100) surface at T ≈ 125K.

UP spectrum (24). The UP spectrum of ~1 monolayer of S_2 deposited on the Mo(100) surface at 200K is shown in Fig. 3.13. The features arising from adsorbed sulfur (4-7 eV) resemble those of sulfur present in an ordered p(2x1) monolayer (Fig. 3.15). Even at these low temperatures the S_2 is dissociated by the clean metal surface.

The sulfur 2P XP spectrum of the multilayer S_2 and the ordered monolayer are shown in Fig. 3.14. The S_2 multilayer exhibits a sharp photoemission feature at 163.7 eV binding energy, very close to the reported value of 164.0 eV for bulk sulfur (25). The spectrum of the monolayer exhibits a clear shift to 162.3 eV, very close to that of sulfur in its -2 formal oxidation state, as in MoS_2 reported at 162.2 eV (25).

The UP spectra of ordered sulfur at monolayer and submonolayer coverages are shown in Fig. 3.15. The monolayer spectrum has two distinct photoemission features at 6.8 eV and 4.6 eV binding energy with respect to the Fermi level. These two features are present in the spectrum of the c(4x2) overlayer but with the low binding energy feature somewhat attenuated. At still lower coverages the low binding energy feature dissappears altogether and only the high binding energy feature remains. This feature remains present throughout the entire coverage range but can be seen to shift down to 6.2 eV at low coverages. Given our previous discussion of the possible existence of two binding sites for the sulfur atom at high coverages these spectra can be given a simple, phenomenological interpretation. We assign the low binding energy peak to photoemission from sulfur atoms in the high coverage binding site and the high binding energy peak to those in the fourfold hollow site. It is not, of course, possible to rule out the argument

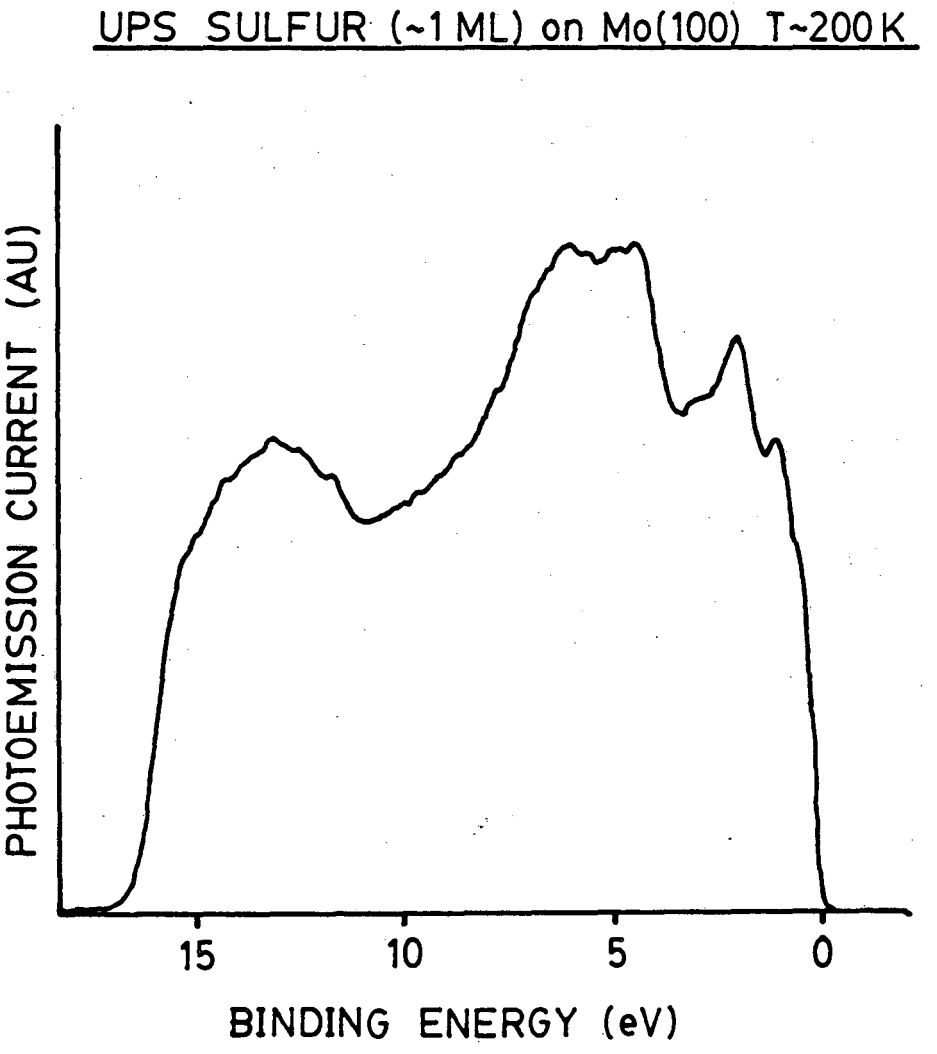

Fig. 3.13 He I UP spectrum of one monolayer of sulfur adsorbed on the Mo(100) surface at T ≈ 200K.

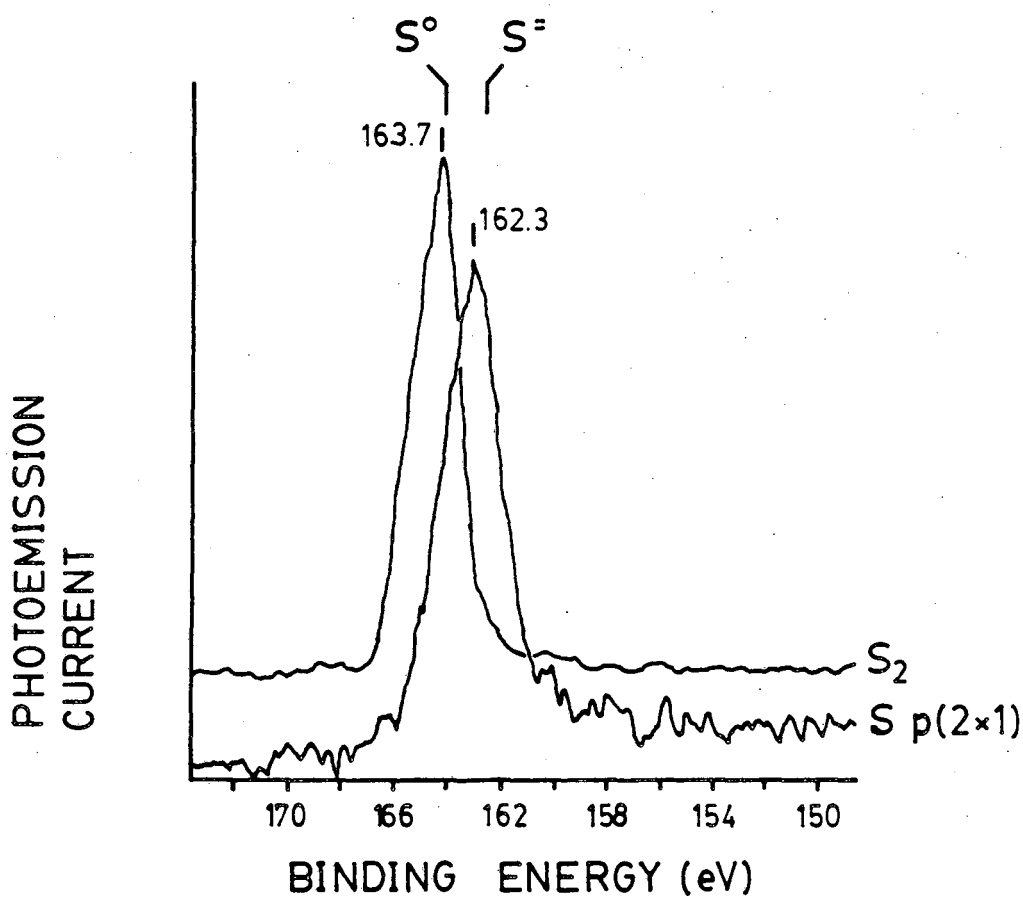

Fig. 3.14 XP spectrum of multilayer S_2 on the Mo(100) surface and the adsorbed sulfur monolayer in the p(2x1) structure.

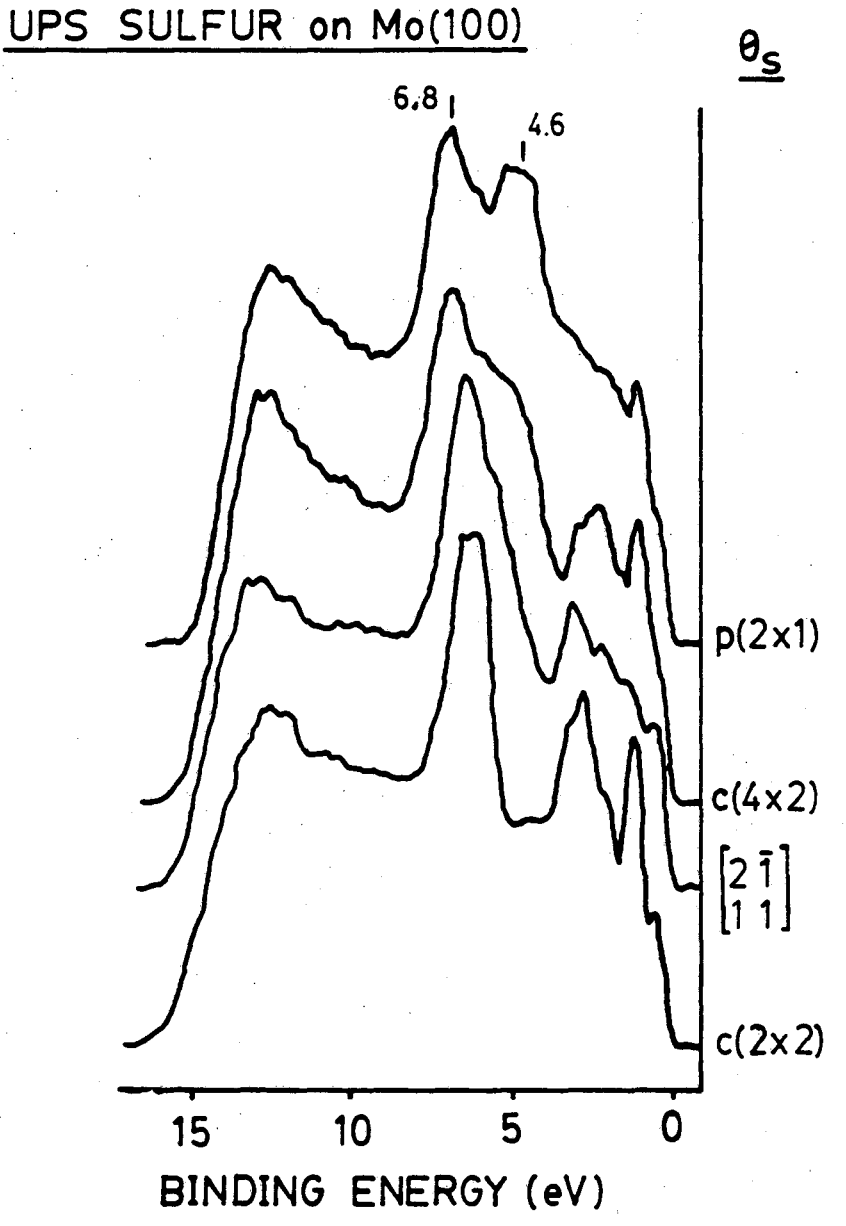

Fig. 3.15 He I UP spectra of sulfur on the Mo(100) surface at several coverages.

that the low binding energy feature appears as a result of interactions between adsorbate atoms.

The adsorption of S on Ni has been studied using UPS several times. It is a case of particular interest because it is one in which a change in binding site with coverage has been proposed (26). Atomic adsorption in either three-fold or four-fold symmetric sites results in the splitting of orbitals into a single orbital of 'a_1' symmetry arising from the p_z atomic orbital and a degenerate pair of 'e' symmetry from the $p_{x,y}$ atomic orbitals. These have been identified on the Ni surface using angle resolving techniques unavailable in this work. On the Ni(111) surface the S p(2x2) structure is formed of atoms in the three-fold hollow sites (27) and the UPS results position the p_z orbital at 4.0 eV and the $p_{x,y}$ orbitals at 5.7 eV (28). The adsorption site of sulfur in the $(\sqrt{3}x\sqrt{3})R30°$ overlayer structure is not known but the suggestion has been made, based on UPS studies, that the S atom bonding site differs from the p(2x2) site (26) and that the orbital energy levels have inverted. The p_z orbital is at 3.8 eV and the $p_{x,y}$ orbital at 6.6 eV. The shifts are 2.5 and -1.9 eV respectively and are of the same magnitude as the the splitting in the two peaks that have been assigned to S atoms in differing binding sites on the Mo(100) surface. The work on the Ni(100) surface has focussed on the p(2x2) and c(2x2) overlayers in which the sulfur atoms are located in the fourfold hollows (29). In this case again there is a shift of energy levels from 4.2 eV (p_z) and 4.9 eV ($p_{x,y}$) in the p(2x2) structure to 5.6 eV (p_z) and 4.4 eV ($p_{x,y}$) in the c(2x2) structure. These shifts are somewhat smaller in magnitude than those observed on the Ni(111) surface but are appreciable and are certainly not associated with any change in adsorption

site. Furthermore, the large dispersion in the p_z orbital energy for the Ni(100) c(2x2) structure has been associated with S-S interactions, which are significant at the half monolayer coverage.

As mentioned above the magnitudes of the shifts in UPS peak positions attributed to changes in binding site are similar to those reported in the case of S on the Ni(111) surface. At the same time shifts induced by changes in overlayer structure and adsorbate-adsorbate interactions are considerable. In the case of S on the Mo(100) surface it would seem that the greatest changes in the UPS spectrum due to such interactions ought to appear in the coverage range immediately in excess of 0.5 monolayers since it is in this coverage regime that sulfur atoms having two nearest neighbours first appear. In fact, the greatest changes occur when the coverage exceeds 0.67 and an overlayer structure forms that can have atoms in two binding sites.

At the half monolayer coverage it is possible to resolve the spectrum into two peaks at 6.7 eV and 5.8 eV below the Fermi level, as shown in Fig. 3.16. As previously mentioned, sulfur atoms bound in fourfold hollow sites should give rise to two sets of molecular orbitals, one having 'a_1' and the other 'e' symmetry. Without angle resolving capability it is not possible to assign the observed peaks and it is clear from the above discussion the assignment cannot be based purely upon their relative positions. The splitting of 0.9 eV is similar to those observed on the Ni(100) and Cu(100) surfaces.

The sulfur 2P XP spectra at coverages in the same range as was used for the UPS measurements are shown in Fig. 3.17. As mentioned above the shift in binding energy on going from bulk sulfur to the chemisorbed monolayer is similar to that observed on comparison with MoS_2. The most

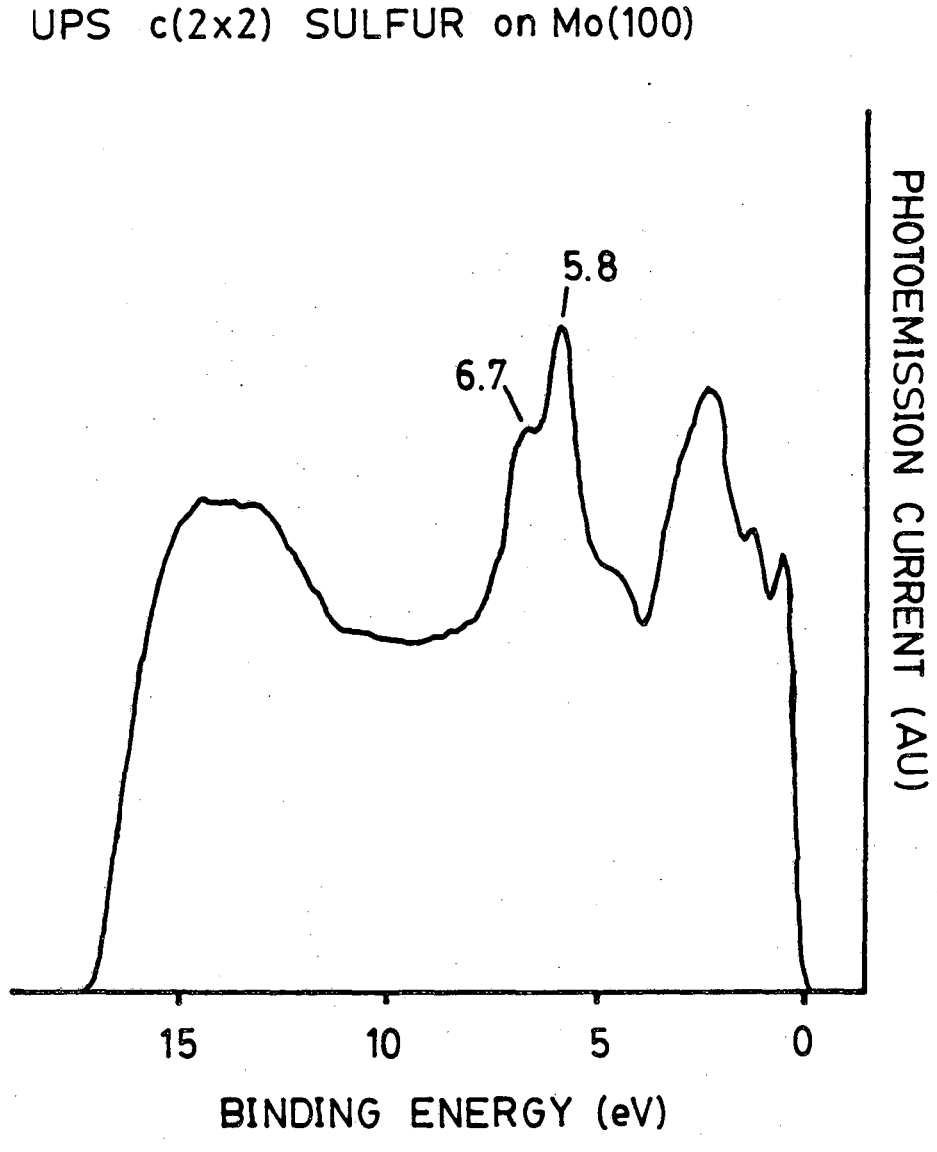

Fig. 3.16 He I UP spectra of sulfur on the Mo(100) surface.
θ_S = 0.5 c(2x2)

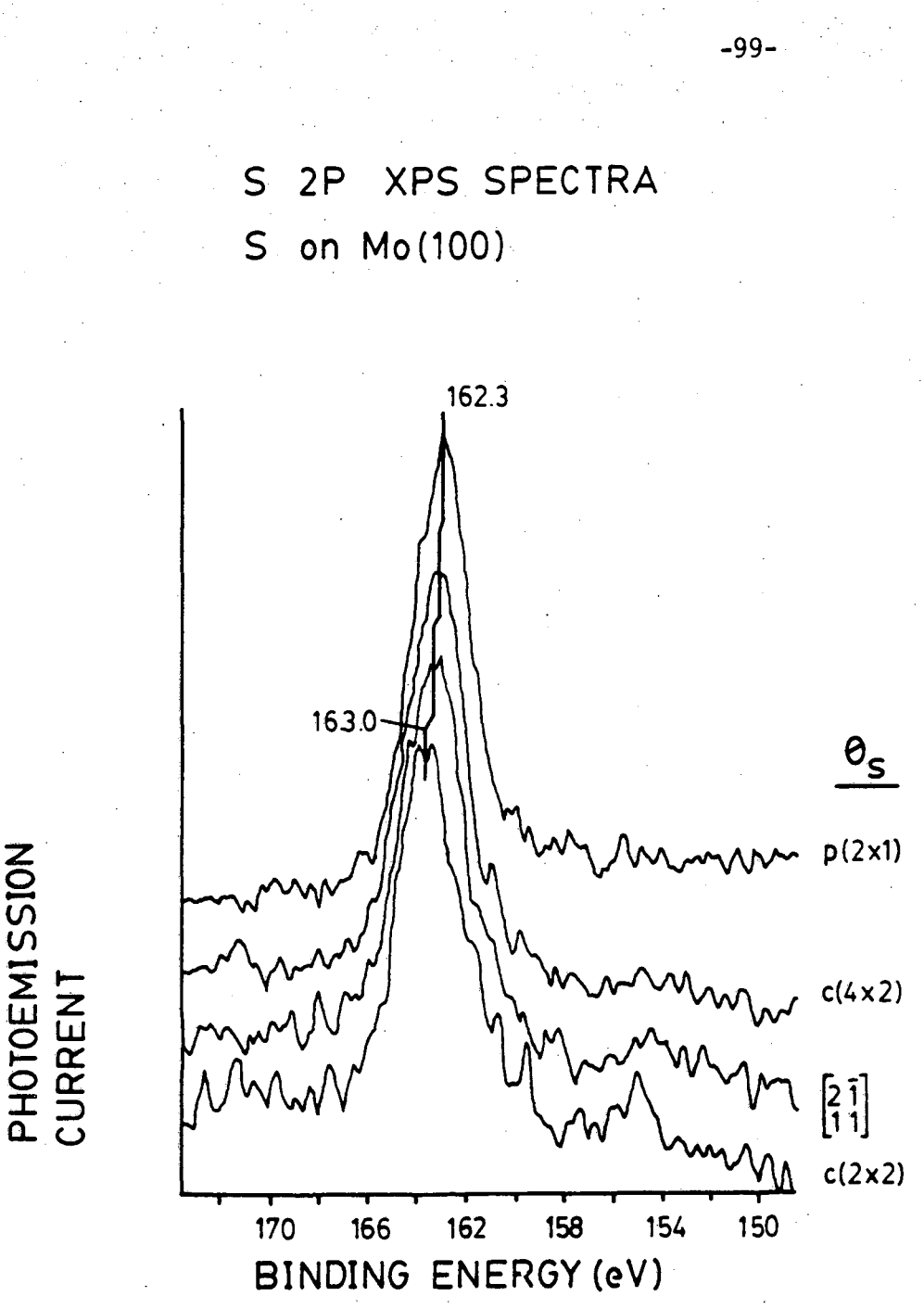

Fig. 3.17 S 2p XP spectra. Sulfur on Mo(100) vs. θ_S.

interesting feature of Fig. 3.17 is the monotonic decrease in binding energy with increasing coverage. This cannot be an effect of coverage dependent changes in the charge transfer between metal and adsorbate. The sign of the binding energy shift upon formation of the sulfur overlayer is indicative of electron transfer from the metal to the sulfur atoms. This is not unexpected given the relative electronegativities of sulfur (2.5) and molybdenum (1.8) (30). A simple model of the surface as a layer of dipoles suggests that with increasing coverage one should observe mutual depolarization as a result of either changes in bond length or decreases in the amount of charge transfer to the adsorbate. Decreases in charge transfer should result in a decrease in the core level binding energy with increasing coverage. The shift that is observed in this case is in the opposite direction.

One might hope to understand the effect in terms of a shift in binding site with coverage. If this were the case, however, an inhomogeneous broadening of the line would be expected on going from the low coverage structure to the p(2x1) monolayer structure in which the LEED results clearly implicate the existence of two binding sites. Such broadening is not observed.

A study of the adsorption of I on Ag has revealed a shift in the core level binding energy with coverage (31,32). This has been discussed and successfully modelled in terms of a direct, initial state interaction between the core electron and the field of surrounding dipoles. Such an interaction is repulsive and will increase with coverage resulting in a lowering of the electron binding energy.

Two studies have measured the work function of the sulfided Mo(100) surface. Maurice et. al. (8) report measurements in the coverage range

0.5-1.0 monolayers using the Kelvin method. The change in work function with respect to the monolayer covered surface varies linearly up to coverages of ~0.9-0.95. This behaviour implies a very low polarizability (33) of the Mo-S bond. The work of Baldinger et. al. (10) reports the work function, measured on a field emission tip, as a function of annealing temperature, having started with an initially fully sulfided surface. These are reported relative to the clean surface. In the temperature range 500K - 1200K there is little variation with $\Delta\phi$= 0.8-0.9V. From 1200K - 1300K there is a sharp drop to $\Delta\phi$= 0.2V and this value decreases slowly to reach zero at a temperature of 1800K. The very sharp change in work function implies a very sharp change in the surface dipole. This would be consistent with a change in sulfur atom binding site in this temperature range from one having a large dipole moment to one having a relatively smaller dipole moment. The results of Sec. 3.2 show that the temperature range from 1200K - 1300K is that in which the overlayer changes from the c(4x2) to the $\begin{vmatrix} 2 & \bar{1} \\ 1 & 1 \end{vmatrix}$ structure.

3.6 Discussion

The objective of this section is to come to some conclusion with respect to the structure of the sulfur overlayers. The question to be addressed is that of the coverage or structure at which the second binding site becomes occupied. A simple model considering two separate binding sites and pair interactions over lengths up to 3/2 the substrate lattice length can be used to discuss this problem. In addition, some conclusion must be reached with respect to the nature of the adsorbate-adsorbate interactions and the binding of sulfur to the metal.

The LEED results clearly indicate that at coverages ≤ 0.5 monolayers, sulfur is adsorbed in islands of c(2x2) structure in which the atoms occupy next-nearest neighbour fourfold hollows. At monolayer coverages the overlayer forms a p(2x1) lattice in which the sulfur atoms must occupy two distinct binding sites. Although the structure is not known it seems reasonable to restrict possibilities to high symmetry sites which leaves one atom adsorbed in the fourfold hollow and the other in a bridging position. The TDS work gives an estimate of 110 kcal/mole for the Mo-S bond strength at low coverages. At higher coverages ≥ 0.67 a second adsorption state is clearly identified having a lower desorption energy, in the range 75-90 kcal/mole. This evidence is insufficient to allow unambiguous identification of two distinct, simultaneously occupied binding sites, since the change in adsorption energy could be a result purely of adsorbate-adsorbate repulsion.

At this point it is helpful to present some model of the metal-sulfur and sulfur-sulfur interactions to facilitate the discussion of possible structures for the overlayer between coverages of 0.5 and 1.0 monolayers. We assume that sulfur atoms come into no closer contact than nearest neighbour distances, that they adsorb only in the hollow and/or bridging positions and that the adsorbate-adsorbate interactions depend only upon separation and not on binding site. With these restrictions in mind we can assign arbitrary values to the heats of adsorption and adsorbate-adsorbate interaction energies that a sulfur atom might feel.

A_4 - adsorption energy of S in hollow site

A_2 - adsorption energy of S in bridging site

B - nearest neighbour interaction energy

C - almost nearest neighbour interaction energy

D - next-nearest neighbour interaction energy

The values of A_4 and A_2 will be negative for exothermic heats of adsorption and the values of the interaction energies B,C, and D will be positive if they are attractive and negative if they are repulsive. Each of the pair configurations giving rise to these interactions are illustrated in Fig. 3.18. If the total energy for any particular overlayer configuration is dominated by these terms it is possible to calculate an average energy per atom for any proposed structure.

At low coverages it is known that the sulfur atoms adsorb in the fourfold hollows and that they coalesce into islands of c(2x2) structure. Within the terms of the model the energy per atom is given by

$$\bar{E} = A_4 + 2D.$$

Although each sulfur atom has four next-nearest neighbours the average interaction energy per atom is given by 2D avoiding double counting of pair interactions. Since these islands are the favoured structure at these coverages this configuration energy must be a minimum among possible configuration energies. Comparison with the energy of a c(2x2) structure in which the atoms are in bridging positions shows that

$$A_4 + 2D < A_2 + 2D$$

$$A_4 < A_2$$

the binding energy in the fourfold hollow is greater than that in the bridging position. The next comparison, between the energy of the very

BINDING SITE and PAIR INTERACTIONS

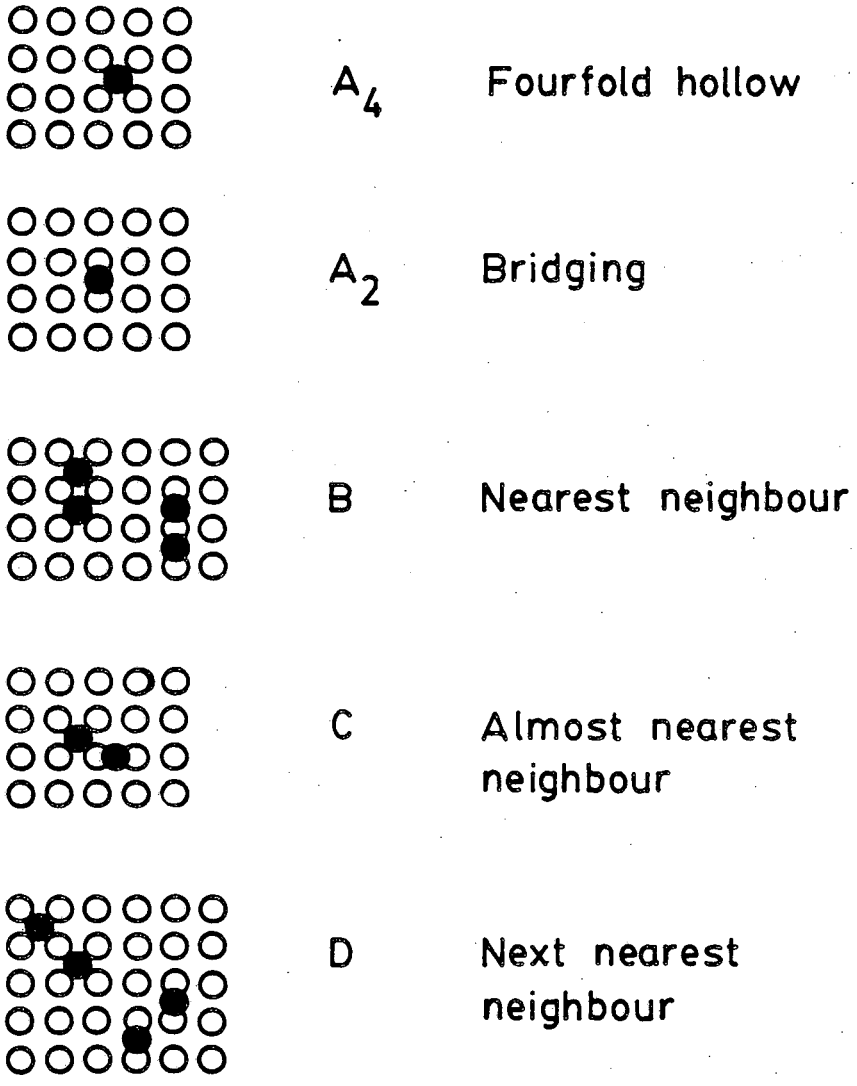

Fig. 3.18 Possible pair configurations of sulfur on the Mo(100) surface with binding sites restricted to fourfold hollows and bridging positions.

low coverage configuration of c(2x2) islands and one in which the atoms are randomly distributed on the surface in fourfold hollows, shows that

$$A_4 + 2D < A_4$$

$$D < 0$$

the next nearest neighbour interaction is attractive as previously suggested. If at low coverages (θ_S<0.5) the overlayer ordered into a p(1x1) lattice the configuration energy would be

$$A_4 + 2B + 2D$$

which, when compared with the c(2x2) configuration energy yields

$$B > 0$$

to show that nearest neighbour interactions are in fact repulsive. This might be expected given that the Van der Waals diameter of sulfur is 3.7 Å(11) while the interatomic separation between two atoms in nearest neighbour sites is 3.14Å.

We must now consider models containing atoms in both hollow and bridging positions to examine the pair interaction (C) between atoms in almost nearest neighbour configurations. At the half monolayer one can envision a p(2x2) lattice having one atom in the fourfold hollow and a second in a bridging site. This structure must have a higher total energy than the true structure.

$$2A_4 + 4D < A_4 + C + A_2 + C$$

$$A_4 - A_2 < 2C - 4D$$

Comparison of the monolayer p(2x1) structure with the possible p(1x1) structure having all atoms in the hollow sites yields

$$A_4 + A_2 + 2B + 4C < 2A_4 + 4B + 4D$$

$$-2B + 4C - 4D < A_4 - A_2 .$$

Combining the two expressions yields

$$-2B + 4C - 4D < 2C - 4D$$

$$C < B .$$

The almost nearest neighbour interactions are less repulsive than the nearest neighbour interactions.

We can now proceed to discuss possible structures for the $\begin{vmatrix} 2 & \bar{1} \\ 1 & 1 \end{vmatrix}$ and c(4x2) overlayer lattices in terms of the model described above. For the $\begin{vmatrix} 2 & \bar{1} \\ 1 & 1 \end{vmatrix}$ lattice the two possible structures are illustrated in Fig. 3.3 It is possible to construst a model in which all atoms sit in bridging positions but, since it is possible to translate such a structure by one half of one substrate lattice length and put all atoms in the favoured hollow sites while maintaining identical adsorbate-adsorbate interactions, this cannot be the lowest energy configuration. Of the two shown in Fig. 3.3 the energy of the structure having both atoms in hollow sites (a) is given by

$$2A_4 + 3B + 2D$$

and that of the other structure (b) by

$$A_4 + A_2 + 2B + 2C .$$

Without some knowledge of the magnitudes of each term it is not possible to determine which structure will be favourable.

In the case of the c(4x2) lattice it is possible to eliminate all structures having either two or three atoms per unit cell in bridging sites based on the arguments made above. Given this restriction the three remaining possibilities are those shown in Fig. 3.5 a,b,c. The configuration energies of the two containing atoms in bridging positions are

$$2A_4 + A_2 + 2B + 4C$$

and

$$2A_4 + A_2 + B + 4C + D$$

for (b) and (c) respectively. Given that $B>0$ and $D<0$ it is clear that (c) should be favoured over (b). The total energy for structure (a) is

$$3A_4 + 4B + 4D.$$

Comparing energies for these two possible remaining structures we get

$$3A_4 + 4B + 4D \rightarrow 2A_4 + A_2 + B + 4C + 2D$$

$$A_4 + 3B + 2D \rightarrow A_2 + 4C$$

Here again, without knowing the magnitudes of the interactions it is impossible to choose between the two structures. If, however, the nearest neighbour repulsion (B) is great enough structure (c) will be favourable and the c(4x2) structure will contain an atom in the bridging position.

From the discussion above it can be seen that as the sulfur coverage exceeds 0.5 monolayers, the surface overlayer shifts from the c(2x2) structure in which the adsorbate-adsorbate interactions are attractive

to structures in which the interactions become repulsive. This effect manifests itself in the appearance of a low temperature shoulder in the sulfur desorption spectra. At low coverages the metal-sulfur bond strength is about 110 kcal/mole, while at the higher coverages the repulsive interactions reduce this to ~75-90 kcal/mole. At the monolayer coverage the mutual repulsion between sulfur atoms is so great that the atomic binding site changes from the fourfold hollow to a mixture of sites, probably bridged and hollow, allowing the atoms to relax into a psuedo-hexagonal lattice.

The studies of sulfur adsorption showed that it was only possible to produce the monolayer p(2x1) structure by adsorption on an initially clean surface followed by annealing. Room temperature adsorption on a surface covered with a c(2x2) overlayer resulted in adsorption up to a coverage of θ_S=0.75, in a c(4x2) structure, after which it was not possible to deposit sulfur to higher coverages. Examination of the c(2x2) and $\begin{vmatrix} 2 & \bar{1} \\ 1 & 1 \end{vmatrix}$ structures that contain atoms only in fourfold hollows shows that they contain next-nearest neighbour fourfold hollows that are vacant. It is possible that these are the sites that are necessary for the dissociation of S_2. None of the possible c(4x2) structures has such sites available and it may be for this reason that it is not possible to dissociatively adsorb sulfur on this surface. If such is the case this is a further argument to suggest that the bridging sites are not occupied at the 2/3 monolayer coverage since, if they were, they would block the adjacent next-nearest neighbour hollow sites.

In the coverage range intermediate between 0.5 and 1.0 monolayers the adsorbate-adsorbate repulsion is continuously increasing. The LEED patterns produced during the adsorption of sulfur in the range 0.5 -

0.67 have been interpreted in terms of an increasing density of anti-phase boundaries between regions having c(2x2) structure (8). This growth model leads to a 2/3 monolayer structure in which all atoms occupy hollow sites. The adsorption studies of S_2 on the sulfided Mo(100) surfaces suggest that an adsorption site consisting of two, next-nearest neighbour, hollow sites is needed to dissociate S_2. The fact that sulfur will adsorb at room temperature on the surface sulfided to a coverage of 2/3 monolayer suggests that this type of site is still present at this coverage and that the bridging sites are not occupied at this coverage. The appearance of a low binding energy peak in the UP spectrum of the surface at 3/4 monolayer coverage and the low temperature desorption peak in the sulfur TD spectrum suggest that at this coverage the high coverage binding site is being populated. Studies of the hydrogenation of sulfur from the surface (Chapter 6) also show that there is a drastic change in the nature of the Mo-S bond at the transition from θ_S=0.67 to θ_S=0.75.

3.7 References

1. L. Peralta, Y. Berthier, J. Oudar, Surf. Sci., 55 (1976) 199
2. J.M. Wilson, Surf. Sci., 59 (1976) 315
3. C.S. Zhang, A.J. Gellman, M.H. Farias, G.A. Somorjai, submitted to Mat. Res. Bull.
4. J.M. Wilson, Surf. Sci., 53 (1975) 330
5. L.J. Clarke, Surf. Sci., 102 (1981) 331
6. M. Salmeron, G.A. Somorjai, R.R. Chianelli, Surf. Sci., 127 (1983) 526
7. M.H. Farias, A.J. Gellman, G.A. Somorjai, R.R. Chianelli, K.S. Liang, Surf. Sci., 140 (1984) 181
8. V. Maurice, L. Peralta, Y. Berthier, J. Oudar, Surf. Sci., 148 (1984) 623
9. J.M. Wilson, Surf. Sci., 57 (1976) 499
10. Th. Baldinger, E. Bechtold, private comm.
11. L. Pauling, The Nature of the Chemical Bond, p.255-260, Cornell Univ. Press, (1960), 3rd ed. Ithaca, NY
12. T.E. Felter, R.A. Barker, P.J. Estrup, Phys. Rev. Lett., 38(20) (1977) 1138
13. S.C. Ying, L.D. Roelofs, Surf. Sci., 125 (1983) 218
14. L.J. Clarke, Surf. Sci., 91 (1980) 131
15. A. Ignatiev, F. Jona, H.D. Shih, D.W. Jepsen, P.M. Marcus, Phys. Rev. B., 11(12) (1975) 4787
16. E.A. Wood, J. Appl. Phys., 35 (1964) 1306
17. H.K.A. Kan, S. Feuerstein, J. Chem. Phys., 50(8) (1969) 3618
18. G. Popov, E. Bauer, Surf. Sci., 122 (1982) 433

19. A. Redondo, Y. Zeiri, W.A. Goddard III, Phys. Rev. Lett., 49(25), (1982) 1847

20. S.L. Weng, E.W. Plummer, Sol. State Comm., 23 (1977) 515

21. S.L. Weng, Phys. Rev. Lett., 38 (1977) 434

22. S.L. Weng, E.W. Plummer, T. Gustafsson, Phys. Rev. B., 18(4) (1978) 1718

23. J.E. Inglesfield, Surf. Sci., 76 (1978) 335

24. J.M. Dyke, L.Golob, N.Jonathan, A. Morris, J. Chem. Soc. Farad. Trans. 2, 71(5) (1975) 1026

25. Handbook of X-ray Photoelectron Spectroscopy, G.E. Muilenberg (ed.) Perkin Elmer Corp. (1978) Minn.

26. T.W. Capehart, C.W. Seabury, G.W. Graham, T.N. Rhodin, Surf. Sci., 120 (1982) L441

27. J.E. Demuth, P.M. Marcus, D.W. Jepsen, Phys. Rev. B, 11 (1975) 1460

28. T.W. Capehart, T.N. Rhodin, Surf. Sci., 83 (1979) 367

29. J.E. Demuth, D.W. Jepsen, P.M. Marcus, Phys. Rev. Lett., 31 (1973) 540

30. L. Pauling, The Nature of the Chemical Bond, p. 93, Cornell Univ. Press (1960) 3rd ed. Ithaca NY

31. S.B. DiCenzo, G.K. Wertheim, D.N.E. Buchanan, Phys. Rev. B, 24(10) (1981) 6143

32. S.B. DiCenzo, G.K. Wetheim, D.N.E. Buchanan, Surf. Sci. 121 (1982) 411

33. J. Topping, Proc. Roy. Soc. (Lond.) A, 114 (1927) 67

34. M.W. Roberts, C.S. McKee, Chemistry of the Metal Gas Interface, Clarendon Press, Oxford, England, 1978

Chapter 4 - The Chemistry of Thiophene on the Mo(100) Surface

4.1 Introduction

Thiophene has been chosen as a model compound for this study of the hydrodesulfurization process due to the fact that it has been used in many studies over dispersed catalysts. Many of the sulfur containing compounds in crude petroleum stocks are derivatives of thiophene and so these have been chosen as standards for the determination of the activity of industrial catalysts. The most commonly used are dibenzothiophene, benzothiophene, and thiophene. In general, dibenzothiophene is more easily desulfurized than benzothiophene which, in turn, is easier to desulfurize than thiophene (1). In this work thiophene has been chosen for a number of reasons. As the smallest of the three, spectroscopic studies can be most readily interpreted. Since the resolution of the electron spectroscopies used in surface analysis is far below that of their gas phase counterparts, this is an important consideration. The catalyst used in this work is a Mo(100) single crystal having a very low total surface area ($\sim$1 cm^2) and thus, in order to obtain measurable rates of HDS, the model compound chosen must be relatively easy to desulfurize. Finally, thiophene is an ideal choice because it has a relatively high vapour pressure at room temperature ($\sim$80 torr) (2), allowing high pressure catalytic reactions to be performed without requiring heating of the entire reactor loop.

The goal of the work presented in this chapter is to understand the chemistry of thiophene adsorbed on well characterized, clean and sulfided Mo(100) single crystal surfaces. Experiments have been performed entirely under UHV conditions and have, in general, involved

the adsorption of thiophene on a prepared surface followed by spectroscopic analysis, either immediately after the adsorption or after heating to induce some reaction. These spectroscopies yield information about the adsorption/desorption kinetics, reaction kinetics, and the nature of intermediate species produced during surface reactions. These have been studied over both the clean metal surface and as a function of sulfur coverage.

Although there are now a number of studies in progress of the chemistry of thiophene on metal surfaces, only five have been completed to date (3,4,5,17,18). The adsorption and desulfurization of thiophene on the Pt(111) surface was studied using near-edge x-ray absorption fine structure (NEXAFS), XP and HREEL spectroscopies (4). This study suggested that the thiophene molecule adsorbs in a compressed monolayer at 150K with its ring tilted away from the surface. Heating to 180K induced some molecular desorption and resulted in a surface covered by a monolayer of thiophene pi-bonded with its ring parallel to surface. Further heating induced desulfurization at temperatures of ~290-350K but left the hydrocarbon chain intact in the form of a Pt metallocycle, slightly tilted from the surface. The desorption and decomposition of thiophene and several substituted thiophenes has also been studied using TDS over a number of Group VIII metal surfaces (5). Again a metallocyclic intermediate was suggested for some metals. This was based purely on the observation of selective dissociation of the α-CH bonds during the initial stages of decomposition over Ni, Ru, and Os. Such regiospecific bond breaking was not, however, observed in the case of the Pt(111) surface in which there is some additional evidence for the existence of a metallocycle. It is certainly possible that the

decompostion kinetics of the metallocycle on the Pt(111) surface may differ from those on other surfaces and that the results are compatible. On the Cu(111) surface the thiophene monolayer was studied using angle resolved UV photoemission spectroscopy, the conclusion being that on this metal surface the molecule is pi-bonded with its ring parallel to the surface after adsorption at room temperature (17). Finally, a very recent study of thiophene adsorption on the Ni(111) surface concluded that, upon heating, the adsorbed thiophene polymerized (18). This concl- was based upon the observation of a desorbing species having mass 69 which was assigned to a five carbon olefin. In addition, IR absorption spectra revealed a feature at 2960 cm^{-1} assigned to a paraffinic C-H stretching mode. It seems unlikely that a polymerized species exists under catalytic conditions since the HDS of thiophene produces only four carbon atom products and it is difficult to understand why a polymeric species should undergo such highly selective hydrogenolysis.

4.2 The Adsorption/Desorption of Thiophene on the Mo(100) Surface

The TD spectra of thiophene adsorbed on the Mo(100) surface have contributions from reversibly adsorbed thiophene, which desorbs molecularly, and H_2 which results from the decomposition of a fraction of the thiophene that is adsorbed irreversibly. Fig. 4.1 shows the molecular desorption spectra after exposure of the clean surface to several different doses of thiophene in the range 0.1L - 15L. These show two high temperature peaks at 360K and 230-290K and a low temperature peak at ~170K. The highest temperature desorption peak has been associated with very small amounts of carbon contamination that could not be

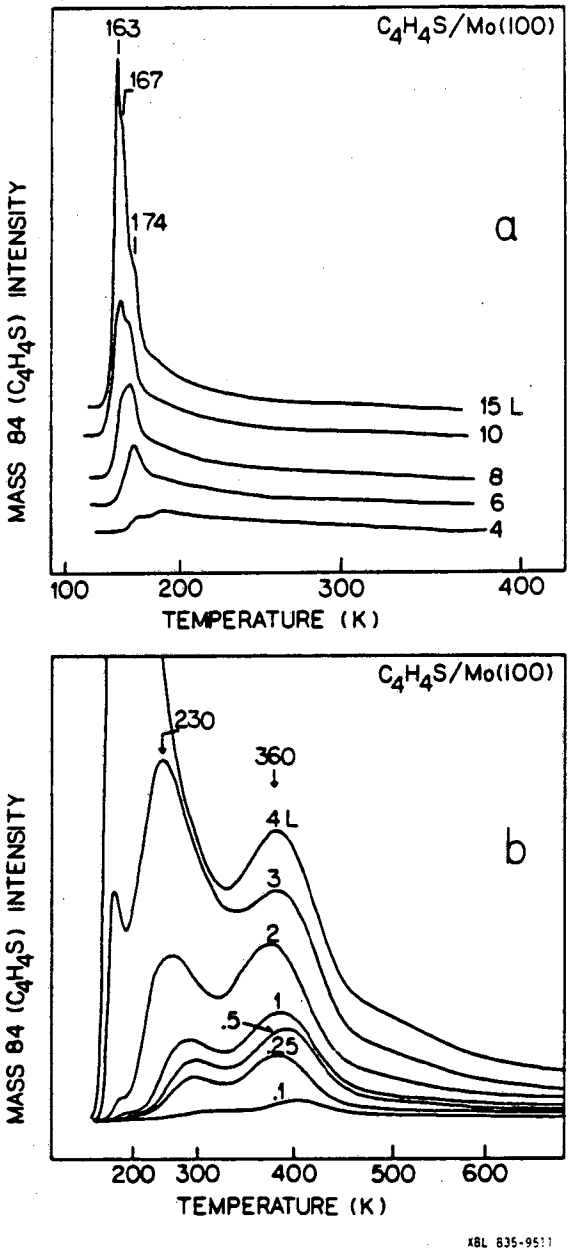

Fig. 4.1 Thermal desorption spectra of thiophene from the clean Mo(100) surface over several different exposures.

completely removed from the surface at the time of these experiments (6). The peak at intermediate temperatures, however, results from desorption from the metal surface. As the thiophene exposure is increased, the area under this peak increases until it saturate at a total exposure of ~3L. The temperature of the peak maximum decreases with exposure from 290K at very low coverages to 230K at saturation. The lowest temperature desorption peak at T < 180K appears at exposures greater than 3L. At the highest exposure, this feature shows a peak at 163K with shoulders at 167K and 174K which appear to grow in sequentially with exposure starting with the 174K peak at 3L. For exposures in excess of 15L the 163K peak grows indefinitely.

The peak at 230-290K has been assigned to reversible molecular adsorption of thiophene to the metal surface. A shift of the desorption peak maximum with coverage can be attributed either to second order desorption kinetics or to a coverage dependent desorption energy (7,19). Given that thiophene adsorbs molecularly, it seems unlikely that the desorption is a second order process. It is much more likely that the desorption energy is coverage dependent due to adsorbate-adsorbate interactions. Assuming first order desorption kinetics and a pre-exponential factor of 10^{13} sec^{-1}, we find that the desorption energy is 16 kcal/mole at low coverages and drops to 13 kcal/mole at the monolayer coverage. The monolayer coverage is believed to occur for exposures of 3L at which the peak area saturates and the low temperature feature begins to appear.

The desorption feature at 163K grows with exposure beyond the range investigated and is due to desorption of multilayers of thiophene. Desorption of the first multilayer (thiophene on thiophene) appears at

174K after an exposure of 3L. After an 8L exposure the first multilayer becomes saturated and a lower temperature peak appears at 167K. For exposures of >15L the lowest temperature peak appears at 163K. The high temperature shoulders on this peak are the result of first and second layer desorption that are influenced by the metal substrate.

4.3 Thiophene Decomposition on Mo(100)

As previously mentioned, a large fraction of the thiophene is irreversibly adsorbed to the Mo(100) surface. Heating of the crystal results in decomposition yielding H_2 desorption into the vacuum and carbon and sulfur deposition on the surface. There is no self-hydrogenation to produce hydrocarbon products that can desorb. In the case of the Pd(111) surface, thiophene decomposition was observed to yield butadiene under UHV conditions and, when co-adsorbed with hydrogen, butenes (8). Apparently, the hydrogenation reactions on Mo are more difficult than on Pd and high hydrogen pressures are necessary if these reactions are to compete with total decomposition.

Fig. 4.2 shows the desorption of hydrogen from the surface during the decomposition of irreversibly bound thiophene. At low initial coverages, there is no molecular desorption and the hydrogen desorption occurs at 340K. Comparison of this desorption peak with the desorption of hydrogen from the clean surface (Fig. 4.3) (9,10) shows that this process is desorption rate limited and appears to result from hydrogen bound in the β_2 state. It appears that the presence of carbon and sulfur on the surface blocks the β_3 hydrogen adsorption state that would yield a desorption peak at 450K. At higher thiophene exposures, a lower

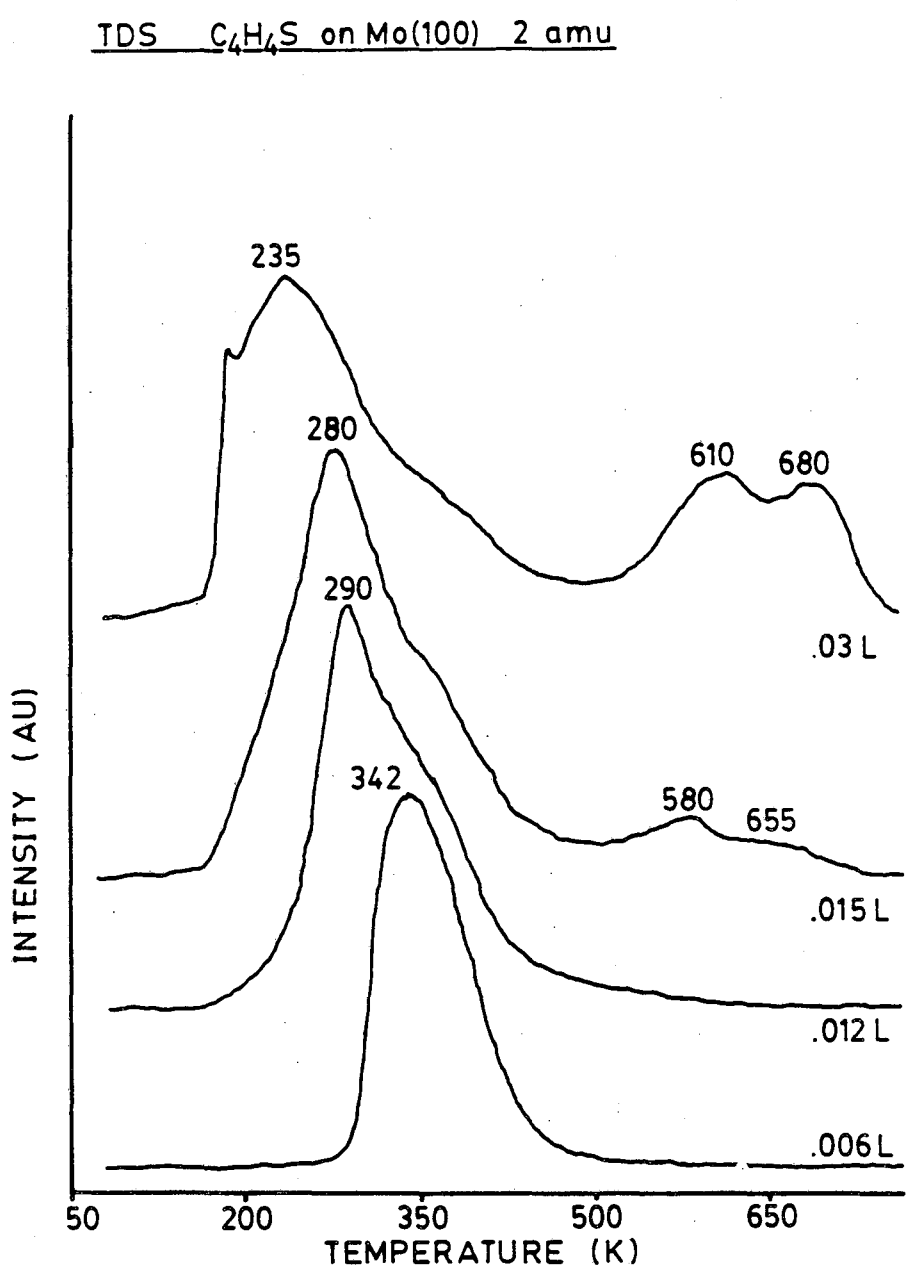

Fig. 4.2 The H_2 desorption spectra resulting from the decomposition of thiophene on the clean Mo(100) surface.

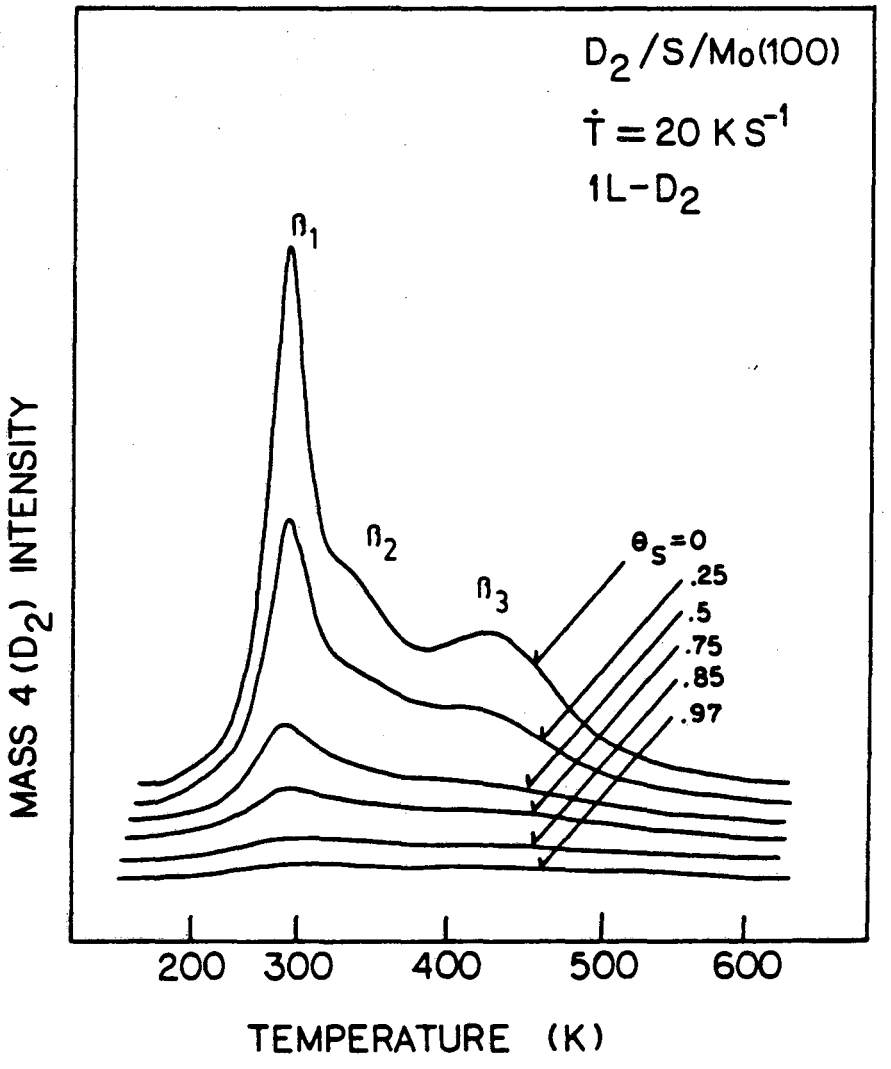

Fig. 4.3 Thermal desorption spectra of D_2 from the clean Mo(100) surface over several different exposures.

temperature desorption feature appears that is reminiscent of the β_1 desorption peak at 290K in Fig. 4.3, but which shifts to temperatures of 230K with increasing exposure, far below the that of the β_1 state The presence of carbon, sulfur and thiophene deposits weakens the metal-hydrogen bond to such an extent that desorption is occuring at temperatures below those at which hydrogen would desorb from the clean metal surface. It is known that coverages of between 0.25 and 0.5 monolayers of sulfur will completely block hydrogen adsorption at ~150K (9).

In addition to the low temperature decomposition and desorption processes, two high temperature hydrogen desorption peaks appear at 620K and 680K after high thiophene exposures. These features appear at temperatures far higher than those at which hydrogen desorbs from the clean surface and thus must originate from C-H bond breaking processes. It is apparent that after starting with high coverages of thiophene, the decomposition process leads to hydrocarbon species that are stable on the surface to temperatures much higher than those that can be reached after starting with a low thiophene coverage on a clean surface.

Figs. 4.4, 4.5, and 4.6 show the desorption spectra of H_2, HD and D_2 from surfaces exposed to αd_2-$C_4D_2H_2S$ in increasing doses. The exposures listed are much lower than those of Fig. 1 due differences in the dosing apparatus. At low coverages, the low temperature peak at 340K shows no selectivity towards either H_2 or D_2. This is not surprising since desorption is the rate limiting step in the decomposition/desorption process. At high coverages, however, there is clearly some selective decomposition pathway that favours α-CD bond breaking at low temperatures. The desorption peak at 230K is clearly dominated by D_2 while the peak at 340K is dominated by H_2. This selectivity supports

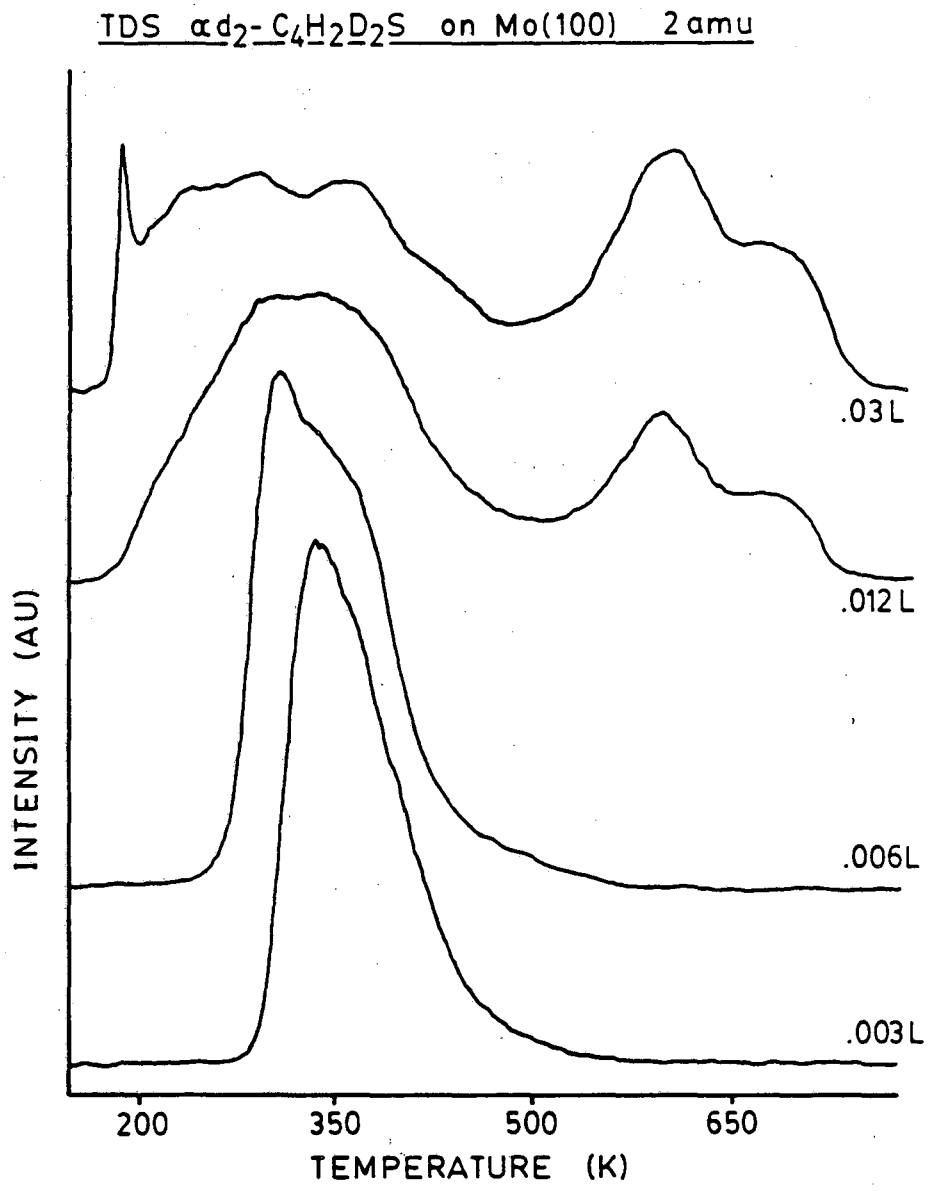

Fig. 4.4 The H_2 desorption spectra resulting from the decomposition of αd_2-$C_4D_2H_2S$ on the clean Mo(100) surface.

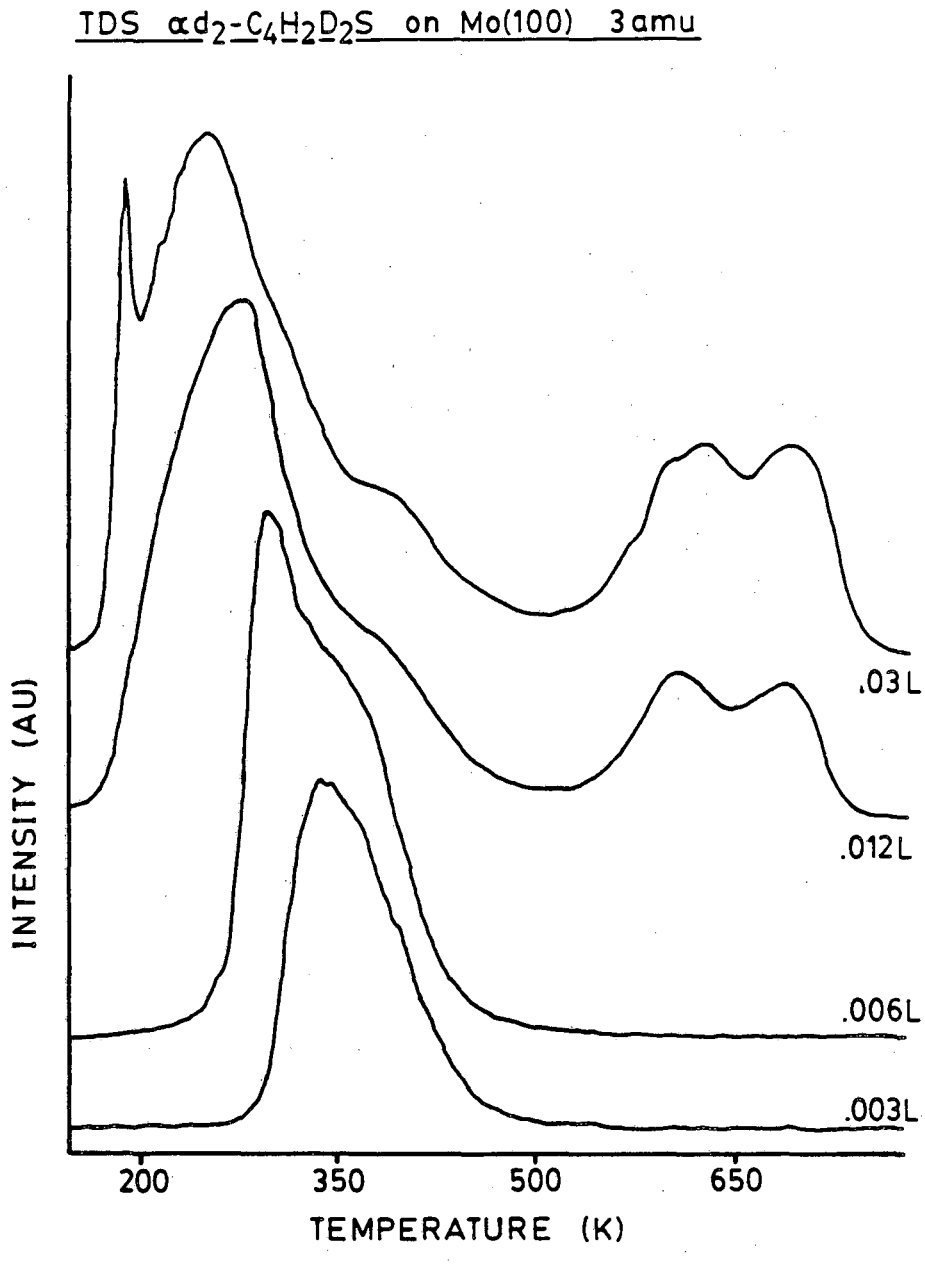

Fig. 4.5 The HD desorption spectra resulting from the decomposition of αd_2-$C_4D_2H_2S$ on the clean Mo(100) surface.

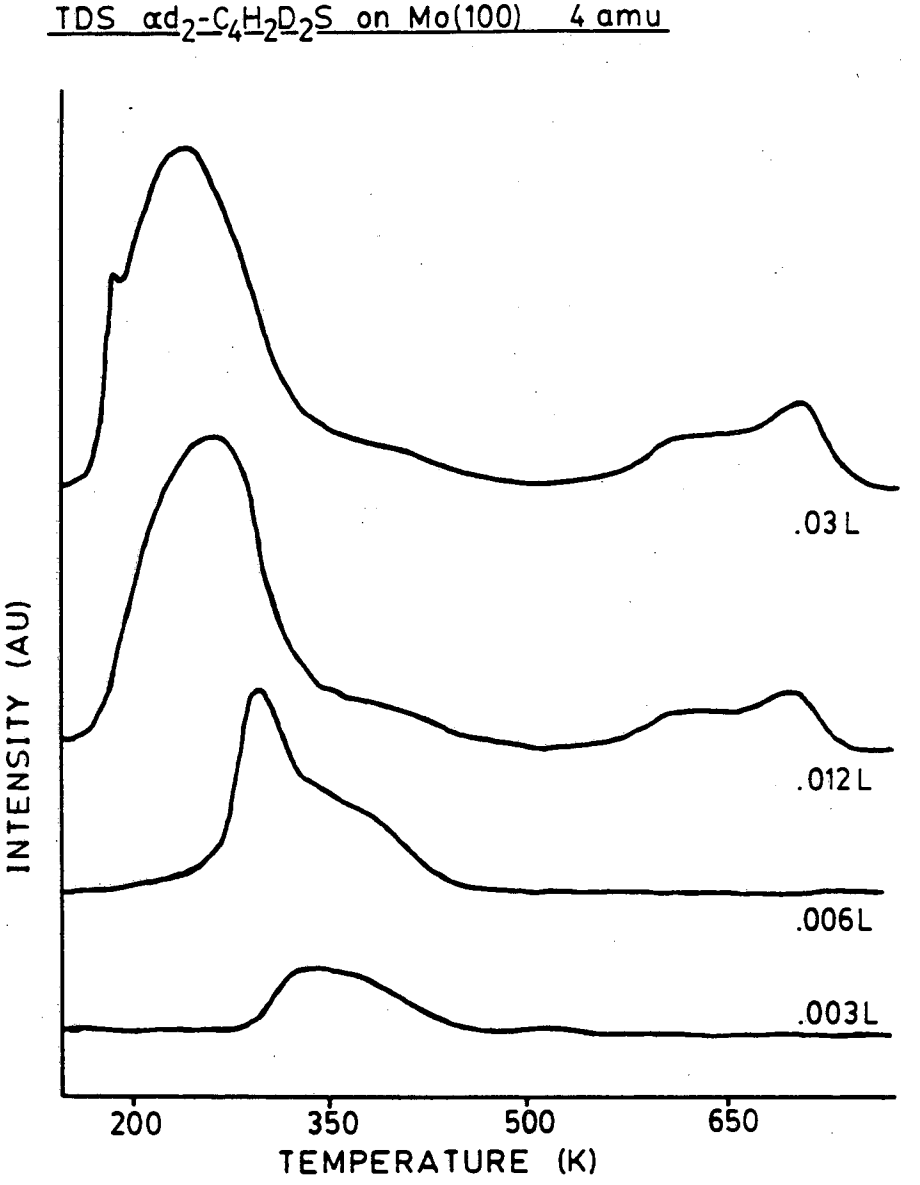

Fig. 4.6 The D_2 desorption spectra resulting from the decomposition of αd_2-$C_4D_2H_2S$ on the clean Mo(100) surface.

the suggestion made above, that at these high thiophene coverages, the low temperature hydrogen evolution is rate limited by decomposition processes. Furthermore, the fact that the α-CD bonds dissociate at lower temperatures than the β-CH bonds suggests an adsorption configuration in which their interaction with the surface is greater.

The high temperature hydrogen desorption peaks at 620K and 680K show selectivity opposite to that of the low temperature peaks. The 620K peak is dominated by H_2 while the 680K peak is dominated by D_2. Apparently this second decomposition route, induced by high thiophene coverages, differs from that at low coverages on the clean surface. There is some indication that these peaks may be induced by the presence of carbon as they increase in size with the initial addition of carbon to the surface (6). It is possible that the deposition of carbon onto the surface, during the low temperature decomposition process, at some point blocks this pathway inhibitting further decomposition until higher temperatures are reached.

To this point it has been assumed that thiophene decomposition in both temperature regimes is complete and that two different mechanisms are being followed. Given the sequence of hydrogen desorption, D_2-H_2-H_2-D_2, it would seem reasonable to suggest a mechanism of dehydrogenation starting with the α-CD bond at position 2 and proceeding in a sequential fashion through positions 3,4 and 5. The relative areas under the peaks argues against such a mechanism since each ought to be of the same height if this mechanism were correct. Fig. 4.7 shows the S 2P XP spectrum taken at various temperatures throughout the decomposition process. The spectra clearly exhibit two peaks, a high binding energy feature (164.3 eV) from sulfur bound in the thiophene ring (11)

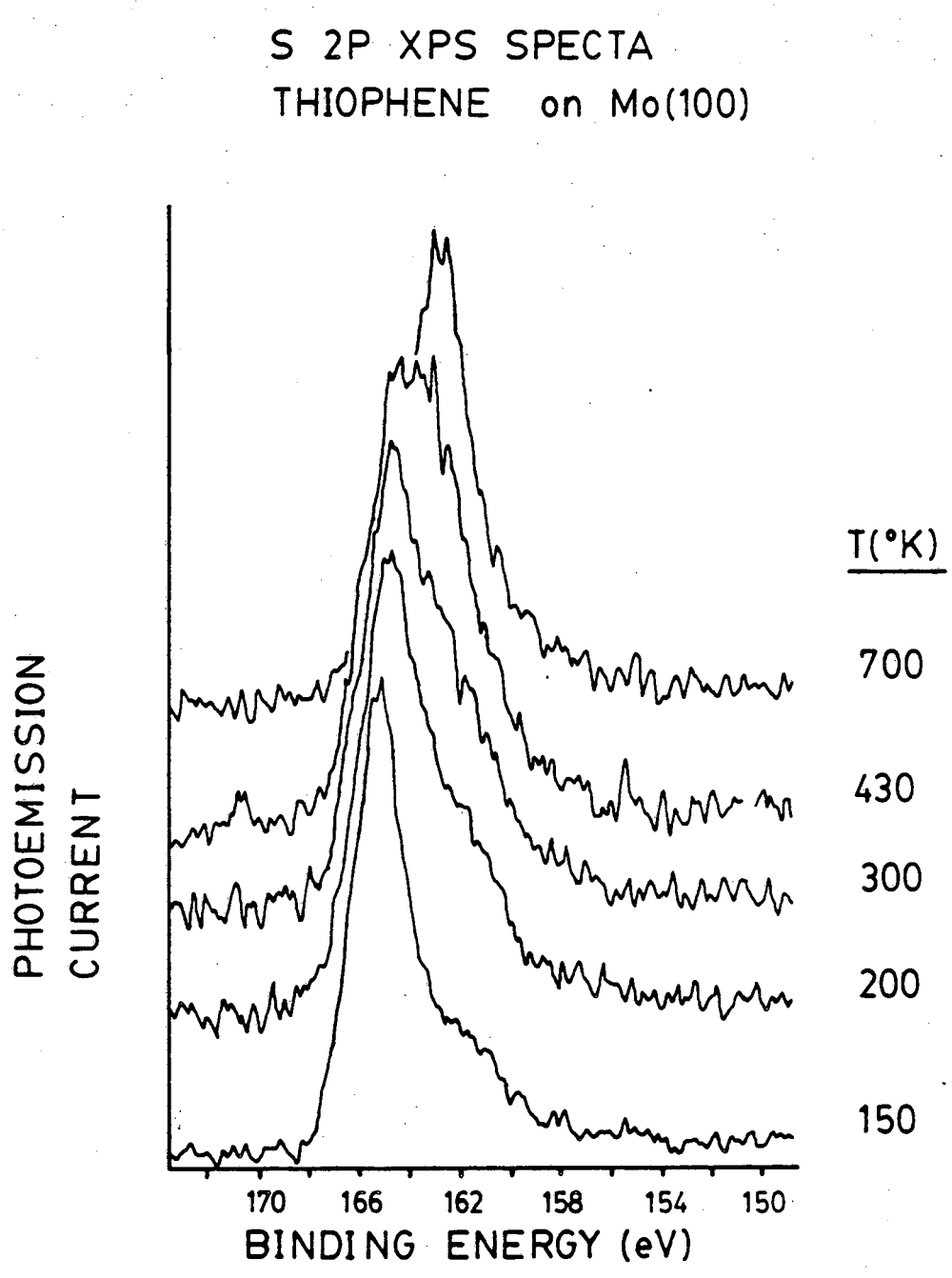

Fig. 4.7 S 2P XP spectra taken during the decomposition of thiophene on the Mo(100) surface.

and a lower binding energy feature (162.3 eV) from sulfur bound directly to the metal surface. It is clear that throughout a wide temperature range thiophenic sulfur is present on the surface, even at 430K, well past the molecular desorption temperature. The S 2P binding energy is strongly dependent upon its local chemical environment, ranging between 160 eV - 169 eV (11). Fig. 4.8 gives the 2P binding energies in a number of sulfur containing organic compounds. In the case of sulfur atoms in saturated environments of the form R-S-R the binding energies range from 162.2 eV - 163.5 eV while in the aromatic thiophene ring it is 164.1 eV. The position of the high binding energy S peak observed during thiophene decomposition on the Mo(100) surface ranges from 164.3 eV at 150K to 163.9 eV at 430K. This shift may be partly the result of a changing work function during the decomposition from 3.9 eV to 4.4 eV. Nevertheless the absolute position of the peak remains characteristic of a sulfur atom bound in the thiophene ring These data strongly support a mechanism in which some thiophene is decomposing throughout the entire temperature range rather than one in which a single species is present on the surface at any given temperature that is undergoing a stepwise dehydrogenation. There must be several species present on the surface at any one time since at the intermediate temperatures there is sulfur, carbon, some sulfur containing hydrocarbon and possibly some other hydrocarbon species that are in some stage of partial dehydrogenation.

Sulfur 2P Binding Energy in Various Compounds

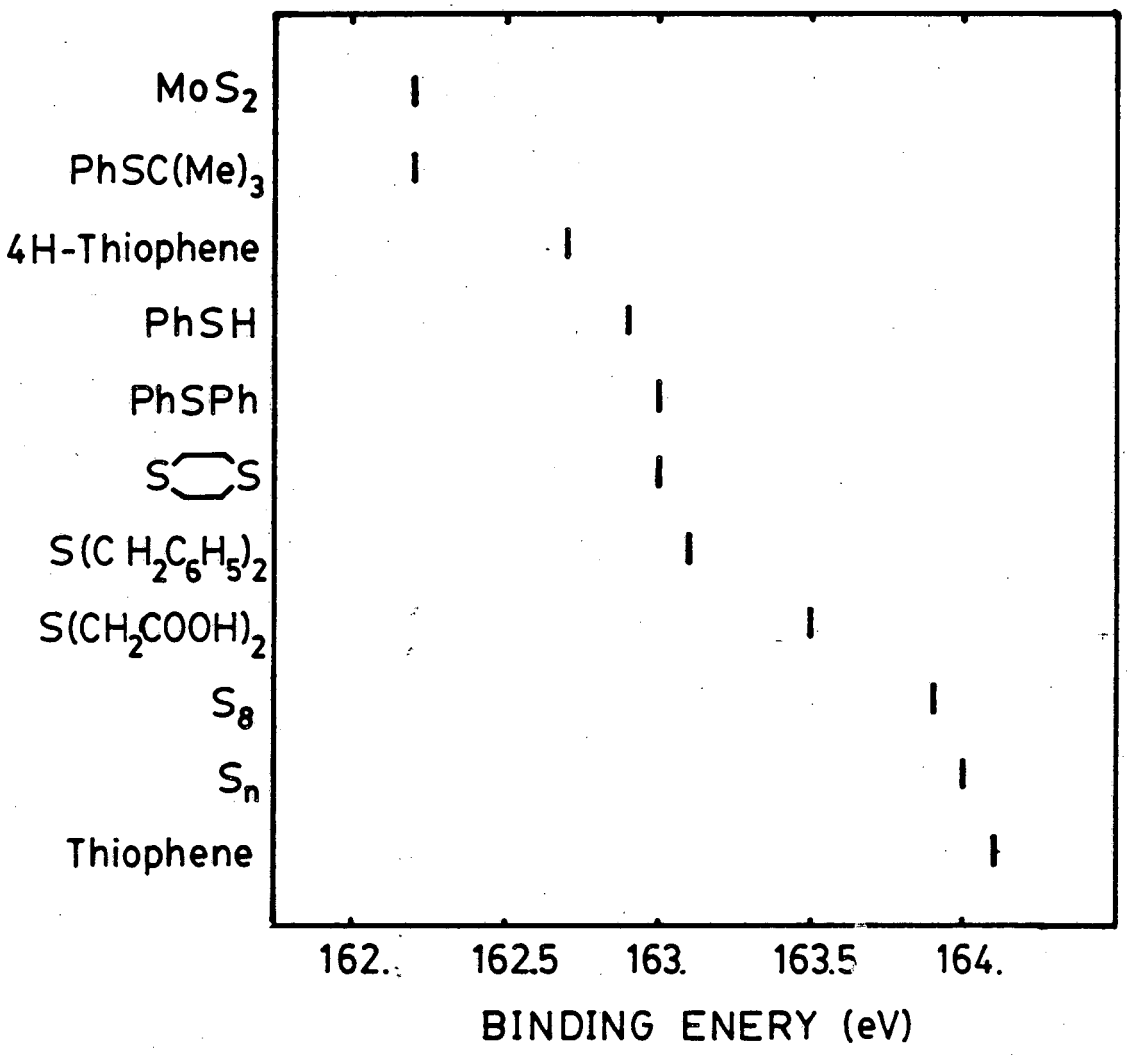

Fig. 4.8 2p binding energies of sulfur atoms in various compounds (11,22).

4.4 Bonding and Coordination of Thiophene to the Mo(100) Surface

UPS and HREELS have been used to study the bonding configuration of the irreversibly adsorbed thiophene molecule. At this point XPS has shown the existence of a thiophene-like molecule present to high temperatures (>430K) that decomposes in the range 600-680K. The TDS of αd_2-$C_4D_2H_2S$ suggests a configuration in which low temperature dehydrogenation favours the α-CD bond. The dehydrogenation reaction at high temperatures is clearly via a different route.

Fig. 4.9 shows the UP spectrum of multilayer thiophene adsorbed on the surface. The photoemission features are poorly resolved but match well with the expected relative positions of the gas phase peaks (12, 20). The work function of this surface is 3.9V. The $1a_2(\pi)$ orbital ionization potential lies at 4.1 eV below the Fermi edge of the metal, or 8.0 eV below the vacuum level while the gas phase I.P. of this orbital is 8.9 eV. We attribute the 0.9 eV difference to relaxation effects in the metal. After heating the crystal to 200K to remove the multilayer the major features of the thiophene photoemission spectrum are still present (Fig. 4.10) but with additional shifts in position due to increased screening by the metal (13). The manifold of the CCσ, CSσ, lowest lying π, and non-bonding orbital ($6b_2$,$9a_1$,$5b_2$,$1b_1$,$8a_1$) photoemission features has been drawn into Fig. 4.10 in the 5.5-9.0 eV binding energy region of the spectrum. It is clear that in order to obtain a good fit with the levels of the multilayer spectrum an increase of ~0.9 eV in relaxation energy must be assumed. Similar shifts of 0.4, 1.7, and 0.3 eV are reported for benzene, acetylene and ethylene, respectively, on comparison of the condensed multilayer spectra with

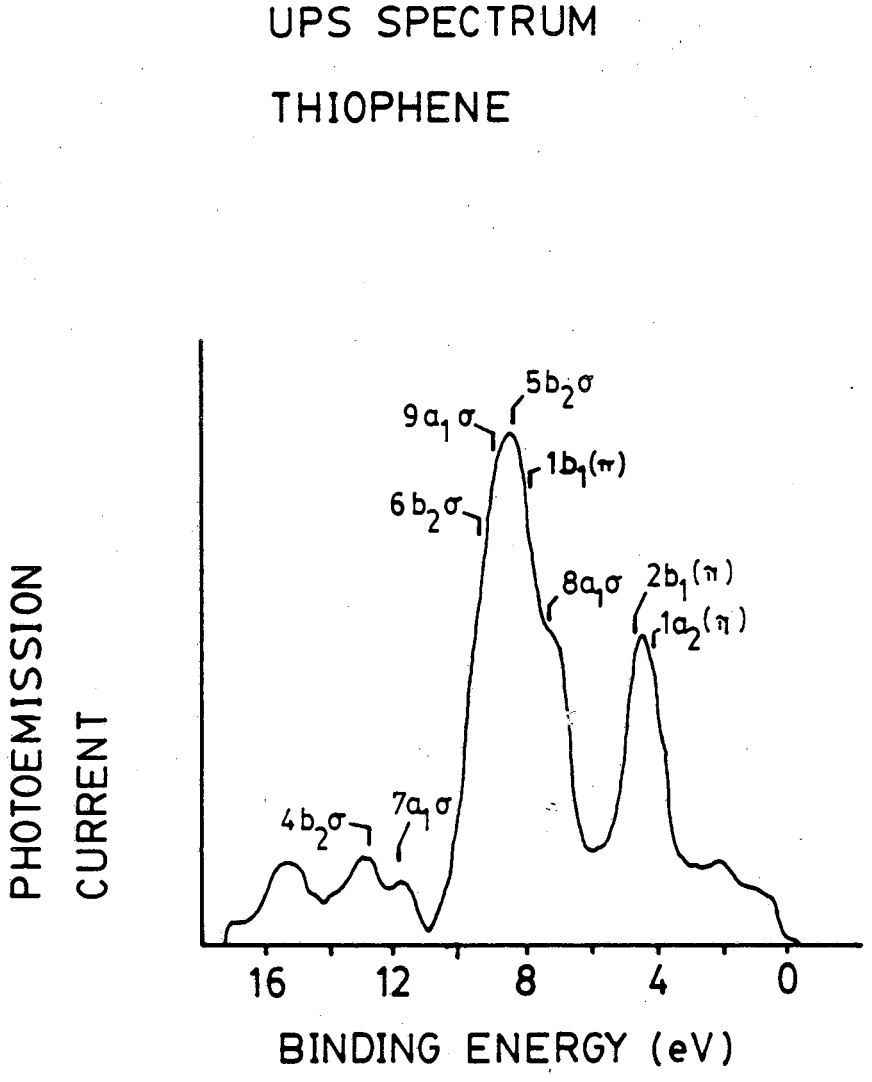

Fig. 4.9 He I UP spectrum of condensed thiophene. T ≈ 125K.

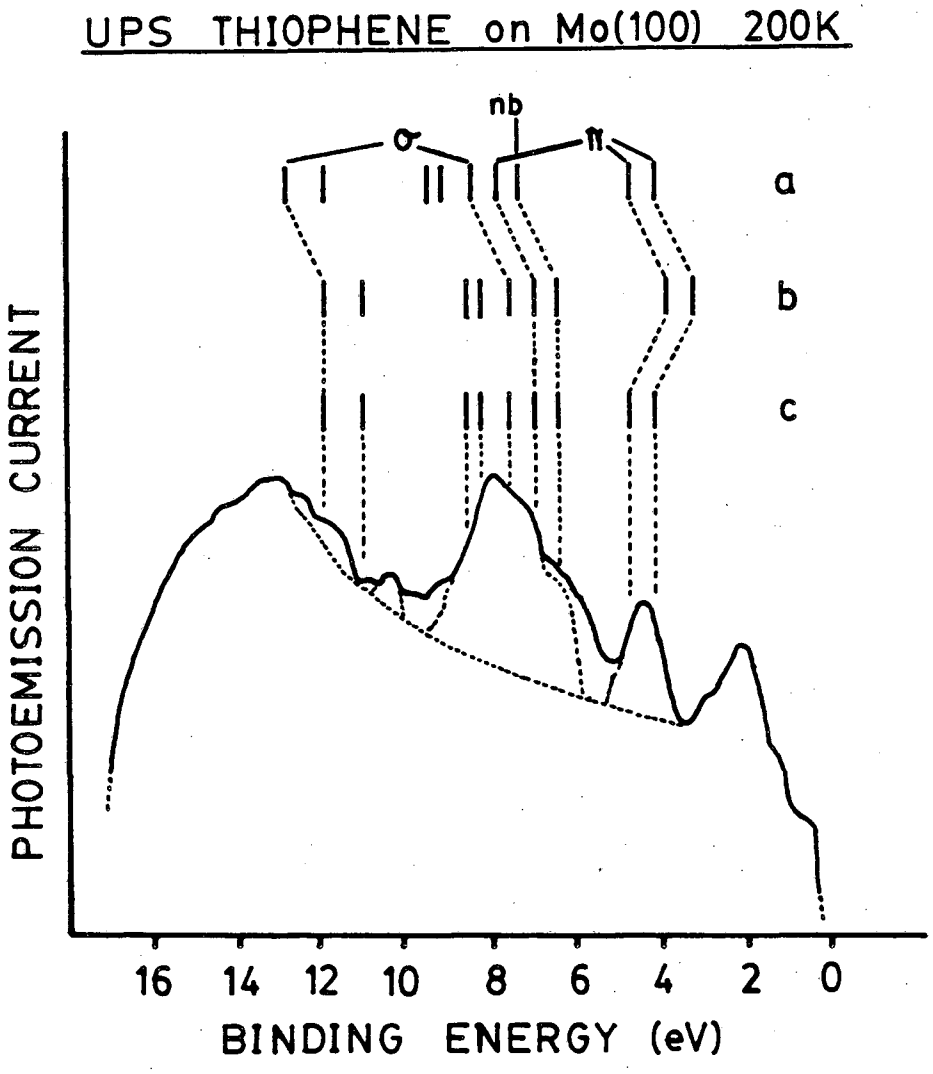

Fig. 4.10 He I UP spectra of chemisorbed thiophene on the Mo(100) surface after heating to 200K. a) Orbital energy levels of the condensed multilayer phase. b) Orbital energy levels shifted to lower binding energy due to increased screening by the metal after desorbing the multilayer. c) Stabilization of the highest lying π-orbitals resulting from bonding interactions with the metal.

those of the chemisorbed monolayer on the Ni(111) surface (13). In addition to the relaxation energy shift, the high lying $2b_1$ and $1a_1$ π orbitals undergo a stabilizing shift in the opposite direction of about -0.9 eV due to bonding overlap with the surface. Such bonding points to a configuration in which the thiophene ring is nearly parallel to the surface. The fate of the $1b_1$ π orbital is unclear. If it is stabilized by bonding with the surface in the same manner as the high lying π orbitals it must be shifted under the manifold of the σ orbital photoemission features. Since it is at a lower energy than the highest lying π orbitals it may be that it does not undergo the same interaction with the metal and is not stabilized by bonding, as is depicted in Fig. 4.9.

There are two region of the spectrum that deserve further discussion. XPS results have shown that even at 200K there is some dissociation of thiophene and some sulfur deposited on the metal. This sulfur is expected to give rise to some photoemission features at about 6 eV binding energy and thus the low binding energy shoulder on the manifold of features about 5.5-9.0 eV must be attributed in part to this sulfur species. In the high binding energy region of the spectum it appears that the $4b_2$ and $7a_1$ orbitals are at higher energy than the above relaxation energy shift would predict. These orbitals are C-H bonding in nature. The assumption that all orbitals should see the same screening effect from the metal is only a simplifying one and not strictly correct. It is possible that the C-H bonds are not in as close proximity to the surface as the CC and CS bonds and thus feel a weaker relaxation shift from the substrate.

Fig. 4.11 shows the UP spectra of thiophene on the Mo(100) surface, after heating to several temperatures. Throughout the temperature range 200-430K the spectra show contributions from the thiophene species described above, π-bonded parallel to the surface. In addition there is an increasing contribution from the Mo-S species at ~6 eV and and from the Mo-C species at ~4.5 eV. The final spectrum taken after heating to 700K, exhibits features that are due purely to sulfur and carbon bound directly to the metal (Fig. 4.12). In addition there is a small photoemission feature in the 200K spectrum at ~10.2 eV binding energy that is clearly present in both the 300K and 430K spectra. There are two points to note about this feature. First, it is in the C-H orbital energy region of the spectrum but must correspond to a strongly perturbed C-H bond if it originates from thiophene. A comparison with the UP spectrum of butadiene, propylene, ethylene and H_2S during their decomposition yields no similar feature. Second, it is worth noting that this feature is persistent throughout the temperature range, suggesting that it arises from some fairly stable hydrocarbon species on the surface, possibly the π-bonded, irreversibly adsorbed thiophene.

Fig. 4.13 shows the HREELS spectrum of condensed thiophene on the Mo(100) surface at T < 100K. Fig. 4.14 shows the corresponding spectra after heating to 200K and 300K while Table 4.1 lists the peak positions and those of gas phase thiophene (14,23). The feature at 1950 cm^{-1} that is present in the spectrum taken at 200K does not appear in any other spectra and is probably an artifact due to coadsorbed CO. The most noticeable features in the low frequency range of the spectra is the appearance of a mode at 300 cm^{-1} in the 200K spectrum and one

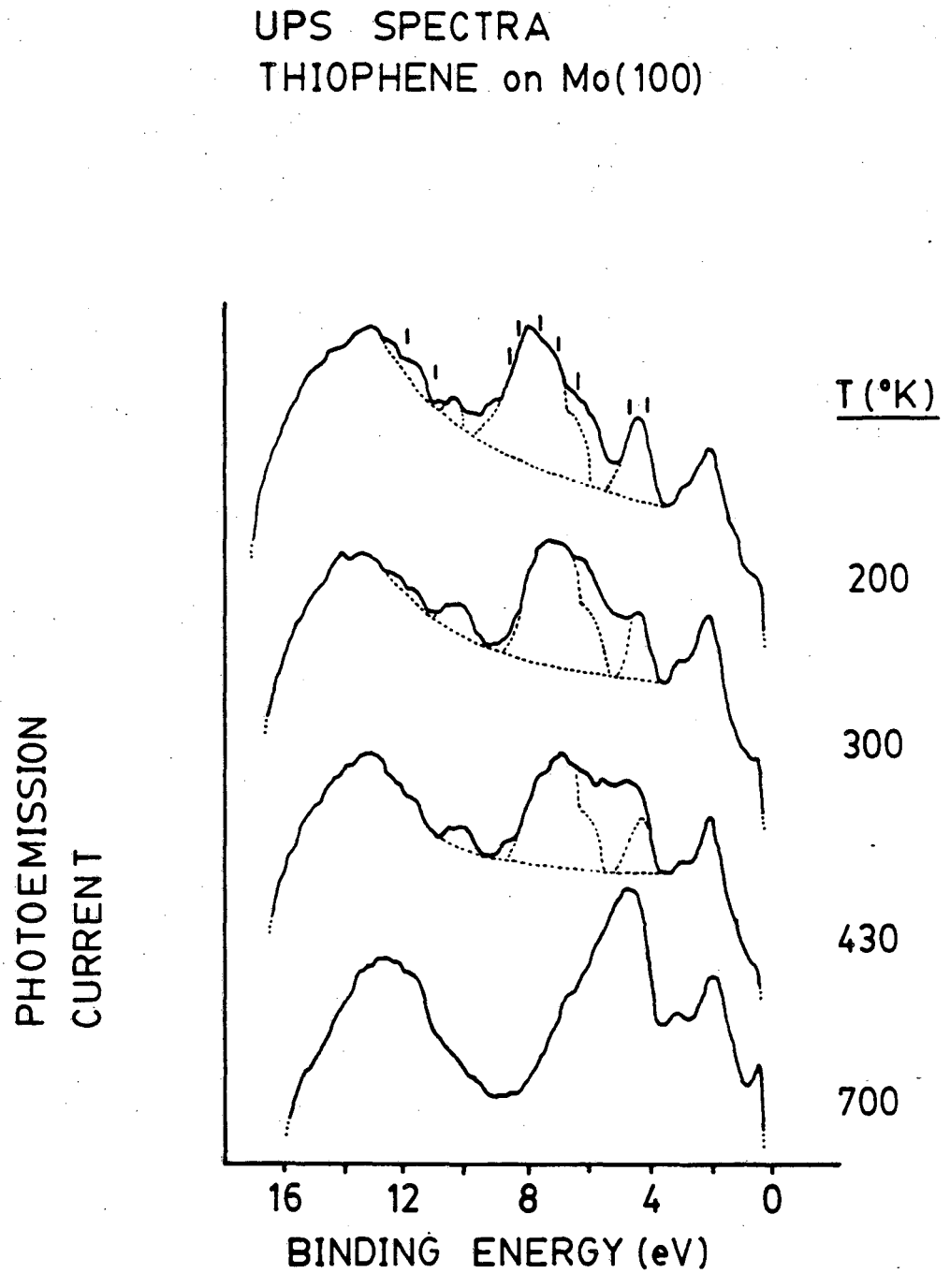

Fig. 4.11 He I UP spectra taken during the decomposition of thiophene on the Mo(100) surface.

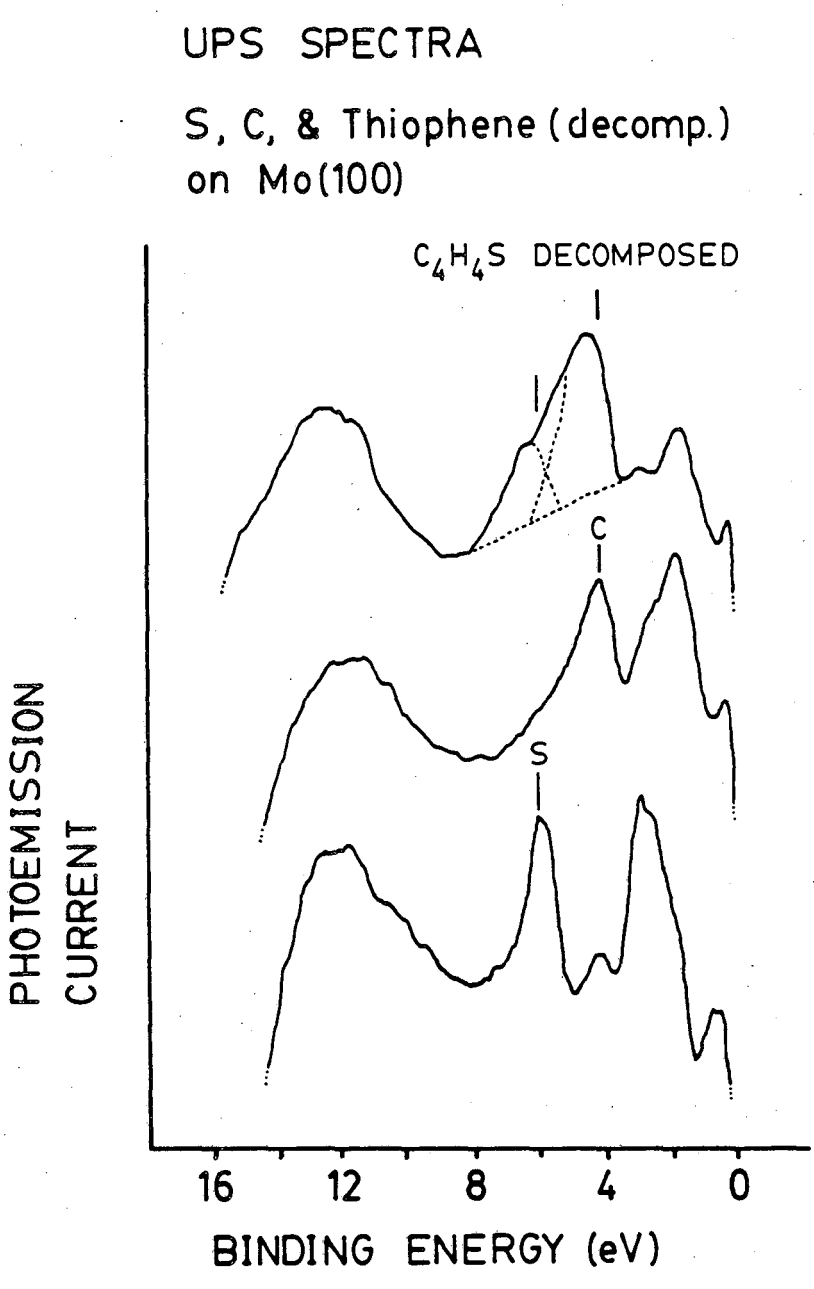

Fig. 4.12 He I UP spectra of decomposed thiophene, sulfur, and carbon on the Mo(100) surface.

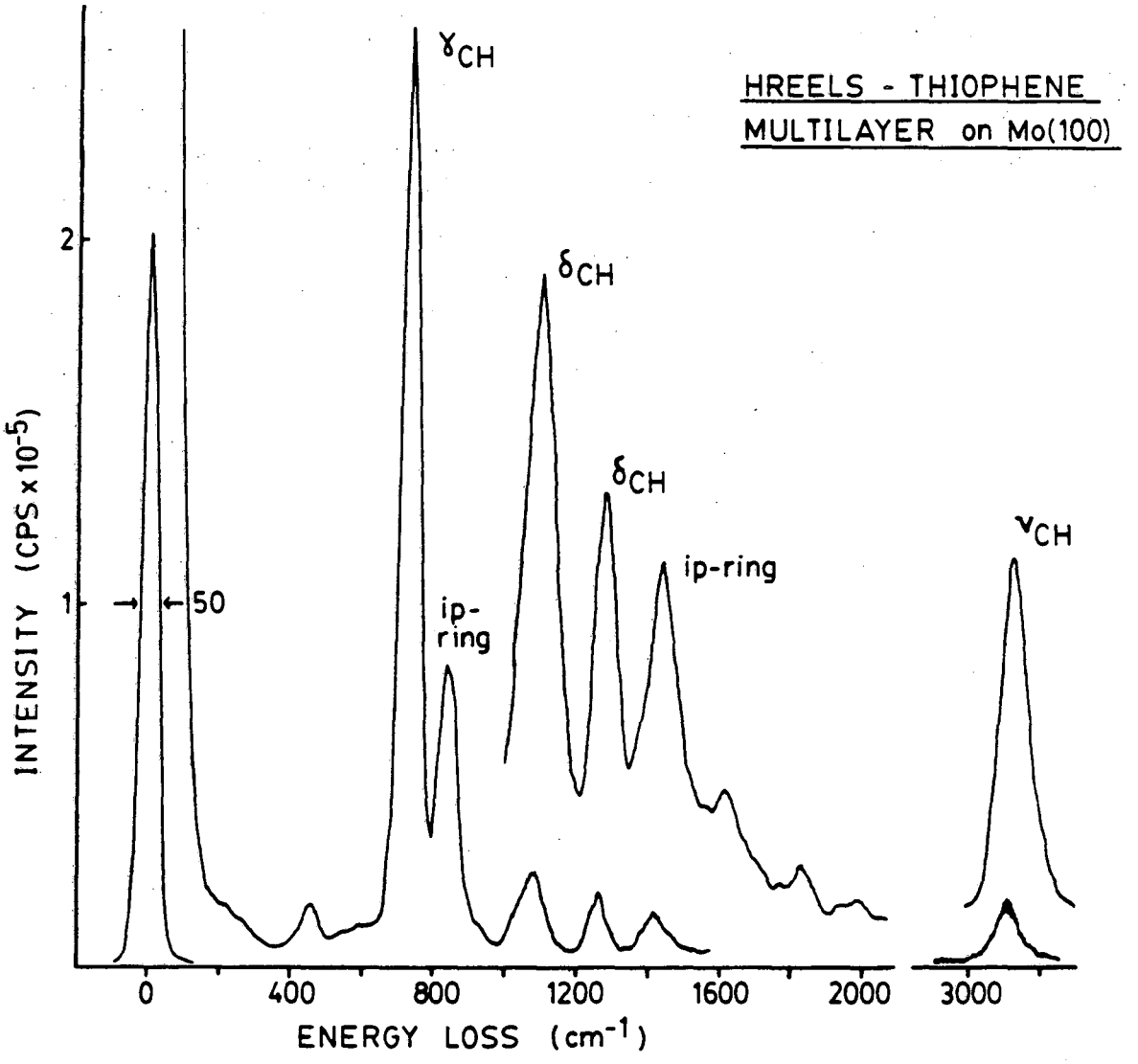

Fig. 4.13 HREEL spectrum of condensed thiophene.

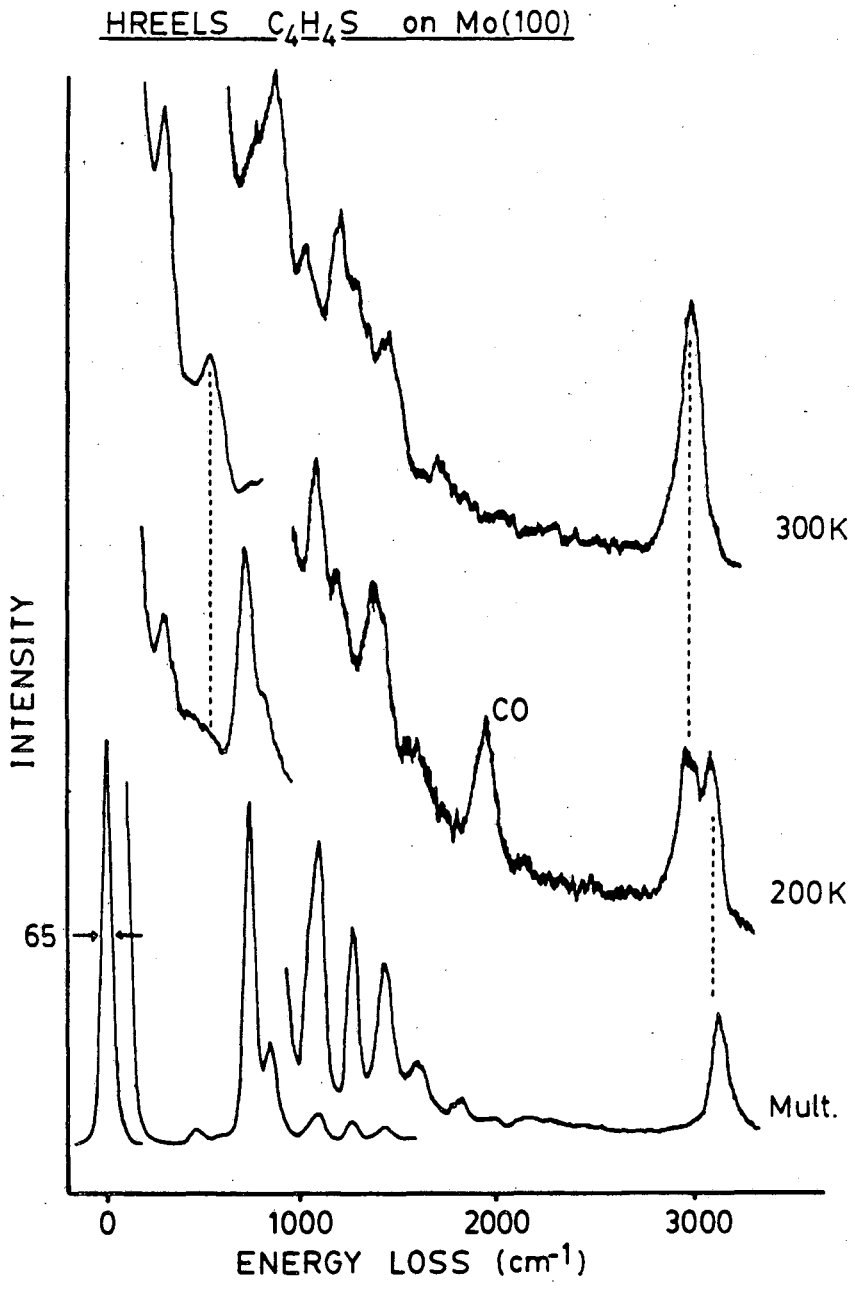

Fig. 4.14 HREEL spectra of thiophene during thermal decomposition on the Mo(100) surface. (Mult. - condensed multilayer)

Table 4.1 C_4H_4S Vibrational Mode Frequencies During Chemisorption and Decomposition on the Mo(100) Surface

Mode Sym.	Mode No.	Mode Classification	Gas Phase Frequency*	Adsorbate Frequencies Mult. <100K	Mono. 200K	Decomp. 300K	Decomp. 450K
a_1	1	CH stretch (M)	3126 cm^{-1}	3120 (S)	3090		
b_1	12	CH stretch	3125				
a_1	2	CH stretch (S)	3098				
b_1	13	CH stretch (S)	3086				
					2980	2990	3000
b_1	14	ip-ring (VW)	1504				
						1440	1450
a_1	3	ip-ring (S)	1409	1420 (S)			
					1380	1350	1380
a_1	4	ip-ring (VW)	1360				
b_1	15	CH ip-bend (S)	1256	1260 (S)		1250	1250
					1190	1180	1190
b_1	16	CH ip-bend	1085				
a_1	5	CH ip-bend (S)	1083	1090 (S)	1090		
a_1	6	CH ip-bend (S)	1036	1040 (S)			
						1020	1010
a_2	9	CH op-bend (VW)	903				
b_1	17	ip-ring (M)	872				
b_2	19	CH op-bend	867				
						870	
a_1	7	ip-ring (VS)	839	840 (VS)	820		840
b_1	18	ip-ring (VW)	751				
b_2	20	CH op-bend (VS)	712	725 (VS)	710	750	
a_2	10	CH op-bend	688				
a_1	8	ip-ring (W)	608				
a_2	11	op-ring (VW)	567				
		Mo-C stretch				530	530
b_2	21	op-ring (W)	452	460 (S)			
		Mo-S stretch			300	300	290

* Gas phase values taken from reference (23).

at 540 cm^{-1} in the 300K spectrum. These are the Mo-S and Mo-C stretching modes respectively and have been assigned from spectra of surfaces covered with adsorbed sulfur and carbon only. In the high frequency region the C-H stretching mode shifts from 3100 cm^{-1} down to 2990 cm^{-1} . Such a "softening" of this mode is indicative of strong interactions with the surface, possibly due to π-bonding of the ring resulting in a weakened C-H bond . Benzene adsorption on the Pt(111) and Ni(111) surfaces is via π-bonding and results in a down shift of the C-H strecthing mode by 60 cm^{-1} (21). At 200K there is still thiophene on the surface that is reversibly adsorbed and weakly perturbed by the metal, having a C-H stretch at 3100 cm^{-1}. The changes in the spectral region from 700 cm^{-1} to 1500 cm^{-1} (the CH bending and ring deformation modes) are dramatic but poorly resolved. At 200K there are modes still present that are only weakly perturbed from the gas phase thiophene modes. After heating to 300K and 450K there is a drastic reduction in the out-of-plane CH modes and new loss features appear at 1180 cm^{-1} and 1020 cm^{-1}. There is very little change in the peak positions over this temperature range, suggesting a stable species on the surface that decomposes at higher temperatures.

Fig. 4.15 and Table 4.2 depict the vibrational modes and list the mode frequencies of dueterated thiophene in gas phase and during adsorption and decomposition on the Mo(100) surface (23). These show the same shifts in CD stretching frequency and appearance of Mo-S and Mo-C modes as in the case of thiophene.

Fig. 4.16 shows the multilayer spectrum of αd_2-$C_4D_2H_2S$ with mode assignments (15). Spectra taken after annealing to 180K and 290K show the same general trends as in the case of C_4H_4S (Fig.4.17). Table 4.3

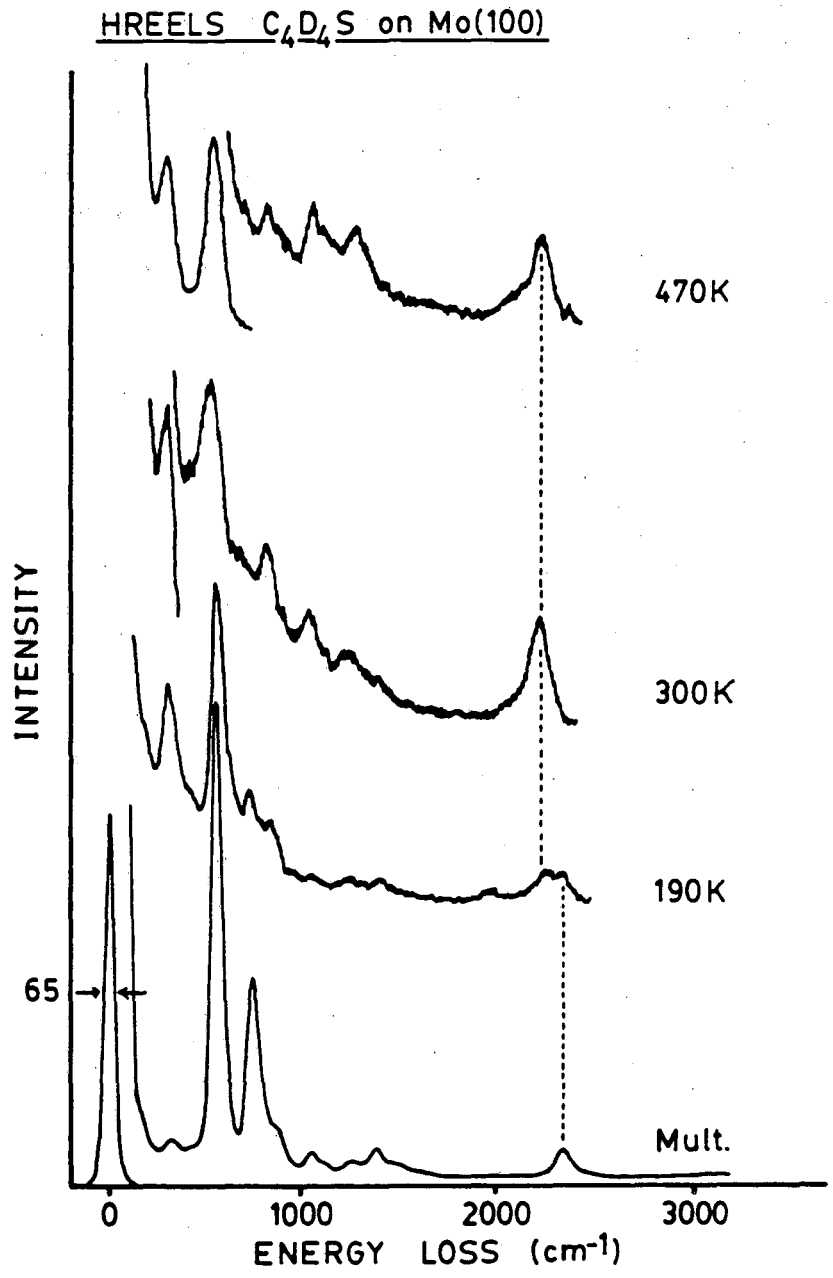

Fig. 4.15 HREEL spectra of C_4D_4S during thermal decomposition on the Mo(100) surface.

Table 4.2 C_4D_4S Vibrational Mode Frequencies During Chemisorption and Decomposition on the Mo(100) Surface

Mode Sym.	Mode No.	Mode Classification	Gas Phase Frequency*	Adsorbate Frequencies Mult. <100K	Mono. 190K	Decomp. 300K	Decomp. 470K
a_1	1	CD stretch (M)	2343 cm^{-1}	2340 (S)	2330		
b_1	12	CD stretch	2340				
b_1	13	CD stretch (S)	2305				
a_1	2	CD stretch (M)	2290				
					2250	2220	2220
							2100
b_1	14	ip-ring (M)	1459	1460 (M)			
a_1	3	ip-ring (S)	1376	1380 (S)	1400	1400	1420
a_1	4	ip-ring (W)	1248	1260 (M)	1250	1250	1280
						1140	1140
b_1	15	CD ip-bend (S)	1034	1030 (S)	1050	1040	1060
a_1	5	CD ip-bend (M)	896				
b_1	16	CD ip-bend (S)	846	850 (S)	840	820	810
a_1	6	CD ip-bend (M)	785				
a_2	9	CD op-bend	752				
b_1	17	ip-ring	752				
a_1	7	ip-ring (VS)	731	730 (VS)	730		
b_1	18	ip-ring (W)	712				
b_2	19	CD op-bend (VW)	684				
a_1	8	ip-ring (VW)	585				
a_2	10	CD op-bend	532				
b_2	20	CD op-bend (VS)	531	540 (VS)	550		
		Mo-C stretch				530	530
a_2	11	op-ring	488				
b_2	21	op-ring	414				
		Mo-S		320	310	280	290

* Gas phase frequencies taken from reference (23).

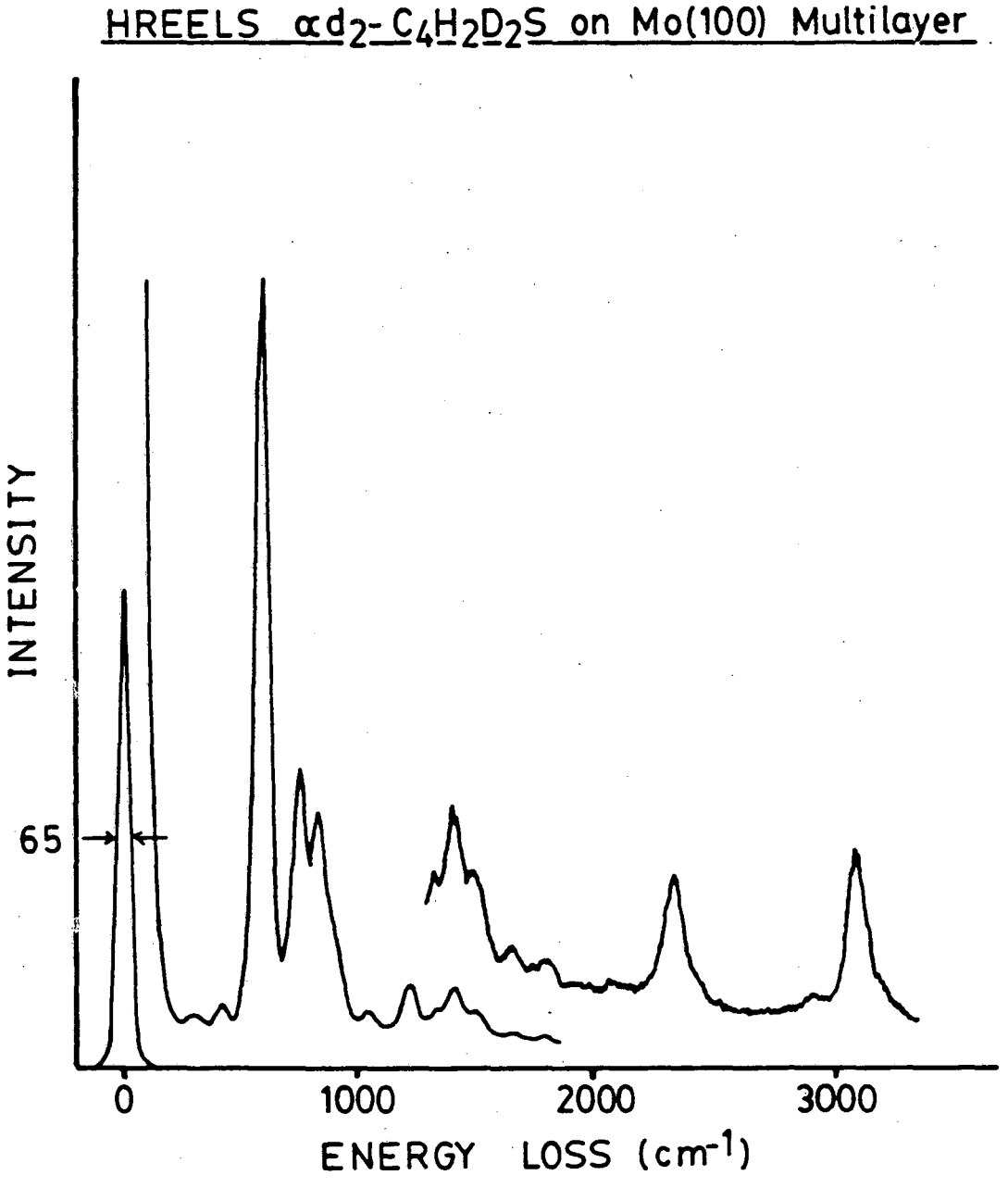

Fig. 4.16 HREEL spectrum of condensed αd_2-$C_4D_2H_2S$.

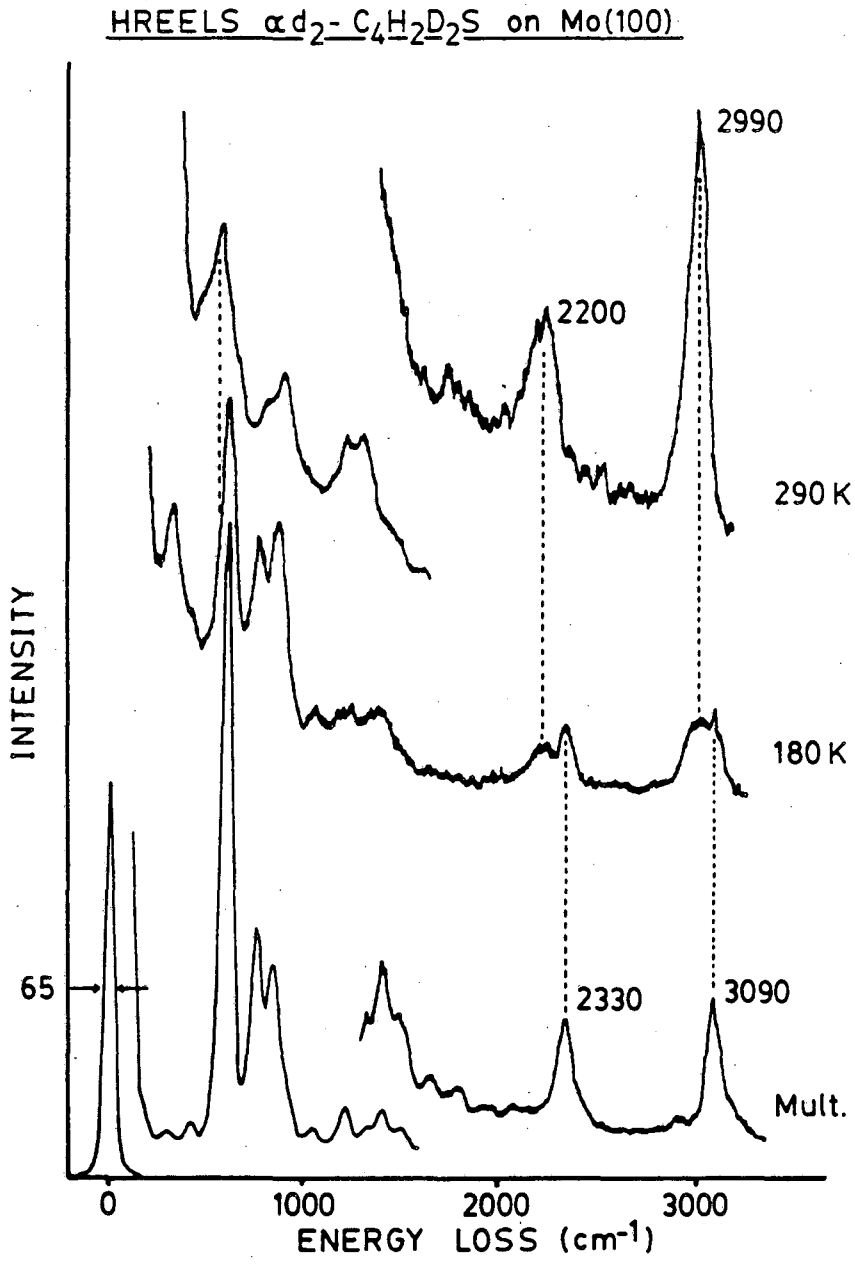

Fig. 4.17 HREEL spectra of αd_2-$C_4D_2H_2S$ during thermal decomposition on the Mo(100) surface.

Table 4.3 αd_2-$C_4H_2D_2S$ Vibrational Mode Frequencies During Chemisorption and Decomposition on the Mo(100) Surface

Mode Sym.	Mode No.	Mode Classification	Gas Phase Frequency*	Adsorbate Frequencies Mult. <100K	Mono. 180K	Decomp. 290K	Decomp. 430K
a_1	2	CH stretch (S)	3101 cm^{-1}	3090 (S)	3090		
b_1	12	CH stretch (S)	3088				
					3000	2990	2980
b_1	13	CD stretch	2368	2330 (S)	2330		
a_1	1	CD stretch (W)	2336				
					2200	2200	2200
b_1	14	ip-ring (VW)	1500	1480 (M)	1480		
						1440	1420
a_1	3	ip-ring (S)	1398	1400 (S)	1370		
a_1	4	ip-ring (S)	1310	1320 (M)			
						1280	1290
b_1	15	CH/CD ip-bend(S)	1215	1220 (S)	1200	1190	1180
a_1	5	CH/CD ip-bend(M)	1044	1040 (M)	1030		
b_1	16	CH/CD ip-bend(M)	918	920 (S)			
a_1	6	CH/CD ip-bend(M)	884				
a_2	9	CH/CD op-bend	881				
						870	
b_2	19	CH/CD op-bend(VS)	818	830 (VS)	840		850
						790	
b_1	17	ip-ring	772				
a_1	7	ip-ring (VS)	754	740 (VS)	760		
b_1	18	ip-ring	745				
a_1	8	ip-ring	616				
a_2	10	CH/CD op-bend	600	600 (VS)	590		
b_2	20	CH/CD op-bend(VS)	584				
		Mo-C stretch				540	530
a_2	11	op-ring	493				
b_2	21	op-ring	419	410 (M)			
		Mo-S stretch		290	310	300	290

* Gas phase frequencies taken from reference (15).

lists the frequencies of the modes of gas phase αd_2-$C_4D_2H_2S$ and its adsorbed counterpart before and during decomposition. The Mo-S (300 cm^{-1}) mode and Mo-C (540 cm^{-1}) mode appear at 180K and 290K respectively, and at 180K there is still some weakly bound thiophene with modes essentially unperturbed from those in the gas phase. It is interesting to note the shifts in the α-CD vs. β-CH stretching frequencies upon entering the irreversibly chemisorbed state. The α-CD mode shifts from 2330 cm^{-1} to 2200 cm^{-1} ($\Delta\nu_{CD}$ = 130 cm^{-1}) while the β-CH mode shifts from 3090 cm^{-1} to 2990 cm^{-1} ($\Delta\nu_{CH}$ = 100 cm^{-1}). Identical changes in the force constants would be expected to give relative shifts of $\Delta\nu_{CH} = \sqrt{2} \times \Delta\nu_{CD}$ and thus a much smaller shift in the α-CD stretch than in the β-CH stretch. The larger shift in the α-CD mode frequency implies that it is more strongly perturbed than the β-CH mode, suggesting that this bond is in closer contact with the surface. One can envision a thiophene molecule π-bonded to the metal with the ring plane close to parallel with the surface but having the sulfur containing end tilted downwards.

The modes of irreversibly adsorbed C_4H_4S, αd_2-$C_4D_2H_2S$, and C_4D_4S at ~300K and ~430K are compared in Fig.s 4.18 and 4.19 respectively. With the exception of differences in the background intensity, the spectra of these compounds change little on raising the temperature. The modes in the region about 1400 cm^{-1} appear in all spectra and it is possible that they originate from the in-plane ring modes of the unperturbed thiophene molecule. The ring modes and CH wagging modes in the region 800-1200 cm^{-1} yield complex spectra which, combined with the lack of resolution, preclude any further assignment.

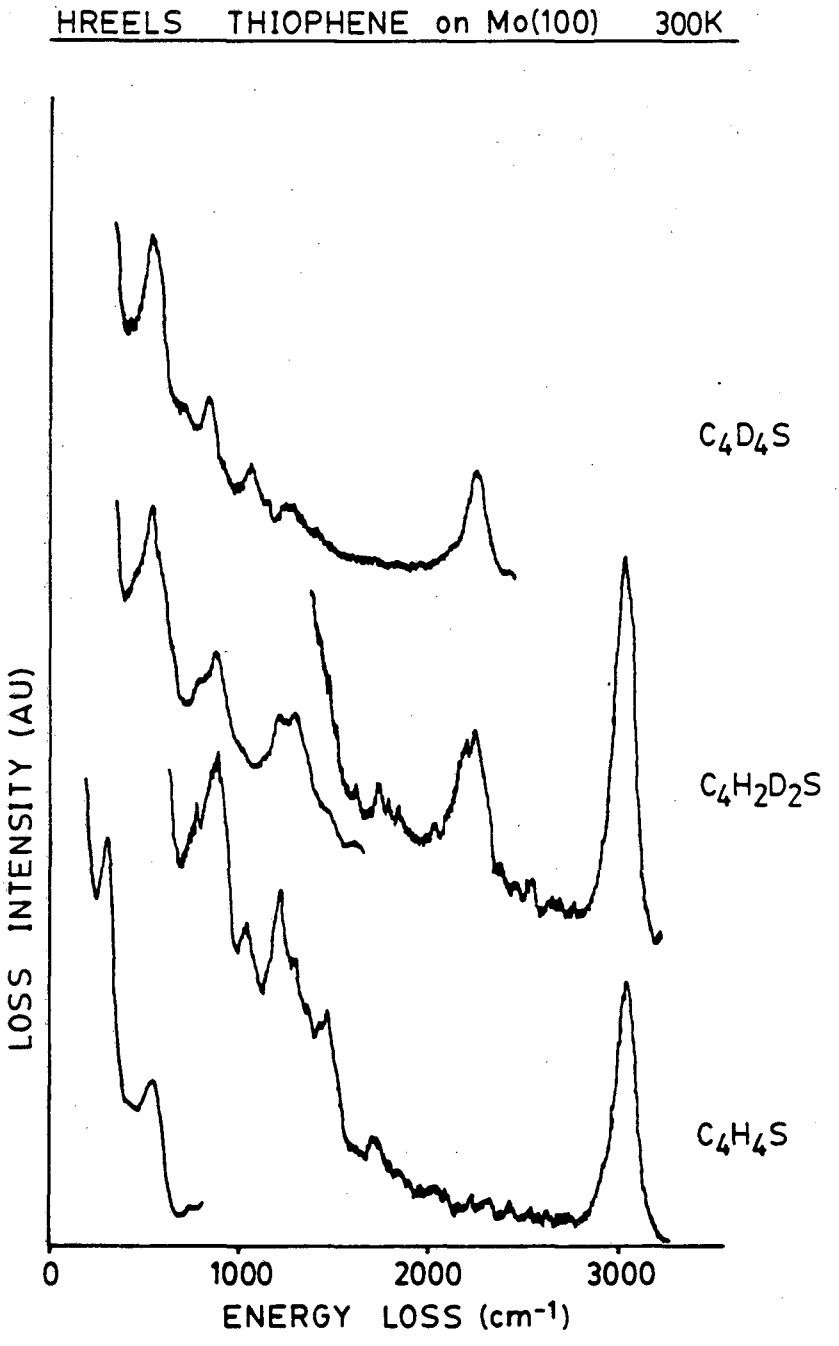

Fig. 4.18 HREEL spectra of C_4H_4S, αd_2-$C_4D_2H_2S$, and C_4D_4S on the Mo(100) surface after heating to 300K.

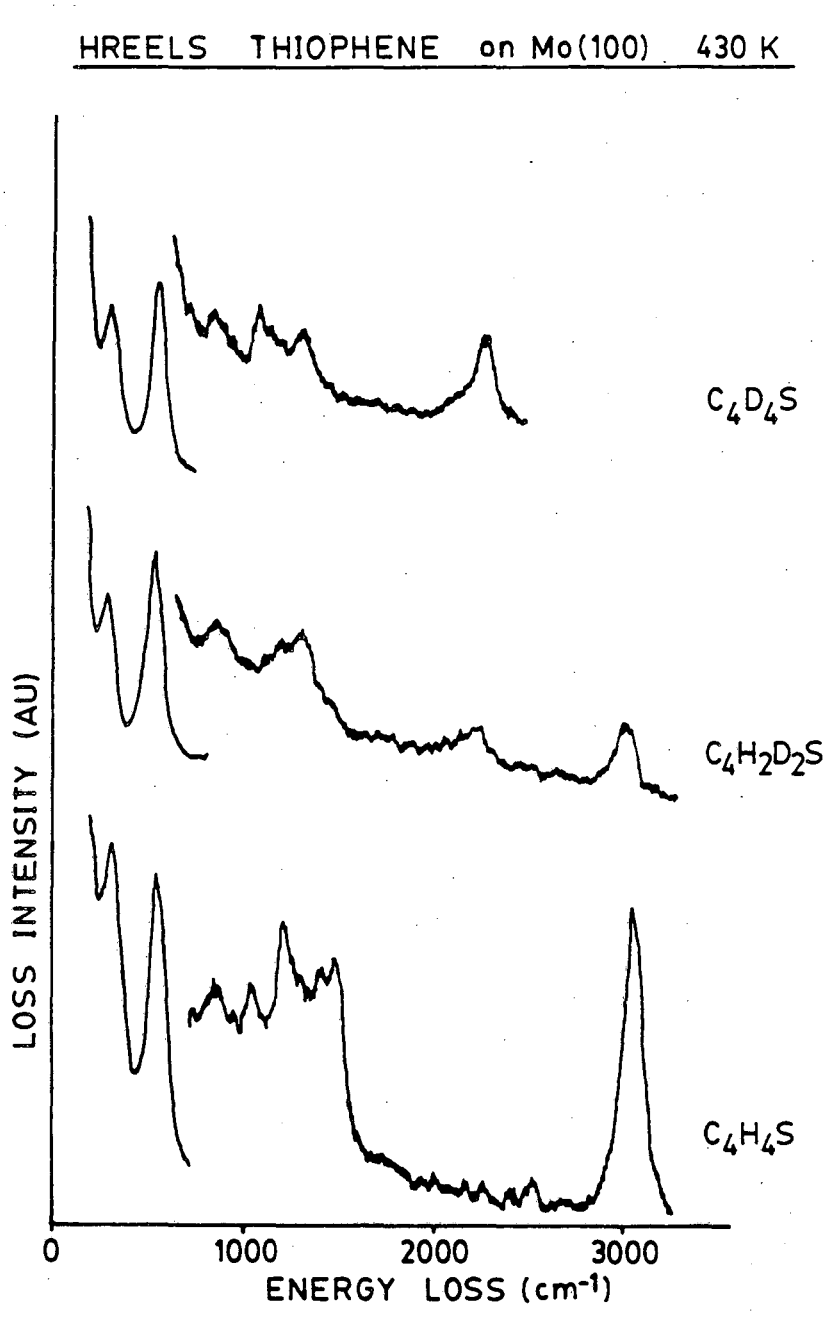

Fig. 4.19 HREEL spectra of C_4H_4S, αd_2-$C_4D_2H_2S$, and C_4D_4S on the Mo(100) surface after heating to 430K.

4.5 Thiophene Coadsorption with Sulfur on the Mo(100) Surface

The primary effect of sulfur on thiophene adsorption on the Mo(100) surface is to reduce the fraction that is adsorbed irreversibly. Fig. 4.20 shows the desorption spectra of thiophene from the sulfided surface over a range of coverages. The sulfiding of the surface increases the fraction desorbing at low temperatures from the condensed multilayer phase. Fig. 4.21 shows the H_2 TDS spectrum from surfaces with varying initial sulfur coverage and a uniform exposure to 1L of thiophene. The amount of H_2 desorption drops monotonically with sulfur coverage to zero at coverages of $\theta_S \approx 0.70$. This decrease in H_2 desorption is accompanied by a simultaneous drop in the amount of sulfur deposited on the surface during decomposition. It appears that the decomposition process may be similar to the dissociative adsorption of S_2 discussed in Chapter 3 which requires at least two next-nearest neighbour fourfold hollows.

The decomposition of thiophene on the half monolayer c(2x2) sulfur structure has been followed by UPS and the spectra are shown in Fig. 4.22. The contribution due to pre-adsorbed sulfur is shaded in the spectrum taken at 175K. The molecular orbital features still appear to have contributions from the π-orbitals at ~4.5 eV and the σ-orbitals in the 6.0-9 eV energy range. These disappear in the temperature range 250K-375K as decomposition occurs and are accompanied by an increase in the photoemission signal in at 4.5 eV due to the formation of a surface carbon deposit. It is interesting to note that, although the bonding to the sulfided surface does not appear to be significantly different from that on the clean surface, there is no photoemission at 10.2 eV binding

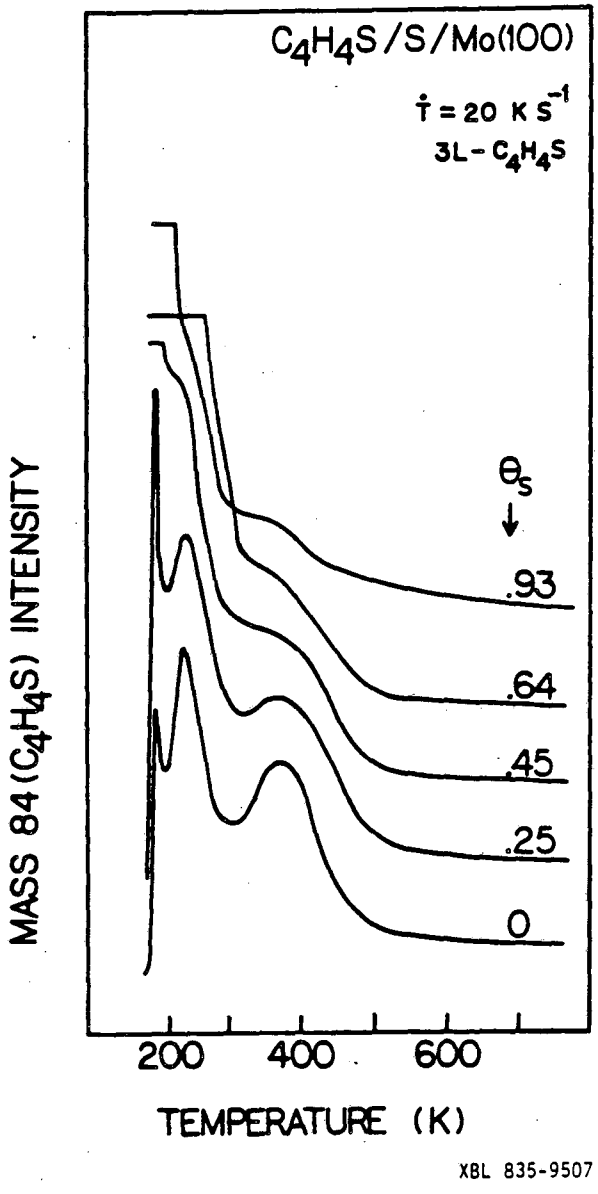

Fig. 4.20 Thermal desorption spectra of thiophene (1L) from the sulfided Mo(100) surface.

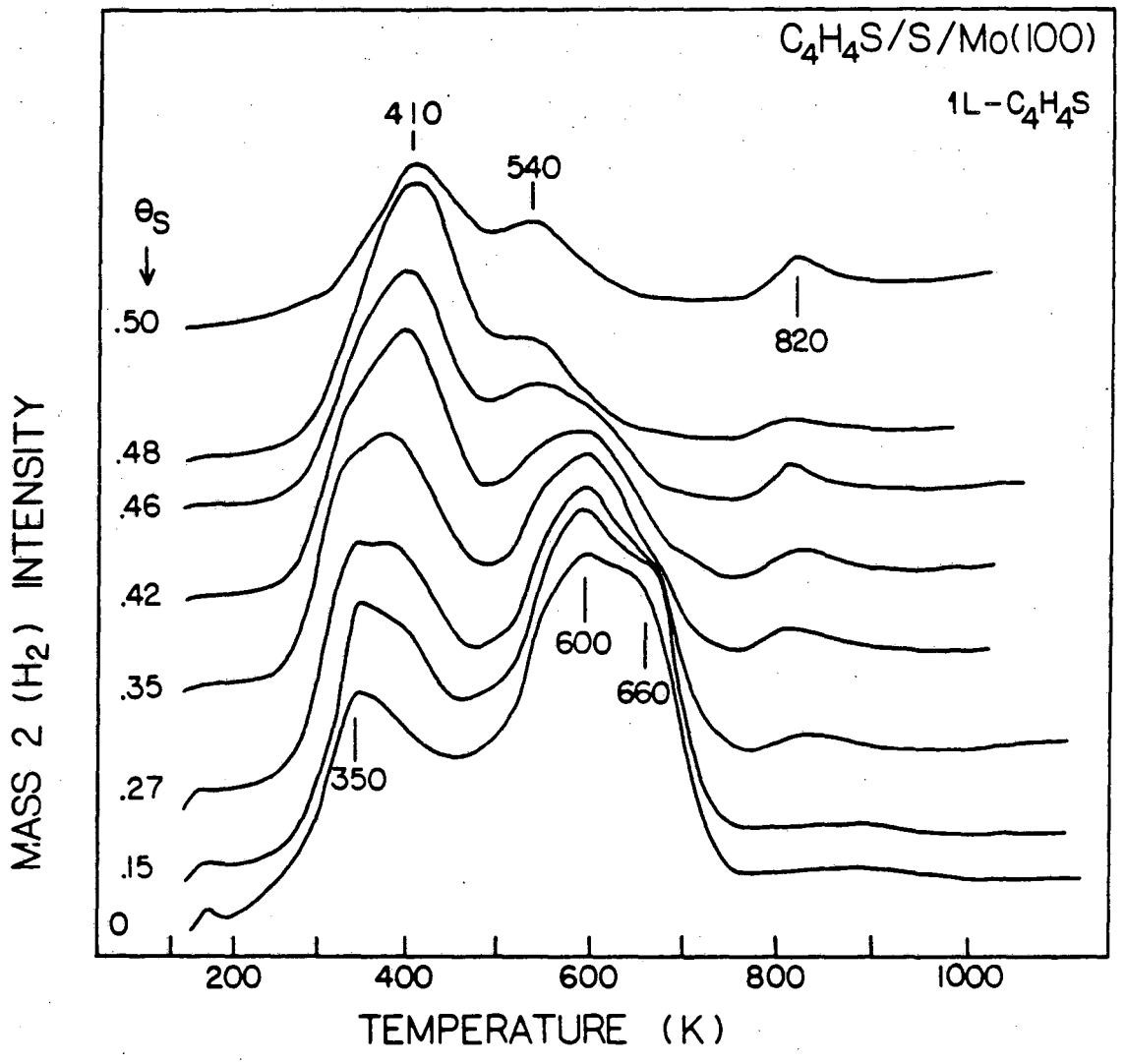

Fig. 4.21 Desorption spectra of H_2 resulting from thiophene decompositi on on the sulfided Mo(100) surface.

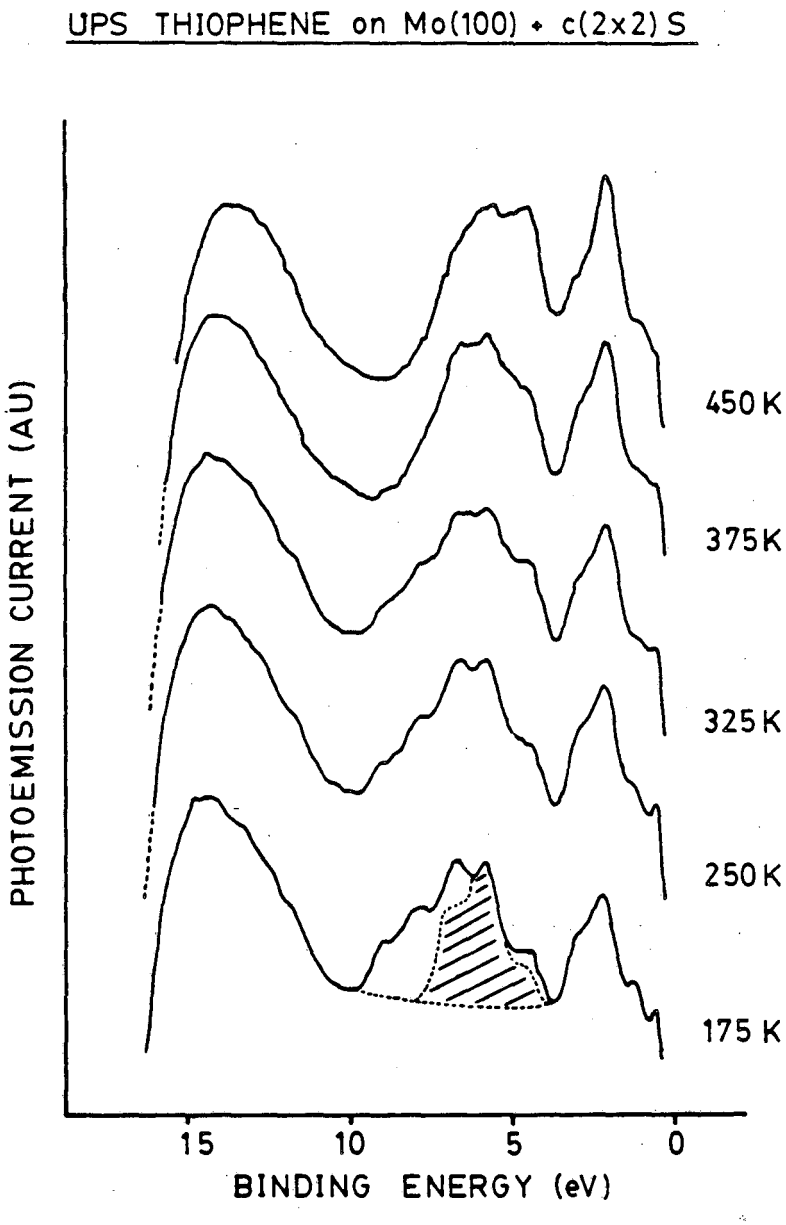

Fig. 4.22 He I UP spectra of thiophene on the sulfided Mo(100) surface with θ_S = 0.5 c(2x2), during desorption and decomposition.

energy. This feature that is characteristic of the surface adsorbate complex on the clean surface is absent on the sulfided surface.

4.6 Discussion

The chemistry of thiophene adsorbed on the Mo(100) surface is clearly very complex, but it has been possible to make some progress in understanding this system. At the simplest level the low temperature adsorption of thiophene on the clean surface can be divided into two catagories. One fraction is reversibly adsorbed and will desorb at temperatures <290K while the remainder enters an irreversibly bound state from which it proceeds to decompose as the temperature is increased. The HREEL and XP spectra at 200K show that both species can co-exist on the surface and that even at these low temperatures some decomposition of the irreversibly bound thiophene has begun.

The reversibly adsorbed thiophene closely resembles molecular, gas phase thiophene in that it exists on the surface in a condensed phase at low temperatures and has vibrational and UP spectra almost identical to those of its gas phase counterpart. Heating to 200K results in the desorption of the bulk of this multilayer phase. At this point some thiophene has entered the irreversibly bound state while some still remains reversibly adsorbed. The interaction of this latter portion with the surface is fairly weak. Desorption occurs in the temperature range 290K - 230K, shifting downward with increasing coverage, indicating a heat of adsorption shifting from 16 kcal/mole to 13 kcal/mole at the higher coverages. The decrease is attributed to adsorbate-adsorbate repulsive interactions.

Decomposition of the irreversibly bound thiophene fragment occurs throughout the temperature range 170K - 650K depositing sulfur and carbon on the metal surface and resulting in the desorption of H_2 into the vacuum. Some of the irreversibly bound thiophene remains intact on the surface with the sulfur atom bound in the organic ring up to temperatures >430K (XPS Fig. 4.7). The ring is π-bonded to the surface with an estimated stabilization of the $1a_2$ and $2b_1$ orbitals of 0.9 eV (UPS, Fig. 4.10). Vibrational spectra show an expected softening of the CH stretching modes (HREELS, Fig. 4.17) and, in particular, a greater weakening of the α-CH bond than of the β-CH bond. This suggests a configuration in which the ring is close to parallel to the surface but with the sulfur containing end closer to the surface than the hydrocarbon chain, as depicted in Fig. 4.23. As is implied in this figure the ring may no longer be perfectly planar. The decomposition of αd_2-$C_4D_2H_2S$ in this form leads to the desorption of D_2 at lower temperatures than H_2 (Fig.s 4.4,4.5,4.6) again supporting the existence of a species in which the α-CH bond is in closer proximity to the surface than the β-CH bond. At low thiophene coverages, however, both H_2 and D_2 desorb simultaneously. In this case the process is rate limited by the desorption of hydrogen and thus selective bond breaking would not be observable in a desorption spectrum.

An alternative bonding scheme is one in which the thiophene molecule is 2,5 di-σ-bonded to the metal through the carbon atoms in the α positions with a double bond between the carbon atoms in the 3 & 4 positions. Such a configuration would account for the shift in CH stretching frequencies from those of an aromatic species (3100 cm^{-1}) towards those of an aliphatic hydrocarbon (2990 cm^{-1}). The S 2P XP

THIOPHENE ADSORPTION STRUCTURE

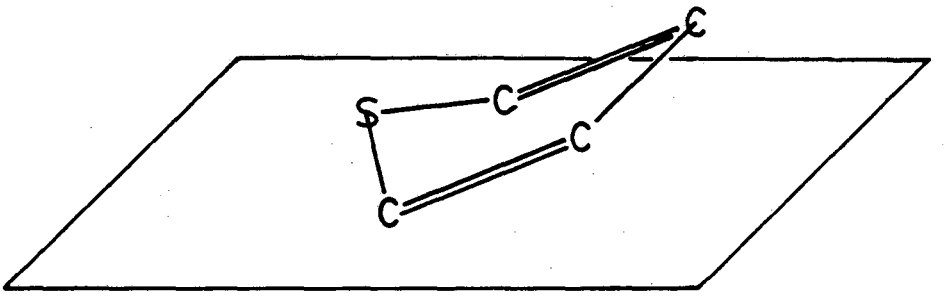

Fig. 4.23 Schematic depiction of a possible adsorption geometry of thiophene on a metal surface. The sketch shows the possible deviation from planarity.

spectra, however, suggest that the sulfur atom remains in an aromatic environment, similar to that in thiophene, up to temperatures >430K. The σ-bonded adsorbate might be expected to have its sulfur atom in an environment similar to that of tetrahydrothiophene in which the S 2P binding energy is 162.7 eV, 1.6 eV less than that observed for adsorbed thiophene. Furthermore, the UP spectra indicate that the thiophene π-orbital system remains intact on adsorption. Table 4.4 lists the CH stretching vibrational frequencies of a number of systems related to the thiophene adsorption complex. In the case of benzene adsorption on the Pt(111) surface, bonding is through the π-orbitals, parallel to the surface and results in a downshifting of the CH stretching frequency by 60 cm^{-1} (21). The π-bonding of thiophene to Cr in the $(C_4H_4S)Cr(CO)_3$ complex results in only very minor shifts in the CH stretching frequencies (25). There is however some decrease in the frequencies of the in-plane CH bending and ring modes accompanied by an increase of the out-of-plane CH wagging mode frequenices. Related systems in which carbon atoms are σ-bonded are the case of 2,5 dihydrothiophene and cyclopentene adsorption on the Pt(111) surface. 2,5 dihydrothiophene resembles a thiophene molecule di-σ-bonded to a metal surface, having aliphatic CH bonds in the α positions and olefinic CH bonds in the β positions. The splitting in these CH vibrational mode frequencies, however, is 150 cm^{-1} which should be easily resolved in the HREELS spectrum if this type of species were to exist on the surface (26). Finally, the adsorption of cyclopentene on the Pt(111) surface has been shown to produce a species that is σ-bonded to the surface (24). In this case a very low frequency CH stretch was observed at 2695 - 2750 cm^{-1}. It is not clear that this arises from the CH bonds adjacent

Table 4.4 CH Stretching Frequencies of Various Gas Phase Species and their Chemisorbed Counterparts

Molecule and Surface	Gas Phase Frequencies (cm^{-1})	Adsorbed Phase Frequencies (cm^{-1})
Thiophene on Mo(100)	3126 (23) 3125 3098 3086	2990
Benzene on Pt(111)	3068 3062	3000 (21)
η^2-cC_5H_8 on Pt(111)	3066 (olfenic) 2958- 2852 (CH_2)	2970 (24) 2890 2695-2750
$(C_4H_4S)Cr(CO)_3$	3116 (25) 3116 3090 3080	
2,5,dihydro-thiophene	3065 (olefinic) (26) 2866-2936 (CH_2)	

to the Pt-C bond, however, if this is the case such a low frequency mode would be expected if thiophene were 2,5 di-σ-bonded to the surface. In conclusion, it seems that while thiophene adsorbed on the Mo(100) surface is more strongly perturbed than thiophene π-bonded in the $(C_4H_4S)Cr(CO)_3$ complex it is not perturbed to the point of being σ-bonded to the metal through its carbon atoms.

The exact sequence of steps involved in the decomposition is not clear. Examination of the C_4H_4S and αd_2-$C_4D_2H_2S$ HREEL spectra taken after heating to 200K show the Mo-S mode at 300 cm^{-1} but no Mo-C mode at 540 cm^{-1} . It seems from this and the XPS study (Fig. 4.7) that some some sulfur has been extracted from the ring at this temperature but that there is no simultaneous decomposition of the remaining hydrocarbon chain. If the remaining hydrocarbon is at all similar to the Pt metallocycle it must be a minority species on the surface. The HREEL spectra of the Mo surface during thiophene decomposition bears no resemblance to that of the Pt(111) surface (4).

At high temperatures (>400K) a second decomposition pathway exists that is only present for initially high thiophene coverages. This process leads initially to H_2 desorption followed by D_2, the reverse of the low temperature process. It has been noted that the initial presence of carbon on the surface leads to an enhancement in the H_2 yield from the high temperature decomposition pathway (6). It is likely that for high thiophene coverages the deposition of carbon onto the surface during the low temperature decomposition at some point blocks further decomposition leading to this high temperature pathway.

Even under UHV conditions, molecular thiophene is stable on the surface to temperatures as high as 600K which is within the range of

temperatures in which HDS reactions have been performed. Although under UHV conditions this adsorbed species will decompose it is possible that in the presence of adsorbed hydrogen this is the precursor to desulfurization leading to the HDS products. The high lying molecular orbitals of thiophene are depicted in Fig. 4.24 (12,16,20). In general, organometallic complexes containing thiophene are π-bonded systems in which the ligand is weakly electron donating. In this case we have observed π-bonding accompanied by a small lowering of the work function also implying electron donation to the metal. A stabilization of the thiophene π orbitals through bonding interaction with the surface would result in a weakening of the CS bonds, especially in the case of the $1b_1\pi$ orbital that is strongly CS bonding. Similarly, any back-donation into the unoccupied $3b_1\pi$ orbital will weaken the CS bond as it is CS anti-bonding. If such weakening of the CS bonds is sufficiently great, and hydrogen is present on the surface hydrogenation of the CS bonds can occur.

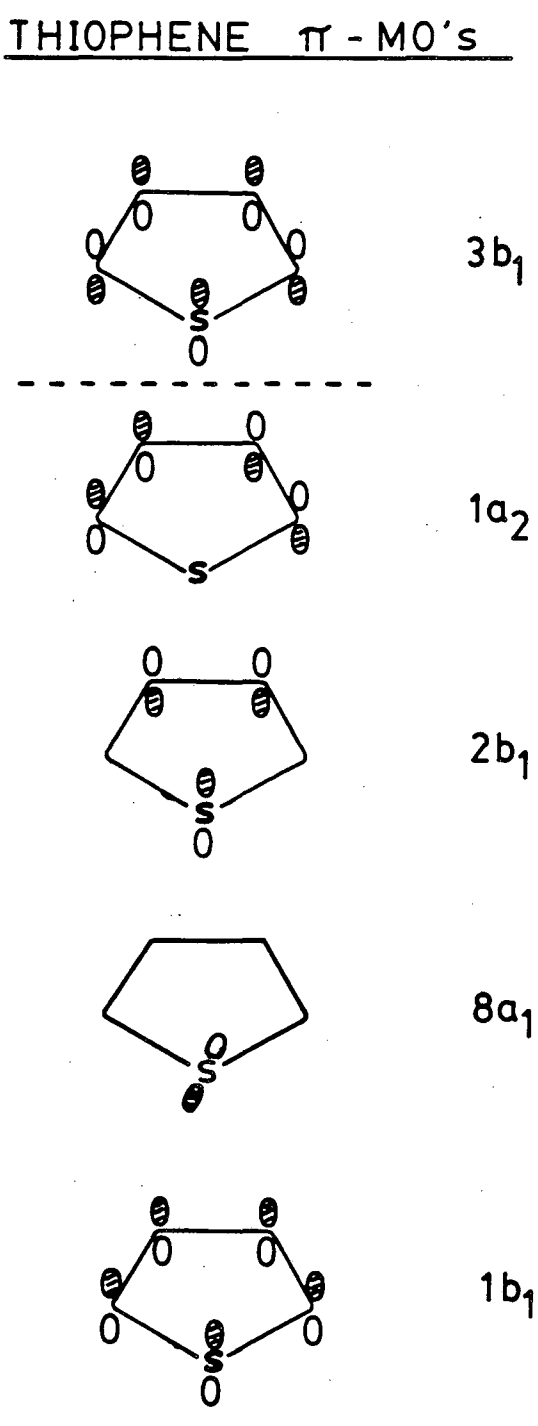

Fig. 4.24 The highest lying molecular orbitals of thiophene.

4.7 References

1. M.L. Vrinat, Appl. Catal., 6 (1983) 137
2. B.J. Zwolinski, R.C. Wilhoit, Handbook of Vapour Press. & Heats of Formation of Hydrocarbons and Related Compounds, API 44-TRC Publications in Sci. & Eng., Texas, 1971
3. A.J. Gellman, M.H. Farias, M. Salmeron, G.A. Somorjai, Surf. Sci., 136 (1984) 217
4. J. Stohr, et al., Phys. Rev. Lett., 53(22) (1984) 2161
5. E.L. Muetterties, et al., to be published
6. D. Kelly, G.A. Somorjai, unpublished work
7. P.A. Redhead, Vacuum, 12 (1962) 203
8. T. Gentle, E.L. Muetterties, private comm.
9. M.H. Farias, A.J. Gellman, G.A. Somorjai, Surf. Sci., 140 (1984) 181
10. H.R. Han, L.D. Schmidt, J. Phys. Chem., 75(2) 1971 227
11. Handbook of X-ray Photoelectron Spectroscopy, G.E. Muilenberg (ed.) Perkin-Elmer Corp., Minn. 1978
12. P.J. Derrick, L. Asbrink, O. Edqvist, B.O. Jonsson, E. Lindholm, Int. J. of Mass Spec., 6 (1971) 177
13. J.E. Demuth, D.E. Eastman, Phys. Rev. Lett., 32(20) (1974) 1123
14. D.W. Scott, J. Mol. Spec., 31 (1969) 451
15. L.M. Sverdlov, M.A. Kovner, E.P.Krainov, Vibrational Spectra of Polyatomic Molecules, Wiley, NY
16. S. Harris, R.R. Chianelli, J. Catal., 86 (1984) 400
17. N.V. Richardson, J.C. Campuzano, Vacuum, 31 (1981) 449
18. G.R. Schoofs, R.E. Preston, J.B. Benziger, Langmuir, 1 (1985) 313
19. J.M. Soler, N. Garcia, Surf. Sci., 124 (1983) 563

20. W. von Niessen, W.P. Kraemer, L.S. Cederbaum, L. Elect. Spec. Rel. Phenom., 8 (1976) 179

21. S. Lehwald, H. Ibach, J.E. Demuth, Surf. Sci., 78 (1978) 577

22. B.J. Lindberg, K. Hamrin, G. Johansson, U. Gelius, A. Fahlman, C. Nordling, K. Siegbahn, Phys. Scr., 1 (1970) 286

23. T. Shimanouchi, Tables of Molecular Vibrational Frequencies Consolidated Volume I, NSRDS-NBS 39, p. 203

24. N. Avery, Surf. Sci., 146 (1984) 363

25. B.V. Lokshin, E.B. Rusach, Yu. D. Konovalov, Izv. Akad. Nauk. SSSR Ser. Khim., 1 (1975) 84

26. W.H. Green, A.B. Harvey, Spectrochimica Acta, 25A (1969) 723

Chapter 5. HDS of Thiophene over Mo Single Crystal Surfaces

5.1 Introduction

The many studies of hydrodesulfurization catalysis can, for the most part, be divided into two catagories. Those aimed at characterizing the nature of the catalyst have been reviewed in Chapter 1. The second category consists of those aimed at studying the reaction mechanism either through variation of reaction conditions to measure kinetic parameters or the variation of the reactants. The work presented here has used metal single crystal surfaces, primarily the Mo(100) surface, as catalysts for the HDS of thiophene at high pressures (1 atm.). Variation of both surface structure/composition and kinetic parameters has been used to determine the nature of the active catalyst and the reaction mechanism.

The kinetic studies of HDS over Mo catalysts have been recently reviewed by Vrinat (1). For the most part these have been performed over high surface area, Co promoted catalysts supported on γ-Al_2O_3. Variation of the reactant pressures has yielded rates that can be fitted to Langmuir-Hinshelwood type rate expressions while the temperature dependence of the rates is used to determine the Arrhenius parameters. This general approach to the study of these reactions has not as yet yielded any consensus as can be seen from Vrinat's review which tabulates seven different rate expressions that have been successfully fitted to experimental data. The reported Arrhenius activation energies range from 3.7 - 26 kcal/mole. The exact source of the discrepancies is uncertain but it is clear that when working with such poorly characterized and complex catalysts, minor differences in preparative proceed-

ures can result in different catalytic behaviour. Furthermore, the extreme complexity of such catalysts makes interpretation of results very difficult due to the fact that many reactions can take place on a variety of active sites within the catalyst. The fact that H_2S inhibits desulfurization activity but not hydrogenation activity, for instance, has been used to suggest that these two reactions occur on two distinct catalytic sites (2,3). Changes in product distribution with the addition of a support material also suggest that this further complicates the situation either through reactions occurring on the support or by modifying the nature of the catalytically active sites (4).

Although it has been noted that a large number of rate expressions have been proposed for thiophene HDS there is a general form that appears most frequently or is at least a limiting case of some more complex expressions.

$$r = \frac{kK_TP_TK_HP_H}{(1 + K_TP_T + K_SP_S)^2}$$

Here k is the rate constant, K_i are equilibrium constants, P_i are pressure values and the subscripts T,H,S refer to thiophene, hydrogen and H_2S respectively. This expression implies first order adsorption of both thiophene and hydrogen and adsorption inhibition by both thiophene and H_2S. The product distribution over supported catalysts consists primarily of the three isomers of butene with some fraction of butane and in some cases butadiene. A generalized reaction pathway has been proposed that leads to these products and is depicted in Fig. 5.1 (1,5). The fact that small amounts of butadiene have been observed over some catalysts while no tetrahydrothiophene has been produced has

THIOPHENE HYDRODESULFURIZATION REACTION PATHWAY

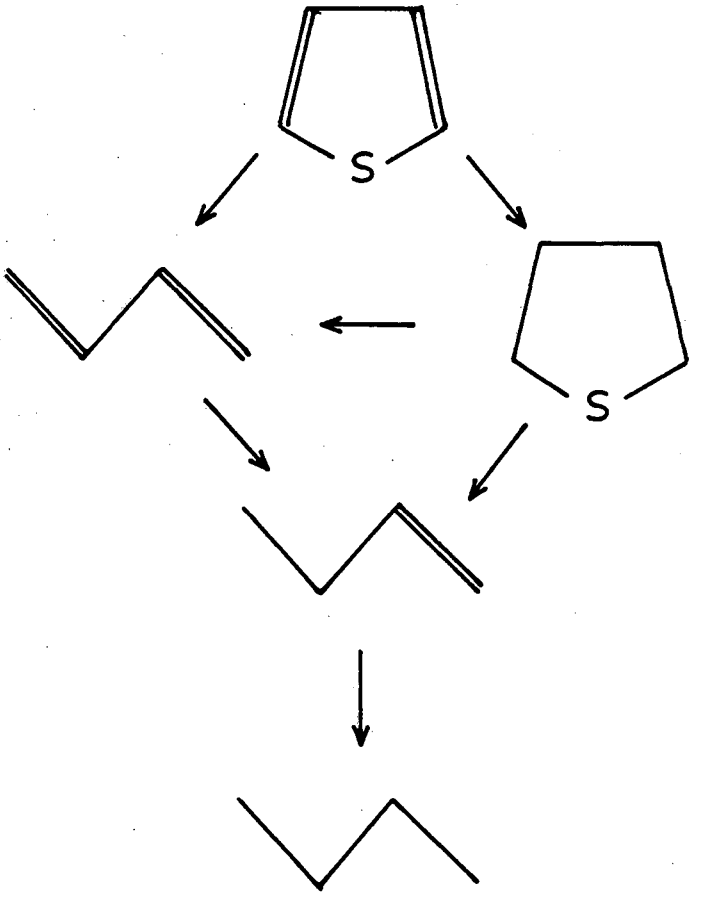

Fig. 5.1 Possible reaction pathways for thiophene HDS.

lead to the conclusion that butadiene is an intermediate in the reaction and that hydrogenation of C-S bonds occurs prior to hydrogenation of C-C bonds (3). In addition it has been shown that the HDS of tetrahydrothiophene yields a different product distribution from that of thiophene (6). Nevertheless this is still a point of contention.

The work described in this chapter has been performed over Mo single crystals that have been well characterized both in terms of composition and structure. The first experiments were aimed at determining whether or not it is possible to catalyze the HDS of thiophene over a metal surface and what similarities this reaction may have to that performed over an industrial catalyst. Following this a number of kinetic experiments were performed over the Mo(100) surface to measure the effects of variations in various reaction parameters. No detailed fitting of rate expressions has been performed although a model is proposed that is consistent with the observed kinetic parameters. It should be noted that this reaction is very complicated, involving the scission of two C-S bonds, the dissociation of H_2 and the formation of two S-H bonds and between two and six C-H bonds. The proposal of a detailed mechanism and the fitting of rates to obtain kinetic constants based purely on kinetic observations would be extremely difficult and of questionable value. It is also worth noting that the kinetic studies performed to date over supported catalysts have all, to my knowledge, focussed on the overall reaction rate, as measured by the disappearance of thiophene or the appearance of C_4 hydrocarbon products. In this study it has been very useful to examine the kinetics of formation of each of the products individually, as not all are identical. Finally, the effects of surface modification have been studied by varying both sulfur coverage and surface structure.

5.2 The Nature of the HDS Reaction

Fig. 5.2 shows the evolution of HDS products into the closed loop batch reactor as a function of time during a reaction in which the feed was 2.5 torr of thiophene and 1.0 atm of H_2 and the crystal temperature was held at 380°C. In this case the crystal was initially clean. The product yields are plotted as turnover numbers (TN, product molecules per surface atom) and the fact that these are in excess of 1 indicates that the reaction is indeed catalytic. Under these conditions the thermodynamic yield is expected to be almost purely butane, indicating that the reaction is kinetically limited. It is clear that while a steady state catalytic reaction takes place over the first one to two hours there is some modification of the surface resulting in a decrease in the rate of butadiene production after this period. Since this deactivation takes place and is not well understood at this point most reactions have been limited in length to ~90 min. and all reported rates are initial rates of reaction measured over the first hour. Total rates of reaction are calculated by summing the appearance rate of all C_4 hydrocarbon products. Since the total conversion of thiophene was always very low (<5%) it was difficult to accurately measure rates of thiophene disappearance. No induction period was observed although the proceedures used would not have been sensitive to an induction period of less than ~5min.

The reaction products are primarily butenes with some butane and butadiene. This product distribution is compared in Fig. 5.3 with that observed over a powdered, unsupported MoS_2 catalyst under similar conditions (6,7). The two are almost identical, suggesting that the HDS

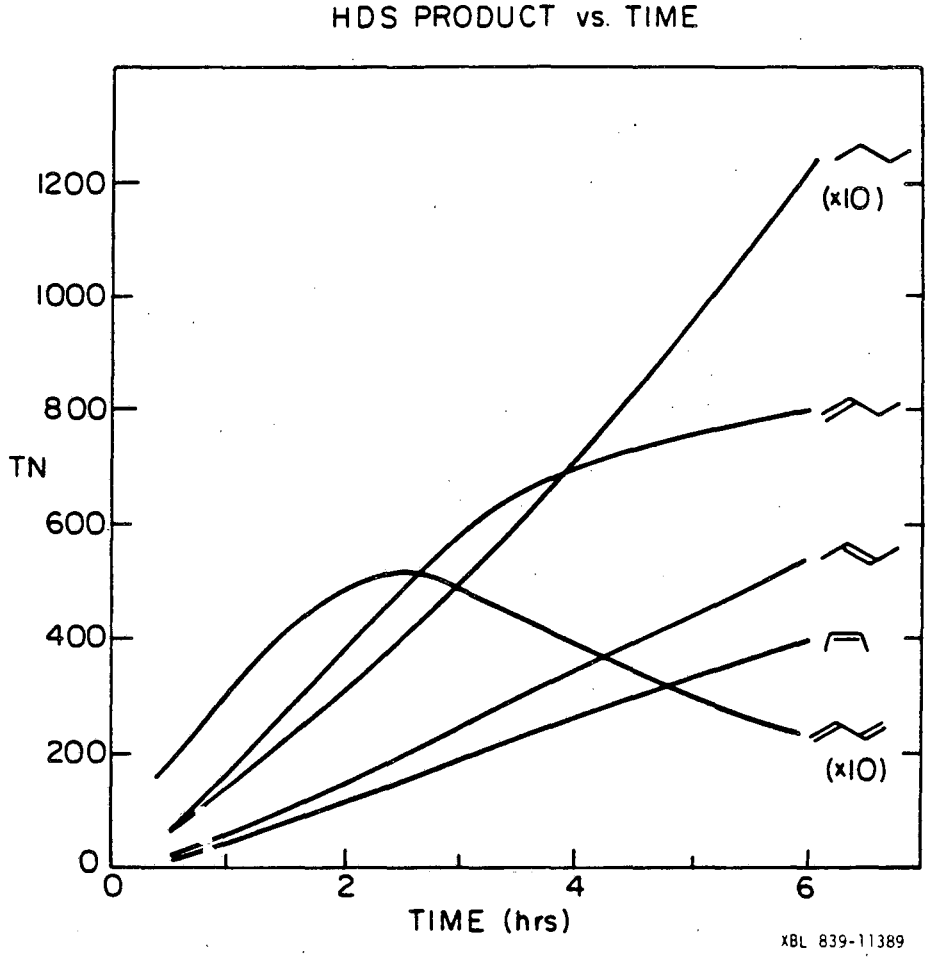

Fig. 5.2 The appearance of thiophene HDS products in reactor with time. T = 380°C, $P(H_2)$ = 780 torr, P(Th) = 2.5 torr

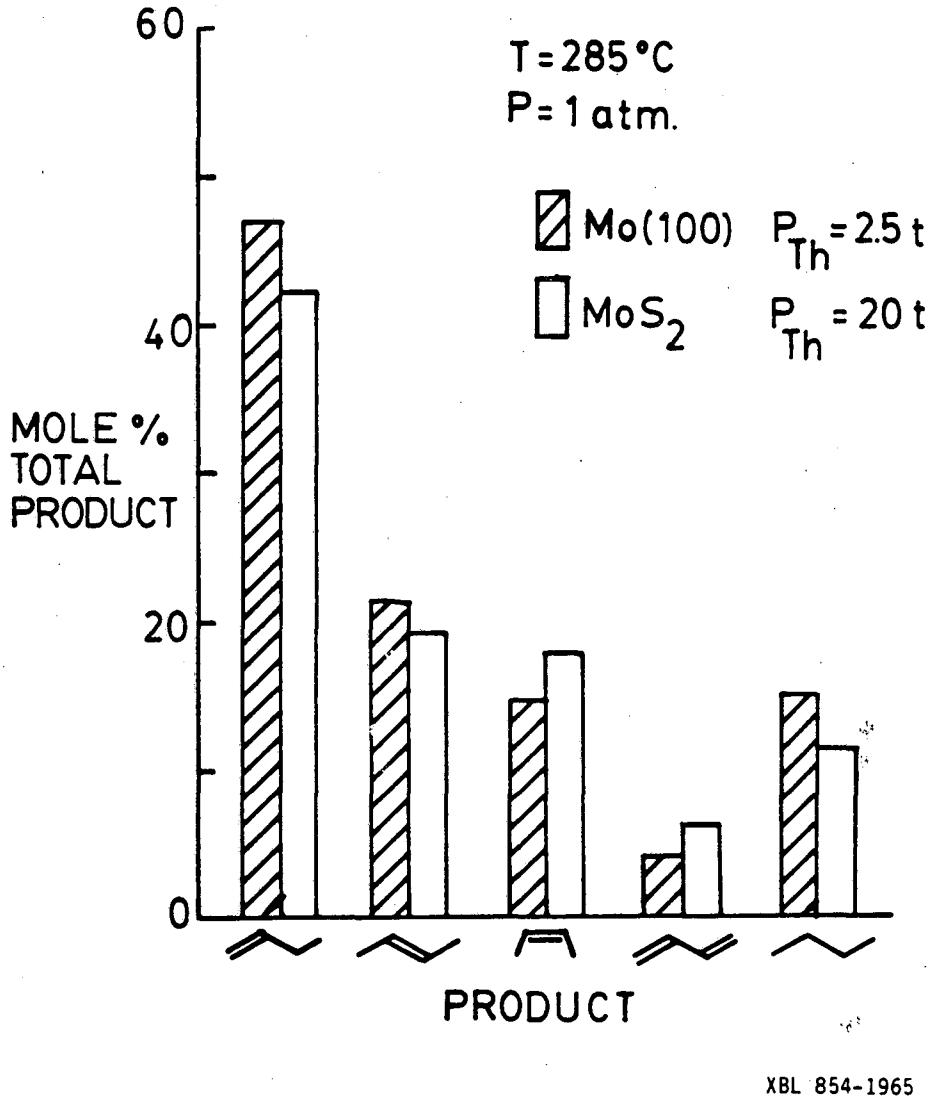

Fig. 5.3 Comparison of the product distibutions from thiophene HDS over the clean Mo(100) surface and powdered MoS_2.

of thiophene over a Mo(100) single crystal proceeds by a mechanism similar to that over the MoS_2 catalyst. A comparison of the absolute reaction rates shows that the single crystal is much more active than the MoS_2 powder. The single crystal gives a turnover frequency of 3.2×10^{-2} molecules/site/sec or 5.3×10^{-7} moles/m^2/sec while the MoS_2 catalyst, with a BET surface area of 67 m^2/gm, had an activity of 2.3×10^{-9} moles/m^2/sec. This in itself is not particularly alarming since it is not clear that the BET measurement is sensitive only to the active surface and the MoS_2 powder probably has a large fraction of inactive surface area composed of the sulfided basal planes of MoS_2 crystallites. Furthermore, several studies have shown that there is very little correlation between the BET surface area and HDS activity for a number of sulfided Mo catalysts (8). A comparison of activity per unit weight of metal shows a similar discrepancy with the single crystal having an activity of 3.4×10^{-4} moles/gm/sec as compared with 2.5×10^{-7} moles/gm/sec for the high surface area catalyst. Apparently only a small fraction of the metal atoms in the MoS_2 are active. Again this is not surprising since a large fraction of Mo atoms are probably not exposed to the reactant mixture.

The long term deactivation of the Mo(100) single crystal catalyst has not been studied in great depth but can be associated with the formation of a MoS_2 overlayer on the surface. Fig. 5.4 shows the typical AES spectrum of the surface after a long reaction time indicating an extremely high sulfur coverage, some carbon, and a small amount of oxygen contamination. The oxygen contamination appeared primarily after exposing the crystal to atmosphere and would disappear after several reactions. It has not been possible to characterize the nature

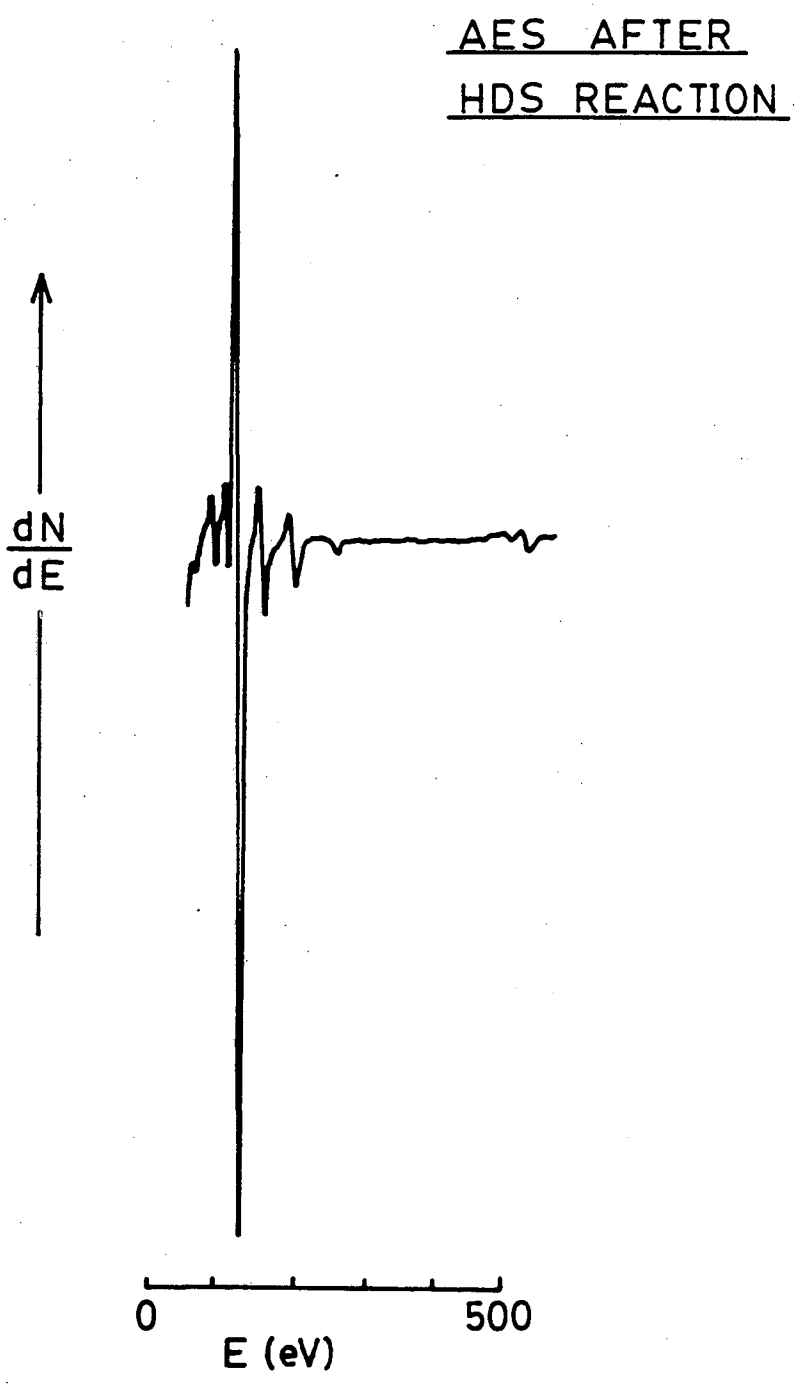

Fig. 5.4 Auger spectrum of the Mo(100) surface after a thiophene HDS reaction. This spectrum is typical of a surface that has become deactivated.

of the sulfur in the sense that it is not known whether the sulfur is present in the form of organic sulfur or bound to the metal surface. Studies using XPS would help answer this point but were not available on the chamber used for these reaction studies. Heating of the sample resulted in the evolution of enormous amounts of hydrogen, probably from the Ta support rods that are known to absorb large amounts of hydrogen. The S_{150}:Mo_{221} AES ratio in Fig. 5.4 approaches the value of ~12:1 observed for a MoS_2 single crystal (9). In general no LEED pattern can be observed from the surface unless the duration of the reaction is fairly short, in which case the sulfur coverage was less than a monolayer and the square lattice due to diffraction from the substrate can be observed. Annealling of a heavily sulfided surface to 800-1100K will produce the LEED pattern shown in Fig. 5.5 with no significant change in the AES spectrum. The LEED pattern in Fig. 5.5a has diffraction spots forming a square lattice, again produced by the substrate, and a circle of diffraction intensity with twelve maxima about its perimeter. These are due to diffraction from two domains of a hexagonal overlayer rotated at 30° with respect to each other. The features in Fig. 5.5b are 2nd and 3rd order diffraction features from this overlayer. The lattice spacing of this hexagonal overlayer is 3.11Å±0.05Å which is almost identical to that of MoS_2 (3.15 Å) (10). This sulfide sulfide structure has been grown on both the Mo(100) and Mo(111) surfaces by exposures to H_2S (~1 torr) at high temperatures (>500°C) and has been determined to be the basal plane of MoS_2. This assessment has been made based upon the above observations and the comparison of electron energy loss (ELS) and LEED I/V measurements with those made on bulk MoS_2(11,12,13). The fact that the overlayer diffraction

Fig. 5.5 LEED pattern of MoS_2 overlayer on the Mo(100) surface produced by annealing of the deactivated, heavily sulfided surface to ~800°C. A) First order diffraction features. B) First, second and third order diffraction features.

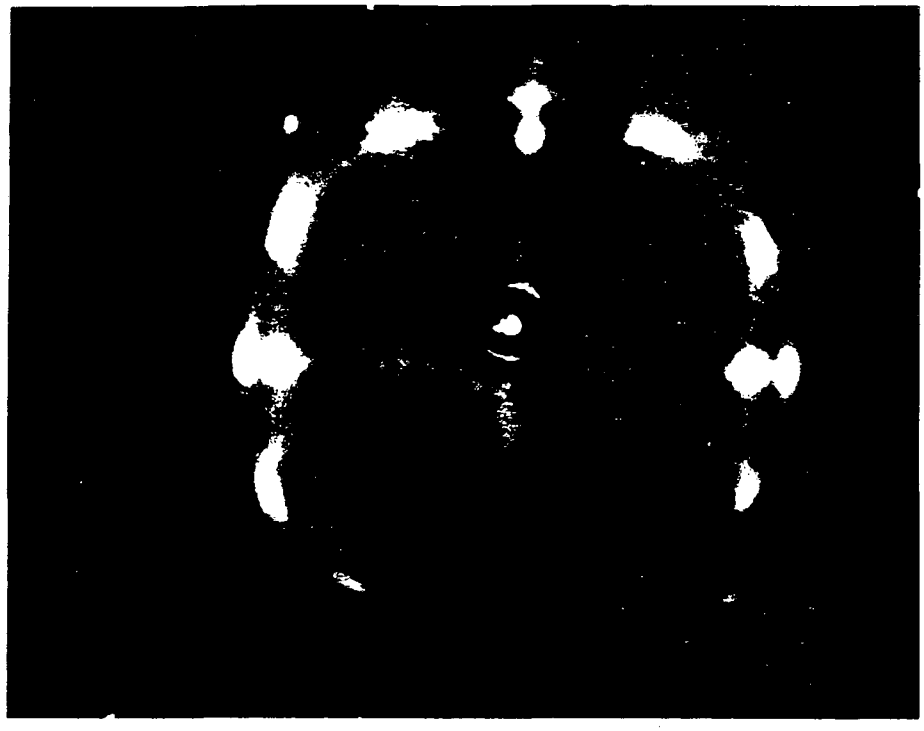

A

B

features are streaked to form concentric rings indicates poor rotational order. The two preferred orientations of the overlayers are shown in Fig. 5.6. On occasion this structure has been observed immediately following an HDS reaction without the need for annealing. This suggests that the surface after most reactions is composed of an MoS_2 overlayer having a high S_{150}:Mo_{221} AES ratio but not sufficiently well ordered to produce a LEED pattern, and that the effect of annealing is merely to induce long range ordering. The fact that these surfaces are composed primarily of the basal plane of MoS_2 explains the decrease in catalytic activity.

In an effort to determine the route that thiophene HDS takes through the proposed pathway (1,5) illustrated in Fig. 5.1, the HDS of tetrahydrothiophene (C_4H_8S) and the hydrogenation of butadiene have been studied over the sulfided single crystal surface. The product distribution of the HDS of tetrahydrothiophene over an initially clean Mo(100) surface is shown in Fig. 5.7. The total reaction rate was 0.49 molecules/site/sec, almost five times that of thiophene HDS. In addition to HDS a simple dehydrogenation reaction produces thiophene at a rate of 0.02 molecules/site/sec. The most striking feature of the distribution is the very large fraction of propylene produced, not apparent in the thiophene HDS product distribution. In all cases of thiophene HDS the rate of hydrogenolysis of C-C bonds was less than 5% of the total reaction rate. Clearly, tetrahydrothiophene is not a likely intermediate in the thiophene HDS reaction.

The tetrahydrothiophene HDS reaction is extremely interesting in its own right, although it has not received a great deal of attention in this study. The production of propylene implies breaking of C-C

PREFERRED ORIENTATIONS

of MoS_2 on Mo(100)

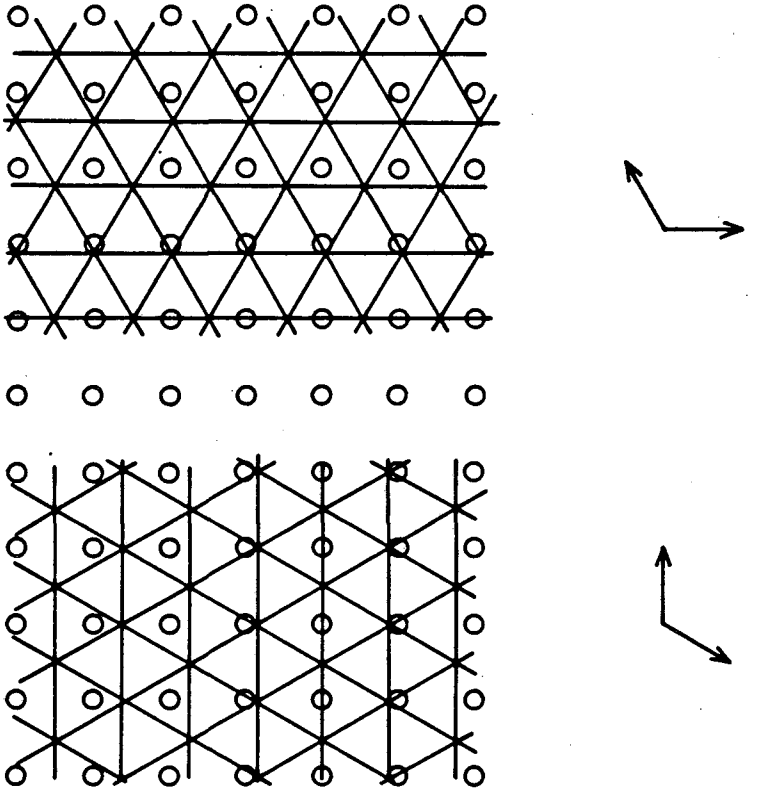

Fig. 5.6 Preferred orientations of the MoS_2 overlayer of the Mo(100) surface.

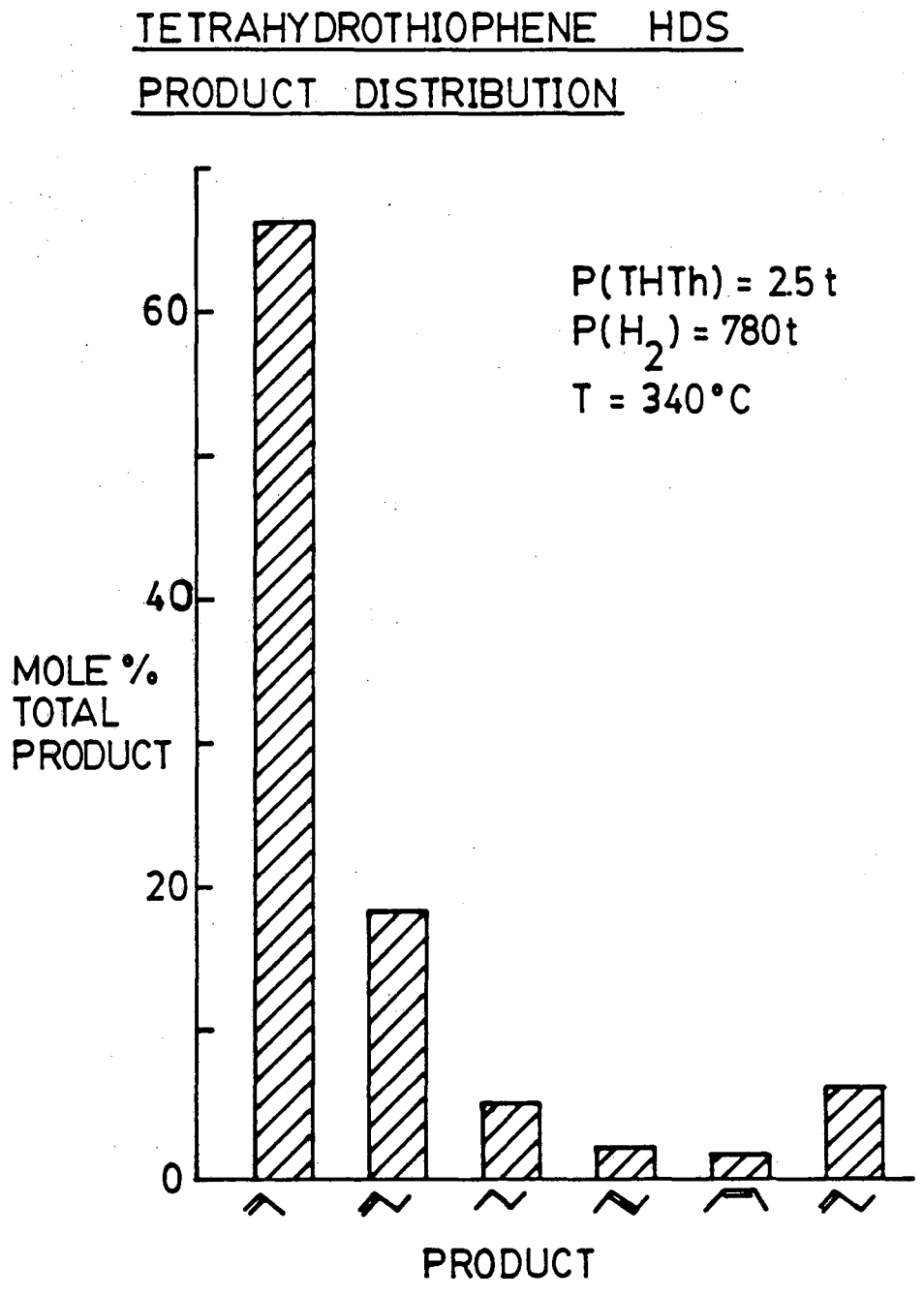

Fig. 5.7 Product distribution of the HDS of tetrahydrothiophene over the clean Mo(100) surface.

bonds but is not accompanied by the simultaneous production of methane. At this point in time no products other than C_3 and C_4 hydrocarbons have been detected. Auger analysis of the surface after the reaction shows no anomalous buildup of carbon to account for the non-stoichiometric reaction, nor is there any apparent contamination of the bulk of the crystal with dissolved carbon. The flame ionization detector used in this work is sensitive only to carbon atoms in a reduced form and so, such possible carbon containing products as CS_2 would not be detectable. The fate of the remaining carbon atom is still under investigation.

One study of the HDS of tetrahydrothiophene over a powdered MoS_2 catalyst reports the production of C_3 hydrocarbons, although in this case the product was allene (C_3H_4) (18). The discrepancy here may lie in the fact that the hydrogen pressure used was 10 torr vs. the 780 torr used in the present study suggesting that in our case allene is an intermediate that is hydrogenated to propylene. Again, no products containing only one carbon atom were detected and the remaining atom was assumed to be left adsorbed on the catalyst. Propylene has been observed as a product of the hydrodeoxygenation (HDO) of furan (14) and once again the fourth carbon atom from the ring was assumed to be remaining on the catalyst. Our investigation over Mo foils showed that during the HDO of both furan and tetrahydrofuran the production of propylene was accompanied by the appearance of CO (15).

Finally, the hydrogenation of butadiene has been studied over a sulfided Mo(100) surface. Fig. 5.8 shows the evolution of products into the reactor during the course of this reaction. It is clear that the hydrogenation of terminal double bonds occurs more readily than does

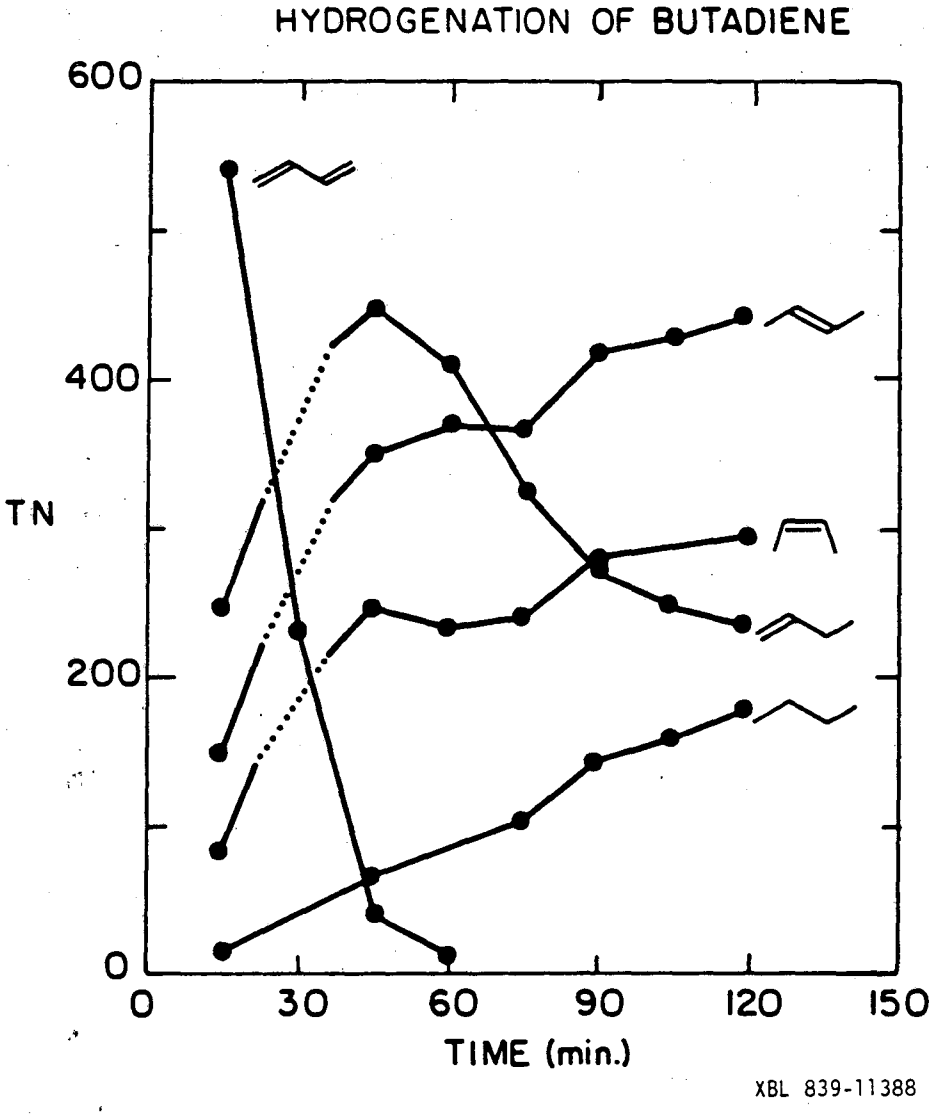

Fig. 5.8 The disappearance of butadiene and appearance of butenes and butane in the ractor during the hydrogenation of butadiene over a sulfided Mo(100) surface.

that of the central double bond. Comparison of the initial yields of butenes and butane with those produced by thiophene HDS shows a strong similarity (Fig. 5.9). It seems that butadiene is a likely intermediate during thiophene HDS while tetrahydrothiophene is not, i.e. that the hydrogenation reaction are much slower than the hydrogenolysis of C-S bonds.

5.3 Kinetics of Thiophene HDS

This section presents the results of a number of kinetic measurements of thiophene HDS made over the clean Mo(100) surface. Description of a model consistent with both these and other results will be reserved for the discussion section of this chapter. An Arrhenius plot of the appearance rates of each of the products is shown in Fig. 5.10. The rate of butadiene production is the only curve that shows Arrhenius type temperature dependence with an activation energy of 14.4 ± 2 kcal/mole. The Arrhenius plots for the butenes have a negative curvature, all having similar temperature dependences. The rate of butane production has strongly non-Arrhenius type temperature dependence showing a decrease in rate with increasing temperature and a maximum at about 600K. A comparison of the reaction rates in a D_2 atmosphere shows no significant change in the reaction rates except at the highest temperature (693K). The isotope effect that might be expected for a reaction whose rate limiting step is hydrogenation is not apparent. An Arrhenius plot of the reaction rates in D_2 (Fig. 5.11) shows the same general behaviour as that for the reaction in H_2. The activation energy for butadiene production is measured as 12.6 ± 2 kcal/mole.

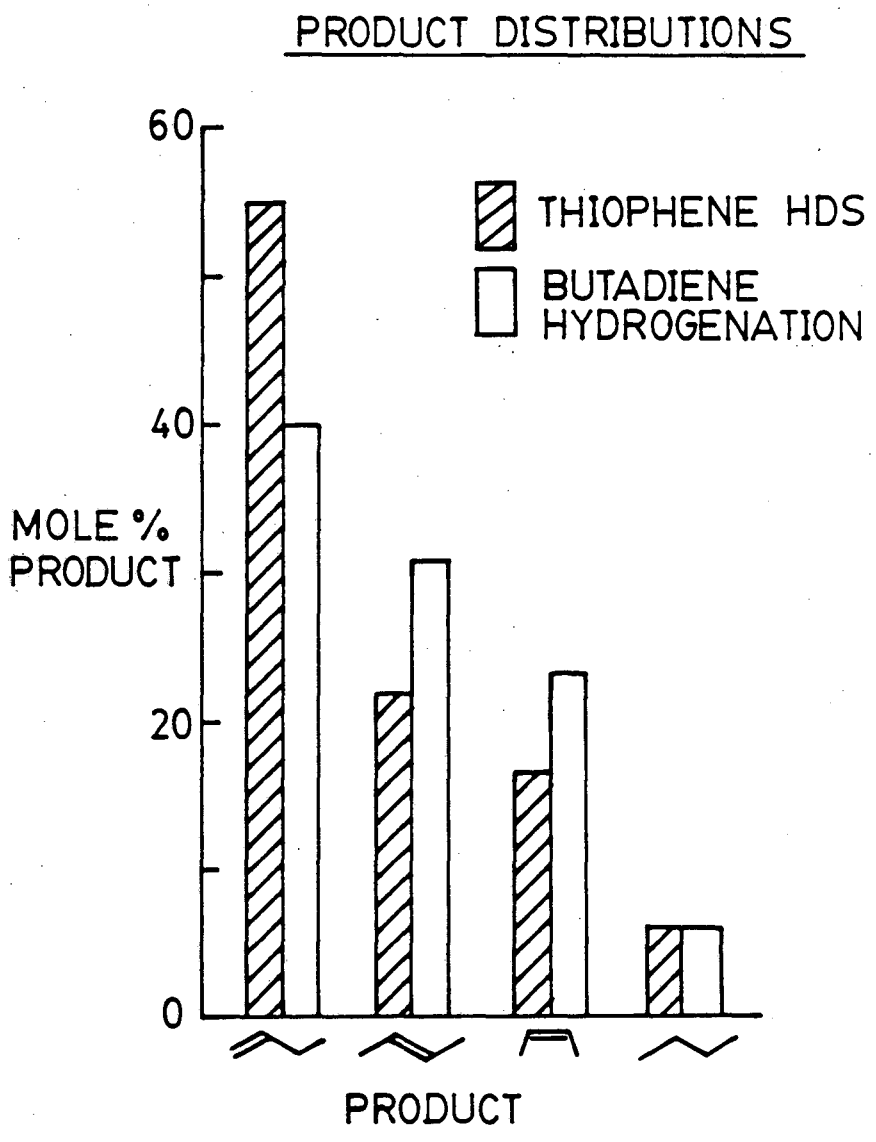

Fig. 5.9 The initial product distribution of the butadiene hydrogenation reaction over the sulfided Mo(100) surface.

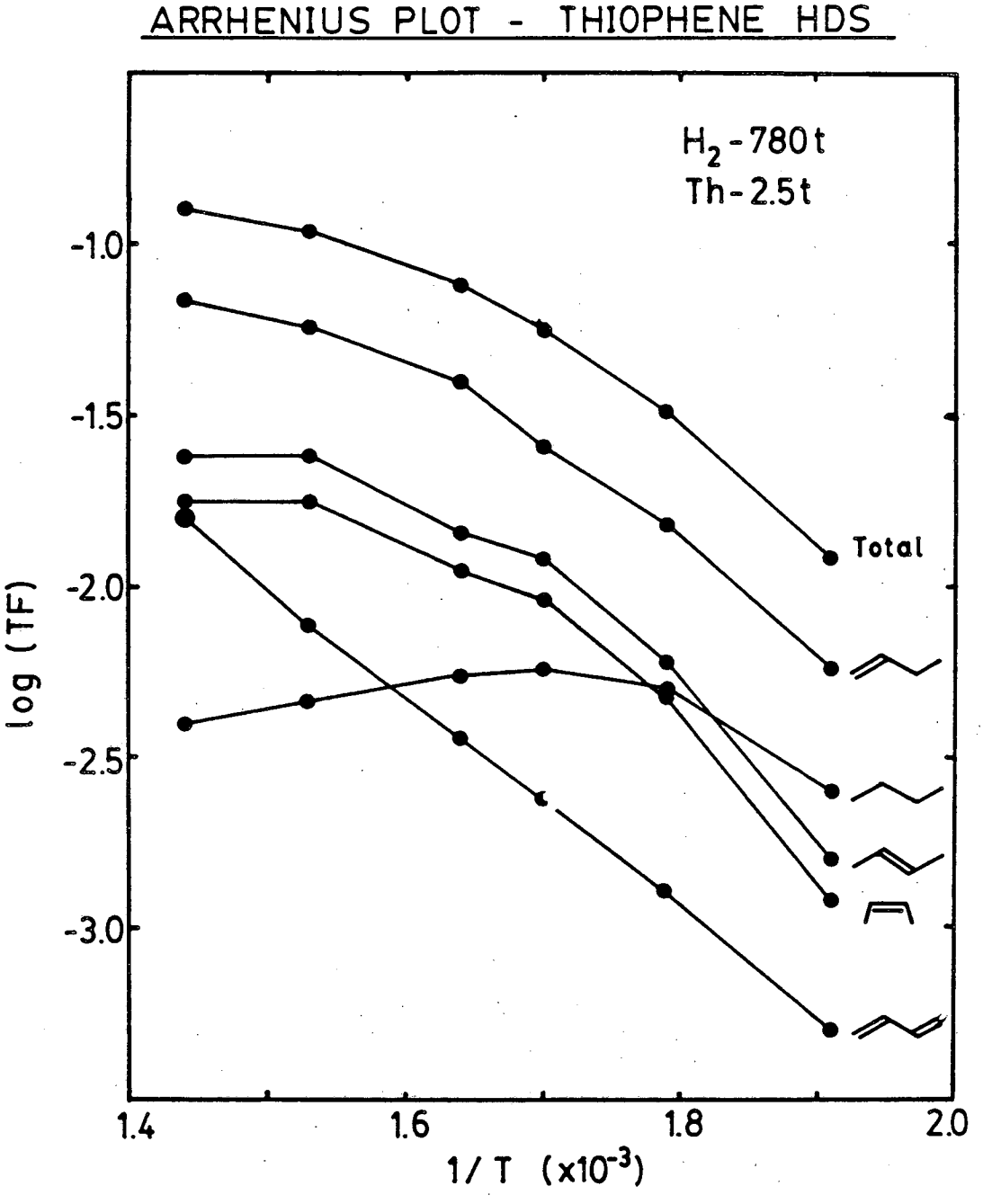

Fig. 5.10 Arrhenius plot of the rates of product appearance during thiophene HDS over the clean Mo(100) surface. $P(H_2)$ = 780 torr, P(Th) = 2.5 torr.

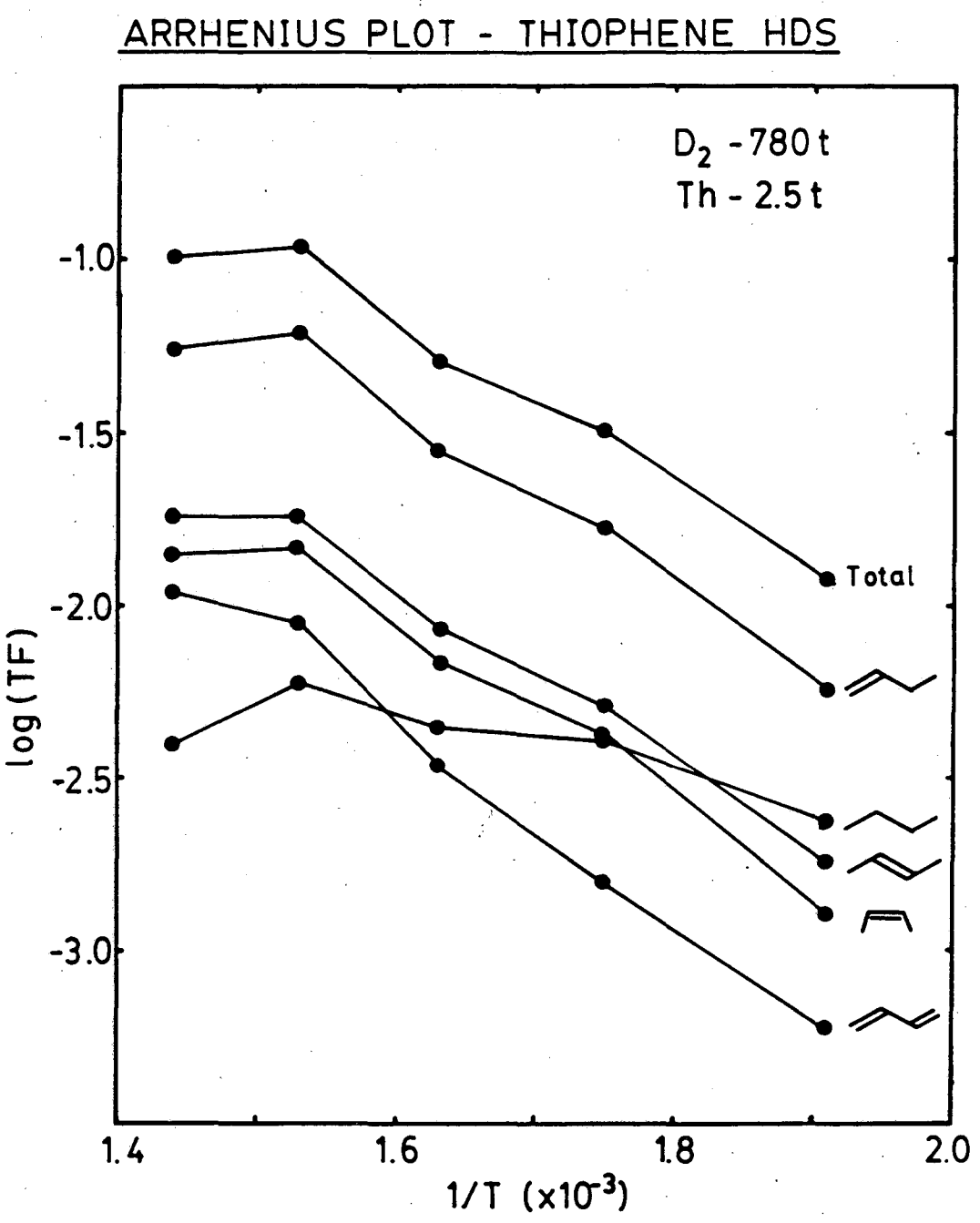

Fig. 5.11 Arrhenius plot of the rates of product appearance during thiophene HDS in deuterium over the clean Mo(100) surface. $P(D_2)$ = 780 torr, P(Th) = 2.5 torr.

Since the butenes are the primary product the total rate of reaction follows their temperature dependence and shows the same non-Arrhenius type behaviour.

Figs. 5.12 and 5.13 are order plots illustrating the dependence of the reaction rates for butadiene, the butenes and butane on both hydrogen and thiophene pressures. The dependence among the three butene isomers shows very little variation. The rate dependence on hydrogen pressure is roughly 0, 1/2, and 1 for butadiene, the butenes, and butane respectively with the measured values listed on the figure. The rate of butadiene production has a first order dependence in thiophene pressure while the hydrogenated products show only very weak dependence. Again, exact values are listed on the figure.

5.4 The Effect of Surface Composition and Structure on Thiophene HDS

The reactions described to this point have all been performed over the initially clean Mo(100) surface, and will be discussed in the following section in terms of a reaction pathway or mechanism yielding some insight into the nature of the reaction intermediates that are present. As yet, though, little information has been obtained about the nature of the catalyst surface composition and structure other than the fact that a large amount of sulfur is present in some form and that after long reaction times the surface is converted to MoS_2. It is clear though that for periods of 1-2 hrs. some catalytic surface exists in steady state, desulfurizing thiophene. The following work attempts to determine the role of sulfur and the effect of surface structure on reaction rates by varying each.

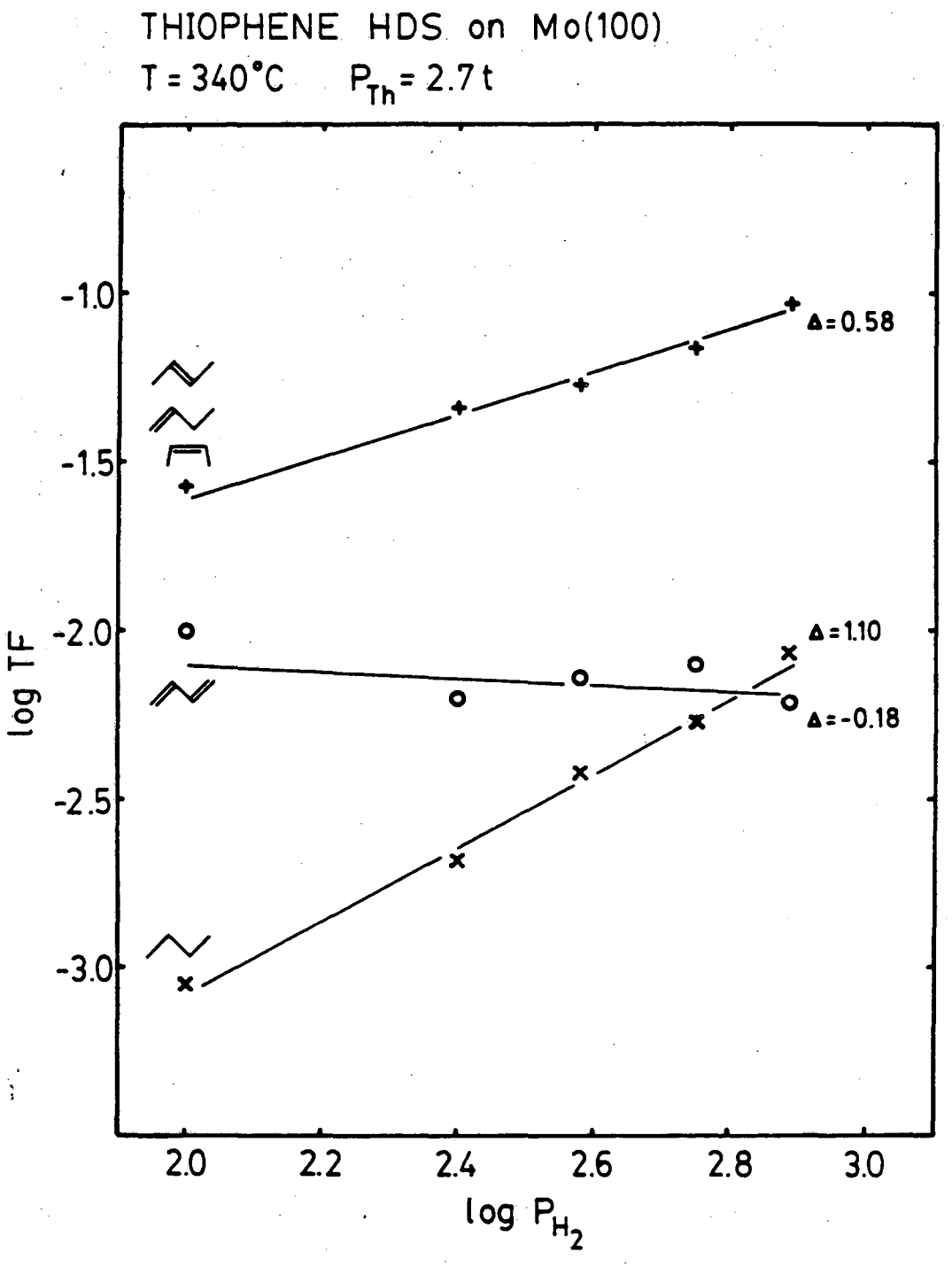

Fig. 5.12 Hydrogen pressure dependence of the product rates of appearance during thiophene HDS over the clean Mo(100) surface. P(Th) = 2.5 torr, T = 340 °C.

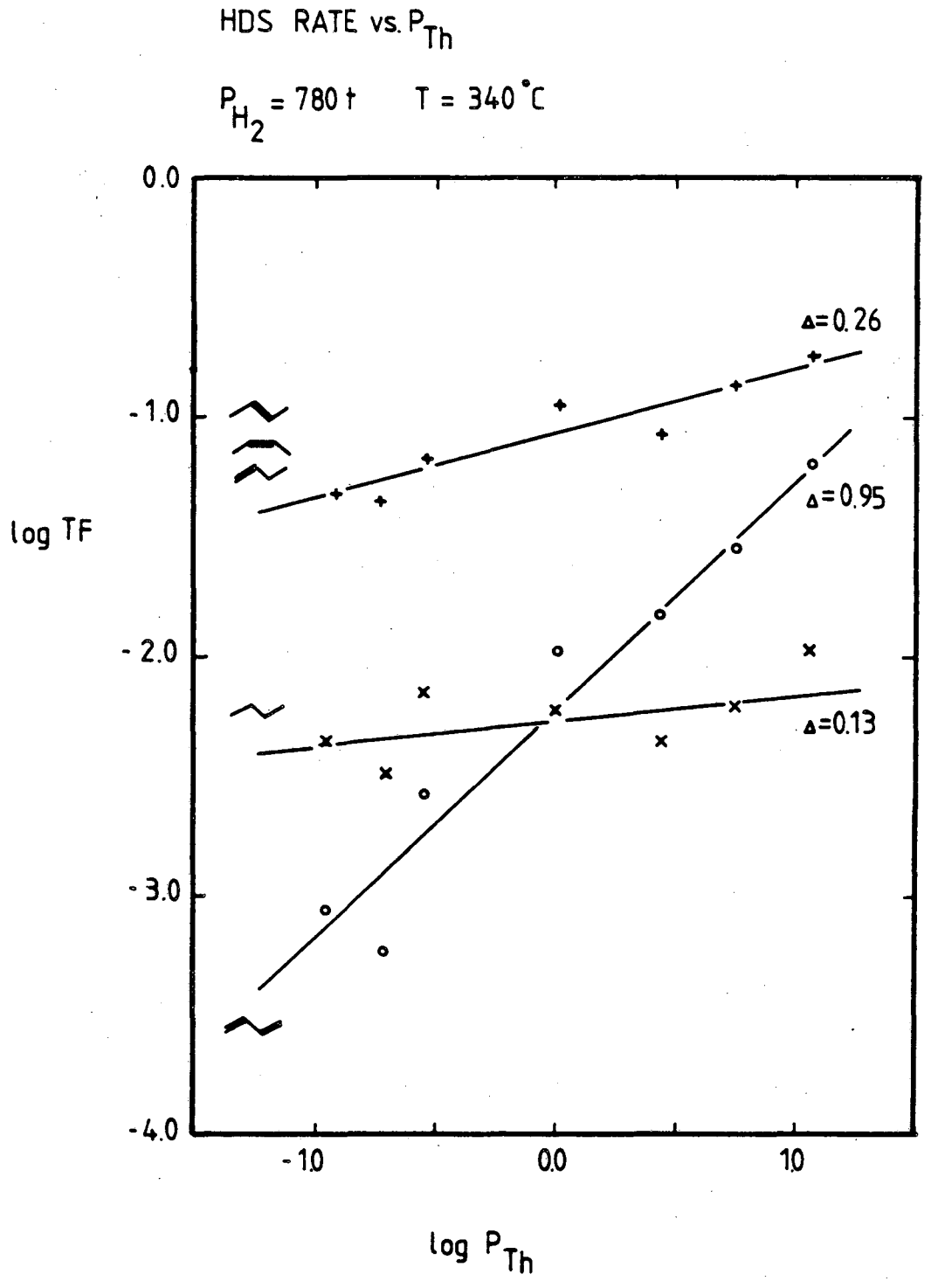

Fig. 5.13 Thiophene pressure dependence of the product rates of appearance during thiophene HDS over the clean Mo(100) surface. $P(H_2)$ = 780 torr, T = 340 °C.

Fig. 5.14 shows the total reaction rate vs. initial sulfur coverage. In the low coverage regime there is a decrease in activity with coverage that continues up to coverages of ~0.6 monolayers, while at higher coverages there is little further variation in the rate. The curve is merely as a visual aid and is not a fit of any function to the data. At low coverages one might expect a linear dependence on the coverage based on the fact that the sulfur overlayer forms islands of c(2x2) structure and thus the rate should be some linear combination of the rate over a clean surface and that over the sulfur layer. At higher coverages it is not clear what is to be expected since the sulfur atom becomes more weakly bound to the metal and begins to populate a second binding site (16).

Fig. 5.15 shows the dependence of the production rates of butadiene, the butenes, and butane individually on the initial sulfur coverage, with each normalized to its rate on the clean surface. The rates of production of the three isomers of butene all have a similar dependence on the sulfur coverage. These and the rate of butane production closely mimic the behaviour of the total reaction rate with initial sulfur coverage. The striking point is that the rate of butadiene production is independent of sulfur coverage. This and the kinetic data suggest that the desulfurization and hydrogenation steps are quite distinct.

The histogram in Fig. 5.16 compares the rates of thiophene HDS over four clean, single crystal Mo surface of different structure. These have all been normalized to assume 10^{15} atoms per cm^2, which is the surface atomic density of the Mo(100) face, and thus are proportional to the activity per unit area. Schematics of the low Miller

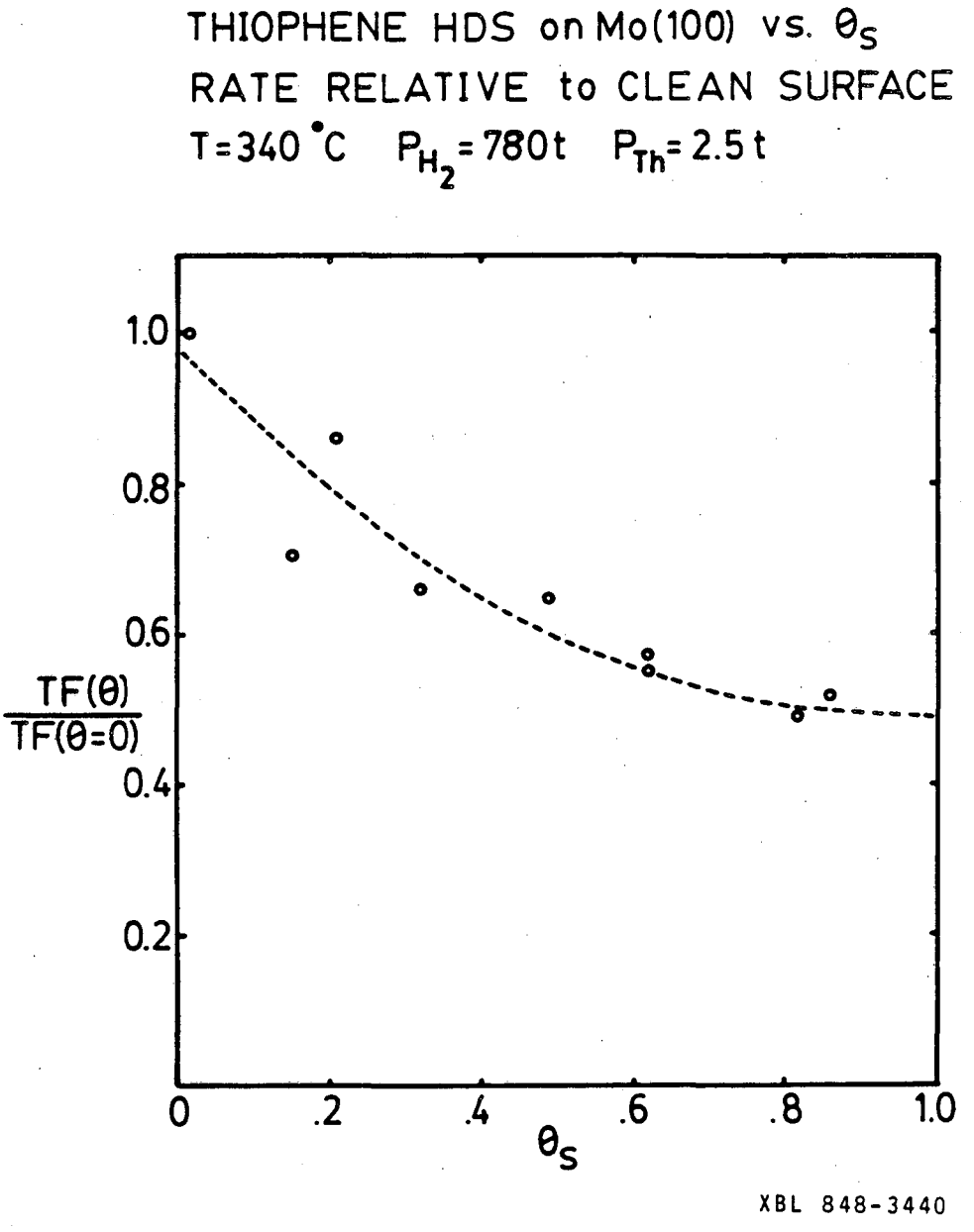

Fig. 5.14 Rate of thiophene HDS vs. initial sulfur coverage of the Mo(100) surface. Rates are given relative to those on the clean surface. $P(H_2)$ = 780 torr, P(Th) = 2.5 torr, T = 340°C.

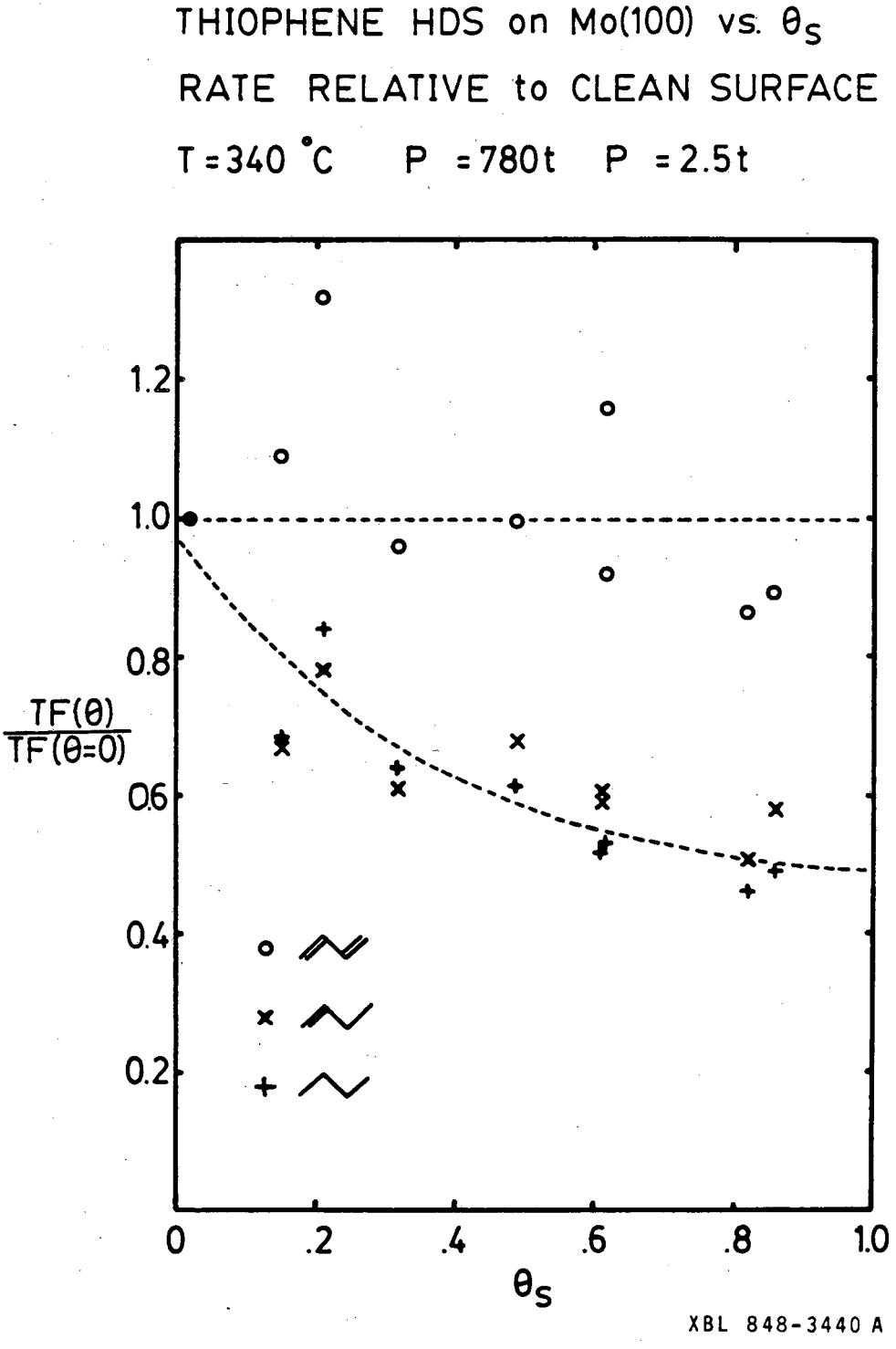

Fig. 5.15 Product rates of appearance vs. initial sulfur coverage of the Mo(100) surface. Rates are given relative to those on the clean surface. $P(H_2)$ = 780 torr, P(Th) = 2.5 torr, T = 340°C.

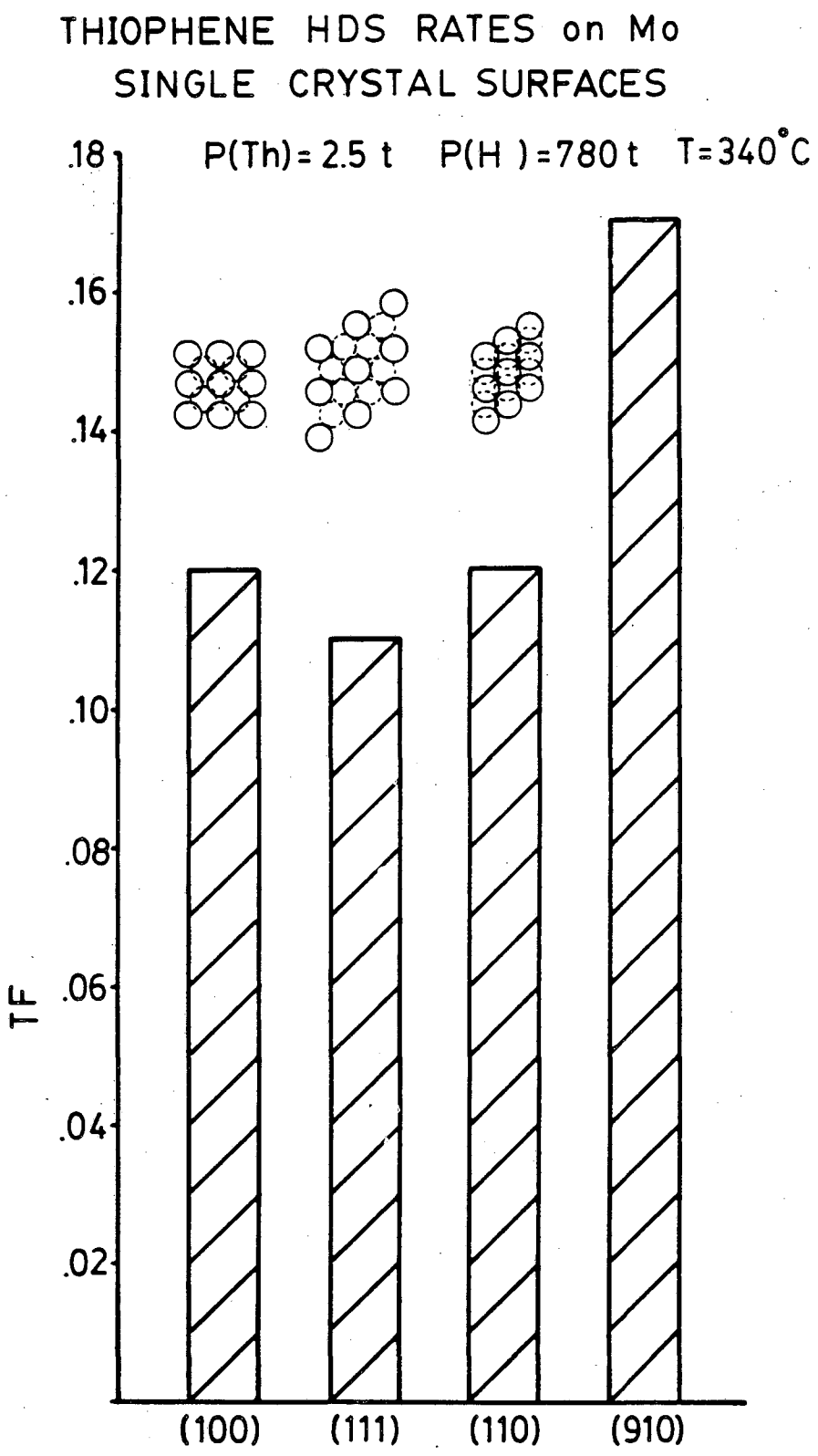

Fig. 5.16 Comparison of the rates of thiophene HDS over the Mo(100), Mo(110), Mo(111) and Mo(910) surfaces. $P(H_2)$ = 780 torr, P(Th) = 2.5 torr, T = 340°C.

index faces are included in the figure and the Mo(910) face is depicted in Fig. 5.17. There are no dramatic variations in activity from one face to the next, indicating a structure insensitive reaction. Nor are there any significant variations in product distributions.

5.5 Discussion

The second section of this chapter has shown that the catalytic hydrodesulfurization of thiophene in hydrogen can be carried out over the Mo(100) surface and that this reaction closely mimics that performed over a powdered MoS_2 catalyst, at least with respect to the product distribution. The reaction over the initially clean surface proceeds with a turnover frequency of 0.11 ± .03 at a temperature of 340°C and reactant pressures of 2.5 torr thiophene and 780 torr hydrogen. The activity of the catalyst is constant over a period of about one hour after which a deactivation process begins to become apparent that has been associated with the formation of an MoS_2 overlayer. Comparison of the product distribution with those of tetrahydrothiophene HDS and butadiene hydrogenation suggest that that reaction proceeds via initial desulfurization yielding butadiene that is subsequently hydrogenated to the butene and butane products.

The kinetic parameters of the reaction over the clean Mo(100) surface suggest a fairly complex reaction scheme. The first point of interest is the dependence of the reaction rates on the crystal temperature. The non-Arrhenius temperature dependence of the butenes and butane products, and in particular the maximum in the rate of butane production suggest a depletion of the surface in one of the reactant

Mo (910)

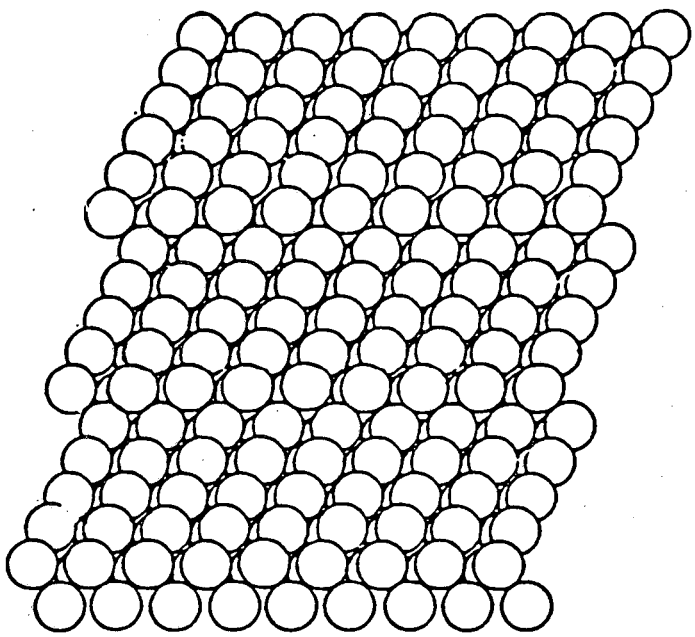

Fig. 5.17 Illustration of the Mo(910) surface.

species with increasing temperature. Such an effect occurs because the observed rate constant in a surface reaction can often be composed of both true rate constants and adsorption equilibrium constants (17). Considering the simple case of a unimolecular reaction in which a gas phase molecule (A_g) is in equilibrium with its adsorbed counterpart (A_a), and $A_a \rightarrow B_a$ with B_a desorbing immediately.

$$A_g \rightleftharpoons A_a \qquad K_A = A \exp(\Delta H_A/RT)$$

$$A_a \rightarrow B_a \qquad k_r = A' \exp(-E_a/RT)$$

$$B_a \rightarrow B_g \qquad k_d \qquad (k_d >> k_r)$$

The surface coverage of A_a will be given by

$$\theta_A = \frac{K_A P_A}{1 + K_A P_A}$$

and thus the reaction rate by

$$r_A = \frac{k_r K_A P_A}{1 + K_A P_A} \quad .$$

The Arrhenius plot gives an apparent activation energy of

$$\frac{d \ln(r)}{d (-1/RT)} = E_a - \Delta H_A + \frac{\Delta H_A K_A P_A}{1 + K_A P_A} \quad .$$

At low temperatures θ_A will be ~1 and fairly independent of temperature and the slope of the plot will give the correct activation energy of E_a. At high temperatures $K_A P_A$ will become very small and the apparent activation energy will be $E_a - \Delta H_A$ which can be negative if $\Delta H_A > E_a$.

In the present case the depletion of the surface in hydrogen

coverage can explain the observed Arrhenius plots. Since the production of butadiene is independent of hydrogen pressure it is expected that, if this is the case, its rate of appearance will obey Arrhenius type kinetics. The fact that the butenes all have approximately half order dependence in hyrogen pressure means that they should have similar temperature dependences, having rate expressions of the form

$$r_1 = \frac{k_1 K_H^{1/2} p_H^{1/2}}{1 + K_H^{1/2} p_H^{1/2}} = k_1 f(T)$$

with k_1 depending upon the butene isomer and f(T) being the hydrogen adsorption isotherm at a given pressure. The butane production rate, being first order in hydrogen pressure, is expected to have a stronger dependence on hydrogen coverage and should have a rate expression given by

$$r_2 = \frac{k_2 (K_H^{1/2} p_H^{1/2})^2}{(1 + K_H^{1/2} p_H^{1/2})^2} = k_2 f^2(T) \quad .$$

If this analysis is correct and sufficient to explain the non-Arrhenius behaviour of the rates the the ratio r_1^2/r_2 should have the form

$$\frac{r_1^2}{r_2} = \frac{k_1^2}{k_2} \quad .$$

Since k_1 and k_2 are simple rate constants the plot $\ln(r_1^2/r_2)$ vs. 1/T should be linear. This plot is shown in Fig. 5.18 and, in fact, is linear through all but the highest temperatures, having a slope giving $2E_1-E_2=21$ kcal/mole, where E_1 and E_2 are the activation energies for the butene and butane production rate constants respectively. The

$\log(r_1^2/r_2)$ vs. $1/T$

r_1 - Butene r_2 - Butane

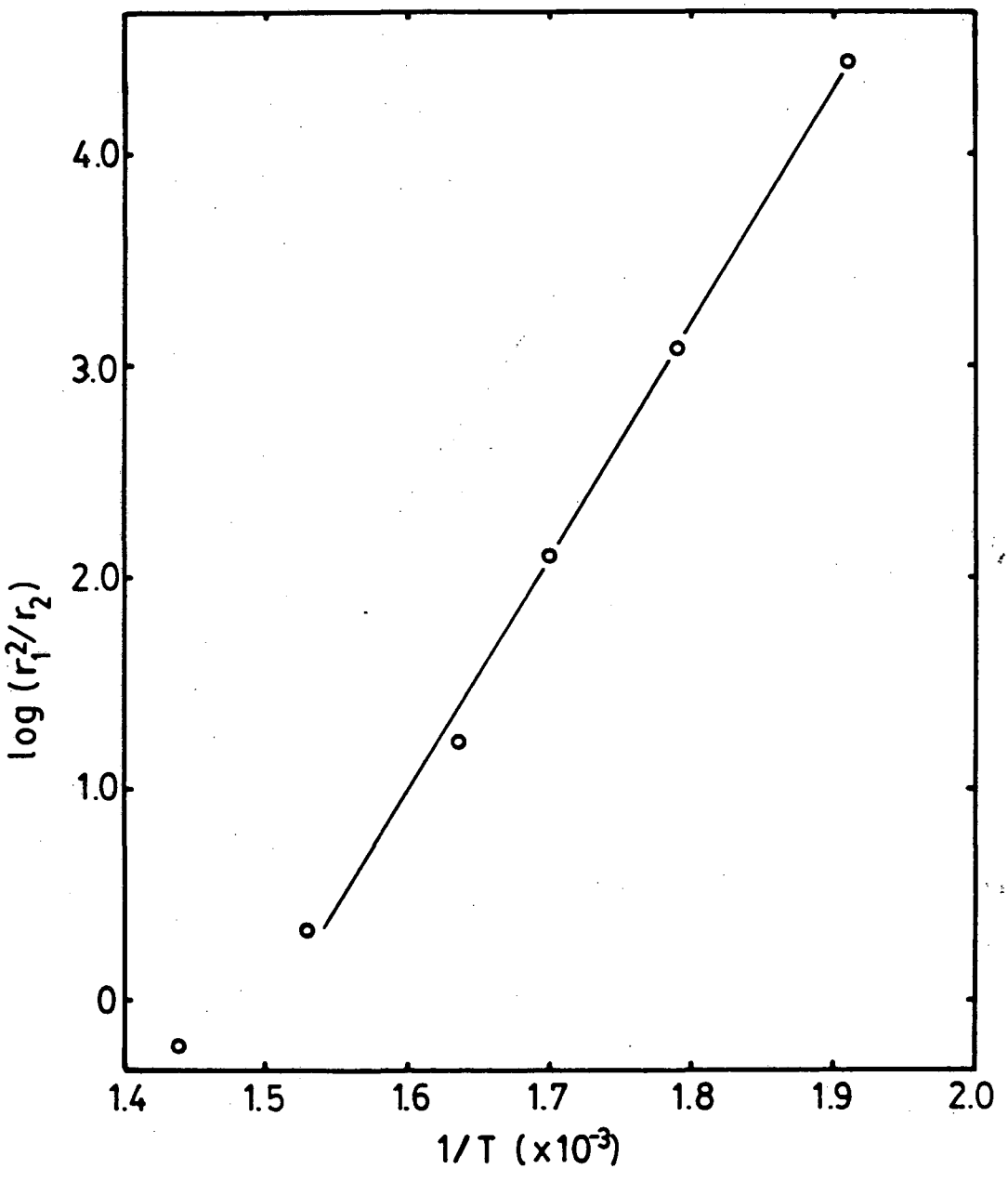

Fig. 5.18 Plot of (r_1^2/r_2) vs. $1/T$. r_1 is the rate of butene production and r_2 the rate of butane production during thiophene HDS. $P(H_2)$ = 780 torr, P(Th) = 2.5 torr.

hydrogen pressure dependence of the reaction rates was measured at 613K ($1/T = 1.63 \times 10^{-3}\ K^{-1}$). The fractional order of the butene production suggests that the hydrogen coverage at this temperature is in the low coverage regime of the equilibrium adsorption isotherm and that the adsorption is indeed dissociative.

In examining the kinetics of the HDS reaction the first product of interest is butadiene. Its rate of appearance is independent of hydrogen coverage in spite of the fact that its formation requires the creation of at least two C-H bonds. The fact that the rates of butene and butane production depend on hydrogen pressure, and the arguments made above, rule out the likelyhood of a hydrogen saturated surface. It would only be possible to argue along these lines by invoking the existence of two hyrogen adsorption sites, one saturated in hydrogen that is responsible for desulfurization, leading to butadiene, and a second that is poor in hydrogen and produces the hydrogenated products. The other possible reason for a zero-order hydrogen pressure dependence is that the surface is saturated in butadiene and that the reaction is rate limited by its desorption. This can be eliminated based upon the fact that the rate of butadiene production has a first order dependence on the thiophene pressure.

The butadiene kinetics can be explained by a reaction mechanism in which the rate limiting step occurs prior to hydrogenation and the subsequent hydrogenation and butadiene desorption steps are fast.

$$Th_g \overset{k_1}{\rightarrow} T_a \underset{H}{\overset{k_2}{\rightarrow}} T_1 \underset{H}{\overset{k_3}{\rightarrow}} T_2 \underset{H}{\overset{k_4}{\rightarrow}} T_3 \underset{H}{\overset{k_5}{\rightarrow}} \text{Butadiene}_a \overset{k_6}{\rightarrow} \text{Butadiene}_g$$

Here Th_g represents gas phase thiophene, T_a a species resulting from

thiophene adsorption that has not been hydrogenated by surface hydrogen, and T_1, T_2 and T_3 are partially hydrogenated intermediates in the reaction pathway leading from T_a to adsorbed butadiene. The rate limiting step could be adsorption of thiophene or some undetermined step leading to the species T_a that is then hydrogenated to butadiene. The point at which sulfur is extracted from the ring and desorbs as H_2S cannot be determined. If thiophene adsorption is the rate limiting step it is difficult to understand the origin of the 14 kcal/mole activation energy since this represents an unusually high barrier for a molecular adsorption process . A possible rate limiting step might be the breaking of C-S bonds to form a metal-sulfur species and some hydrocarbon fragment, both of which can be hydrogenated. This mechanism will be ruled out in Chapter 6 by some independent measurments of the rates of hydrogenation of the Mo-S bond. A final alternative, that has been proposed in the literature, is an intra-molecular desulfurization reaction leading to H_2S and a diacetylene-like species that must be hydrogenated at four points to yield butadiene (6,19). At this point the exact nature of the rate limiting step cannot be defined in any more detail than to reiterate that it occurs prior to any of the hydrogenation steps.

The rates of appearance of the hydrogenated products are dependent upon hydrogen pressure and almost independent of thiophene pressure. These kinetics suggest an intermediate in the hydrogenation pathway that is saturating its available adsorption sites. If such a species were present in equilibrium with butadiene, or any of the precursors to butadiene, the equilibrium expression for its coverage would be

$$K_7 \cdot \theta_B \cdot \theta_H(1-\theta_{BH}) = \theta_{BH}(1-\theta_H)$$

where θ_B is the coverage of butadiene or the precursor to butadiene that, when hydrogenated yields the species BH. θ_{BH} is the coverage of this intermediate that will lead to butene and butane production. Note that the above expression assumes no competition for binding sites between butadiene and BH or between hydrogen and hydrocarbons. If butadiene is weakly bonded to the surface through its π-orbitals it may be relatively insensitive to the exact site that it occupies. A singly hydrogenated butadiene molecule, on the other hand might specifically require a fourfold hollow site with which to form a metal-carbon σ-bond. The non-competitive coadsorption of hydrogen and hydrocarbons has also been observed related study of the hydrogenation of butadiene over Pt(110) surfaces (20). Given that the hydrogen coverage is low the equlibrium coverage of BH is given by

$$\theta_{BH} = \frac{K_7 \theta_B \theta_H}{1 + K_7 \theta_B \theta_H}$$

which, for a large value of the equilibrium constant, will be approximately unity, independent of the pressure of either reactant. A subsequent hydrogenation step to yield butene would have a rate expression of

$$r_1 = k_8 \theta_{BH} \theta_H$$

which would be independent of thiophene pressure and have a half order dependence on the hydrogen pressure, as observed.

The first order dependence of the butane production in hydrogen pressure implies a second equilibrium step involving hydrogen, before the final hydrogenation steps. If the above mentioned intermediate BH is in equilibrium with a second species BH_2 that ultimately leads to butane production then the equilibrium expressions become

$$K_7\theta_B\theta_H(1-\theta_{BH}-\theta_{BH_2}) = \theta_{BH}(1-\theta_H)$$

and $$K_{10}\theta_{BH}\theta_H = \theta_{BH_2}(1-\theta_H)$$

and the final coverages of each are given by

$$\theta_{BH} = \frac{K_7\theta_B\theta_H}{1 + K_7\theta_B\theta_H + K_7K_{10}\theta_B\theta_H^2}$$

$$\theta_{BH_2} = \frac{K_7K_{10}\theta_B\theta_H^2}{1 + K_7\theta_B\theta_H + K_7K_{10}\,\theta_B\theta_H^2}$$

The denominator is still dominated by the term $K_7\theta_B\theta_H$, if K_{10} is not large, because θ_H^2 is small. The coverages are

$$\theta_{BH} \approx 1$$

and $$\theta_{BH_2} \approx K_{10}\theta_H$$

not affecting the butene production kinetics. The hydrogenation of the BH_2 species to butane will have a rate given by

$$r_2 = k_{11}K_{10}\theta_H^2$$

which will be first order in hydrogen pressure and independent of

thiophene pressure, as observed. The suggestion that K_{10} is not large is consistent with the fact that butene production is much greater than butane production.

The hydrogenation reactions following desulfurization are fairly complex and the kinetic studies described above can do little to determine the details of the process. More extensive studies of the butadiene and butene hydrogenation and isomerization reactions might be of some interest. Those performed in this work have shown primarily that the distribution of butenes and butanes produced by the hydrogenation of butadiene is similar to that produced by thiophene HDS. Examination of Fig. 5.8 shows that butadiene hydrogenation is much faster than butene hydrogenation and that it is the terminal double bonds of the butenes that are hydrogenated preferentially. The isomers of 2-butene, produced both by butadiene hydrogenation and 1-butene isomerization, hydrogenate at a very slow rate.

The above analysis of the kinetics of thiophene HDS have yielded a mechanistic pathway that conforms to the observed behaviour and is outlined in Fig. 5.19. Needless to say such a model is not unique in explaining the data and the attempt has been made to avoid specification of any mechanistic details to as great an extent as possible. Nevertheless, the model does embody three points that it would seem are difficult to avoid in any interpretation of the data. First, the hydrogen coverage of the catalytic surface varies, under our conditions, in the temperature range 250°C - 425°C resulting in non-Arrhenius type temperature dependences for the rates of production of butane and butene. At a temperature of 340°C the coverage is at the low end of the hydrogen adsorption isotherm and thus varies as the half order

THIOPHENE HDS KINETIC PATHWAY

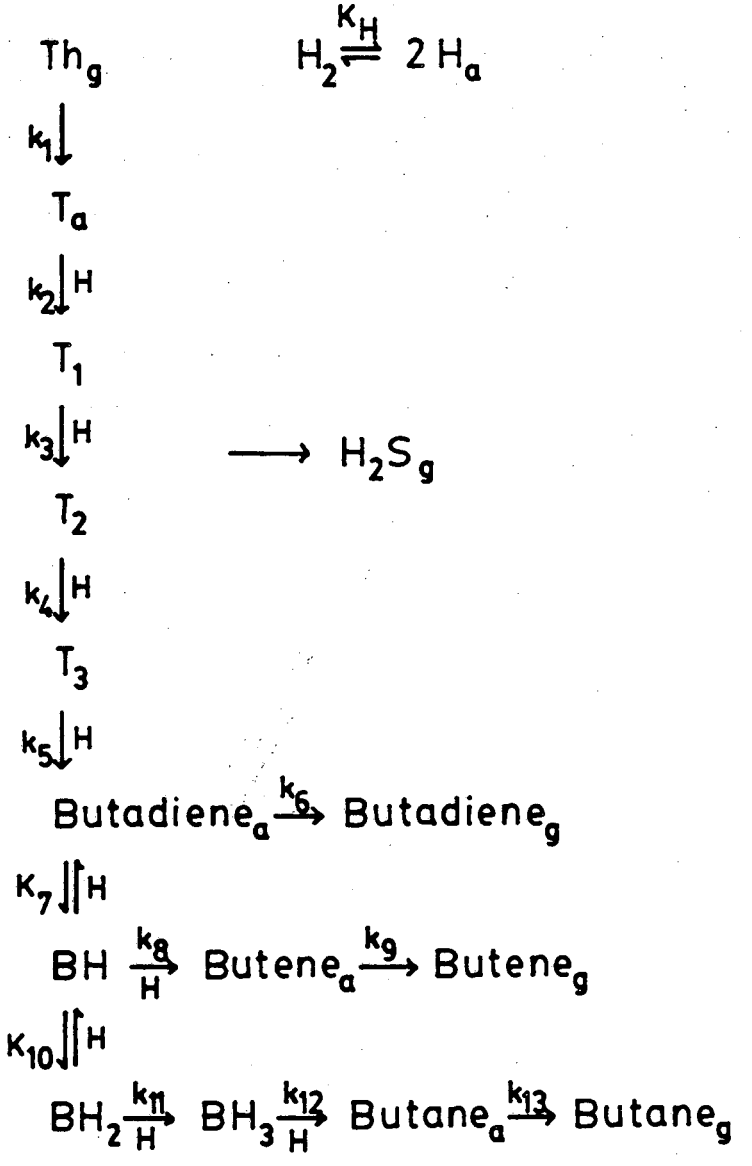

Fig. 5.19 A mechanistic pathway for thiophene HDS that is consistent with the observed kinetics.

power of the hydrogen pressure. Second, the rate determining step in the production of butadiene occurs prior to any hydrogenation steps, in spite of the fact that this product requires the formation of at least two C-H bonds. This results in the observed first order dependence on thiophene pressure and apparent independence of hydrogen pressure. Finally, the hydrogenated products are produced via an intermediate whose coverage saturates its available adsorption sites, resulting in an independence of thiophene pressure.

The initial sulfiding of the surface, under UHV conditions, prior to the HDS reaction resulted in a decrease in the activity at low coverages which continued to decrease up to a coverage of ~0.6 beyond which the further addition of sulfur had very little effect. The activity of the surface at these coverages had dropped to almost half that of the clean surface. The inhibition of the reaction rate at low coverages is caused by sulfur atoms adsorbed in the fourfold hollow sites, that must remain adsorbed on the surface during the reaction. Evidence has been presented in Chapter 3 for the presence of a second sulfur adsorption site that is less tightly binding than the hollow site and is only populated at high coverages. The fact that the addition of sulfur to the surface at these high coverages has little additional effect on the reaction rate suggests that the sulfur in this second binding site is easily reduced and that removal of sulfur from this site is relatively fast. In other words a reaction that is initiated on a surface that is initially covered with one monolayer of sulfur results in an immediate reduction of this coverage to the point at which only hollow sites are occupied. Immediate reduction implies a reaction that is fast on the time scale by which HDS rates are measured

(<< 15 min.)

Since sulfur atoms adsorbed in the fourfold hollow sites remain present on the surface, reducing the reaction rate, for periods of time that are long on the scale of the reaction rate (>10 sec.) suggests an interesting reaction mechanism for the desulfurization step. Three possible mechanisms for this step are depicted in Fig. 5.20. It is clear that thiophene HDS cannot proceed via initial cleavage of the C-S bonds to deposit sulfur into the fourfold hollows as in Fig. 5.20a. If such a mechanism were to occur over the initially clean surface, the hollow sites would be saturated within seconds of starting the reaction and the rate would be identical to that observed over the surface sulfided under UHV conditions. The reaction would be rate limited by sulfur removal from the surface, a step that appears to be very slow. A second possible mechanism for the desulfurization step would be deposition into the high coverage binding site from which it is apparently removed relatively quickly (Fig. 5.20c). If this is the case, however, it would seem necessary to assume that the sulfur removal from the high coverage site is faster than diffusion into the fourfold hollow. It seems more likely that the desulfurization step proceeds via direct hydrogenation of the C-S bonds to produce H_2S without ever forming a strongly bound metal sulfur intermediate, as depicted in Fig. 5.20b. This might occur via direct hydrogenolysis of C-S bonds by surface hydrogen or an intramolecular dehydrodesulfurization, neither of which would deposit sulfur onto the metal. These ideas can be tested by independent measurements of the rate of reduction of sulfur adsorbed on the metal surface, discussed in Chapter 6.

THIOPHENE DESULFURIZATION MECHANISMS

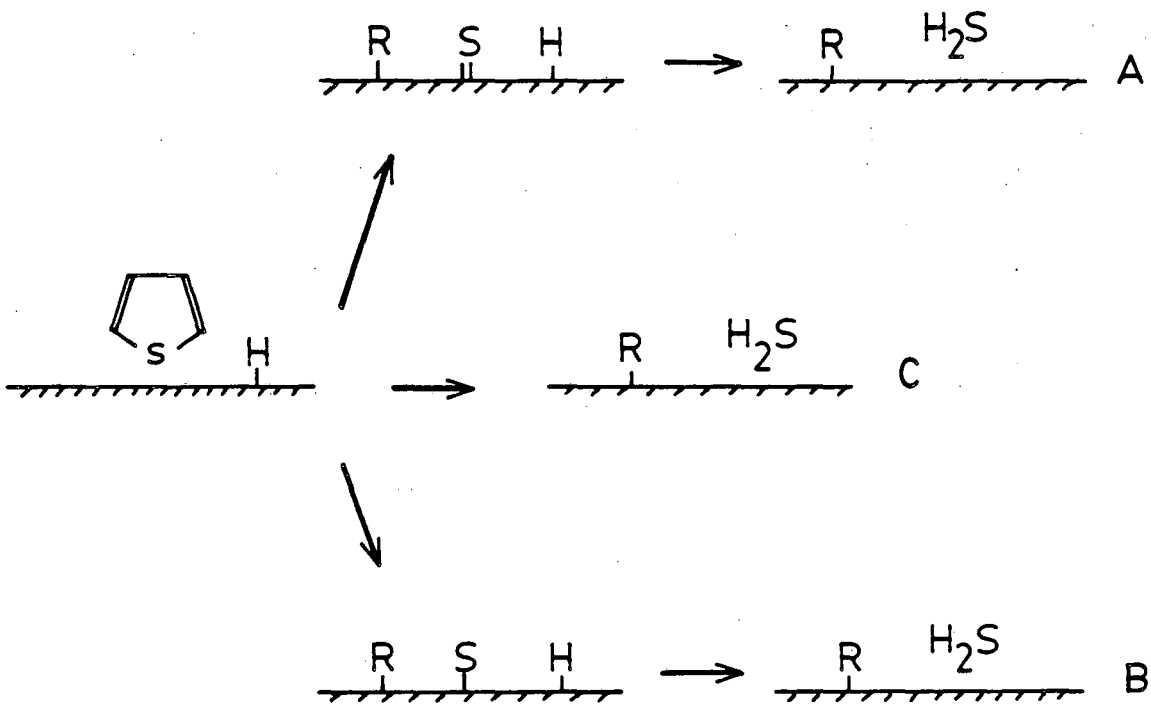

Fig. 5.20 Possible mechanisms for the initial desulfurization of thiophene. A) The Lipsch-Schuit mechanism involving deposition of sulfur onto the catalyst followed by reduction by surface hydrogen. B) A similar mechanism in which the sulfur atom is in a very weakly bound intermediate state. C) Direct extrusion of sulfur from the thiophene ring to form H_2S without the intermediate formation of an Mo-S species.

The final point of interest with respect to the effects of sulfur on the reaction rates is that while the intial adsorption of sulfur on the surface does reduce the rate of production of the butenes and butanes it has no apparent effect on the rate of butadiene production. This observation is consistent with the arguments made on the basis of kinetic measurements that the hydrogenated products are formed via some intermediates that saturate their available adsorption sites. The adsorbed sulfur atom in the fourfold hollow site directly blocks the formation of the species referred to as BH and BH_2. The route to butadiene production proceeds without the need to form a strong bond to the metal and appears to proceed either on or at least in the presence of the sulfur overlayer.

5.7 References

1. M.L. Vrinat, J. Appl. Catal., 6 (1983) 137
2. D.H. Broderick, B.C. Gates, AIChE J., 27 (1981) 663
3. P.J. Owens, C.H. Amberg, Adv. Chem. Series, 33 (1961) 182
4. E. Furminsky, Catal. Rev.- Sci. Eng., 22(3) (1980) 371
5. F.E. Massoth, G. MuraliDhar, Fourth Int. Conf. on the Chemistry and Uses of Molybdenum, Climax Moly. Co., Golden Co. 1982
6. S. Kolboe, Can. J. Chem., 47 (1969) 352
7. S. Kolboe, C.H. Amerg, Can. J. Chem., 44 (1966) 2623
8. S.J. Tauster, T.A. Pecoraro, R.R. Chianelli, J. Catal., 63 (1980) 515
9. M. Salmermon, G.A. Somorjai, A. Wold., R.R. Chianelli, K.S. Liang, Chem. Phys. Lett., 90 (1982) 105
10. J.A. Wilson, A.D. Yoffe, Advan. Phys., 18 (1969) 193
11. J.M. Wilson, Surf. Sci., 53 (1975) 330
12. J.M. Wilson, Surf. Sci., 57 (1976) 499
13. J.M. Wilson, Surf. Sci., 59 (1976) 315
14. E. Furminsky, Ind. Eng. Chem. Prod. Res. Dev., 22 (1983) 31
15. M.A. Logan, A.J. Gellman, G.A. Somorjai, unpublished work
16. A.J. Gellman, M. Asscher, G.A. Somorjai, in press
17. C.N. Satterfield, Heterogeneous Catalysis in Practice, p. 52, McGraw-Hill, 1980, New York
18. M.R. Blake, M. Eyre, R.B. Moyes, P.B. Wells, Bull. Soc. Chim. Belg., 90(12) (1981) 1293
19. R.J. Mikovsky, A.J. Silvestri, H. Heinemann, J. Catal., 34 (1974) 324

20. S. Pinol, Y.Berthier, J. Oudar, C.R. Acad. Sc. Paris, t. 300, Serie II, No. 12, 1985

Chapter 6. Hydrogenation of Sulfur on the Mo(100) Surface

6.1 Introduction

The previous chapters have presented studies of both the sulfided Mo(100) surface and the HDS of thiophene over these surfaces. The overall mechanistic pathway is initiated by a desulfurization process leading to the formation of butadiene. Subsequent hydrogenation of an adsorbed hydrocarbon intermediate results in butene and butane production. The mechanism of the initial step is in question and so it is the aim of this chapter to ascertain the nature of this reaction via direct measurements of the rates of sulfur hydrogenation from the metal surface.

The model most frequently proposed for such a reaction is that originally described by Lipsch and Schuit (1). Initial adsorption of the sulfur containing organic molecule is postulated to be at an anion vacancy on the catalyst surface (in this case an oxygen or sulfur vacancy). The exact geometry and nature of the bonding is not specified although a number of discussions have been made on the basis of theoretical calculations (2,3) suggesting that thiophene should bond through its lone pair electrons on the sulfur atom. The results of this work and other surface science studies of thiophene adsorption on metal surfaces point to a π-bonded configuration (Chapter 4). Subsequent hydrogenation of the C-S bonds leads to butadiene and the deposition of sulfur onto the catalyst surface. Final steps involve the reduction of the adsorbed sulfur to H_2S and the further hydrogenation of the butadiene. It should be noted, however, that there is very little direct evidence for this mechanism other than a series of experiments

using a catalyst labelled with ^{35}S in a vein similar to those reported in this work (4). These showed that for the HDS reaction of dibenzothiophene over a sulfided Mo catalyst there is a labile sulfur species, present on the catalyst, that is an intermediate in the reaction leading to H_2S.

It is possible to envision a number of HDS mechanisms that do not proceed via the formation of an Mo-S species. Direct hydrogenation of C-S bonds to yield H_2S and a surface bound hydrocarbon intermediate is one such possibility. Such a mechanism has been suggested leading from dibenzothiophene to mercaptobiphenyl which is then hydrogenated to biphenyl and H_2S (5). In the case of thiophene HDS a mechanism has been proposed, similar to that of an alcohol dehydration reaction, in which the desulfurization occurs by an intra-molecular hydrogenation of the sulfur atom leaving diacetylene as the hydrocarbon product (6). Investigations of the HDS of thiophene in D_2 showed that the sulfur containing product was H_2S rather than D_2S, in direct agreement with this mechanism (7). Such a reaction does not require the formation of a metal sulfur bond but is impossible in the case of dibenzothiophene.

The results of Chapter 5 show that the sulfiding of the Mo(100) surface under UHV conditions results in a decrease in the rate of thiophene HDS relative to that over the clean surface. The inhibition is most noticeable at low sulfur coverages and is associated with the blocking of active surface area by a strongly bound sulfur species that is stable on the surface under reaction conditions. At higher coverages (>0.6) the further addition of sulfur to the surface has little effect on the reaction rate. Previous work has shown that at high coverages the metal sulfur bond strength is reduced from its low coverage value

of 110 kcal/mole to a value of 75-90 kcal/mole, and the suggestion has been made that this weakly bound sulfur species may be readily reduced from the metal surface and thus have little effect on the HDS activity. Calculations of the equilibrium coverages of sulfur in H_2 (1 atm., 340°C), using 110 kcal/mole and 80 kcal/mole respectively for the bond strengths of the two Mo-S species respectively, show that the steady state coverage of the strongly bound species is almost unity while that of the weakly bound species is $\sim 5 \times 10^{-4}$.

The experiments performed in this work have used a ^{35}S isotope to make direct measurements of the rate of sulfur removal from the metal surface during exposure to H_2 and to the reaction mixture. The surface has been sulfided under UHV conditions with ^{35}S and then exposed either to H_2 or the reaction mixture. Periodic removal from the high pressure cell allows determination of the amount of ^{35}S remaining on the surface by monitoring of its β^- emission. Using this approach it is possible to discriminate between sulfur that has been deposited directly on the metal surface vs. sulfur that has been deposited in the form of adsorbed thiophene or via the decomposition of thiophene.

6.2 Mo(100)-S Reduction in H_2

The labelled ^{35}S sulfur overlayer on the Mo(100) surface produced a β^- signal of ~1800 cpm from the crystal at a coverage of θ_S=0.75 on initial reciept of the labelled material. Exposure of the surface to H_2 (1 atm.) at 340°C for 5 min. results in no measureable loss of ^{35}S from the surface. Fig. 6.1 shows the loss of ^{35}S from the surface at a

^{35}S HYDROGENATION on Mo(100) at θ_S°=.75

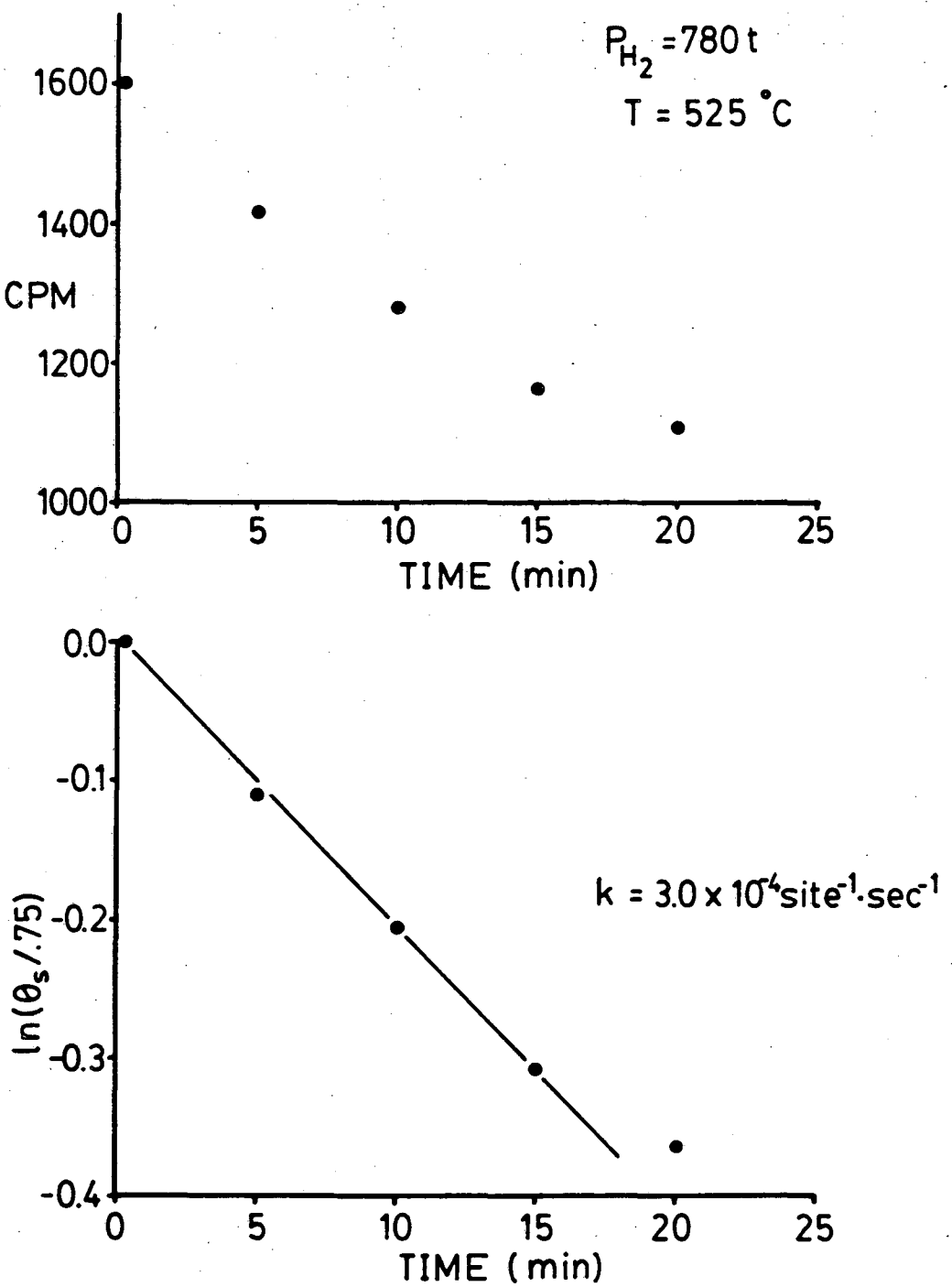

Fig. 6.1 A) Decrease in ^{35}S signal with time during reduction in H_2. Initial coverage was θ_S = 0.75, T = 525°C, P(H_2) = 780 torr. B) Plot of ln(θ_S/0.75) vs. t shows first order kinetics.

temperature of 525°C and a corresponding fit to a first order kinetic equation used to find the rate constant for removal, $k=3.0 \times 10^{-4}$ $site^{-1} \cdot sec^{-1}$.

$$r = \frac{d\theta}{dt} = k\theta$$

Note that this rate constant is dependent on θ_H, and even at these temperatures is less than the measured rates of thiophene HDS at 340°C of 0.11 $site^{-1}sec^{-1}$. Kinetic measurements of the rate of sulfur removal find an activation energy of 13.9 kcal/mole in the temperature range 400°C - 550°C and an order in hydrogen pressure of 0.34 over the pressure range 50 torr to 780 torr (Fig. 6.2 & 6.3). Extrapolation of the Arrhenius plot to 340°C yields a rate of $\sim 2 \times 10^5$ sec^{-1}, about four orders of magnitude less than the observed HDS rate. The reduction of S, bound to the metal surface, by hydrogen is not a step that is involved in the HDS of thiophene as it, necessarily, would be the rate limiting step.

The rates of sulfur removal from the surface were measured at several initial sulfur coverages (Fig. 6.4). Although the rates were measureable at 500°C for coverages of 0.75, at coverages of $\theta_S \leq 0.67$ there was no measureable reduction in the ^{35}S signal after treatment in H_2 for 5 min. Repetitive exposures would result in the buildup of contaminant sulfur and carbon from the reaction loop and the displacement of sulfur. It is interesting to note that that the coverage at which it becomes possible to remove the sulfur is $\theta_S \leq 0.67$. It is at this coverage that the sulfur atoms begin to populate the high coverage binding site rather than the fourfold hollow site.

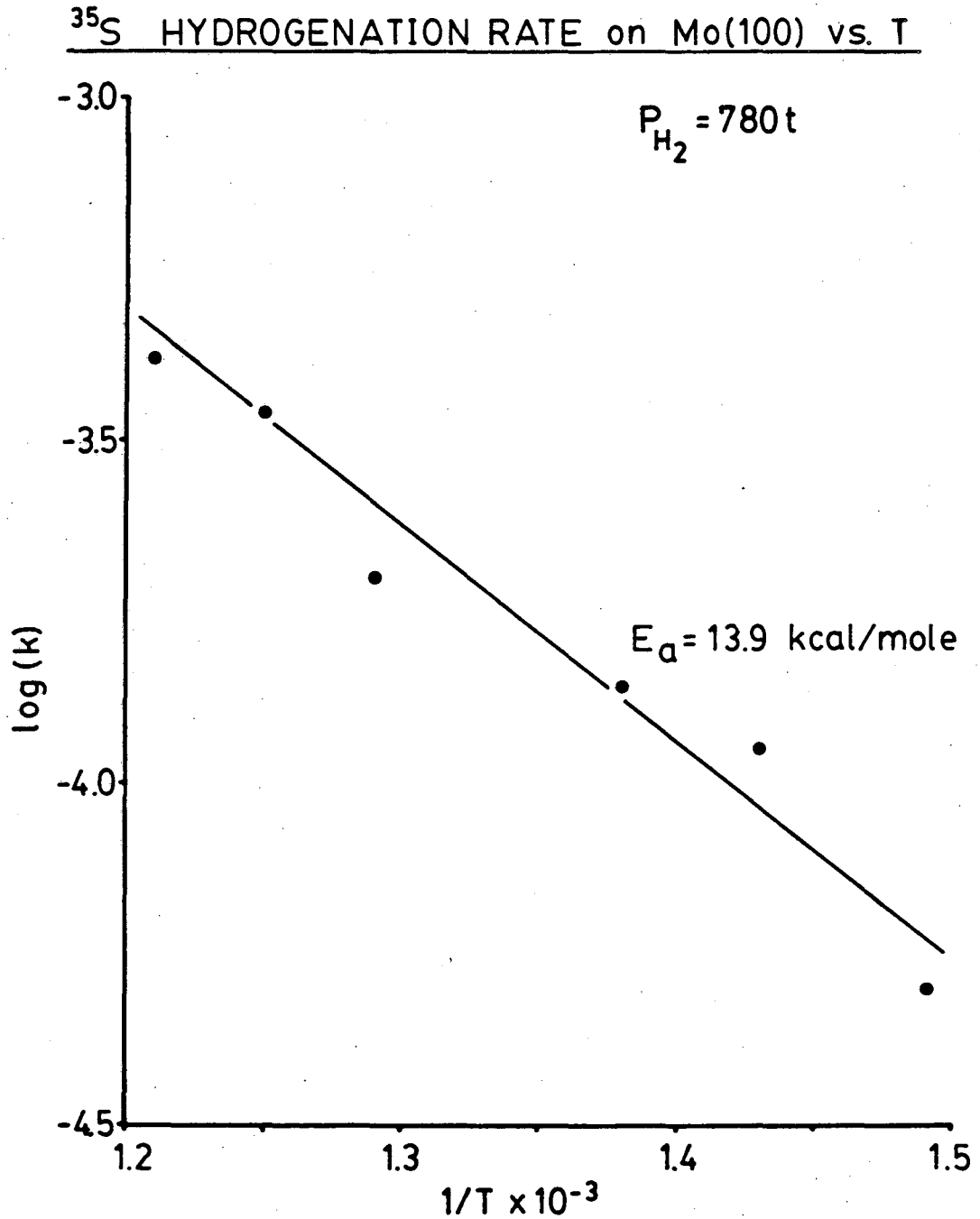

Fig. 6.2 Arrhenius plot of the rate constant for sulfur removal in hydrogen. $P(H_2)$ = 780 torr

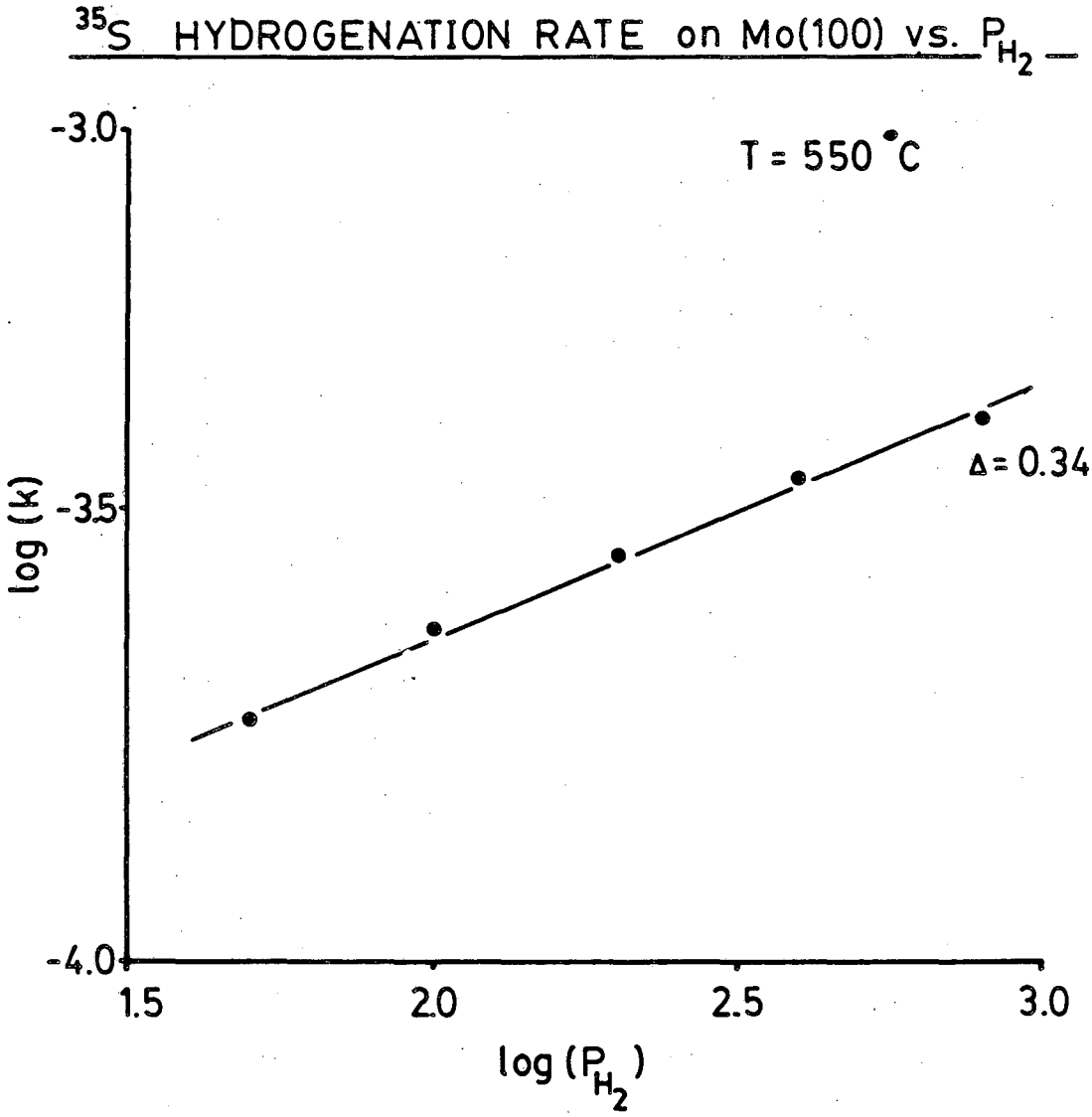

Fig. 6.3 Order plot of the rate constant for sulfur removal vs. hydrogen pressure. T = 550°C

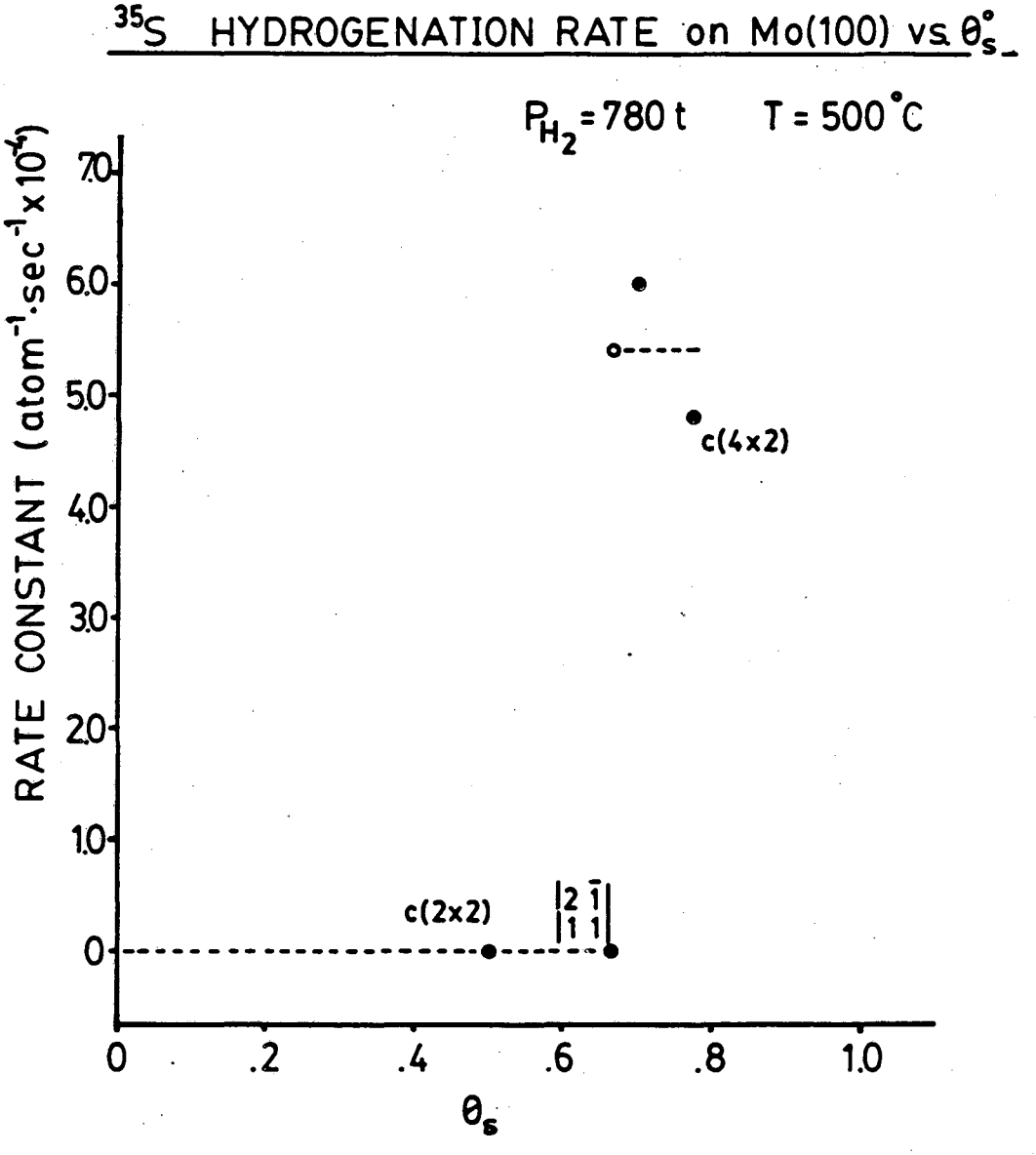

Fig. 6.4 Rate constant for sulfur removal vs. sulfur coverage. Reaction times were limited to 5 min. to minimize the effects of contamination by background hydrocarbons. T = 500°C, $P(H_2)$ = 780 torr

6.3 Mo(100)-S Reduction under HDS Conditions

In addition to studying the reduction of sulfur overlayers in H_2, similar measurements have been made in the presence of the HDS reaction mixture. The kinetic measurements show the the reaction is much different from that in pure H_2 (Fig. 6.5-6.7). The most pronounced effect of the addition of thiophene to the reaction mixture is a marked increase in the rate of sulfur removal. Under conditions of T = 345°C, $P(H_2)$ = 780 torr and P(Th) = 1 torr, very close to those used to study the HDS reaction, the removal rate constant is 6.8×10^{-4} sec^{-1}, greater than 30 times that observed in pure H_2, but still far lower than the observed thiophene HDS rate.

An Arrhenius plot of the rate over a temperature range of 225°C - 440°C shows a distinct break at ~380°C with a change of slope from 7.2 kcal/mole in the low temperature regime to 32.2 kcal/mole in the high temperature regime. Such a change is characteristic of a change of mechanism rather than a reduction in the surface concentrations of reactants, as was observed for the thiophene HDS reaction. The sulfur removal rate has been measured at 325°C, in the low temperature regime, over a range of reactant concentrations and been shown to be independent of either thiophene or hydrogen pressure. This is true even for very low concentrations of thiophene as it was observed that after performing reactions with thiophene several reactions in pure hydrogen were necessary to remove the trace amounts of contaminant thiophene to a level at which the sulfur removal rates were characteristic of those in pure H_2.

There was no significant difference in rates between surfaces

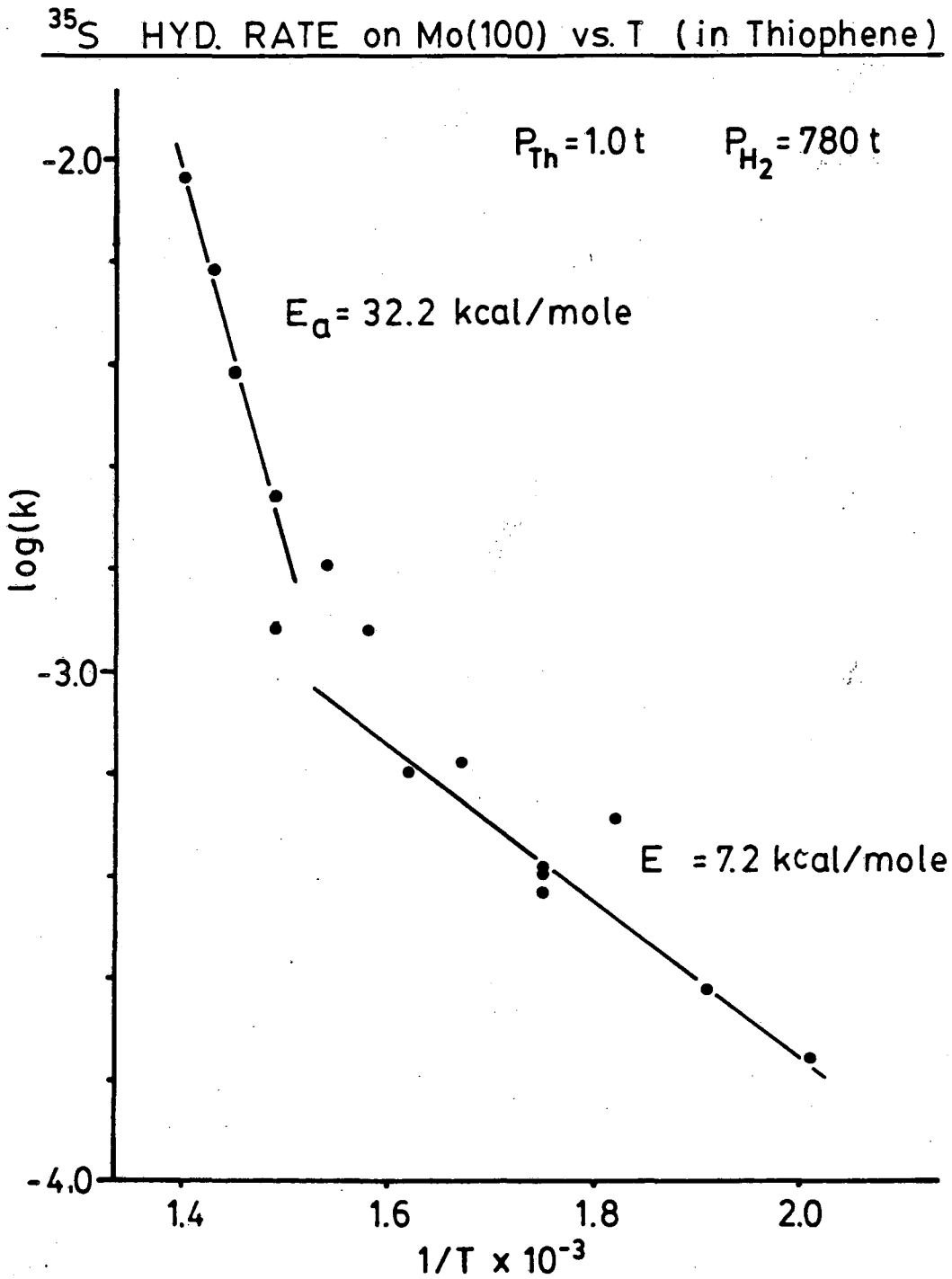

Fig. 6.5 Arrhenius plot of rate constants for sulfur removal in both thiophene and hydrogen. P(Th) = 1.0 torr, $P(H_2)$ = 780 torr

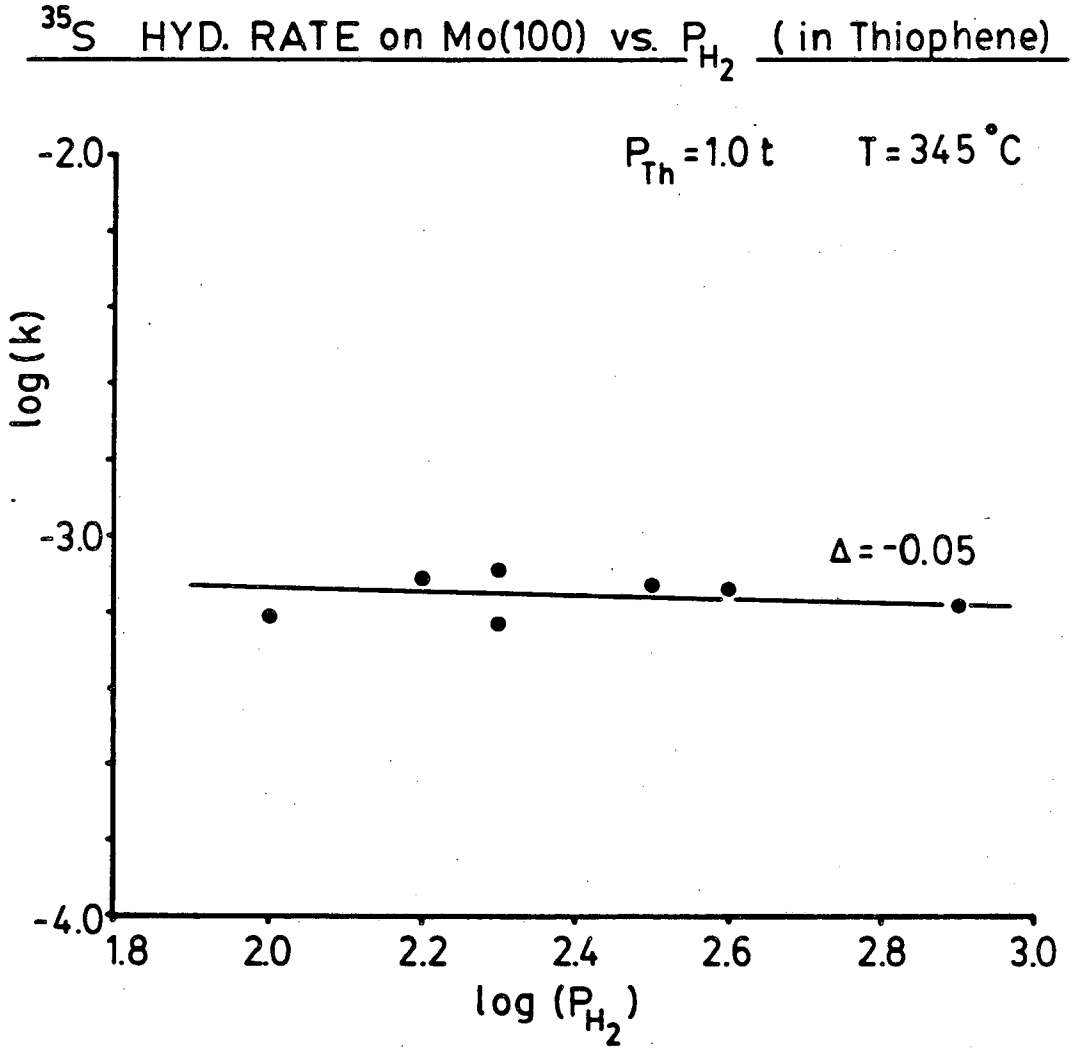

Fig. 6.6 Order plot of the rate constant for sulfur removal vs. hydrogen pressure. P(Th) = 1.0 torr, T = 345°C

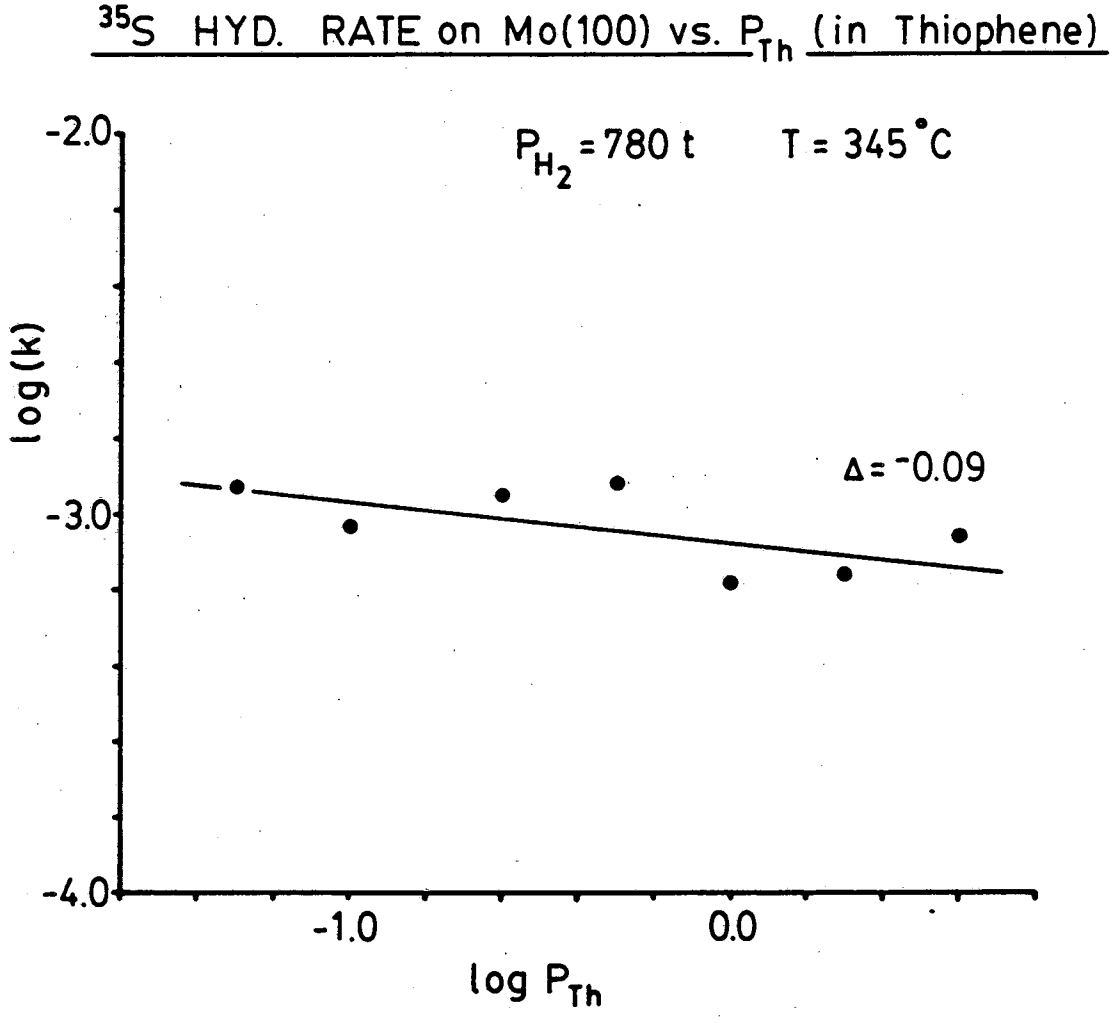

Fig. 6.7 Order plot of the rate constant for sulfur removal vs. thiophene pressure. $P(H_2)$ = 780 torr, T = 345°C

starting with θ_S = 0.5 and θ_S = 0.75 as was observed in the case of pure H_2. In the cases in which thiophene was included in the reactant mixture even sulfur atoms bound in the fourfold hollow sites could be displaced, although its residence time on the surface is still very long, i.e. ~1500 sec. The sulfur deposited on the surface before the an HDS reaction remains on the surface for periods much longer than those of either the reactants or the products.

6.4 Discussion

The two most important results of this work and their implications on HDS catalysis can be understood in terms of the results of sulfur adsorption on the Mo(100) surface and of thiophene HDS over these surfaces. The rate of hydrogenation of adsorbed sulfur to H_2S is much slower than the rate of hydrodesulfurization under the same conditions. This result eliminates the Lipsch-Schuit mechanism depicted in Fig. 6.8 of desulfurization in which the sulfur is first adsorbed onto the metal as a result of hydrogenolysis of C-S bonds and is subsequently hydrogenated. If such were the case the hydrogenation reaction would be rate limiting and the reaction rates much slower than those observed. It is not, of course, possible to rule out a mechanism in which the sulfur atom is deposited onto the surface in a very weakly bound state from which it is easily reduced. The nature of such a state, however, would be much different from any observed under UHV conditions. Its heat of adsorption must be sufficiently low that its reduction to H_2S is much faster than any exchange reaction with sulfur bound directly to

THIOPHENE DESULFURIZATION MECHANISMS

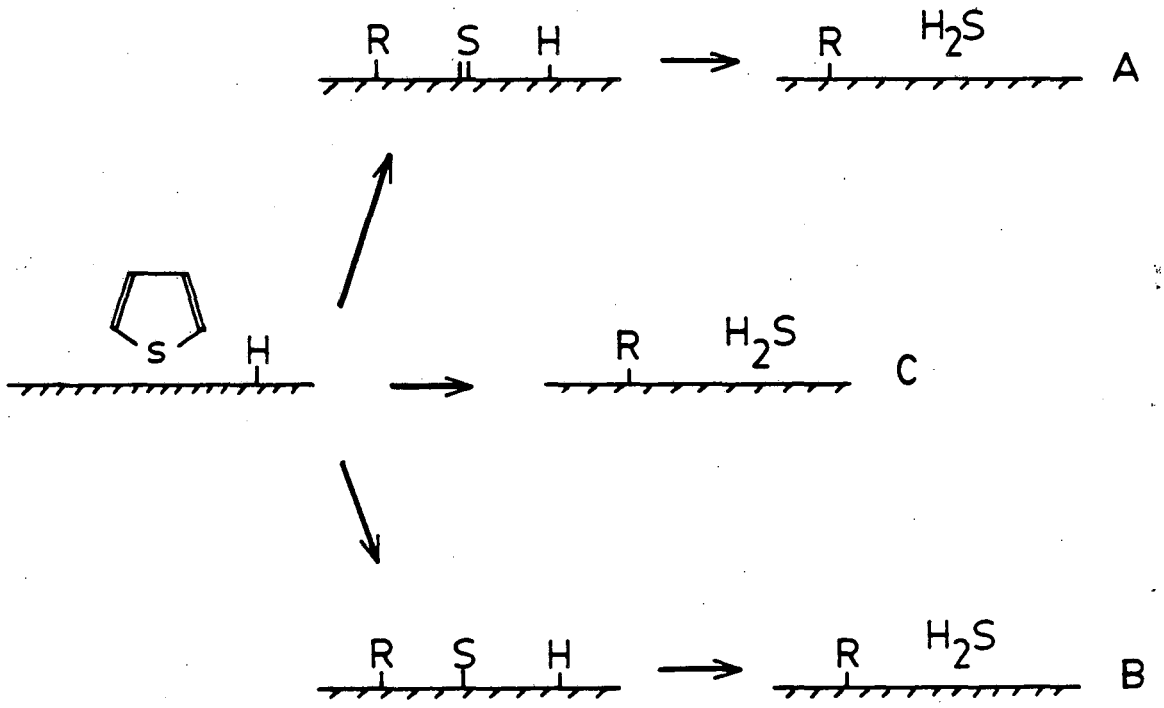

Fig. 6.8 Possible mechanisms for the initial desulfurization of thiophene. A) The Lipsch-Schuit mechanism involving deposition of sulfur onto the catalyst followed by reduction by surface hydrogen. B) A similar mechanism in which the sulfur atom is in a very weakly bound intermediate state. C) Direct extrusion of sulfur from the thiophene ring to form H_2S without the intermediate formation of an Mo-S species.

the metal. It is difficult to understand what the driving force would be for the breaking of C-S bonds to form such a species.

The kinetic studies of thiophene HDS have shown that the initial steps to produce butadiene are independent of hydrogen pressure and first order in thiophene pressure. This has been discussed in terms of a rate determining step that occurs prior to any hydrogenation steps. The fact that butene production is of fractional order in hydrogen pressure has suggested that the hydrogen coverage is low and the first order dependence on thiophene pressure rules out a mechanism in which one of the hydrocarbon intermediates leading to butadiene is saturating the surface. Finally, the activation energy of the rate determining step has been found to be ~14 kcal/mole. Two mechanisms for the initial desulfurization step are consistent with the observations of this work. A reaction in which hydrogenolysis of C-S bonds by adsorbed hydrogen, yielding H_2S and an adsorbed hydrocarbon intermediate that is readily reduced to butadiene, proceeds without the intermediate formation of an Mo-S bond. In this case the rate determining step is one occuring prior to the hyrogenolysis step, either the adsorption of thiophene or the production of some activated adsorption state in which the hydrogenolysis can occur. It is unlikely that simple chemisorption is activated, however, studies of thiophene chemisorption on the Mo(100) surface (Chapter 4) showed the existence of an adsorption state, stable to high temperatures (>450K), that was only produced upon heating to ~200K. Although no direct correlation to the high pressure reaction can be made, such a species might be hydrogenated at high pressures to yield the HDS products. The second mechanism that is consistent with the current work is that proposed by Kolboe (6), which

is a dehydrodesulfurization reaction. The production of H_2S occurs intramolecularly leading to adsorbed diacetylene. It seems reasonable to suggest that such an initial step would be activated and might be rate limiting. Furthermore the hydrogenation of diacetylene to butadiene would be expected to be very fast (8). Such a mechanism would not be possible in the case of dibenzothiophene but labelling studies of the HDS of this compound have shown that it does proceed via a Lipsch-Schuit type mechanism.

The measurements of sulfur hydrogenation in H_2 show that the hydrogenation of the high coverage sulfur species is faster than that of the low coverage species ($\theta_S < 0.67$). This was predicted from the study of the rates of the thiophene HDS reactions at various different initial sulfur coverages, in which the low coverage sulfur was found to have a strong inhibiting effect while increases past $\theta_S \sim 0.6$ caused little additional change. The coverage at which the sulfur can be reduced is that at which the high coverage binding site, postulated to be a bridging site, becomes populated. The present results provide further evidence that there is some change in the bonding of sulfur to the surface on going from the $\begin{vmatrix} 2 & \bar{1} \\ 1 & 1 \end{vmatrix}$ structure to the c(4x2) structure.

The details of the role that preadsorbed sulfur plays in determining the reaction rate are unclear. In the presence of thiophene all ^{35}S can be reduced from the metal surface, but on a scale that is much longer than the reaction rate. The pre-adsorbed sulfur selectively inhibits the hydrogenation reactions leading to the butenes and butane production but not the desulfurization reaction leading to butadiene. Kinetic studies suggest that the hydrogenated products are formed via a partially hydrogenated intermediate that saturates its available

binding site on the surface, thus leading to the very weak dependence of the butenes and butane rates of production on the thiophene pressure. The presence of pre-adsorbed sulfur blocks binding sites for such an intermediate. A zeroth order explanation for the shape of the rate vs. θ_S curve would be that sulfur adsorbed in the fourfold hollow sites ($\theta_S \leq 0.67$) remains on the surface permanently, blocking adsorption sites for the intermediate leading to the hydrogenated products. Sulfur adsorbed on the surface at coverages greater than 0.67 is present in the high coverage binding site and is reduced from the surface very quickly, until the concentration of adsorbed sulfur reaches 0.67, and thus has very little effect on the reaction rate. Such an ideal situation would be expected to result in a linear decrease of the rate in the coverage regime $0 < \theta_S < 0.67$ and for $\theta_S \leq 0.67$ a rate equal to that at $\theta_S = 0.67$. While the results presented here approximate such a process the situation is clearly much more complicated due to the fact that the removal of sulfur from the high coverage sites is not infinitely fast, nor is removal rate of sulfur from the low coverage site, zero. Furthermore, in the presence of thiophene there is some deposition of sulfur onto the surface, albeit at a rate much less than that of the reaction.

The sulfur reduction kinetics in pure hydrogen can be modelled very well by a simple scheme of hydrogen adsorption followed by a sequential hyrogenation of sulfur atoms and finally, desorption of H_2S.

$$H_{2g} \rightarrow 2H_a$$

$$S + H_a \rightarrow SH$$

$$SH + H_a \rightarrow SH_2$$

$$SH_2 \rightarrow H_2S_g$$

The fact that the hydrogen pressure dependence is zero indicates that the first step of hydrogen adsorpton is not rate limiting. Unfortunately, it was not possible to cover a great enough range of hydrogen pressures to allow determination of which step among the remainder is rate limiting.

The final point of interest in this study is the dramatic influence of thiophene on the rate of sulfur reduction. Very low pressures of thiophene resulted in an enhancement of the reduction rate by as much as an order of magnitude. The rate increase may be due either to a change in the metal-sulfur bonding due to the presence of co-adsorbed thiophene or a change in the reaction mechanism.

The reduction of sulfur in pure H_2 has been noted to occur at a faster rate as the Mo-S bond is weakened on increasing the coverage past 0.67 monolayers. This bond weakening is due to a change in the sulfur adsorption site with coverage, induced by repulsive interactions between adsorbed sulfur atoms. If such an effect were produced by the presence of thiophene a similar increase in the reaction rate would be expected. Such an effect, however, would be expected to manifest itself in terms of a decrease in the reaction activation energy. At temperatures of 390°C - 440°C this is clearly not the case as the apparent activation energy increases from 14 kcal/mole to 32 kcal/mole on introducing thiophene. In the lower temperature range, outside that accessible when working just with H_2, the activation energy is lowered by the presence of thiophene. The pre-exponential factor and the kinetics,

however, are also different suggesting a new sulfur removal mechanism.

It is interesting to note that the removal rate of sulfur in the HDS mixture is independent of both thiophene and hydrogen pressures. The studies of HDS kinetics point to the existence of a hydrocarbon intermediate that is saturating the surface and is in equilibrium with hydrogen on the surface. Its concentration is independent of both thiophene and hydrogen pressures. It is possible that such a species serves as a source of hydrogen for sulfur removal accounting both for the enhancement in the reaction rate and the observed kinetic parameters. The presence of a carbonaceous deposit serving as a source of hydrogen during hydrogenation reactions has been discussed elsewhere (9). In the case of ethylene hydrogenation over Pt(111) and Rh(111) surfaces such deposits have been identified as ethylidyne moieties (10,11). In this case, however, the nature of such a species is unknown, and should be the subject of further investigation.

6.6 References

1) J.M.G. Lipsch, G.L.A. Schuit, J. Catal., 15 (1969) 179

2) A.J. Duben, J. Phys. Chem., 82(3) (1978) 348

3) S. Harris, R.R. Chianelli, J. Catal., 86 (1984) 400

4) C.G. Gachet, E. Dhainaut, L. de Mourgues, J.P. Candy, P. Fouilloux, Bull. Soc. Chim. Belg., 90(12) (1981) 1279

5) G.H. Singhal, R.L. Espino, J.E. Sobel, J. Catal., 67 (1981) 446

6) S. Kolboe, Can. J. Chem., 47 (1969) 352

7) R.J. Mikovsky, A.J. Silvestri, H. Heinemann, J. Catal., 34 (1974) 324

8) B.C. Gates, J.R. Katzer, G.C.A. Schuit, Chemistry of Catalytic Processes, p. 263, McGraw-Hill Inc., New York, 1979

9) S.M. Davis, Ph.D. Thesis, U.C. Berkeley, Berkeley CA, 1981

10) F. Zaera, Ph.D. Thesis, U.C. Berkeley, Berkeley CA, 1984

11) F. Zaera, G.A. Somorjai, J. Am. Chem. Soc., 106 (1984) 2288

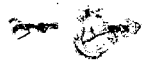

LAWRENCE BERKELEY LABORATORY
TECHNICAL INFORMATION DEPARTMENT
UNIVERSITY OF CALIFORNIA
BERKELEY, CALIFORNIA 94720